https://dspace.org/

Electrochemical studies of metal-ligand equilibria involving chelating ligands

Uwamariya, Valentine

2006-04-24
http://hdl.handle.net/10539/349

Downloaded from a DSpace repository. https://dspace.org/

ELECTROCHEMICAL STUDIES OF METAL–LIGAND EQUILIBRIA INVOLVING CHELATING LIGANDS

Dissertation submitted to the Faculty of Sciences, University of the Witwatersrand, South Africa, for the degree of **Master of Science**

By

Valentine UWAMARIYA

Supervised by:

- **Prof. Ignacy Cukrowski**
- **Dr. Alvaro Silva de Sousa**

SCHOOL OF CHEMISTRY

UNIVERSITY OF THE WITWATERSRAND

JOHANNESBURG

SOUTH AFRICA

January 2005

Declaration

I hereby declare that this dissertation is my own work. It is submitted for the fulfillment of the degree of Master of Science in the Faculty of Sciences of the University of the Witwatersrand. This dissertation has never been submitted before for any degree or examination in any other university.

…….

V. UWAMARIYA

18 day of January 2005

In memory of my Father

To my Mother

To my Sons

Abstract

Metal-ligand models and complex stability constants of newly synthesised chelating ligands, N,N'-bis(2-hydroxycyclopentyl)-ethylenediamine (Cyp_2EN) and N,N'-bis(2-hydroxycyclohexyl)-ethylenediamine (Cy_2EN), with metal ions Cd^{2+}, Cu^{2+}, Ni^{2+}, Pb^{2+} and Zn^{2+} were established in this work. Stability constants were determined by Glass Electrode Potentiometry (GEP) and polarography as electrochemical techniques. A new concept, termed Virtual Potentiometry (VP), was also used for the evaluation of stability constants. In this concept, polarographic or polarographic + potentiometric data were evaluated using potentiometric computer software (ESTA). This concept assisted in obtaining a final model for Cd–Cyp_2EN and Pb–Cyp_2EN systems. It could refine M(HL) complex inaccessible via polarographic study of Pb–Cyp_2EN system and refined the hydroxo–complex $ML_2(OH)$ that in turn was inaccessible using GEP for Cd–Cyp_2EN system. For all metals studied, the complexes ML formed with the ligand Cy_2EN were found more stable than the complexes ML formed with the ligand Cyp_2EN. The complex M(HL) was obtained for all systems studied, but it seemed to be a minor species. The complex ML_2 was obtained in different systems studied with the ligand Cy_2EN while this complex was only found in Cd–Cyp_2EN system. In several systems potentiometric (ESTA) and voltammetric (3D–CFC) software could not distinguish which hydroxo–complexes were present as these species were formed in the pH range where the ligand was fully deprotonated. Selectivity trends for Cyp_2EN and Cy_2EN were compared and related to DHEEN as a function of metal ion radius. It was observed that the large metal ions were favoured by the addition of cyclopentyl bridges in DHEEN while the small metal ions were favoured when cyclohexyl bridges were added.

Acknowledgements

I would like to express my sincere thanks and appreciations for the support that I received throughout this work to the following people:

- My supervisor Prof. Ignacy Cukrowski for his guidance, understanding, financial assistance and intellectual input. His enthusiasm is greatly appreciated.
- My co-supervisor Dr. A.S. de Sousa for providing samples of ligands used in this work, his intellectual input, understanding and proof reading of this dissertation,
- The entire "Electrochemistry Team" for their understanding co–operation and invaluable assistance inside and outside the laboratory,
- All members of my family: parents, husband, brothers and sisters for their support, love and encouragement. I could not have coped without them.
- My sister Chantal who became the mother of my sons while I was away,
- All my friends for their love, support and encouragement

I wish also to acknowledge the Rwandan Government for its financial support. Finally my Greatest Thanks go to GOD who gave me strength and perseverance throughout this work.

Table of Contents

Declaration ii

Dedication iii

Abstract iv

Acknowledgments v

Table of Contents vi

List of Figures x

List of Symbols and Abbreviations xx

List of Tables xxv

Chapter 1: Introduction

1.1. Concept of metal complex in aqueous solution 1

1.1.1. Overview of metal complexes 1

1.1.2. Types of complex equilibria in solution 2

1. 2. Chelating complexes 4

1.2.1. Chelate effect 5

1.2.2. Use of chelates in medicine 7

1.3. Effect of oxygen and nitrogen donor atoms in ligand design 8

1.3.1. Neutral and negatively charged oxygen donor atom 8

1.3.2. Neutral saturated nitrogen donor 11

1.4. Measurement and Application of Stability Constants 11

1.4.1. Measurement of stability constants 11

1.4.2. Applications of stability constants 13

1.4. Aim of the research 14

Chapter 2: Theory and Data Treatment

2.1. Glass Electrode Potentiometry 15

2.1.1. Prediction of Stability constant by potentiometry 15

2.1.2. Generalities on glass electrode potentiometry (GEP) 16

2.1.3. Use of GEP in the determination of stability constants 18

2.1.4. Analysis of potentiometric data 20

2.2. Polarography 25

2.2.1. General introduction 25

2.2.2. Principles of Direct Current Polarography (DCP) 27

2.2.3. Principles of Differential Pulse Polarography (DPP) 30

2.2.4. Use of Polarography in Metal-Ligand Equilibrium Study 31

2.3. Theory of Virtual Potentiometry 37

Chapter 3: Experimental

3.1. Reagents 40

3.2. Preparation of the solutions used 40

3.3. Glass Electrode Potentiometry 42

3.3.1. Experimental set-up 42

3.3.2. Experimental procedure 43

3.4. Polarography 45

3.4.1. Experimental set-up 45

3.4.2. Experimental procedure 46

Chapter 4: Results and Discussion

4.1. Protonation constants of the ligands Cyp_2EN and Cy_2EN 49

4.2. Glass electrode potentiometric study of Cd-Cyp_2EN 52

4.2.1. Data refinement 52

4.2.2. Complex formation function 54

4.2.3. Species distribution diagram 55

4.3. Polarographic study of Cd–Cyp$_2$EN system 56

4.3.1. Data fitting 56

4.3.2. Modelling of experimental data from DC$_{tast}$ 59

4.4. Study of Cd-CypEN by potentiometry + polarography 68

4.5. Study of Pb–Cyp$_2$EN system by GEP 71

4.5.1. Data refinement 71

4.5.2. Complex formation function $\overline{Z}_M$ 72

4.5.2. Species distribution diagram 73

4.6. Polarographic study of Pb–Cyp$_2$EN system 74

4.6.1. Data treatment 74

4.6.2. Modelling of experimental data from DPP ratio L_T:M_T 50 75

4.7. Study of Pb-Cyp$_2$EN by polarography + potentiometry 83

4.8. Study of Cu–Cyp$_2$EN, Ni–Cyp$_2$EN and Zn–Cyp$_2$EN by GEP 85

4.8.1. Cu–Cyp$_2$EN system 85

4.8.2. Study of Ni–Cyp$_2$EN system 89

4.8.3. Study of Zn–Cyp$_2$EN system 93

4.9. Polarographic study of Cd-Cy$_2$EN system 97

4.9.1. Data fitting 97

4.9.2. Modelling for experimental data from DC-tast 100

4.10. Glass electrode potentiometric study of Cd–Cy$_2$EN system 105

4.10.1. Data refinement 105

4.10.2. Complex formation curve 107

4.10.3. Species distribution diagram 108

4.11. Comparison between GEP and DC_{tast} for Cd–Cy_2EN system 111

4. 12. Study of Pb–Cy_2EN system by GEP 115

4.12.1. Data treatment 115

4.12.2. Complex formation curve 116

4.12.3. Species distribution diagram 117

4.13. DC_{tast} polarographic study of Pb-Cy_2EN 118

4.14. Study of Cu–Cy_2EN, Ni–Cy_2EN and Zn–Cy_2EN by GEP 121

4.14.1. Cu–Cy_2EN system 121

4.14.2. Ni–Cy_2EN system 126

4.14.3. Zn–Cy_2EN system 130

4.15. Effect of the addition of cyclic moiety in the pendant donor groups of diamine 134

4.15.1. Comparison of Cyp_2EN with DHEEN 134

4.15.2. Comparison of Cy_2EN with DHEEN 136

4.15.3. Comparison of Cyp_2EN with Cy_2EN 137

Chapter 5: Conclusion 140

References 144

Appendix 148

List of Figures

Figure 1.1: Diagrammatic representation of a metal ion, Ni (II), in water, showing its inner and outer sphere of coordinated water (A), the formation of an outer–sphere complex with sulphate (B), and an inner–sphere complex with sulphate where the sulphate ligand is directly bonded to the Ni^{2+} ion (C) [5]. 3

Figure 1.2: The effect of neutral oxygen donor atom on complex stability. Relationship between the change in complex stability, Δlog *K*, that occurs on adding 2–hydroxyethyl groups to alanine (•) or ethereal oxygens to oxalate (o), and the ionic radius of the metal ion. Ionic radii are from [5] and are for octahedral coordination, except for Cu(II) which is square planar. Formation constants are from [13] 9

Figure 1.3: Relationship between log K_1 for chelating ligands containing negatively charged oxygen donors groups and log K_1 for the formation of the hydroxide complex, for a variety of metal ions. The ligands shown are catechol (•), 5–nitrosalicylic acid (o), kojate (▪) and malonate (□). Formation constants at ionic strength zero and 25°C are from [13]. The intercept at log 55.5 is expected from theories of chelate effect from [29] and [30]. 10

Figure 1.4: Structure of the ligands studied in this work 14

Figure 2.1: Calibration curve of GE performed by titration of 15 ml of 0.01 M HNO_3 with 0.02 M NaOH 18

Figure 2.2: Example of DC–waves recorded at different pH on Pb-Cyp_2EN system L_T:M_T ratio 50. *a* and *a'* represent the limiting current

I_d, *b* and *b'* represent the half-wave potential $E_{1/2}$, *c* and *c'* represent the residual current. Circles and solid lines represent the recorded and fitted curves, respectively. 28

Figure 2.3: Example of differential pulse polarogram recorded on Cd-Cyp_2EN system L_T: M_T ratio 200 at pH 3.1, ionic strength 0.1 in $NaNO_3$ and 25°C. $[M_T] = 1.99 \times 10^{-5}$ M and $[L_T] = 3.98 \times 10^{-3}$ M. 31

Figure 4.1: Experimental (circles) and fitted (solid line) protonation curves from the titration of the ligand Cyp_2EN at ionic strength 0.1 M and 25°C, $[L_T] = 5 \times 10^{-3}$ M (in 0.01 M HNO_3); titration by 0.01 M NaOH. 49

Figure 4.2: Experimental (circles) and fitted (solid line) protonation curves from the titration of the ligand Cyp_2EN at ionic strength 0.1 M and 25°C, $[L_T] = 5 \times 10^{-3}$ M (in 0.01 M HNO_3); titration by 0.01M NaOH. 50

Figure 4.3: Experimental (circles) and calculated (solid lines) potentiometric complex formation curves for Cd–Cyp_2EN system at 25°C and ionic strength 0.1 M in $NaNO_3$. The model used is M(HL), ML, and ML_2. 54

Figure 4.4: Species distribution diagram of Cd–Cyp_2EN system for L_T:M_T ratio 3 at 25°C and ionic strength 0.1 M in $NaNO_3$. $[L_T] = 2.99 \times 10^{-3}$ M and $[M_T] = 1.00 \times 10^{-3}$ M. The model used was M(HL), ML and ML_2 together with all known $Cd_x(OH)_y$ species from the combined refinement..... 55

Figure 4.5: Example showing how the system became less reversible when the pH increased for Cd–Cyp_2EN system. L_T:M_T ratio 200 studied by DPP at 25°C and ionic strength 0.1 M in $NaNO_3$.

$[M_T] = 1.99 \times 10^{-5}$ M and $[L_T] = 3.98 \times 10^{-3}$ M. The circles and solid lines indicate experimental and fitted curves, respectively 58

Figure 4.6: Variation in limiting diffusion current for Cd–Cyp_2EN system studied by DC_{tast} at L_T:M_T ratio 200, initial $[M_T] = 1.99 \times 10^{-5}$ M and $[L_T] = 3.98 \times 10^{-3}$ M, at 25°C and ionic strength 0.1 M in $NaNO_3$. The dashed line and triangles indicate the normalised limiting diffusion current; the squares indicate the expected current when complexes are not formed. 59

Figure 4.7: Variation in half–wave potential vs. pH for Cd–Cyp_2EN system studied by DC_{tast} at L_T:M_T ratio 200, initial $[M_T] = 1.99 \times 10^{-5}$ M and $[L_T] = 3.98 \times 10^{-3}$ M, at 25°C and ionic strength 0.1 M in $NaNO_3$ 61

Figure 4.8: Variation in half–wave potential vs. log [L] for Cd–Cyp_2EN system studied by DC_{tast} at L_T:M_T ratio 200, initial $[M_T] = 1.99 \times 10^{-5}$ M and $[L_T] = 3.98 \times 10^{-3}$ M, at 25°C and ionic strength 0.1 M in $NaNO_3$ 63

Figure 4.9: Virtual half-wave potential as a function of log [M] for Cd–Cyp_2EN system studied by DC_{tast} at L_T:M_T ratio 200, initial $[M_T] = 1.99 \times 10^{-5}$ M and $[L_T] = 3.98 \times 10^{-3}$ M, at 25°C and ionic strength 0.1 M in $NaNO_3$. 64

Figure 4.10: Experimental and calculated complex formation curves for Cd–Cyp_2EN system studied by DC_{tast} at L_T:M_T ratio 200, initial $[M_T] = 1.99 \times 10^{-5}$ M and $[L_T] = 3.98 \times 10^{-3}$ M, at 25°C and ionic strength 0.1 M in $NaNO_3$. The circles indicate the experimental corrected shift in DC_{tast} half-wave potential calculated for each data point. The solid line represents the CCFC for the optimised M–L model 65

Figure 4.11: Species distribution for Cd–Cyp_2EN system ratio L_T:M_T 200 studied by DC_{tast} at 25°C and ionic strength 0.1 M in $NaNO_3$. $[L_T] = 3.98 \times 10^{-3}$ M and $[M_T] = 1.99 \times 10^{-5}$ M. 67

Figure 4.12: Species distribution diagram for Cd–Cyp_2EN system using the results from GEP + VP-DC and conditions from potentiometry. $[L_T] = 3.00 \times 10^{-3}$ M and $[M_T] = 1.00 \times 10^{-3}$ M 69

Figure 4.13: Species distribution diagram for Cd–Cyp_2EN system by GEP + VP-DC calculated using polarographic conditions and the model obtained when the stability constant of ML(OH) was fixed at 7.9 $[L_T] = 3.98 \times 10^{-3}$ M and $[M_T] = 1.99 \times 10^{-5}$ M. 70

Figure 4.14: Complex formation curves for Pb–Cyp_2EN system studied by potentiometry at 25°C and ionic strength 0.1 M in $NaNO_3$. Circles, triangles and diamonds represent experimental points for L_T:M_T ratio 1, 2, and 3, respectively. The solid lines represent the fitted curves..... 72

Figure 4.15: Species distribution diagram for Pb–Cyp_2EN system calculated using the results from the combined refinement and potentiometric conditions for L_T:M_T ratio 1. $[L_T]=2.00 \times 10^{-3}$ M and $[M_T] = 2.00 \times 10^{-3}$ M..... 73

Figure 4.16: Pb–Cyp_2EN system studied by DPP at L_T:M_T ratio 50. The dashed line indicates the normalised peak height (triangles). Squares represent expected peak height if the metal complexes were not formed (if the observed decrease at high pH is only caused by dilution of the sample). $[M_T] = 8.01 \times 10^{-5}$ M and $[L_T] = 4.029 \times 10^{-3}$ M. 75

Figure 4.17: Variation in virtual peak potential versus pH for Pb–Cyp_2EN system L_T:M_T 50 ratio studied by DPP at 25°C and ionic strength 0.1 M in $NaNO_3$. [M_T] = 8.01 × 10^{-5} M and [L_T] = 4.029 × 10^{-3} M. 77

Figure 4.18: Variation in virtual peak potential versus log [L] for Pb–Cyp_2EN system at 25°C and ionic strength 0.1 M in $NaNO_3$. [M_T] = 8.01 × 10^{-5} M, and [L_T] = 4.029 × 10^{-3} M. 79

Figure 4.19: Experimental (circles) and calculated (solid line) complex formation curves for Pb–Cyp_2EN system for the model ML, ML(OH) and $ML(OH)_2$.[M_T] = 8.01 × 10^{-5} M and [L_T] = 4.029 × 10^{-3} M. ..... …….. 80

Figure 4.20: Observed potential compared to the virtual potential in terms of slope and E^o for Pb-Cyp_2EN system. The experimental conditions are 25°C and ionic strength 0.1 M in $NaNO_3$. [M_T] = 8.01 × 10^{-5} M and [L_T] = 4.029 × 10^{-3}M 81

Figure 4.21: Species distribution diagram for Pb–Cyp_2EN system L_T:M_T ratio 50 studied by DPP at 25°C and ionic strength 0.1 M in $NaNO_3$. [M_T] = 8.01 × 10^{-5} M and [L_T] = 4.029 × 10^{-3} M. 82

Figure 4.22: Complex formation curves for Cu–Cyp_2EN system studied at different ratios by GEP at 25°C and ionic strength 0.1 M in $NaNO_3$. Model M(HL), ML, ML(OH), and $ML(OH)_2$. 87

Figure 4.23: Species distribution diagram for Cu–Cyp_2EN system studied at 25°C and ionic strength 0.1 M in $NaNO_3$. The model used is from the combined refinement and conditions for L_T:M_T ratio 2. [L_T] = 2.668 × 10^{-3} M and [M_T] = 1.337 × 10^{-3} M 88

Figure 4.24: Experimental (points) and calculated (solid lines) complex formation curves for Ni-Cyp_2EN system studied at different ratios by GEP at 25°C and ionic strength 0.1 M in $NaNO_3$. Model M(HL), ML, ML(OH) and $ML(OH)_2$. 91

Figure 4.25: Species distribution diagram for Ni–Cyp_2EN system L_T:M_T ratio 3 at 25°C and ionic strength 0.1 M in $NaNO_3$. $[L_T] = 2.99 \times 10^{-3}$ M, $[M_T] = 1.00 \times 10^{-3}$ M. The model used is from the combined refinement..... 93

Figure 4.26: Experimental (circles) and calculated (solid line) complex formation curves for Zn–Cyp_2EN system studied at 25°C and ionic strength 0.1 M in $NaNO_3$. Model M(HL), ML, ML(OH) and $ML(OH)_2$. 95

Figure 4.27: Species distribution diagram for Zn–Cyp_2EN system studied at 25°C and ionic strength 0.1 M in $NaNO_3$. The values of stability constants used are from the refinement of L_T:M_T ratio 2. $[M_T] = 1.332 \times 10^{-3}$ M and $[L_T] = 2.667 \times 10^{-3}$ M..... 96

Figure 4.28: Behaviour of some of DC–waves recorded for Cd–Cy_2EN system ratio 47 studied at 25°C and ionic strength 0.1 M in $NaNO_3$. $[M_T] = 1.05 \times 10^{-4}$ M and $[L_T] = 4.985 \times 10^{-3}$ M. 97

Figure 4.29: Example showing how DC–waves were fitted for Cd–Cy_2EN ratio 47 system studied at 25°C and ionic strength 0.1 M in $NaNO_3$, $[M_T] = 1.05 \times 10^{-4}$ M and $[L_T] = 4.98 \times 10^{-3}$ M. This wave was recorded at pH 6.2..... 99

Figure 4.30: Example showing the difference in limiting current (ΔI_d) and half wave potential ($\Delta E_{1/2}$) when one tries to estimate the limiting current for one wave. The circles indicate the observed points, the triangle

indicates the estimated one wave, the solid line in red indicates the fitted curve, and the solid line in pink indicates the background current. 100

Figure 4.31: Variation in virtual half–wave potential vs. pH for Cd–Cy_2EN system studied by DC_{tast} at L_T: M_T ratio 47, $[M_T] = 1.05 \times 10^{-4}$ M and $[L_T] = 4.98 \times 10^{-3}$ M, at 25°C and ionic strength 0.1 M in $NaNO_3$ 101

Figure 4.32: Variation in virtual half–wave potential vs. log [L] for Cd–Cy_2EN system studied by DC_{tast} at L_T:M_T ratio 47, initial $[M_T] = 1.05 \times 10^{-3}$ M and $[L_T] = 4.98 \times 10^{-3}$ M, at 25°C and ionic strength 0.1 M in $NaNO_3$. 102

Figure 4.33: Experimental (circles) and calculated (solid line) complex formation curves for Cd–Cy_2EN system ratio 47 studied by DC_{tast}. The experimental conditions are those for Figure 4.32. 104

Figure 4.34: Experimental (points) and calculated (solid line) potentiometric complex formation curves for Cd–Cy_2EN system studied at 25°C and ionic strength 0.1 M in $NaNO_3$. Model M(HL), ML, ML_2, ML(OH) and ML $(OH)_2$. 108

Figure 4.35: Species distribution diagram for Cd–Cy_2EN system studied by potentiometry at 25°C and ionic strength 0.1 M in $NaNO_3$. $[M_T] = 1 \times 10^{-3}$ M and $[L_T] = 3 \times 10^{-3}$ M. Model M(HL), ML, ML_2, ML(OH) and $ML(OH)_2$ from combined refinement. 109

Figure 4.36: Species distribution diagram for Cd–Cy_2EN system studied by potentiometry at 25°C and ionic strength 0.1 M in $NaNO_3$. $[M_T] = 1 \times 10^{-3}$ M and $[L_T] = 3 \times 10^{-3}$ M. Model M(HL), ML, ML_2, ML(OH) and $ML_2(OH)_2$ from combined refinement. 109

Figure 4.37: Species distribution diagram for Cd–Cy_2EN system studied by GEP at 25°C and ionic strength 0.1 M in $NaNO_3$. $[M_T] = 1 \times 10^{-3}$ M and $[L_T] = 3 \times 10^{-3}$ M. Model M(HL), ML, ML_2, ML(OH) and $ML_2(OH)$ from combined refinement 110

Figure 4.38: Complex formation curves using the model from GEP, and polarographic conditions for L_T:M_T ratio 47. $[M_T] = 1.05 \times 10^{-4}$ M and $[L_T] = 4.98 \times 10^{-3}$ M. Circles represent experimental points from DC_{tast} and solid line indicates the fitted curve for the model M(HL), ML, ML_2, ML(OH) and $ML(OH)_2$ from GEP. 112

Figure 4.39: Complex formation curves using the model from GEP, and polarographic conditions for L_T:M_T ratio 47. $[M_T] = 1.05 \times 10^{-4}$ M and $[L_T] = 4.98 \times 10^{-3}$ M. Circles represent experimental points from DC_{tast} and solid line indicates the fitted curve for the model M(HL), ML, ML_2, ML(OH) and $ML_2(OH)_2$ from GEP. 113

Figure 4.40: Complex formation curves using the model from GEP, and polarographic conditions for L_T:M_T ratio 47. $[M_T] = 1.05 \times 10^{-4}$ M and $[L_T] = 4.98 \times 10^{-3}$ M. Circles represent experimental points from DC_{tast} and solid line indicates the fitted curve for the model M(HL), ML, ML_2, ML(OH) and $ML_2(OH)$ from GEP. 113

Figure 4.41: Experimental (points) and fitted (solid lines) potentiometric complex formation curves for Pb–Cy_2EN system studied at 25°C and ionic strength 0.1 M in $NaNO_3$. Model M(HL), ML, ML(OH) and $ML(OH)_2$. 117

Figure 4.42: Species distribution diagram for Pb–Cy_2EN system studied by GEP at 25°C and ionic strength 0.1 M in $NaNO_3$. The model used is

M(HL), ML, ML(OH) and $ML(OH)_2$ from the combined refinement and conditions for L_T:M_T ratio 3. $[M_T] = 1.01 \times 10^{-3}$ M and $[L_T] = 3.00 \times 10^{-3}$ M. 118

Figure 4.43: Behaviour of different waves recorded for Pb–Cy_2EN system L_T:M_T ratio 29 studied by DC_{tast} at 25°C and ionic strength 0.1 M in $NaNO_3$. $[M_T] = 1.017 \times 10^{-4}$ M and $[L_T] = 2.989 \times 10^{-3}$ M. 119

Figure 4.44: Experimental (circles) and calculated (solid line) complex formation curves obtained using the model from potentiometry (MHL, ML, ML(OH) and $ML(OH)_2$) and polarographic conditions. $[M_T] = 1.017 \times 10^{-4}$ M and $[L_T] = 2.989 \times 10^{-3}$ M. 120

Figure 4.45: Experimental (points) and calculated (solid line) potentiometric complex formation curves for Cu–Cy_2EN system studied by GEP at 25°C and ionic strength 0.1 M in $NaNO_3$. The model used is M(HL), ML, ML(OH) and $ML(OH)_2$ from the combined refinement. 123

Figure 4.46: Species distribution diagram for Cu–Cy_2EN system studied by GEP at 25°C and ionic strength 0.1 M in $NaNO_3$. The model used is from the refinement of L_T:M_T ratio 3: ML, ML(OH) and $ML(OH)_2$. $[M_T] = 1.01 \times 10^{-3}$ M and $[L_T] = 2.99 \times 10^{-3}$ M. 124

Figure 4.47: Species distribution diagram for Cu–Cy_2EN system studied by GEP at 25°C and ionic strength 0.1 M in $NaNO_3$. The model used is from the combined refinement and potentiometric conditions for L_T:M_T ratio 3: M(HL), ML, ML_2, ML(OH) and $ML(OH)_2$. $[M_T] = 1.01 \times 10^{-3}$ M and $[L_T] = 3.00 \times 10^{-3}$ M. 125

Figure 4.48: Experimental (points) and calculated (solid lines) complex formation curves for Ni–Cy_2EN system studied by GEP at 25°C and ionic strength 0.1 M in $NaNO_3$. The model used is M(HL), ML, ML_2, ML(OH) and $ML(OH)_2$ from the combined refinement 128

Figure 4.49: Species distribution diagram for Ni–Cy_2EN system studied by GEP at 25°C and ionic strength 0.1 M in $NaNO_3$. The model used is M(HL), ML_2, ML, ML(OH) and $ML(OH)_2$ from the refinement of L_T:M_T ratio 3. $[M_T] = 1.01 \times 10^{-3}$ M and $[L_T] = 2.99 \times 10^{-3}$ M..... 129

Figure 4.50: Experimental (points) and calculated (solid line) complex formation curves for Zn–Cy_2EN system studied by GEP at 25°C and ionic strength 0.1 M in $NaNO_3$. The model used is M(HL), ML, ML_2, ML(OH) and $ML(OH)_2$ from the combined refinement. 132

Figure 4.51: Species distribution diagram for Zn–Cy_2EN system studied by GEP at 25°C and ionic strength 0.1 M in $NaNO_3$. The model used is M(HL), ML_2, ML, ML(OH) and $ML(OH)_2$ from the refinement of L_T:M_T ratio 2. $[M_T] = 1.34 \times 10^{-3}$ M and $[L_T] = 1.67 \times 10^{-3}$ M..... 133

Figure 4.52: Plot of change in complex stability relating to metal ion size when passing from DHEEN to Cyp_2EN. 135

Figure 4.53: Plot of change in complex stability relating to metal ion size when passing from DHEEN to Cy_2EN. 136

Figure 4.54: Plot of change in complex stability relating to metal ion size when passing from Cyp_2EN to Cy_2EN..... 138

List of symbols and abbreviations

HSAB: Hard and Soft Acids and Bases

EDTA: Ethylenediamine tetraacetic acid

TMDTA: Trimethylenediaminetetraacetic acid

ΔH: Enthalpy of formation

ΔS: Entropy of formation

PAS: Para–Amino Salicylic acid

LF: Ligand Field

K_{eq}: Equilibrium constant

Cyp_2EN: N, N'-bis(2-hydroxycyclopentyl)-ethylenediamine

Cy_2EN: N, N'-bis(2-hydroxycyclohexyl)-ethylenediamine

DHEEN: N, N'-2-hydroxyethylenediamine

β_{ML_n} : Thermodynamic overall stability constant for the complex ML_n

$K_1 \ldots K_n$: Stepwise stability or formation constants

$[M_T]$: Metal total concentration

$[L_T]$: Ligand total concentration

[M]: Free metal concentration

[L]: Free ligand concentration

e.m.f.: Electromotive force

GEP: Glass Electrode Potentiometry

CGE: Combination Glass Electrode

GE: Glass electrode

IUPAC: International Union of Pure and Applied Chemistry

L_T:M_T: Ligand to metal ratio

pH: Negative logarithm of the free proton concentration

ESTA: Equilibrium Simulation and Titration Analysis

X_n: Activity of the component *n*

C_j: Activity of the complex *j*

NC: Number of component appearing in complexes

r_{jn}: Stoichiometric coefficient of complex *j* and component *n*

T_i^c : Total concentration for component *i*

T_i^r : Total concentration for each component at each point

C_i^v : Initial vessel concentration for component *i*

C_{im}^B : Burette concentration

v_m : Burette titer volume

V^o : Initial vessel volume

NB: Number of Burettes

E_k^o : Electrode response intercept potential

E_k^{IS} : Electrode selectivity potential

E_k^{LJ} : Liquid junction potential

$\overline{Z}_H$: Proton formation function

H_T: Total hydrogen ion concentration

K_w: Dissociation constant of water

$\overline{Z}_M$: Metal formation function

β_{H_nL} : Overall protonation constant for the ligand H_nL

pA: Negative logarithm of the free ligand concentration

DME: Dropping Mercury Electrode

mV/s: millivolts per second

SCE: Standard Calomel Electrode

µA: Micro-ampere

DCP: Direct current Polarography

I: Current

E: Potential

I_d: limiting diffusion current

n: number of electrons

D: diffusion coefficient

m: Flow rate of mercury

t_d: drop time

C: Concentration of the electroactive species in the bulk solution

DC: Direct current

$E_{1/2}$: Half–wave potential

E^o: Standard redox potential

R: Gas constant (= 8,31 $J.mol^{-1}.K^{-1}$)

T: Temperature

$C_O(O)$: surface concentration of oxidised species

$C_R(O)$: Surface concentration of reduced species

F: Faraday constant (= 96,500 C/ mol)

D_O: Diffusion coefficient of oxidised form

D_R: Diffusion coefficient of reduced form

DPP: Differential Pulse Polarography

E_p: Peak potential

I_p: Peak current

E_M: Half–wave or peak potential of free metal ion

E_C: Half–wave or peak potential of the complexed metal ion

j: Number of ligands in a complex ML_j

$\Delta E_{1/2}$: Difference between the half–wave potential of free metal ion and the half–wave potential of complexed metal ion

I_d(M): Limiting diffusion current of free metal ion

I_d(C): Limiting diffusion current of complexed metal ion

I(C): Current of complexed metal ion

I(M): Current of free metal ion

$\Delta E_p(i)$: Shift in the peak potential at i^{th} pH value

$[M_T](i)$: Metal total concentration at i^{th} pH value

$[M_{Free}](i)$: Free metal ion concentration at i^{th} pH value

$I_p(M_{Comp})(i)$: Height of the DPP peak recorded at i^{th} pH value

$I_p(M_{Free})(i)$: Calculated DPP peak height of the free metal ion, one would be observed at i^{th} pH value if complexes are not formed

ECFC: Experimental Complex Formation Curve

CCFC: Calculated (or Computed) Complex Formation Curve

CFC: Complex Formation Curve

$E(virt)$: Virtual potential

$E_{1/2}(virt)$: Virtual half–wave potential

DET: Dynamic Equivalence point Titration

MET: Monotonic Equivalence point Titration

m_{KHP}: Amount of Potassium Hydrogen Phtalate

M_{KHP}: Molecular mass of Potassium Hydrogen Phtalate

K_{sp}: Solubility product

V_L: Volume of the ligand solution

V_M: Volume of the metal ion solution

$V_{Back.}$: Volume of the background solution

ppt.obs.: Observed precipitation

ppt. pred.: Predicted precipitation

pK_a: protonation constant

I_r: Reduction current

I_b: Background current

X: Applied potential

I_d: Limiting diffusion current

δ: Delta: parameter which is close to 1 for a reversible electrochemical process

$w_{1/2}$: Peak width

VP: Virtual Potentiometry

List of Tables

Table 1.1: Formations constants of complexes of copper (II) with nitrogen donor ligands of differing denticity [5]..... 5

Table 1.2: Thermodynamics of complex formation of EDTA (five–membered chelate ring involving both N–donors) compared with TMDTA (six–membered ring involving both N–donors) 6

Table 1.3: Methods available for determining complex equilibrium Constants 12

Table 3.1: Preparation of samples for different L_T:M_T ratios studied by GEP 45

Table 3.2: Preparation of sample for different L_T:M_T ratios used in polarographic study of Cyp_2EN with Cd^{2+} and Pb^{2+}..... 47

Table 3.3: Preparation of the sample for different L_T:M_T ratios used in polarographic study of Cy_2EN with Cd^{2+} and Pb^{2+}..... 48

Table 4.1: Protonation constants of the ligands Cyp_2EN and Cy_2EN at 25°C and ionic strength 0.1 M in $NaNO_3$ 51

Table 4.2: Protonation constants of some open–chain amines [74]..... 52

Table 4.3: Model and stability constants obtained from GEP for Cd–Cyp_2EN system..... 53

Table 4.4: Model and stability constants obtained for Cd–Cyp_2EN system studied by DC_{tast}, L_T:M_T ratio 200 68

Table 4.5: Model and stability constants obtained for Cd–Cyp_2EN system at 25°C and ionic strength 0.1 M in $NaNO_3$. 69

Table 4.6: Model and stability constants obtained for Pb–Cyp_2EN system studied by GEP at 25°C and ionic strength 0.1 M in $NaNO_3$ 71

Table 4.7: Model obtained for Pb–Cyp_2EN system studied at different ratios by DPP and DC_{tast}. 80

Table 4.8: Stability constants obtained for Pb–Cyp_2EN system using the concept of virtual potentiometry 83

Table 4.9: Final model proposed for Pb-Cyp_2EN system at 25°C and ionic strength 0.1 M in $NaNO_3$ 84

Table 4.10: Proposed model and stability constants for Cu–Cyp_2EN system studied by GEP at 25°C and ionic strength 0.1 M in $NaNO_3$. 86

Table 4.11: Change in acid and base concentrations for Cu–Cyp_2EN system studied by GEP at different L_T:M_T ratios..... 87

Table 4.12: Model and stability constants for Ni–Cyp_2EN system studied by GEP at 25°C and ionic strength 0.1 M in $NaNO_3$ 90

Table 4.13: Change in acid and base concentrations for Ni–Cyp_2EN system at different L_T:M_T ratios..... 91

Table 4.14: Model and stability constants for Zn–Cyp_2EN system studied by GEP at 25°C and ionic strength 0.1 M in $NaNO_3$ 94

Table 4.15: Stability constants obtained from DC_{tast} for Cd–Cy_2EN system L_T:M_T ratio 47 105

Table 4.16: Stability constants for Cd-Cy_2EN system studied by GEP at different L_T:M_T ratios..... 106

Table 4.17: Change in acid and base concentrations for Cd–Cy_2EN system at different L_T:M_T ratios 107

Table 4.18: Proposed model and stability constants for Cd–Cy_2EN system 114

Table 4.19: Model and stability constants for Pb–Cy_2EN system studied by GEP at 25°C and ionic strength 0.1 M in $NaNO_3$. 115

Table 4.20: Change in acid and base concentrations for Pb–Cy_2EN system at different L_T:M_T ratios 116

Table 4.21: Model and stability constants for Cu–Cy_2EN system studied by GEP at different L_T:M_T ratios 122

Table 4.22: Change in acid and base concentrations for Cu–Cy_2EN system at different L_T:M_T ratios 123

Table 4.23: Stability constants of complexes for Ni–Cy_2EN system studied by GEP at 25°C and ionic strength 0.1 M in $NaNO_3$. 127

Table 4.24: Change in acid and base concentrations for Ni–Cy_2EN system studied by GEP at different L_T:M_T ratios 128

Table 4.25: Model and stability constants of complexes for Zn–Cy_2EN system studied by GEP at 25°C and ionic strength 0.1 M in $NaNO_3$ 131

Table 4.26: Change in acid and base concentrations for Ni–Cy_2EN system at different L_T:M_T ratios 131

Table 4.27: Formation constants of ML complexes for Cyp_2EN and DHEEN showing the effect of cyclopentyl bridges on complex stability in relation to metal ion size. 135

Table 4.28: Formation constants of ML complexes for Cy_2EN and DHEEN showing the effect of cyclohexyl bridges on complex stability in relation to metal ion size. 137

Table 4.29: Formation constants of ML complexes for Cyp_2EN and Cy_2EN showing the effect of changing the cyclopentyl to cyclohexenyl bridges on complex stability in relation to metal ion size 137

Chapter 1: Introduction

1.1. Concept of metal complex in aqueous solution

1.1.1. Overview of metal complexes

The metal complexes are compounds containing a central atom or ion, which is usually a metal but may be any electron acceptor, and which is surrounded by several electron donor groups that are generally referred to as *ligands*. The complex which may be either charged or neutral tends to retain its identity even in solution, although of course both dissociation and replacement of the original ligands may occur [1]. The theory of hard and soft acids and bases (HSAB) [2] has been used to identify appropriate ligands donors. Hard acids (i.e. Na^{+}, Mg^{2+}, Ca^{2+}, Al^{3+}) or bases (i.e. OH^{-}, NO_3^{-}, SO_4^{2-}) are normally small, highly charged atoms that have electron distributions that are not easily polarised. Soft acids (i.e. Hg^{2+}, Pb^{2+}, Cd^{2+}) and bases ($S_2O_3^{2-}$, CN^{-}, C_2H_4) tend to be lower charged, are larger and have much more diffuse and polarisable electronic distributions. Generally, hard metal ions (acids) form stable complexes preferentially with hard donors [3]. In all cases the properties of the solvent must be considered. In aqueous solution the aquo–complexes are formed. In the presence of a second ligand, the stepwise substitution of the ligand molecules for the co-ordinated water molecules occurs. If this second ligand is also a neutral molecule, the charge of the successive complexes is the same as that of the central ion. For example, increasing the concentration of ammonia in the solution of cobalt (II) perchlorate causes the following reactions to take place:

$$Co(H_2O)_6^{2+} + NH_3 \rightleftharpoons Co(H_2O)_5NH_3^{2+} + H_2O$$

$$Co(H_2O)_5NH_3^{2+} + NH_3 \rightleftharpoons Co(H_2O)_4(NH_3)_2^{2+} + H_2O$$

And the last equilibrium is:

$Co(H_2O)(NH_3)_5^{2+} + NH_3 \rightleftharpoons Co(NH_3)_6^{2+} + H_2O$

The intermediate species Co $(H_2O)_n(NH_3)_{(6-n)}^{2+}$ where n=1, 2, 3, 4, 5 are in fact mixed ligand complexes [4].

1.1.2. Types of complex equilibria in solution

Considering the charge and size of the metal ions, it is obvious that in solution they cannot exist freely, but they are associated with the counter ion(s) or other components of the solution having no-bonding electron pair(s) [4]. In aqueous solution, the counter ions are the molecules of water itself. When a ligand bonds covalently to a metal, the resulting complex is sometimes referred to as an *inner–sphere complex*. In inner sphere complex, ligands replace water molecules from the inner coordination sphere, and form bonds directly to the metal ion. In this instance the ligand occupies a clearly defined site within the coordination shell of the metal. An *outer–sphere complex* is formed when an inner-sphere complex is weakly linked through electrostatic, Van der Waals' or hydrogen-bonding to further groups. In general these groups do not occupy specific sites around the metal [1, 5]. Outer–sphere complexes are important in the kinetics of complex formation since all complex–formation processes appear to involve initial formation of an outer–sphere complex, followed by entry of the ligand into the inner–sphere [6]. The Figure 1.1 taken from [5] shows the example of inner and outer sphere of Ni (II) with water and sulphate.

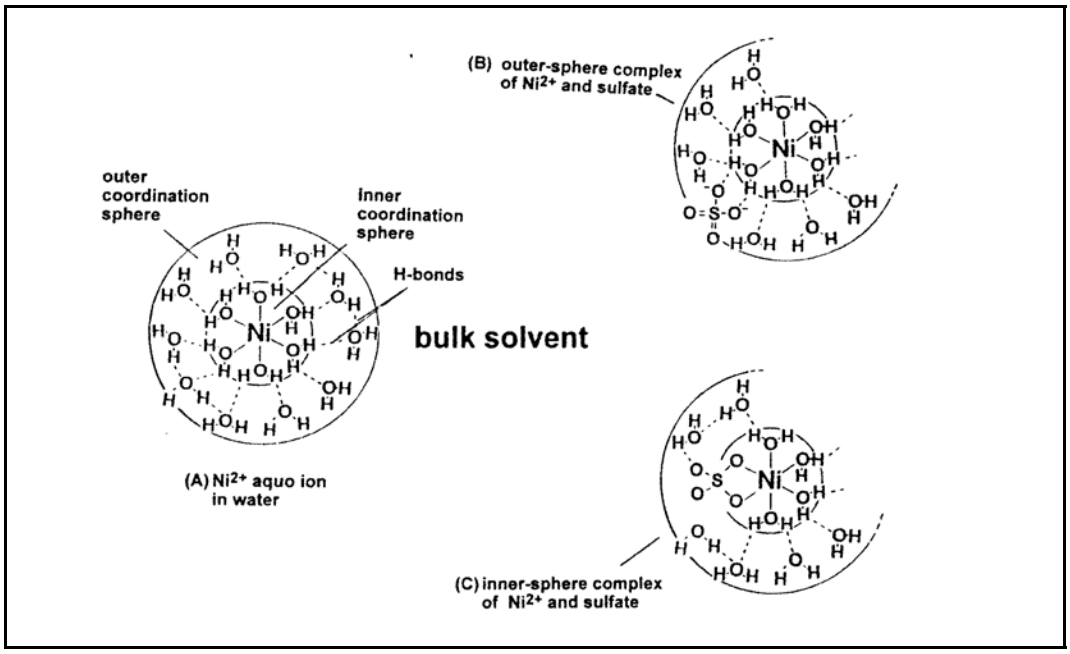

Figure 1.1: Diagrammatic representation of a metal ion Ni (II), in water, showing its inner and outer sphere of coordinated water (A), the formation of an outer–sphere complex with sulphate (B), and an inner–sphere complex with sulphate where the sulphate ligand is directly bonded to the Ni^{2+} ion (C) [5].

If the ligand is an anion, then during stepwise complex formation, the positive charge of the metal ion is gradually neutralized, and often happens that an overcompensation of the charge of the central ion occurs and complex anions are formed [4]:

$$Al^{3+}+F^{-} \rightleftharpoons AlF^{2+}$$

$$AlF^{2+}+F^{-} \rightleftharpoons AlF_2^{+}$$

$$AlF_5^{3+}+F^{-} \rightleftharpoons AlF_6^{3-}$$

If the ligand has more than one donor atom bridged, the resulting complex is said to be a *chelate complex* and the process is called *chelation* [7]. If the ligand is a cyclic molecule with three or more potential donor atoms in a ring, it is termed *macrocyclic ligand*. The complexes formed with this kind of ligand are more stable

than chelating ligands [8]. There is also a possibility for the formation of the *protonated complexes*. For example; the protonation of the complexes of multidentate ligands may take place according to the following reaction [4].

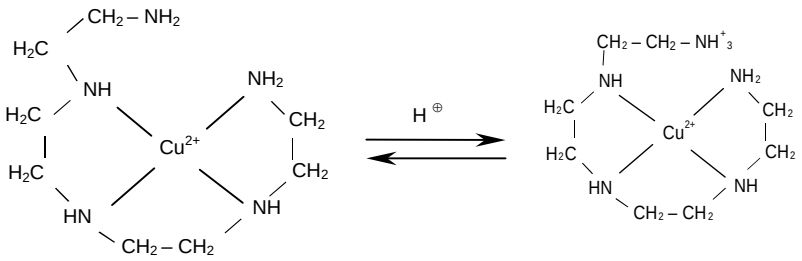

If the central atoms are more than one, the resulting complexes is said to be *polynuclear*. The polynuclear complexes may be *homo- or heteropolynuclear* depending on whether the metal centres are the same or different [4].

Ligands can also be classified according to their level of preorganisation, that is, how nearly the free ligands are arranged as required in the final complex. The order of level increases with the order of stability of complexes formed by these ligands. This can be presented as follow: *unidentate ligands* < *chelating ligands* < *macrocyclic ligands* < *cryptand ligands* [9].

1. 2. Chelating complexes

Chelate complexes are of particular importance because of their generally greater stability than the complexes of the corresponding unidentate ligands. This greater stability, known as the *chelate effect* gives rise to their widespread applications. The word *denticity* is used to describe how many donor groups the chelating agent has available for metal ion bindings; thus unidentate ligands only have one donor

group available, whereas polydentate have many [1]. Table 1.1 illustrates the effect of introducing chelate ring in ammonia molecule.

Table 1.1: Formations constants of complexes of copper (II) with nitrogen donor ligands of differing denticity [5].

Ligand	ammonia	ethylenediamine	triethylenetetramine
Denticity	1	2	4
Log β	$\log \beta_4 = 13.0$	$\log \beta_2 = 19.6$	$\log \beta_1 = 20.1$

1.2.1. Chelate effect

In general, polydentate ligands form more stable complexes than unidentate ligands. The chelate effect is associated with the improved stability of metal complexes containing chelate rings compared to the stability of similar complexes that contain none or fewer rings [10]. The chelate effect may be counteracted by adverse energy changes due to necessary conformational variations during complex formation, especially when strained rings are formed [1]. In order to determine the origin of the chelate effect, the concept of entropy and enthalpy must be considered. The enthalpy effects are related to many parameters: the variations of bonds with the donor or acceptor abilities of the ligand and the metal ion, the ligand field's effect, the steric and electrostatic repulsion between ligand and donor group in the complex, the conformation of the free ligand and the coulombic forces involved in chelating ring formation. The entropy effects are related to the number, size, and arrangement of chelate rings, but also to the difference in configurational entropy between free and coordinated ligand [1]. Schwarzenbach explained the chelate effect in terms of the first atom had attached

itself to the metal ion, the second and subsequent donor atom could move only in a restricted volume about the metal ion [11]. This effect meant that the entropy of these subsequent donor atoms was greatly reduced as compared with an equal number of unidentate ligand. The Schwarzenbach's model predicted that the stability of complexes with larger chelate rings would be of lower complex stability than those with small chelate rings, because of the larger volume to which the chelate ring would be restricted when coordinated to the metal ion by only one donor atom. This seems to be true in general, but it was observed that the decrease in formation constants that occurs as chelate ring size is increased should be an entropy effect, whereas, at least for chelating size less than seven, the enthalpy effect is predominant [5, 12]. Table 1.2 illustrates an example of thermodynamics of complex formation of EDTA (five–membered chelate ring) compared with TMDTA (six–membered) [5, 12].

Table 1.2: Thermodynamics of complex formation of EDTA (five–membered chelate ring involving both N–donors) compared with TMDTA (six–membered ring involving both N–donors) [6, 12]

		EDTA			**TMDTA**		
Metal Ion	**Ionic Radius (Å)**[b]	**log K_1**	**ΔH** [a]	**ΔS** [a]	**log K_1**	**ΔH** [a]	**ΔS** [a]
Cu^{2+}	0.57	18.70	– 8.2	58	18.82	– 7.7	60
Ni^{2+}	0.69	18.52	– 7.6	59	18.07	– 6.7	60
Zn^{2+}	0.74	16.44	– 4.9	59	15.23	– 2.3	62
Cd^{2+}	0.95	16.36	– 9.1	44	13.83	– 5.4	45
Ca^{2+}	1.00	10.61	– 6.6	26	7.26	– 1.7	27
La^{3+}	1.03	15.46	– 2.9	61	11.28	+ 3.8	64
Pb^{2+}	1.18	17.88	– 13.2	38	13.70	– 6.4	41

[a] units for ΔH and ΔS are $kcal.mol^{-1}$ and $cal.deg^{-1}.mol^{-1}$, respectively, and data are from [13]
[b] data are from [14]

1.2.2. Use of chelates in medicine

Treatments of metal intoxication and clinical diagnosis with imaging agents are two areas where chelating agents are already in use [15]. There are a number of fields that currently require specific ligand design for selective metal complexation. These fields encompass the design of ligands for treatment of metal intoxication [16], the need of complexes to act as agents in the body and the selective extraction of precious metals in hydrometallurgy. Much attention is currently being given to the field of nuclear medicine and the design of radiopharmaceuticals. These radiopharmaceuticals have a diagnostic and/or therapeutic application and the radionuclides used are invariably metals [10]. Most generally, all chelators are considered to be removers of heavy metal toxicity. The ability of EDTA and its derivatives to form stable complexes with several metal ions allows their use as probes in various areas in chemistry, biology and medicine. Complexation of radioactive metals with EDTA reagents has found extensive utility in medicine [17]. EDTA is the most common chelator that has been used to also reverse the effect of arterial plaque, thus preventing further strokes and/or heart attacks [18]. A variety of insulin–mimetic organic chelates of VO^{2+} have been investigated as potential therapeutic agents for treatment of diabetes [19]. Metal chelates of P–amino salicylic acid (PAS) with Cu(II), Ni(II), Co(II), Fe(II), Mn(II), and Zn(II) have been screened for antifungal activities against a series of pathogenic and non–pathogenic fungi. The chelates in comparison to PAS were found to possess remarkable antifungal potential [20].

1.3. Effect of oxygen and nitrogen donor atoms in ligand design

The classification of acids and bases into hard and soft (HSAB) by Pearson [2] is a useful starting point for donor atom selection in ligands design. The HSAB classification may provide a preliminary guide for donor atom selection, but in fact, for effective ligand design, a much more detailed consideration of each type of donor atom is needed [15]. Due to the fact that the ligands studied in this work contain oxygen and nitrogen as donor atoms, only these donor groups are considered in this section.

1.3.1. Neutral and negatively charged oxygen donor atom

The neutral oxygen donor has become of great interest because it is the donor atom of the most common solvent (water) and secondary because it is a donor atom in the crown ethers and cryptands [21]. The examination of a large amount of data reveals that *the addition of groups containing neutral oxygen donor atoms to an existing ligand leads to an increase in selectivity of the ligand for large over small metal ions* [22–25]. This rule may be expressed graphically as seen in Figure 1.2 (taken from [5]) where the change in complex stability ($\Delta \log K$) is plotted as a function of metal ion radius on addition of neutral oxygen group to a variety of ligands. The origin of the preference of neutral oxygen donors for large metal ion is from the fact that all crown ethers and cryptands form exclusively five–membered chelate rings on complex formation. This is important in relation to a further rule of ligand design which states that *the increase of chelate ring size from five–membered to six–membered will favour ligand selectivity for small over large metal ion* [26, 27]. The presence of five membered

chelating rings will promote selectivity for large metal ions. This selectivity is derived from purely geometric arguments [28].

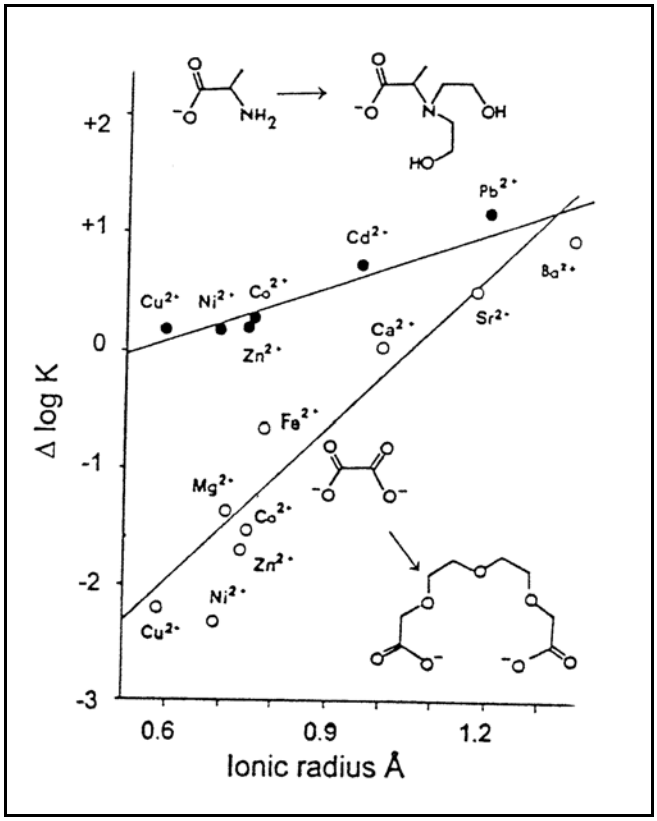

Figure 1.2: The effect of neutral oxygen donor atom on complex stability. Relationship between the change in complex stability, $\Delta\log K$, that occurs on adding 2–hydroxyethyl groups to alanine (•) or ethereal oxygens to oxalate (o), and the ionic radius of the metal ion. Ionic radii are from [5] and are for octahedral coordination, except for Cu(II) which is square planar. Formation constants are from [13].

The negatively charged oxygen donor occurs in the form of the carboxylate, the phenolate, the hydroxamic acid and the phosphoric acid groups as well as in ligands such as acetylacetonate and tropolonate. The effect of the negatively charged oxygen donor on complex stability appears to depend on the acidity (affinity of the metal ion for the OH^- ion) of the metal ion considered [5, 12]. This is observed in Figure 1.3 where the log K_1 of ligands containing

negatively charged RO^- is plotted against log $K_1(OH^-)$ for each metal ion (taken from [12]).

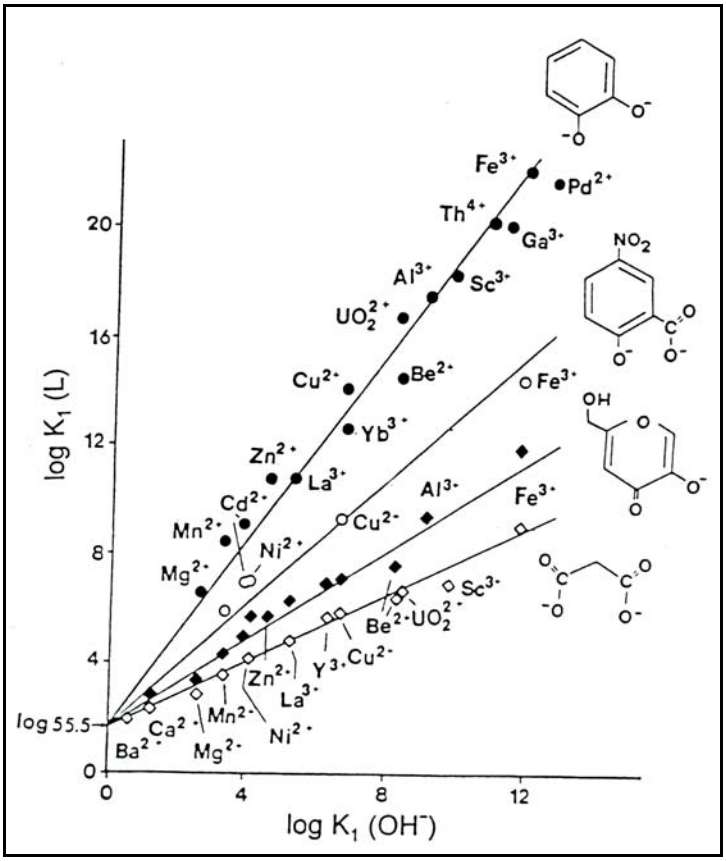

Figure 1.3: Relationship between log K_1 for chelating ligands containing negatively charged oxygen donors groups and log K_1 for the formation of the hydroxide complex, for a variety of metal ions. The ligands shown are catechol (•), 5–nitrosalicylic acid (o), kojate (▪) and malonate (□). Formation constants at ionic strength zero and 25°C are from [13]. The intercept at log 55.5 is expected from theories of chelate effect from [29] and [30].

The selectivity of the ligand for a more acidic metal ion (e.g. Fe^{3+}, Al^{3+}) over a less acidic metal ion (e.g., Zn^{2+}, Cu^{2+}) will be increased by an increase in the number and basicity of the charged oxygen groups. Steric effects usually lead to a drop in complex stability of smaller metal ions such as Be^{2+} [12].

1.3.2. Neutral saturated nitrogen donor

The neutral saturated nitrogen donor displays stronger coordinating properties with many metal ions than does neutral oxygen donor. The order of basicity toward metal ions is $NH_3 < RNH_2 < R_2NH < R_3N$ in the gas phase [31]. In water, the steric hindrance between the added alkyl groups and waters of salvation leads to a decrease in complex stability along this series [32]. The addition of N-alkyl groups result in increased steric strain that is accompanied by significant decreases in complex stability and ligand field (LF) strength. The LF strength is a measure of the overlap in the M–L bonds, which is decreased with increasing M–L bond lengths due to the steric crowding caused by N alkyl groups [33].

1.4. Measurement and Application of Stability Constants

1.4.1. Measurement of stability constants

Wherever metal ions and ligands are present, equilibria between them will be established. Equilibrium constants are then fundamental to understand the behaviour of metal ions in aqueous solution and the stability of complexes that may form. The development of the measurement of stability constants and their use paralleled the development of the instrumentation for their measurement [5]. The stability constant is a quotient consisting of the products of the activities of the products of the reaction raised to the appropriate power divided by the products of the reactants also raised to the appropriate power in accordance with the following reaction and equation:

$$aA + bB \rightleftharpoons cC + dD, \qquad K_{eq} = \frac{a_C^c . a_D^d}{a_A^a . a_B^b} \qquad (1)$$

However, because concentrations closely parallel activities under controlled conditions involving both temperature and ionic strength, it is the practice to determine equilibrium concentration constants in place of activity constants. The equilibrium concentration constant would then be represented by the following equation:

$$K'_{eq} = \frac{[C]^c [D]^d}{[A]^a [B]^b} \qquad (2)$$

The use of concentration in Equation 2 has an advantage: the concentration of the species involved can be substituted directly into the mass balance equations used in solving the equations for the equilibrium constant of formation constant of the metal ion complexes that are formed in solution [34]. In general, any method can be used for measuring equilibrium constant or complex equilibria if it can measure the concentration of at least one of the species in equilibrium in which a metal complex is formed. The concentration of that species plus stoichiometry of the solution provides the information necessary to calculate the concentrations of all species present at the equilibrium. Table 1.3 below shows the methods used in the determination of stability constants.

Table 1.3: Methods available for determining complex equilibrium constants [5]

Standards Methods

- Potentiometry
- Spectrophotometry
- Specific metal ion electrodes
- Nuclear magnetic resonance spectroscopy
- Polarography
- Ion exchange
- Colorimetry

Ionic conductivity

Distribution between two phases

Reaction kinetics

Partial pressure measurement

Solubility measurements

Competition Methods for Strong Complexes

Ligand-ligand competition measured potentiometrically

Ligand-ligand competition measured spectrophotometrically

Metal-metal competition measured spectrophotometrically

Metal-metal competition measured polarographically

Amphoteric Metal ion

1.4.2. Applications of stability constants

Stability constants are fundamental for understanding the behaviour of metal ions in aqueous solution. Such understanding is important in wide variety of areas such as metal ions in biology, biomedical applications, metal ions in the environment, pollution, analytical chemistry, geochemistry, food chemistry, extraction metallurgy and photography [5]. Both plants and animals contain significant quantities of both metal ions and ligands. Some of the essential metal ions are Na, K, Mg, Ca, Fe, Cu, Zn, etc. These metal ions can interact with different ligands found in human serum, such as H_2O, OH^-, Cl^-, HCO_3^-, SO_4^{2-}, F^-, Br^-, I^-, proteins, carbohydrates and carboxylic acids, nucleic acids, lipids and steroids [1]. During the 1950s it was discovered that a number of metal chelates were active anti-viral agents. Chelating agents have found use as antibiotics on the basis of their specificity of complex formation with metal ions [35]. Stability constants of complexes also have an important role in the design of drugs for alleviation of metal poisoning [8]. The formation of complexes in solution is widely used in analytical chemistry in such areas as complexometric titrations, metal-ion

indicators, colorimetric analysis, precipitants and reagents for extracting specific metal ions from solution [1].

1.4. Aim of the research

The aim of this work is the use of electrochemical techniques, such as glass electrode potentiometry (GEP), polarography (DPP and DC_{tast}) and virtual potentiometry (VP), in the modelling of complexation of metal ions with some ligands newly synthesised. This modelling will be a useful tool in designing ligands for selective complexation of metal ions in variety of situations ranging for different applications. The metal ions used in this work are Cd(II), Cu(II), Ni(II), Pb(II) and Zn(II). The ligands newly synthesised are N,N'-bis(2-hydroxycyclopentyl)-ethylenediamine (Cyp_2EN) and N,N'-bis(2-hydroxycyclohexyl)–ethylenediamine (Cy_2EN). Their structures are as follows:

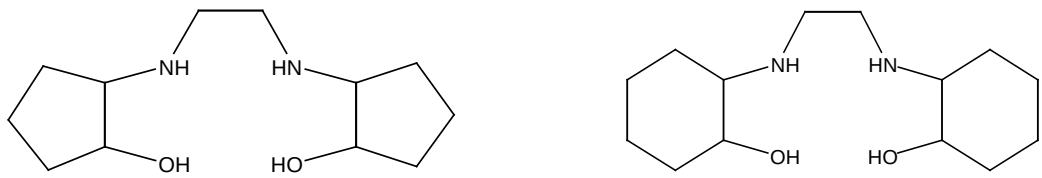

Cyp_2EN **Cy_2EN**

Figure 1.4: Structure of the ligands studied in this work

Chapter 2: Theory and data treatment

2.1. Glass Electrode Potentiometry

2.1.1. Prediction of Stability constant by potentiometry

The formation of metal complexes in solution with a particular ligand must occur via the successive replacement of hydrate molecules [36]. A complexation reaction between a metal ion M, and a ligand, L, whereby the maximum coordination number *n* is developed, may be written as:

$M(H_2O)_n + nL \rightleftharpoons ML_n + nH_2O$

assuming that the ligand is monodentate and no binuclear complex formation occurs. The thermodynamic overall stability constant, β_{ML_n} of the species ML_n is defined by

$$\beta_{ML_n} = \frac{[ML_n]}{[M][L]^n} \qquad (3)$$

Since such complexing processes are regarded as occurring by a series of stages it is possible to write series of n equilibrium expressions for bonding overall stability constants.

$M + L \rightleftharpoons ML,$ $\qquad \beta_1 = [ML]/[M][L]$ (4)

$M + 2L \rightleftharpoons ML_2$ $\qquad \beta_2 = [ML_2]/[M][L]^2$ (5)

$M + 3L \rightleftharpoons ML_3$ $\qquad \beta_3 = [ML_3]/[M][L]^3$ (6)

:

$M + nL \rightleftharpoons ML_n$ $\qquad \beta_n = [ML_n]/[M][L]^n$ (7)

Each of the above equilibrium refers to the overall formation reaction in one stage of each complex species. It is also possible to express the formation reaction in

terms of constants referring especially to the addition of ligand in a stepwise manner in the following way:

$M + L \rightleftharpoons ML$, $K_1 = [ML]/[M][L]$ (8)

$ML + L \rightleftharpoons ML_2$ $K_2 = [ML_2]/[ML][L]$ (9)

$ML_2 + L \rightleftharpoons ML_3$ $K_3 = [ML_3]/[ML_2][L]$ (10)

:

$ML_{n-1} + L \rightleftharpoons ML_n$ $K_n = [ML_n]/[ML_{n-1}][L]$ (11)

The constants $K_1 \ldots K_n$ are known as the stepwise stability or formation constants. It is evident that a relationship exists between the step and overall constants [1].

$$\beta_n = K_1 \times K_2 \ldots \times K_n \quad (12)$$

If the total concentrations of metal ion and ligand are $[M_T]$ and $[L_T]$, the average number of ligands bound to each metal ion is given by

$$\bar{n} = \frac{[L_T]-[L]}{[M_T]} = \frac{[ML]+2[ML_2]+\mathrm{K}\ n[ML_n]}{[M]+[ML]+[ML_2]\mathrm{K}\ [ML_n]} \quad (13)$$

$$= \frac{\beta_1[L]+2\beta_2[L]^2+\mathrm{K}\ n\beta_n[L]^2}{1+\beta_1[L]+\beta_2[L]^2+\mathrm{K}\ \beta_n[L]^n} \quad (14)$$

where $[L]$ is the free ligand concentration. $[L]$ can be measured and the function $\bar{n}$ may be solved for the stability constants β_n [37].

2.1.2. Generalities on glass electrode potentiometry (GEP)

Potentiometric measurements involve the measurement of e.m.f. between a sensing and a reference electrode. The reference electrode is most often a calomel or

Ag/AgCl electrode. Actually, the most used type of pH-electrode is the combination glass electrode (CGE), which incorporates both glass and reference electrode in one body. A line diagram [38] of this cell can be written as follows:

Glass membrane selectively binds H^+

$$\underbrace{\text{Ag}\,(s)\,|\,\text{AgCl}\,(s)\,|\,\text{Cl}^-(aq)}_{\text{Outer reference electrode}}\;\underbrace{\|\,\text{H}^+\,(aq,\text{ outside})}_{\substack{\text{H}^+\text{ outside glass}\\ \text{Electrode}\\ \text{(analyte solution)}}}\;\Big|\;\underbrace{\text{H}^+\,(aq,\text{ inside})}_{\substack{\text{H}^+\text{ inside}\\ \text{glass electrode}}}\;\underbrace{\|\,\text{Cl}^-(aq)\,|\,\text{AgCl}\,(s)\,|\,\text{Ag}\,(s)}_{\substack{\text{Inner reference}\\ \text{electrode}}}$$

The two reference electrodes (outer and inner) measure the electric potential difference across the glass membrane. The salt bridge is the porous plug at the bottom of the combination electrode [38]. The GE is the most widely used indicator electrode for pH determinations used in the laboratory. It operates on the principle that the potential difference between the surface of a glass membrane and a solution is a linear function of pH [39]. Since GE measures hydrogen ion concentration relative to their reference half-cells; they must be calibrated periodically to ensure accurate, reproducible measurements. Calibration is normally carried out by having a series of solutions of known ionic composition and measuring the response of the electrode [1]. The calibration of GE in terms of hydrogen ion concentration may be performed following IUPAC recommendations which are based on the use of designated buffer solutions. An alternative procedure is to perform a titration of strong acid with strong base as a source of solutions with known hydrogen ion concentration. Figure 2.1 shows an example of the calibration curve of GEP using acid-base titration. The GE must be calibrated because its standard potential and the response slope vary with the age

and the pre-treatment of the electrode. The calibration must be performed frequently, usually before each individual titration [40].

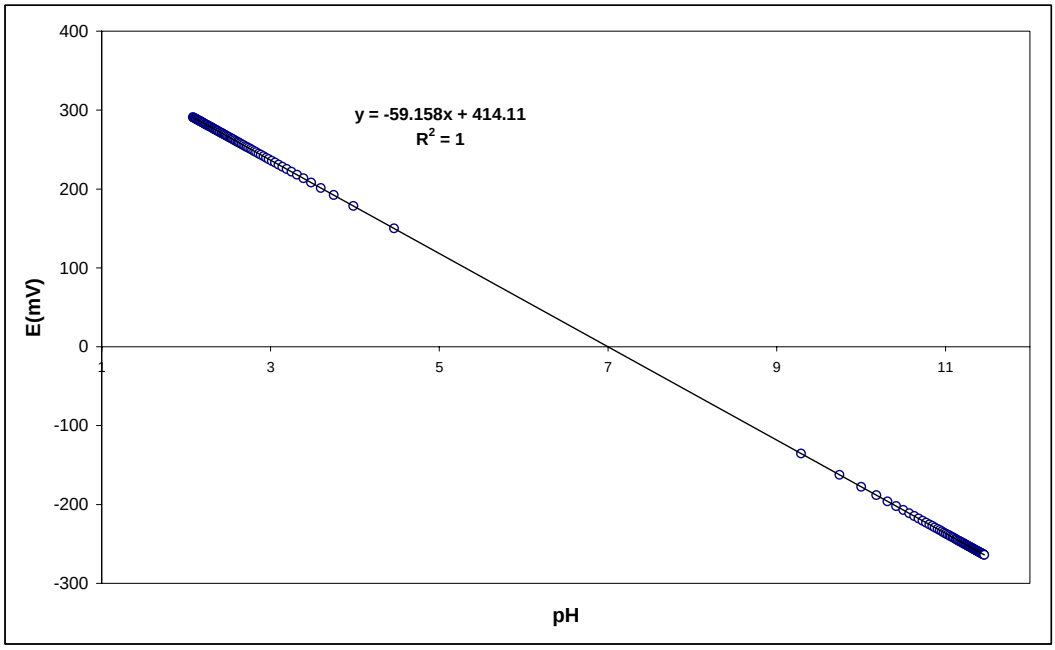

Figure 2.1: Calibration curve of GE performed by titration of 15 ml of 0.01 M HNO_3 with 0.02 M NaOH

2.1.3. Use of GEP in the determination of stability constants

In glass electrode potentiometric speciation study, one measures the activity of a hydrogen ion in the solution, the variation in the proton activity is characteristic for a particular metal–ligand model studied at a particular and fixed L_T:M_T ratio [41]. Potentiometry is well established and most frequently used in speciation studies. Over 80 % of the stability constants reported in the literature are from this technique. Potentiometric measurements were first used for the measurement of stability constants by Arrhenius, Ostwald and Nernst who provided the basis for the introduction of electrodes responding reversibly and selectively to only one species present in solution. Only ligands which were not

protonated could be measured. Also determinations were limited to metal ions for which metal electrodes were characterized by potentials which responded reversibly to the concentrations of their cations [5]. Subsequently work on the glass electrode (which is very sensitive to the hydrogen ion activity or concentration) and appropriate potentiometric apparatus for the measurement of hydrogen ion with considerable accuracy were developed [42].

When stability constants are determined from pH data the experiment can be carried out in one of two ways. The change of pH can be measured as a function of the ligand concentration [43]. Alternatively the pH can be measured as a function of the concentration of acid, or alkali, added to a constant total metal and total ligand concentration [37]. Another approach, with limited applications, concerns the study of weak complexes by carboxylate ligands. This involves treating a metal solution with a buffer mixture containing H_nL and its sodium salt [1]. Although pH measurement has been widely used to determine stability constants, there are a number of limitations to the method. The major limitation in the use of potentiometry is the essential requirement that a suitable electrode exists. Electrodes develop potentials that are dependent on the activities of the species present. These potentials originate from two main types of phenomena, namely oxidation-reduction equilibria and the formation of ionic concentration gradients across membranes. As a result of the occurrence of complex formation processes in solutions, the total (analytical) and free (equilibrium) concentrations of the components involved in the equilibrium are different [1]. GEP also cannot be used under conditions of extreme pH. The pH range is usually limited to 2-12, because below pH 2 and above pH 12, the liquid junction potential change and thus exert an

appreciable influence on the measured value [5]. The GEP method is inapplicable at very low total metal concentrations because under these conditions [M_T] is close to zero and the response of GE is not accurate. It is also inapplicable for very stable complexes such as those formed by some transition metal ions with EDTA [1] because the protons are unable to compete effectively with such metal ions for the ligand. Such complexes may, however, be studied by replacing the proton with another metal ion that can compete effectively with the metal ion under test and be detected potentiometrically or by some other method. Since aqueous solutions always contain hydroxide ions and most metal ions form not only hydroxo-species but also polynuclear species, care must be taken either to work in sufficiently acidic solutions that hydroxo-complex formation is negligible or to take it into account during the analysis of the data [1]. As stability constants and measured potential are temperature dependent, it is extremely important to control the temperature to at least ± 0.1°C.

2.1.4. Analysis of potentiometric data

a. Description of ESTA program

The program ESTA (Equilibrium Simulation and Titration Analysis) was used in the refinement of potentiometric data. ESTA is a computer program library that performs calculations concerned with competitive aqueous solution equilibria. This program can take into account variations in ionic strength and the associated changes in activity coefficients. The major objective is to provide a flexible tool for investigating phenomena associated with chemical interactions in solution and for their quantitative characterisation [44].

The ESTA library contains different program modules (ESTA0, ESTA1, ESTA2, ESTA3, ESTA4, ESTA5, ESTA6, ESTA7 and ESTA8), but the calculations are performed by two main modules [45, 46]:

i. Simulation module (ESTA1)

ESTA1 produces results on a point by point basis. By setting up and solving the mass–balance equations (Equation 15), ESTA1 can determine a single value for almost any of the parameters which characterize a titration.

$$\{C_j\} = \beta_j \prod_{n=1}^{NC} \{X_n\}^{r_{jn}} \tag{15}$$

where $\{C_j\}$ is the activity of the complex, $\{X_n\}$ is the activity of the component, NC is a number of components appearing in complexes, and r_{jn} is a stoichiometric coefficient of complex j and component n.

The activity of a complex $\{C_j\}$ is related to the activity of the component, $\{X_n\}$, from which it is formed by its formation constant, β_j.

Equation 15 can be rewritten in terms of the concentrations and activity coefficients γ in the following way:

$$\gamma_j [C_j] = \beta_j \prod_{n=1}^{NC} (\gamma_n [X_n])^{r_{jn}} \tag{16}$$

or

$$[C_j] = \Gamma_j \beta_j \prod_{n=1}^{NC} [X_n]^{r_{jn}} \tag{17}$$

where

$$\Gamma_j = \left(\prod_{n=1}^{NC} \gamma_n^{r_{jn}} \right) / \gamma_j \tag{18}$$

For each component, the total concentration, summed over the free concentration and all NJ complexes, is

$$T_i^c = [X_i] + \sum_{j=1}^{NJ} r_{ji} [C_j] \tag{19}$$

In the context of titrations, the real total concentration of each component at each point is given by:

$$T_i^r = \frac{C_i^v . V^o + \sum_{m=1}^{NB} C_{im}^B . v_m}{V^o + \sum_{m=1}^{NB} v_m} \tag{20}$$

where C_i^v represents the initial vessel concentration for component *i*, C_{im}^B represents the burette concentration, v_m represents the burette titer volume, V^o represents initial vessel volume, and *NB* represents the number of burettes. For speciation calculations, given NC real total concentration T_i^r from the experiment, one can solve for NC free concentrations by putting $T_i^r = T_i^c$.

In potentiometric titrations, the free concentration is known and is obtained from an experimentally determined e.m.f. ESTA relates this e.m.f to the activity of the electrode ion as follows:

$$E_k = E_k^o + E_k^{IS} + E_k^{LJ}, \tag{21}$$

where k = 1, 2, 3…, E_k^o is the electrode response intercept, E_k^{IS} is the electrode selectivity and E_k^{LJ} is the liquid junction potential.

ii. Optimisation module (ESTA2)

ESTA2 is used when it is desired to determine, for one or more parameters, the best values, based on least squares procedure applied to a whole system of titrations. The following parameters can be refined: formation constants, vessel and burette concentrations, electrode intercept, electrode slope and initial vessel volume. The total number of titrations is dimensioned to 20 and the total number of points to 1000 but these can be varied if necessary. A file of titration data containing the optimized parameter values and with a format identical to ESTA can be generated as an output [47].

b. The protonation formation function

The protonation formation function is defined as

$$\overline{Z}_H = \frac{H_T - H + OH}{L_T} \tag{22}$$

where H_T is the total hydrogen ion concentration and $OH = K_w/H$ (23)

The proton formation function $\overline{Z}_H$ is plotted against $pH = -\log [H]$. This equation is used to evaluate both the observed and calculated functions E_k^{obs} and E_k^{calc}.

In the absence of the metal, the proton formation function becomes

$$\overline{Z}_H = \frac{[boundH]}{L_T} \tag{24}$$

where $[boundH]$ is given as

$$[boundH] = H_T - H + [OH] = H_T - H + K_w H^{-1} \tag{25}$$

where OH is the hydroxide ion, and K_w is the dissociation constant of water, then

$$\overline{Z}_H = \frac{\left(H_T - H + K_w H^{-1}\right)}{L_T} \tag{26}$$

where H_T and L_T are known from the analytically determined concentrations and K_w is a known value from the literature. Since H is measured by glass electrode, $\overline{Z}_H$ can be calculated at a number of pH values. It will then be possible for the protonation curve to be plotted, i.e., $\overline{Z}_H$ vs. pH. Such curve helps in giving valuable information about the state of the ligand at a particular pH range [46, 47]. For this study, $\overline{Z}_H$ was used in the determination of protonation constants of ligands and in the prediction of stability constants for different complexes present in a solution.

c. The metal formation function $\overline{Z}_M$

The metal formation function is defined as the average number of ligand bound to the metal.

$$\overline{Z}_M = \frac{L_T - A(1 + \sum_n \beta_{H_n L} H^n)}{M_T} \tag{27}$$

where n is the number of protons, L_T and M_T are the total ligand and metal concentrations, respectively, and $\beta_{H_n L}$ is the overall protonation constant for the ligand $H_n L$.

A is defined as

$$A = \frac{(H_T - H + OH)}{(\sum_n n\beta_{H_n L} H^n)}. \tag{28}$$

where H_T and H are total and free proton concentrations, respectively. OH represents hydroxide concentration.

In this study, $\overline{Z}_M$ was used in the modelling of M–L systems and in the refinement of computed stability constants. $\overline{Z}_M$ is plotted against pA, where pA is the negative logarithm of the free ligand concentration. A number of titrations with different ligand to metal ratios are usually performed by starting at low and ending at high pH or vice versa.

After the completion of the model, the calculated β values from Equation 27 are used in the calculation of protons. The validity of the model is checked by the comparison of the resulting calculated formation and the experimental curves. The functions $\overline{Z}_H$ and $\overline{Z}_M$ were used here to analyse the data and they shown that they were valuable, but they should be taken as only a mathematical transformation of the data.

2.2. Polarography

2.2.1. General introduction

Polarography is a dynamic electrochemical technique which makes use of current-voltage relationship under conditions of concentration polarisation of an indicator electrode [48]. Basically, polarography consists of electrolysing a solution of the type described, between a dropping mercury electrode (DME) and some reference electrode; the DME usually functioning as a cathode. The DME consists simply of a series of small mercury droplets that are formed from the end of a fine capillary [49]. The potential of the working electrode is increased at typical rate of 2-5 mV/s and the current in microamperes is recorded to give a

polarogram. This polarogram is a plot of current at the working electrode as a function of potential applied to the working electrode [50].

Before any potential is applied it is necessary to flush the working solution with some inert gas, such as nitrogen or argon, in order to remove dissolved oxygen which causes interference by itself undergoing reduction, in two stages, within the normal potential working range [50]. As the potential is increased cathodically from zero, only very small current flows. This current is called residual current. This is essentially a charging current arising from the charging of the double layer at each drop and is non-faradaic. The residual current may also contain small (faradaic) components due to the presence of reducible impurities in the solution, usually introduced through the necessary high concentration of supporting electrolyte. Only the residual current flows until the decomposition reduction potential of the reducible ionic species is reached. At this point, the ions, designated M^{n+}, begin to be discharged owing to their reduction by the following process [50]:

$$Mn^{+} + ne^{-} \rightleftharpoons M(Hg)$$

The product of the electrode reaction has been written here as M(Hg) since very often the metal atoms produced are absorbed into the mercury drop in the form of an amalgam. A steep rise in current is now observed and, with a further small increase in applied potential, the rise will continue. However, the M^{n+} ions arrive at the DME by the relatively slow process of natural diffusion. Since the rate of reduction increases with the applied potential, a point is eventually reached at which the ions are reduced as fast as they diffuse across the concentration gradient set up at the electrode solution interface [51].

Mercury as an electrode material has two important advantages. The first relates to the kinetics of hydrogen evolution on mercury; that is extremely slow, allowing study of aqueous electrolytes in neutral or alkaline solutions over a wide potential range, from ca. -2.0 to + 0.3 V vs. SCE, above which mercury dissolves. The second advantage is that by employing a simple capillary tube, the liquid mercury forms drops with a lifetime of few seconds. As each drop forms and falls from the electrode, the surface of the mercury is kept clean and free of adsorbed impurities. The additional advantage includes the facts that currents through the drops (order of 1mm diameter) are small (order of 1μA), so the composition of the electrolyte does not change during a measurement, and mercury is a relatively inert metal, reacting chemically with few electrolytes [5, 50, 51].

2.2.2. Principles of Direct Current Polarography (DCP)

Heyrovský invented the original polarographic method, conventional direct current polarography (DCP), and Heyrovský and Shikata constructed the first polarograph in 1925 [49, 52]. DCP involves the measurement of current flowing through the dropping mercury electrode (DME) as a function of applied potential. Under the influence of gravity, mercury drops grow from the end of a fine glass capillary until they detach. If an electroactive species is capable of undergoing a redox process at the DME, then an S-shaped current-potential relation is usually observed. This is called a polarographic wave. Figure 2.2 illustrates the response obtained from a reduction reaction where the current (I) increases over a particular potential (E) range until it reaches a limiting value. The

limiting current is the diffusion-controlled limiting current (I_d). This I_d is of interest in analytical measurements as it is proportional to the concentration of reactant. Ilkovic first put the measurement of this current on a theoretical basis, and his equation is [48]:

$$I_d = 706nD^{1/2}\, m^{2/3}\, t_d^{1/6}\, C \qquad (29)$$

where n is the number of electrons, D is the diffusion coefficient, m is the flow rate of mercury, t_d is the drop time, and C is the concentration of the electroactive species in the bulk solution. The half-wave potential $E_{1/2}$ is another important parameter of the DC polarogram. This is the potential at which the current reaches half of its limiting value (see Figure 2.2).

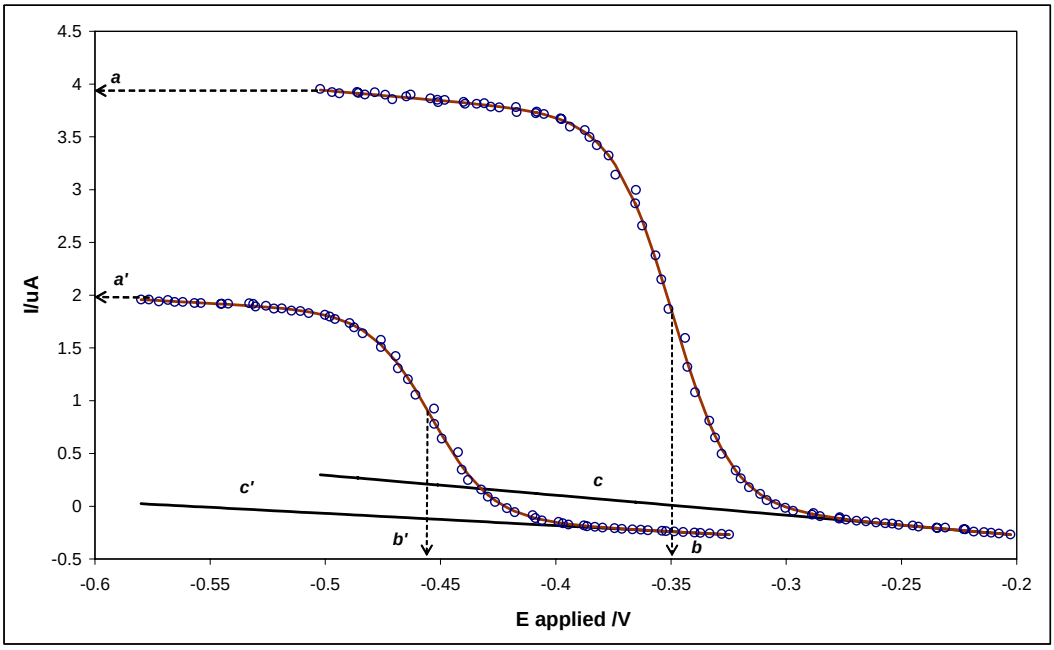

Figure 2.2: Example of DC–waves recorded at different pH on Pb-Cyp$_2$EN system L_T:M_T ratio 50. *a* and *a'* represent the limiting current I_d, *b* and *b'* represent the half-wave potential $E_{1/2}$, *c* and *c'* represent the residual current. Circles and solid lines represent the recorded and fitted curves, respectively.

The value of the half-wave potential is independent of the concentration of electroactive species and is characteristic of that species. Therefore it can be used

for qualitative characterisation of the species, and is the foundation of qualitative analysis. The shape of the DC polarogram is also very important to the overall characterisation of the electrode process. If the reduction electrochemical reaction is reversible and controlled by diffusion, the potential (E) is related to the concentrations of reactant and product by the Nernst equation:

$$E = E° + (RT/nF)\ln(C_O(0)/C_R(0)) \quad (30)$$

where $E°$ is the standard redox potential, R is a gas constant, T is temperature, $C_O(0)$ and $C_R(0)$ are the surface concentrations of species Ox and Red, respectively. The shape of the DC polarographic wave is then derived by combining the Nernst and Ilkovic equations as follows

$$E = E_{1/2} + (RT/nF)\ln((I_d - I)/I) \quad (31)$$

or

$$I = I_d / [1 + \exp((nF/RT)(E - E_{1/2}))] \quad (32)$$

where

$$E_{1/2} = E° + (RT/nF)\ln(D_R/D_O) \quad (33)$$

Since the diffusion coefficients of oxidised and reduced forms, D_O and D_R, are often almost equal, then $E_{1/2} = E°$. When $I = I_d/2$, then $E = E_{1/2}$ [53].

If the potential of the DME is at the limiting current region of the DC polarogram, and all electro-active species reach the electrode surface, the magnitude of the limiting current will be controlled by diffusion, and not by the kinetics of heterogeneous electron-transfer step or homogeneous solution kinetics. Since it is assumed that all the ions or molecules present initially at the electrode surface will be electrolysed immediately as the potential is applied in the limiting current

region, the concentration of the electro-active species approaches zero in a very thin layer near the electrode surface. The concentration gradient established at the electrode-solution interface causes ions to diffuse towards the electrode surface. Since the current flowing through the cell will be proportional to the quantity of material that can be electrolysed, the limiting current is proportional to the rate at which the electroactive substance can diffuse toward the electrode surface [52].

2.2.3. Principles of Differential Pulse Polarography (DPP)

The most convenient technique for studying speciation and determining stability constants is DPP. The current is sampled only as a short pulse when the drop has reached almost full size [5]. The potential wave-form consists of small pulses with constant amplitude superimposed upon a staircase wave-form. The current is sampled twice, before and after the pulse, and the difference between these two current values is recorded and displayed versus the applied potential on a step. The measured signal is the difference in currents measured before and after the application of the pulse. A peak is observed with a peak maximum near $E_{1/2}$ if the process is reversible [54, 55]. The peaks of current as a function of applied potential are obtained, rather than waves, which makes the detection of minor species much easier, provided that the process is electrochemical reversible [51]. Figure 2.3 shows an example of a differential pulse polarogram. The peak potential and its corresponding current are designated by E_p and I_p, respectively.

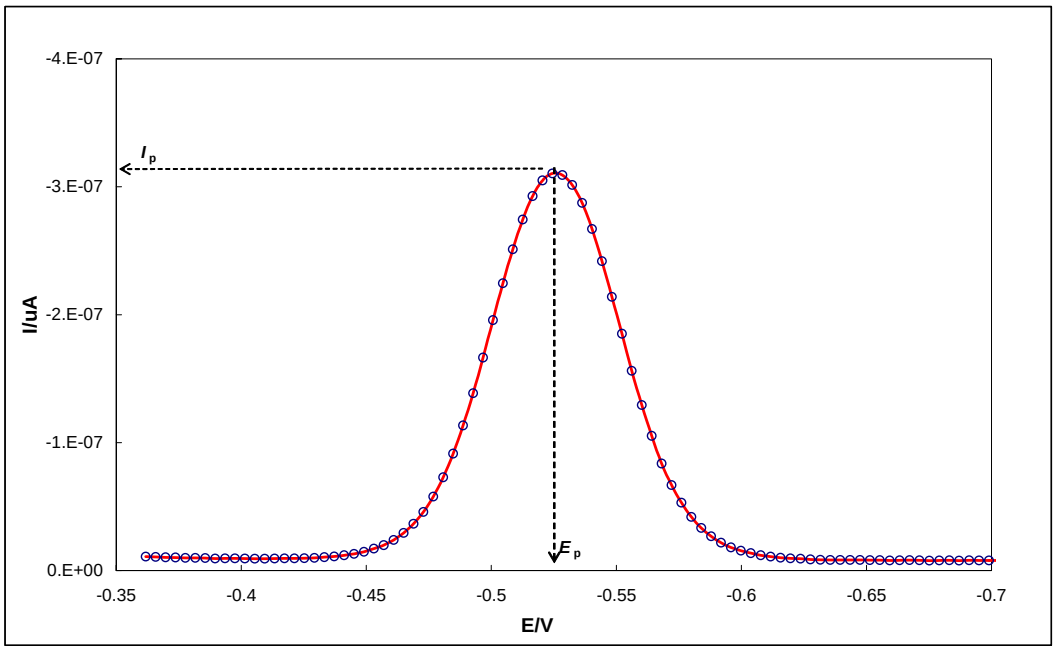

Figure 2.3: Example of differential pulse polarogram recorded on Cd-Cyp_2EN system L_T:M_T ratio 200 at pH 3.1, ionic strength 0.1 M in $NaNO_3$ and 25°C. $[M_T] = 1.99 \times 10^{-5}$M and $[L_T] = 3.98 \times 10^{-3}$M.

2.2.4. Use of Polarography in Metal-Ligand Equilibrium Study

i. Polarographic study of metal complexes at fixed pH

The use of polarography in metal-ligand equilibrium studies dates back to more than 60 years when Lingane [56] reported a derived equation describing a shift in half-wave potential as a function of the excess of a ligand at a fixed pH. The Lingane equation can be written, at 25° C as:

$$E = E_M - E_c = \frac{0.0592}{n}\log_{10}\beta_{ML_j} + \frac{0.0592}{n}\log_{10}[L]^j \qquad (34)$$

where E_M and E_c are the half-wave potentials (or in the case of DPP, the peak potentials) of the free metal ion and the complexed metal ion, respectively, $[L]$ is the free ligand concentration and j is the number of ligands in a complex ML_j. This method was developed for a metal-ligand system where a single complexed species (ML_j) is formed [56]. Ten years later DeFord and Hume [57] reported a

mathematical expression for the analysis of the change in half-wave potential of a metal ion with changes in the concentration of the complexing agent,

$$anti\log\left(\frac{0.4343\times nF}{RT}\Delta E_{1/2}+\log\frac{I_d(M)}{I_d(C)}\right)=\sum_{0}^{n}\beta_{ML_j}\left[L_{excess}\right]^j \qquad (35)$$

where $\Delta E_{1/2}$ represents the difference between the half wave potential of free metal ion and the half–wave potential of complexed metal ion, $I_d(M)$ and $I_d(C)$ represents the limiting diffusion current for free and complexed metal ion, respectively. Equation 35 was derived on similar assumptions and conditions as those reported by Lingane. This made the identification of the successive complexes ML_j and the determination of their stability constants possible [57]. Their method has the advantage over the Lingane method in that it allows the calculation of stability constants for the ligand-metal system when several complexes are formed in a stepwise manner [50]:

$$F_0[L]=\beta_0+\beta_1[L]+\beta_2[L]^2+\mathrm{K}+\beta_n[L]^n\ , \qquad (36)$$

where β_0 is the stability constant of the zero complex by which, by definition has the value 1.

$$F_1[L]=\left[\frac{F_0[L]-1}{[L]}\right]=\beta_1+\beta_2[L]+\mathrm{K}+\beta_n[L]^{n-1} \qquad (37)$$

$$F_2[L]=\left[\frac{F_1[L]-\beta_1}{[L]}\right]=\beta_2+\beta_3[L]+\mathrm{K}+\beta_n[L]^{n-2} \qquad (38)$$

The procedure is continued in this manner until all N complexes have been accounted:

$$F_N[L]=\left[\frac{F_{N-1}[L]-\beta_{N-1}}{[L]}\right]=\beta_N \qquad (39)$$

In 1961, Schaap and McMasters described a polarographic method for the study of mixed complexes and applied it to determine the stability constants of the mixed complexes of Cu^{II} and Cd^{II} [58]. The method of Schaap and McMasters is a logical extension of the DeFord and Hume method applied to the metal-ligand system where two ligands were competing in complex formation reaction with the same metal ion. This method of studying metal complexes at a fixed pH and varying the ligand concentration has recently been found to have several weaknesses, especially when several metal-complexes are formed simultaneously at a particular pH of a solution. In this case, the extended Lingane equation also cannot be used as a tool for the stability constant evaluation. It is because in the extended Lingane equation, only one complex can be included and a shift in the peak potential as well as variation in the peak height are attributed only to one metal complex. As a result, the calculated stability constant is higher than it should be [59].

ii. The analysis of polarographic data at fixed L_T: M_T ratio and varied pH

The new approach of studying metal ions with protic ligands by polarography has been described by Cukrowski [59], where Lingane equation is expanded and the effect of pH included. The expended Lingane equation is presented as follows:

$$\Delta E - \frac{RT}{nF}\ln\frac{I(C)}{I(M)} = \frac{RT}{nF}\ln\beta_{ML_j(OH)_b} + j\frac{RT}{nF}\ln[L] + b\frac{RT}{nF}\ln[OH^-] \qquad (40)$$

where $I(C)$ and $I(M)$ are the current for complexed and free metal, respectively, $[M]$ and $[L]$ denote the free metal ion and ligand concentrations, respectively. The overall reaction is as follows:

$$M + jL + bOH \rightarrow ML_j(OH)_b$$

or

$$M + jL + bH \rightarrow M(H_bL_j)$$

where [L] is calculated from known pH, total ligand concentration [L_T], and stepwise protonation constants (K_1, K_2, K_3...) of the ligand:

$$[L] = [L_T]/(1 + K_1[H] + K_1K_2[H_2] + \mathrm{K}) \quad (41)$$

However ΔE is related to a single β value and if a number of species are formed simultaneously, then Equation 40 assumes that one complex is formed, which is a big limitation when simultaneous and consecutives complexes are formed. The computed value is always too large. Recently, Cukrowski has developed a new approach, which involves equation based on mass balance-equations for labile, mixed or non-labile complexes at fixed L_T:M_T ratio and varied pH [60–62].

The formation of labile complexed metal species can be identified when polarography is employed by, for example, a shift in a differential pulse polarographic peak. The shift is measured as a replacement of the DPP peak along the potential scale measured versus the DPP peak potential of uncomplexed metal ion $E_p(M_{Free})$ in a background of a particular electrolyte solution. A speciation study of labile metal species can be performed either at a fixed pH value or various pH values of a single sample solution. The latter method usually involves a titration of a sample with a standard base solution. In both speciation techniques a series of measurements is performed that result in a number of peak potentials of complexed metal species E_p (M_{comp}) (i). These values, E_p (M_{comp}) (i), are then compared with a single value of E_p (M_{Free}) to evaluate the shift in the peak potential caused by the formation of complexes due to either the excess of the

ligand or the change in the pH value. From the above it follows that the value of E_p (M_{Free}) is of a great importance when modelling metal species and evaluation of their stability constants is performed by polarography. It has been demonstrated that protonated and hydroxo complexes can also be studied by polarography at a fixed L_T:M_T ratio and various pH values.

It has been demonstrated that, when the polarographic experiment is performed on a labile metal-ligand system at a fixed L_T:M_T ratio and varied pH, experimentally available data can be related by the following Equation provided that a single and well shaped DPP peak is observed

$$\Delta E_p(i) - \frac{RT}{nF}\ln\frac{I_p(M_{Comp})(i)}{I_p(M_{Free})(i)} = \frac{RT}{nF}\ln\frac{[M_T](i)}{[M_{Free}](i)} \qquad (42)$$

where

$$\Delta E_p(i) = E_p(M_{Free}) - E_p(M_{Comp})(i) \qquad (43)$$

In Equation 42 $\Delta E_p(i)$ represents a shift in a peak potential observed from the DPP experiment at each pH(i) value to which the metal-ligand system was adjusted in a polarographic cell, $[M_T](i)$ and $[M_{Free}](i)$ stand for the total and free metal ion concentration, respectively, at each ith pH(i) value, $I_p(M_{comp})(i)$ is a height of the DPP peak recorded at an ith pH(i) value and represents all labile metal species in a solution, $I_p(M_{Free})(i)$ is a calculated DPP peak height of the metal ion M(aq) one would observe at an ith pH(i) value with an assumption that complexes of the metal M were not formed [63]. Note that Equations 42 and 43 are applicable at any voltammetric study.

The total metal ion and ligand concentrations ([M_T] and [L_T]) are known at any stage of the experiment. They can be expressed by the following mass-balance equations:

$$[M_T] = [M] + \sum_{p=1}\sum_{q=1}\sum_{r=0} p\beta_{M_pL_qOH_r}[M]^p[L]^q[OH]^r + \sum_{x=1}\sum_{y=1} x\beta_{M_xOH_y}[M]^x[OH]^y \quad (44)$$

$$[L_T] = [L] + \sum_{p=1}\sum_{q=1}\sum_{r=0} q\beta_{M_pL_qOH_r}[M]^p[L]^q[OH]^r + [L]\sum_{k=1}\beta_k^H[H]^k \quad (45)$$

where $\beta_{M_pL_qOH_r}$ and β_k^H stay for the overall stability and protonation constants, respectively, and [M], [L], [H] and [OH] are the free metal ion, free ligand, proton and hydroxide concentrations respectively. In case of the formation of complexes involving the protonated form of a ligand, e.g. M(HL), the term $[M]^p[L]^q[OH]^r$ would be replaced by $[M]^p[L]^q[H]^r$ [64].

In Equation 42 $I_p(M_{Comp})(i)$ stands for the DPP peak potential obtained at each *i*th pH(*i*) value to which the metal–ligand system was adjusted in a polarographic cell. The value of an uncomplexed metal ion is of special importance as it is a single experimental parameter versus which the shift in the peak potential $\Delta E_p(i)$ is estimated. It is commonly accepted that this should be a peak potential of a metal ion obtained in the absence of the ligand to make sure that its value is not influenced by the formation of metal complexes. Modelling of species formed and optimization of stability constants will be achieved by the use of polarographic experimental and calculated complex formation curves (ECFC and CCFC). The ECFC is simply the left–hand side of Equation 42 when plotted vs. pH [65–67].

$$\Delta E_p(i) - \frac{RT}{nF}\ln\frac{I_p(M_{Comp})(i)}{I_p(M_{Free})(i)} = f(pH) \quad (46)$$

It is called the experimental polarographic complex formation curve because all terms in Equation 46 are available from polarographic experiment. The theoretical curve, CCFC, is obtained by varying the metal–ligand species formed (modelling of a metal–ligand system) and optimization of their stability constants in such a way that the calculated corrected shift in the peak potential fits best the experimental corrected shift.

The CCFC is obtained when the right–hand side of Equation 42 is plotted vs. pH [68–70].

$$\frac{RT}{nF} \ln \frac{[M_T(i)]}{[M_{Free}(i)]} = f(pH) . \qquad (47)$$

2.3. Theory of Virtual Potentiometry

Polarography is a dynamic electrochemical technique and any attempt to rigorously describe processes occurring at the electrode-solution interface must involve many complex processes, among them thermodynamics, kinetics (homogeneous and heterogeneous), transport etc. Often it is impossible to arrive to a solution that would allow theoretically reproduction of observed polarograms. This is the reason why in polarography the change in the observed signal, e.g., $\Delta E_{1/2}$ or ΔE_p rather than theoretically predicted position of a curve is used when the study of metal complexes are of interest. This generally employed approach has however a significant weakness and this is seen from Equations 42 and 43, where all recorded curves are compared with a single value of E(M). It is well-known that the nonlinear curve fitting operations will generate more reliable values for fitted parameters with an increase in the number of experimental points recorded. The

problem with refinement of many polarographic experimental data points collected on a solution adjusted to many pH(i) values is that all the recorded data are compared with a single experimental point, e.g., the shift in the peak or half-wave potential is used and not the observed values (E_p or $E_{1/2}$) at each pH(i). As a result, the computed optimised stability constants must change with the change in the value of E(M) even though the metal-ligand model, the overall fit of CCFC in ECFC and standard deviations in stability constants will remain virtually the same. It means that one has to establish the value of E(M) with as high accuracy and certainty as possible. Unfortunately, it is not always possible to obtain a reliable value for E(M). One of examples might be a study of highly acidic metal ions, such as Bi(III). Bismuth undergoes hydrolysis already at pH 0 which means that the recorded polarographic curve represents two bismuth species, Bi(aq) and Bi(OH) [64]. This implies that the value in E(M) is not directly available from the experiment. One of the advantages of studying metal complexes by polarography is a possibility of working with a large excess of a ligand. This, however, might introduce significant uncertainty in the E(M) value that might be different in the absence and the presence of the large concentration of a ligand.

The term $\frac{I_p(M_{Comp})}{I_p(M_{Free})}$ seen in Equation 42 represents the normalized change in the intensity of the recorded polarographic signal. The change in the recorded current (I_d or I_p) can be attributed to a change in the diffusion coefficients of different labile metal complexes formed as well as to the formation of polarographically inactive metal complexes. The theoretically and thermodynamically expected positions of the polarographic signal, along the potential scale, can be written as follow:

$$\left(E(comp) + \frac{RT}{nF} \ln\left(\frac{I(comp)}{I(M)} \right) \right)_{x(i)} = E(virt)_{x(i)} \quad (48)$$

and it can be calculated at any pH (i) from available experimental data. There is a well defined relationship between $E_{1/2}$ and the standard redox potential if the system under investigation can be regarded as thermodynamically fully reversible. Due to this relationship, the proposed virtual potential $E(virt)$ can be interpreted as a thermodynamic potential of a virtual sensor obtained from dynamic, non-equilibrium polarographic data. The virtual potentiometric sensor is metal-ion non-specific and should be able to work for any metal ion that is polarographically active and is reduced reversibly. The virtual potentiometric sensor should have unlimited linear response with a theoretical Nernstian slope. The experimental parameters such as pulse height and width are kept fixed throughout the whole differential pulse polarographic experiment. This means that the concept of $E_p(virt)$ must also be valid with an unlimited linear response shifted in E^o *b*y a fixed number of mV when compared with a linear response of virtual probe generated from $E_{1/2}(virt)$ values. The concept of virtual potentiometric sensor implies that it should be possible to employ potentiometric software, such as ESTA, in the refinement of stability constants using, in principle, data coming from a dynamic electrochemical technique [64]. Virtual potential, rather than observed potential should be used in the prediction of slopes for the validation of proposed model. This new concept will be used here in the discussion of results. $E_{1/2}(virt)$ and E_p ($virt$) will be used instead of $E_{1/2}$(observed) and E_p (observed) when plotted vs. pH, log [L] and log [M] [71].

Chapter 3: Experimental

3.1. Reagents

The ligands N,N'-bis(2-hydroxycyclopentyl)-ethylenediamine (Cyp_2EN F.W 228.33) and N,N'-bis(2-hydroxycyclohexyl)-ethylenediamine (Cy_2EN F.W 256.39) were both synthesized by de Sousa and were used as received. The other reagents are for analytical grade: Nickel Chloride ($NiCl_2$, F.W. 129.62, 98 % pure), Zinc Nitrate hexahydrate ($Zn(NO_3)_2.6H_2O$, F.W. 297.48, 98 % pure), Cadmium Nitrate tetrahydrate ($Cd(NO_3)_2.4H_2O$, F.W. 308.47, 98 % pure) and Lead Nitrate ($Pb(NO_3)_2$, F.W. 331.20, 99% pure) were obtained from ALDRICH. Copper Nitrate trihydrate ($Cu(NO_3)_2.3H_2O$, F.W. 241.60, 99.5 % pure) and Potassium Hydrogen Phtalate (KHP, F.W. 204.23, 99 % pure) were obtained from MERCK, Sodium nitrate ($NaNO_3$, F.W. 84.99, 98 % pure) and Sodium Hydroxide (NaOH, F.W. 40.00, 98 % pure) were purchased from UNILAB. Nitric Acid (HNO_3, F.W. 63.01, 65 % pure and d = 1.41 kg/l) was obtained from SAARCHEM. Deionised water used in the preparation of solutions was prepared by passing distilled water through a milli-Q-water purification system (Millipore, Bedford, MA, USA).

3.2. Preparation of the solutions used

The titrant solution of NaOH with a concentration of approximately 0.01 M was prepared by weighing out the required amount of NaOH and dissolving in a solution of 0.09 M $NaNO_3$. The 0.01 M solution of HNO_3 was also prepared in 0.09 M $NaNO_3$. Both of the above mentioned solutions were

standardised before further use. The stock solutions of Cd^{2+}, Cu^{2+}, Ni^{2+}, Pb^{2+}, and Zn^{2+} were prepared by weighing the required mass of the appropriate metal salt.

In potentiometric titrations, the concentration of the stock solutions of metals was 4×10^{-3} M. They were prepared in standardised solution of about 0.01 M HNO_3 + 0.09 M $NaNO_3$. The stock solutions of the ligands was prepared by weighing out the required amount of the ligand and dissolving it in the same solution as that one used in the preparation of the metal solution. (0.01 M HNO_3 + 0.09 M $NaNO_3$). The concentration of the ligand stock solution was also 4×10^{-3} M.

In polarographic titrations, the concentration of NaOH was 0.02 M NaOH in 0.08 M $NaNO_3$ for the study of Cd–Cyp_2EN and Pb–Cyp_2EN systems with the same stock solutions of metal and ligand as those used in potentiometry. The solution of 0.05 M NaOH in 0.05 M $NaNO_3$ was used as titrant for Cd–Cy_2EN and Pb–Cy_2EN systems. The stock solution of the ligand Cy_2EN was 1×10^{-2} M and was prepared in a solution of 0.02 M HNO_3 + 0.08 M $NaNO_3$. The stock solution of the metals was 3×10^{-2} M prepared in the same solution of 0.02 M HNO_3 + 0.08 M $NaNO_3$.

All experiments were performed at ionic strength 0.1 M using $NaNO_3$ as the background electrolyte.

3.3. Glass Electrode Potentiometry

3.3.1. Experimental set-up

The potentiometric titrations were performed in Metrohm jacketed glass vessel equipped with a magnetic stirrer model Metrohm 801 and thermostatted at 25 ± 0.1°C by water circulating from a constant temperature bath. The *e.m.f.* of the cell was measured using the Metrohm combination glass electrode model 6.0234.100 and the titrations were performed using an autotitrando model Metrohm 809 and a digital burette model Metrohm 800 Dosino. The standardisation of the acid and base solutions was achieved by dynamic equivalence point titration (DET) in which the equivalent point was reached by addition of different volumes of the titrant at each dosing step; the combination glass electrode (CGE) calibration and metal-ligand titration was performed by monotonic equivalence point titration (MET) in which the equivalent point was reached by addition of the same volume of the titrant at each dosing step. In the metal-ligand study, the minimum waiting time between consecutive additions of a titrant was 5 minutes, which was important for drift-controlled measurements. Measured value acceptance only took place when the minimum waiting time had elapsed, even when the measured value drift had already been achieved. The maximum waiting time was 8 minutes; if measured value drift had not yet been achieved, then the measured value was accepted after the maximum waiting time had elapsed. The volume increment, which is the volume to be added at each dosing step, was 0.1 ml. The signal drift, i.e., the alteration in the measured value of potential per minute, was set to 0.5 mV/min. High purity nitrogen was used for deaeration of the sample solutions.

3.3.2. Experimental procedure

A stock solution of NaOH was standardised every week using KHP, and a stock solution of HNO_3 was standardised every month using a standardised solution of NaOH. Before and after running any experiment, the CGE was calibrated using these two solutions.

i. Standardisation of NaOH using KHP

A solution of NaOH was placed in the burette of the autotitrando, and a small amount of KHP was weighed out and dissolved in the cell using a solution of 0.1 M $NaNO_3$. The solution of KHP was titrated by a solution of NaOH until the end point was reached. The end point was used to determine the actual concentration of NaOH by the following equation:

$$[NaOH] = m_{KHP}.1000/ M_{KHP}.V_{NaOH} \quad (49)$$

where m_{KHP} represents the amount of KHP dissolved in the cell, M_{KHP} represent the molecular mass of KHP and V_{NaOH} represents the volume of NaOH added to reach the equivalence point.

The experiment was repeated at least three times and the average was taken as the standard concentration of the standardised NaOH solution.

ii. Standardisation of HNO_3 using standardised solution of NaOH

An appropriate volume of 0.01 M HNO_3 solution was placed in the titration cell. This solution was titrated with a standardised solution of 0.01 M NaOH. The volume of NaOH at the end point was used to determine the concentration of nitric acid solution as follows:

$$[HNO_3] = V_{NaOH}.\ C_{NaOH}/V_{HNO3} \quad (50)$$

where V_{NaOH} represents the volume of NaOH added to reach the equivalent point; C_{NaOH} represents the concentration of standardised solution of NaOH, and V_{HNO3} represents the volume of HNO_3 placed in the titration cell.

The experiment was repeated at least three times and the average was considered as the standard concentration of the standardised HNO_3 solution.

iii. Glass electrode calibration

Before and after running an experiment, the glass electrode was calibrated using the standardised solutions. Calibration of the electrode involved titration of 15 ml of standardised HNO_3 solution with a standardised solution of NaOH. A sufficient number of points had to be taken for pH intervals before and after the equivalence point. An increased number of data points in these pH regions facilitated the linear fitting of the titration data, affording more accurate values of the Nernstian slope and E^o for the electrode.

vi. Determination of protonation constants

In order to study the metal complexes of novel ligands, the protonation constants of these ligands must initially be determined. In the determination of protonation constants, 20 ml of 5×10^{-3} M of the ligand prepared in standardised solution of 0.01 M HNO_3 was titrated with a standardised solution of 0.01 M NaOH. Three titrations were performed and analysed simultaneously for getting the values of protonation constants.

v. Determination of stability constants for different complexes formed

To determine stability constants for metal complexes, different ligand to metal ratios were considered. These ratios were prepared using different volumes of the metal and ligand stock solutions, respectively. The resultant solution in the titration cell was then titrated with a standardised solution of NaOH (see Table 3.1).

Table 3.1: Preparation of samples for different L_T:M_T ratios studied by GEP

Ratio L_T:M_T	V_L (ml)	V_M (ml)	[L_T]	[M_T]
0.5*	5	10	0.00133 M	0.00266 M
1	7.5	7.5	0.002 M	0.002 M
1.45**	8.1	6.9	0.00216 M	0.0149 M
2	10	5	0.00266 M	0.00133 M
3	12	4	0.003 M	0.001 M

*Was used only in the study of Zn–Cyp_2EN system
** Was used only in the study of Cu–Cyp_2EN system

The above procedure was used for all metals studied with the ligands Cyp_2EN and Cy_2EN.

3.4. Polarography

3.4.1. Experimental set-up

All experiments were performed in a Metrohm (Herisau, Switzerland) jacketed glass vessel, equipped with a magnetic stirrer and thermostatted at 25.0 ± 0.1°C by water circulating from a constant temperature bath. The potential of a combination glass electrode and pH= $-\log_{10}$ [H] of solutions were measured to

within ± 0.1 mV (± 0.001 pH unit) with a Φ 72 pH meter (Beckman) or 713 pH meter (Metrohm). A model 6.0234.100 combination glass electrode (Metrohm) was used. Differential pulse and direct current polarograms were obtained with the use of 757 VA computrace (Metrohm) or a computer controlled, in-house built, on instrumental set-up controlled by Labview programs. A multimode electrode (Metrohm model 6.1246.020) was employed as the working electrode and used in the dropping mercury electrode mode with a drop time of 2 s. A silver/silver chloride electrode (3 M KCl) and a platinum electrode (both from Metrohm) were used as reference and auxiliary electrodes, respectively. A pulse height of 50 mV and a step height of 4 mV were used. High purity nitrogen was used for deaeration of the sample solutions.

3.4.2. Experimental procedure

The CGE was calibrated before and after running metal-ligand titration. As the ligands were very basic and polarography had to be performed at very high L_T:M_T ratios, the solution of the ligand used was prepared in 0.01 M HNO_3 + 0.09 M $NaNO_3$ for the ligand Cyp_2EN and in 0.02 M HNO_3 + 0.08 M $NaNO_3$ for the ligand Cy_2EN. The solutions of NaOH and HNO_3 were standardised as described for potentiometric titrations.

i. Polarographic study of Cyp_2EN with Cd^{2+} and Pb^{2+}

After the cell was cleaned with a solution of 0.05 M HNO_3 and rinsed with deionised water, different ligand-metal ratios were prepared. According to the species distribution diagrams obtained using the ligand-metal model from

potentiometry, the first polarogram recorded at pH 3 was considered as the polarogram of metal ion only, because the complexes started to form above that pH. Different ratios were prepared as follows:

Table 3.2: Preparation of the sample for different L_T:M_T ratios used in polarographic study of Cyp_2EN with Cd^{2+} and Pb^{2+}

Metal	V_L (ml)	V_M (ml)	$[L_T]$	$[M_T]$	L_T:M_T ratio
Cd	25	0.5	3.92×10^{-3}M	7.84×10^{-5}M	50
	25	0.125	3.98×10^{-3}M	1.99×10^{-5}M	200
Pb	24.5	0.5	4.03×10^{-3}M	8.01×10^{-5}M	50
	27	0.3	5.51×10^{-3}M	6.62×10^{-5}M	83*

* The ligand and metal concentrations of the stock solution were 5.55×10^{-3} M and 9.02×10^{-3} M respectively

Polarograms were recorded after the pH increment of approximately 0.1– 0.15 pH units. Standardised NaOH solution with the same ionic strength as the test solution was used as the titrant. A set of between 50 to 60 polarograms was obtained for each L_T:M_T ratio.

ii. Polarographic study of Cy_2EN with Cd^{2+} and Pb^{2+}

The procedure employed was the same as for Cyp_2EN ligand, and different ligand to metal ratios were prepared by using different volumes of the ligand, metal and 0.1 M $NaNO_3$ stock solution as shown in Table 3.3. Polarograms were recorded after the pH increment of approximately 0.05 - 0.08 pH units. Standardised NaOH solution of the same ionic strength as the test solution was used as the titrant. A set of between 80 to 90 polarograms was obtained for each L_T:M_T ratio.

Table 3.3: Preparation of the sample for different L_T: M_T ratios used in polarographic study of Cy_2EN with Cd^{2+} and Pb^{2+}

Metal	V_L (ml)	V_M (µl)	$V_{Back.}$ (ml)	$[L_T]$	$[M_T]$	L_T:M_T ratio
Cd	10	70	10	4.98×10^{-3} M	1.05×10^{-5} M	47
	20	35	_	9.98×10^{-3} M	5.25×10^{-5} M	192
Pb	12.5	85	12.5	4.98×10^{-3} M	1.02×10^{-5} M	49
	7.5	85	17.5	2.99×10^{-3} M	1.02×10^{-5} M	29

Chapter four: Results and discussion

4.1. Protonation constants of the ligands Cyp_2EN and Cy_2EN

In order to study the metal complexes of novel ligands, the protonation constants of the ligands were initially determined. Two protonation constants can be expected according to the structure of the ligands Cyp_2EN and Cy_2EN as shown by the following reactions:

$$H + L = HL \qquad K_1^H = \frac{[HL]}{[H][L]} \qquad (51)$$

$$H + HL = H_2L \qquad K_2^H = \frac{[H_2L]}{[H][HL]} \qquad (52)$$

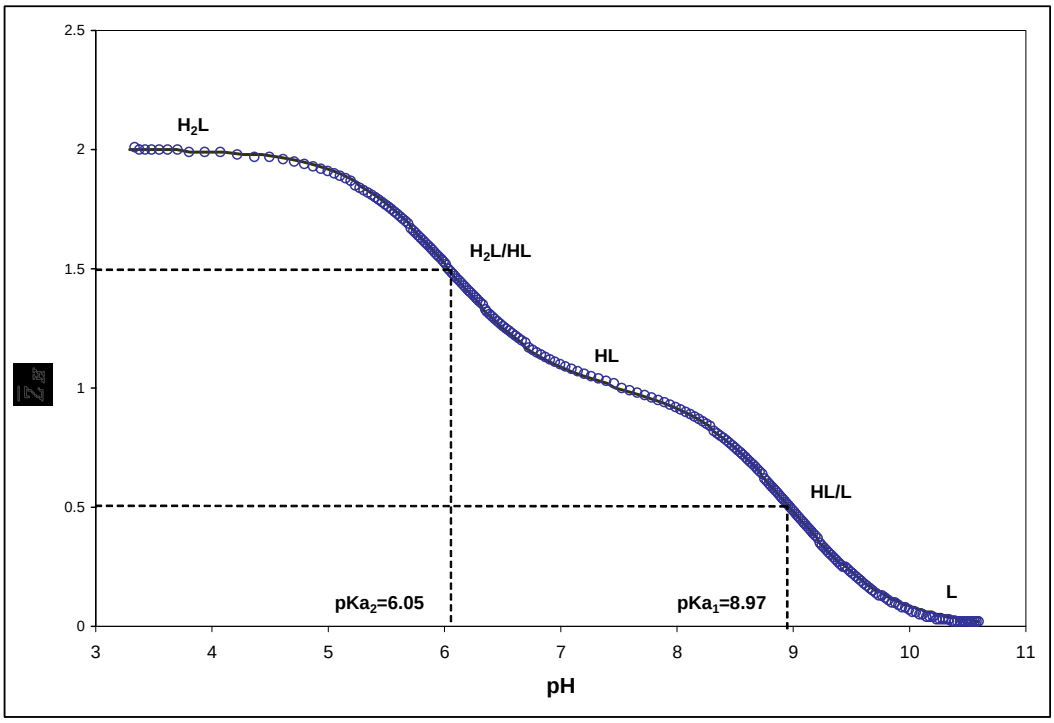

Figure 4.1: Experimental (circles) and fitted (solid line) protonation curves from the titration of the ligand Cyp_2EN at ionic strength 0.1 M and 25°C, $[L_T] = 5 \times 10^{-3}$ M (in 0.01 M HNO_3); titration by 0.01M NaOH.

In the determination of protonation constants, three titrations were performed and the values obtained by fitting of an appropriate model to the

acquired data were considered as the final results of protonation constants. The protonation formation function $\overline{Z}_H$ shows in which pH range different forms of the ligand are predominant. For the ligand Cyp_2EN, the form H_2L of the ligand is predominant below pH 6, the predominant form between pH 6 and 9 is HL, and the ligand is fully deprotonated above pH 10 (see Figure 4.1).

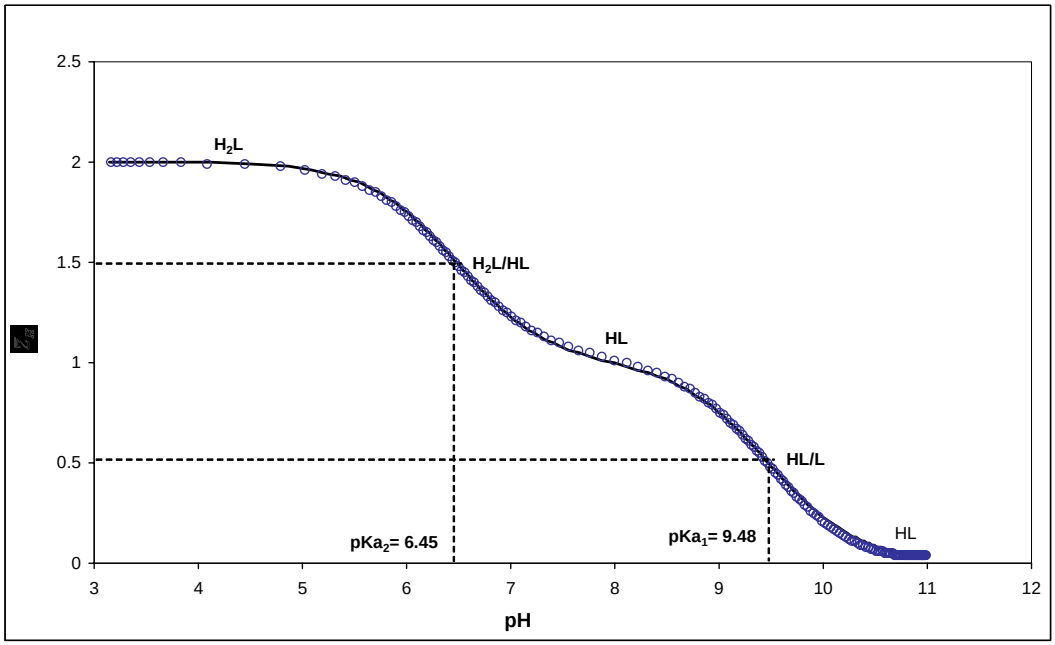

Figure 4.2: Experimental (circles) and fitted (solid line) protonation curves from the titration of the ligand Cy_2EN at ionic strength 0.1 M and 25° C, $[L_T] = 5 \times 10^{-3}$ M (in 0.01 M HNO_3) ; titration by 0.01 M NaOH.

The ligand Cy_2EN was also studied under the same conditions as those used in the study of the ligand Cyp_2EN. The Figure 4.2 shows that the form H_2L of the ligand Cy_2EN is predominant below pH 6.5, from pH 6.5, the form HL starts to be predominant up to pH 9.5. The form L is predominant above pH 9.5, where the ligand becomes fully deprotonated. The values of protonation constants obtained for the ligands Cyp_2EN and Cy_2EN are presented in Table 4.1. As explained in Chapter 3, three titrations were performed for each ligand using the same total

ligand (L_T) concentration (5×10^{-3}M). The final results were obtained in a simultaneous refinement of data from all titrations.

Table 4.1: Protonation constants of the ligands Cyp_2EN and Cy_2EN at 25° C and ionic strength 0.1 M in $NaNO_3$

p*K*a	Cyp_2EN				Cy_2EN			
p*K*a$_1$	8.93 (03)	8.97 (02)	8.97 (02)	8.97 (02)	9.51 (01)	9.477 (004)	9.473 (004)	9.483 (003)
p*K*a$_2$	6.03 (04)	6.04 (03)	6.07 (03)	6.05 (02)	6.44 01)	6.448 (005)	6.473 (005)	6.454 (003)
R – F	0.0103	0.0122	0.0115	0.0130*	0.0257	0.0172	0.0127	0.0175*

* Results from 3 titrations combined during refinement operation

The values of the first protonation constants, 8.97 and 9.48 for Cyp_2EN and Cy_2EN, respectively, are to be expected for amine ligands possessing amino–donor atoms. The ligands Cyp_2EN and Cy_2EN are not easily soluble, especially the ligand Cy_2EN, because of the aliphatic contribution of the cyclopentyl and cyclohexyl moieties. This is the reason why it was necessary to prepare the ligand solution in an acidic medium. Compared to the open-chain amine (see Table 4.2), one can see that pK_a values of open-chain amines are slightly larger than pK_a values of Cyp_2EN and Cy_2EN. Due to the fact that the ligands in Table 4.2 have the same donor atoms, the difference between pK_a values is small, but one can suggest that the inductive effect is slightly high in open–chain amines.

The protonation constants for Cyp_2EN and Cy_2EN seen in Table 4.1 were used in the modelling of different systems studied in this work (Cd–Cyp_2EN, Cu–Cyp_2EN, Ni–Cyp_2EN, Pb–Cyp_2EN, Zn–Cyp_2EN, Cd–Cy_2EN, Cu–Cy_2EN, Ni–Cy_2EN, Pb–Cy_2EN, Zn–Cy_2EN).

Table 4.2: Protonation constants of some open–chain amines [74]

Ligand	p*K*a$_1$	p*K*a$_2$	Temperature	Ionic strength
Ethylenediamine	9.95	7.11	25° C	0.1
Methylenediamine	9.81	6.85	25° C	0.1
1, 2-butylenediamine	9.66	6.65	25° C	0.1
DL –1, 2– dimethylethylenediamine	9.70	6.60	25° C	0.1
Meso –1, 2– dimethylethylenediamine	9.76	6.63	25° C	0.1

4.2. Glass electrode potentiometric study of Cd-Cyp$_2$EN

4.2.1. Data refinement

Three titrations were performed from pH 2.5 to pH 8.4, at 25 ± 0.1 ° C and ionic strength of 0.1 M in $NaNO_3$. The pK_w was 13.78 for these conditions. Complex formation was generally evident starting from pH 3. Consequently, data points at pH < 3 were eliminated from the refinement process as these points relate to the neutralisation of the acidic medium in which the ligand was initially prepared. Data points in the interval 3 ≤ pH < 8.4 were only used for the refinement process to obtain the appropriate model of the present species, since precipitation was observed at pH ≥ 8.4. The data from the three titrations were combined and refined simultaneously for the final model. Figure 4.3 shows the complex formation curves after the refinement of all three titrations. During refinement operation, it was observed that different ratios gave almost the same values of stability constants for different complexes formed when acid and base concentrations were refined simultaneously. The change in the concentration of the base and acid was always less than ± 4 % but the change in the computed

stability constants was significant and final values could be regarded as improved as seen in Table 4.3. The concentrations of standardised base and acid solutions were 0.0100 M and 0.0103 M, respectively.

Note that, when the species distribution diagram was calculated using stability constants from the combined refinement and potentiometric conditions for L_T:M_T ratio 1, it was observed that the complex ML_2 presented a significant percentage in the solution. It was then decided to fix the stability constant of ML_2 complex in the refinement of L_T:M_T ratio 1.

Table 4.3: Model and stability constants obtained from GEP for Cd–Cyp_2EN system

L_T:M_T ratio	M(HL)	ML	ML_2	R-Factor	Remarks *
1 $[L_T] = 2.00 \times 10^{-3}$ M $[M_T] = 2.00 \times 10^{-3}$ M	11.56 (01) 11.29 (01)	4.285 (006) 3.98 (01)	rejected Fixed at 7.20	0.00639 0.00479	Raw data Acid and base refined $[H^+] \Rightarrow$ 0.0100715 M $[OH^-] \Rightarrow$ 0.0096065 M
2 $[L_T] = 2.67 \times 10^{-3}$ M $[M_T] = 1.34 \times 10^{-3}$ M	11.69 (01) 11.35 (01)	4.33 (01) 3.99 (01)	7.39 (05) 7.19 (01)	0.00708 0.00259	Raw data Acid and base refined $[H^+] \Rightarrow$ 0.0102241 M $[OH^-] \Rightarrow$ 0.0097739 M
3 $[L_T] = 2.99 \times 10^{-3}$ M $[M_T] = 1.00 \times 10^{-3}$ M	Rejected 11.34 (01)	3.61 (03) 3.97 (01)	7.09 (04) 7.31 (01)	0.01044 0.00257	Raw data Acid and base refined $[H^+] \Rightarrow$ 0.0102621 M $[OH^-] \Rightarrow$ 0.0100401 M
Combined refinement	11.47 (03) 11.31 (01)	4.19 (02) 3.96 (01)	7.04 (11) 7.24 (01)	0.04219 0.00412	Raw data Acid and base refined R1: $[H^+] \Rightarrow$ 0.01006 M $[OH^-] \Rightarrow$ 0.00959 M R2: $[H^+] \Rightarrow$ 0.010221 M $[OH^-] \Rightarrow$ 0.00976 M R3: $[H^+] \Rightarrow$ 0.010251 M $[OH^-] \Rightarrow$ 0.01001 M

* Initial concentration of $[H^+]$ in the cell was 0.0103 M; initial concentration of $[OH^-]$ in the burette was 0.010 M

4.2.2. Complex formation function

The following metal-ligand model M(HL), ML, and ML_2 resulted in the lowest standard deviations in the refined stability constants and R factor, as well as better fit of the calculated in the experimental potentiometric complex formation curves $\overline{Z}_M$ (see Figure 4.3). The complex formation curves of Cd–Cyp_2EN system do not show the back-fanning feature in Figure 4.3. This can explain the reason why hydroxospecies were rejected during the refinement operations. Due to the precipitation that occurred early (at pH=8.4), the Figure 4.3 does not show clearly the formation of the ML_2 complex.

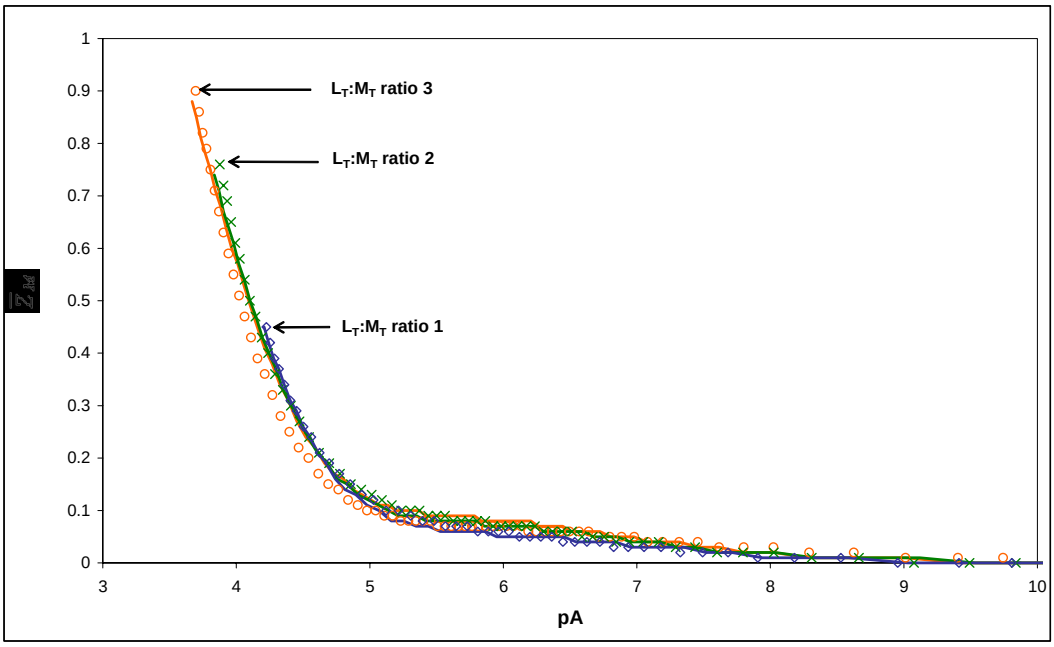

Figure 4.3: Experimental (circles) and calculated (solid lines) potentiometric complex formation curves for Cd–Cyp_2EN system at 25° C and ionic strength 0.1 M in $NaNO_3$. The model used is M(HL), ML, and ML_2.

The formation of M(HL) complex is predicted in the pA range between 5.5 and 8 where the slope of the complex formation curves increases with the increase in the L_T:M_T ratio.

4.2.3. Species distribution diagram

The species distribution diagram in Figure 4.4 was calculated for the model M(HL), ML, ML_2 from the combined refinement using conditions for L_T:M_T ratio 3. A species distribution diagram is a powerful tool for assessing concentrations of the species present as a function of pH. The construction of a species diagram starts with the total concentration of each component and its accuracy depends on the quality of all the equilibrium constants [5].

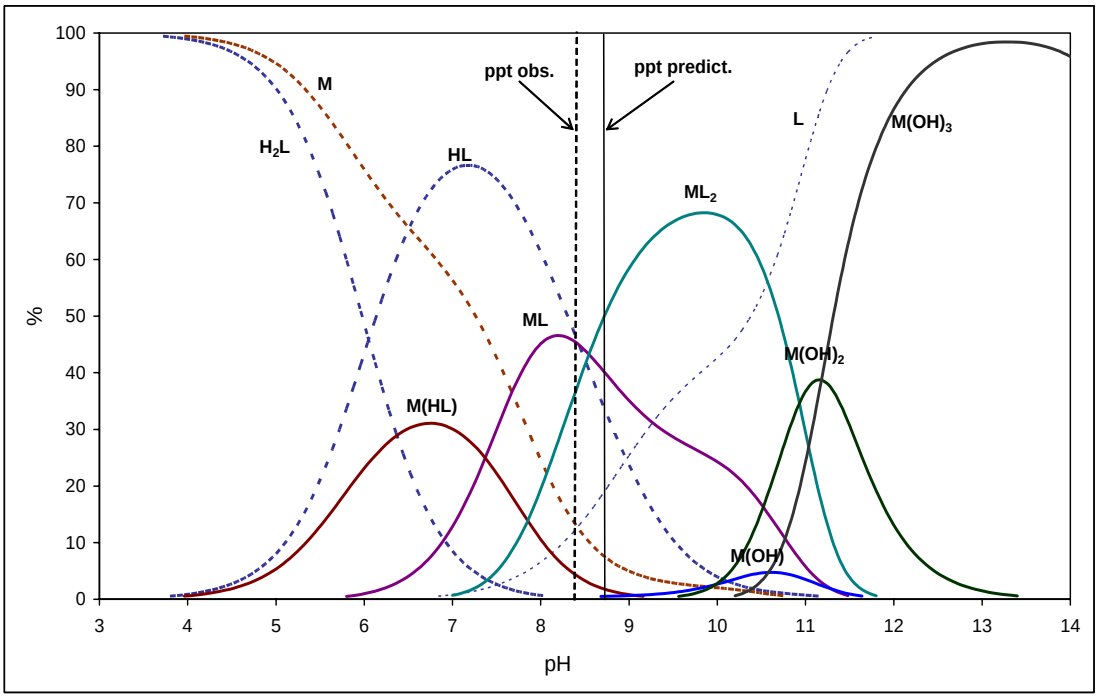

Figure 4.4: Species distribution diagram of Cd–Cyp_2EN system for L_T:M_T ratio 3 at 25°C and ionic strength 0.1 M in $NaNO_3$. $[L_T] = 2.99 \times 10^{-3}$ M and $[M_T] = 1.00 \times 10^{-3}$ M. The model used was M(HL), ML and ML_2 together with all known $Cd_x(OH)_y$ species from the combined refinement.

Figure 4.4 shows that the complex ML_2 should be the major species in the solution if the precipitation had not occurred early. The same Figure also shows that the precipitation occurred at pH 8.4 for L_T:M_T ratio 3. Due to the precipitation which

appeared early, there was no $M_xL_y(OH)_z$ species formed in the solution. Equilibrium constants involving complexes formed are presented as follows:

$Cd^{2+} + Cyp_2EN = Cd(Cyp_2EN)^{2+}$ $$\beta = \frac{[Cd(Cyp_2EN)^{2+}]}{[Cd^{2+}][Cyp_2EN]} \quad (53)$$

$Cd^{2+} + Cyp_2EN + H^+ = Cd(Cyp_2EN)^{3+}$ $$\beta = \frac{[Cd(Cyp_2ENH)^{3+}]}{[H^+][Cd^{2+}][Cyp_2EN]} \quad (54)$$

$Cd^{2+} + 2Cyp_2EN = Cd(Cyp_2EN)_2^{2+}$ $$\beta = \frac{[Cd(Cyp_2EN)_2^{2+}]}{[Cd^{2+}][Cyp_2EN]^2} \quad (55)$$

For L_T:M_T ratios 1 and 2, the precipitation occurred at pH 8 and pH 8.3 respectively, and the predicted precipitation using the solubility product of $Cd(OH)_2$ [74] was at pH 8.2 and pH 8.6, respectively. This can suggest that it was not $Cd(OH)_2$ which precipitated out but one of complexes formed by Cyp_2EN and Cadmium.

4.3. Polarographic study of Cd–Cyp_2EN system

4.3.1. Data fitting

The modelling and refinement of stability constants using the data from polarography were described by Cukrowski [61, 62]. It was observed that the half-wave potential shifts to more negative values of the applied potential when the pH was increased. The DC_{tast} wave is the sum of the reduction and the background currents at any applied potential. For the purpose of fitting experimental polarograms, the reduction current I_r and the background current I_b are given by

$$I_r = \frac{I_d}{10 \times \exp\left[\frac{2 \times \delta \times (X - E_{1/2})}{0.05916} + 1\right]} \quad (56)$$

$$I_b = aX + b \tag{57}$$

where X stands for E_{applied}, I_{d} is the limiting diffusion current and δ is an additional parameter that is close to 1 for reversible electrochemical process. The total observed current from an experiment is given by:

$$y = I_r + I_b \tag{58}$$

The limiting diffusion current I_{d} does not depend on the electrochemical reversibility of the system under consideration. The data was fitted as obtained from the experiment and the values of a and b were allowed to vary as described in Equation 57. This system was also studied by DPP, where the fitting procedure involved Gaussian Equation and Equation of the background current.

$$I_r = I_p \times \exp\left[-\frac{\left(X - E_p\right)^2}{\left[2 \times \left(\frac{w_{1/2}}{2.345}\right)\right]}\right] \tag{58}$$

where I_{r} denotes the differential reduction current of the electrochemically active species, X is the E_{applied} i.e., applied step potential at which the reduction current is measured. The approximation of the background current was performed by means of a linear Equation 57 and the total current (y) was calculated by using Equation 58. The analysis of E_{p}, I_{p} and $w_{1/2}$ for DPP was carried out by using Equations seen above. It was observed that, during the refinement operation, the value of $w_{1/2}$ increased in the course of the experiment, resulting in a small departure from the reversibility when the pH increased as seen in Figure 4.5.

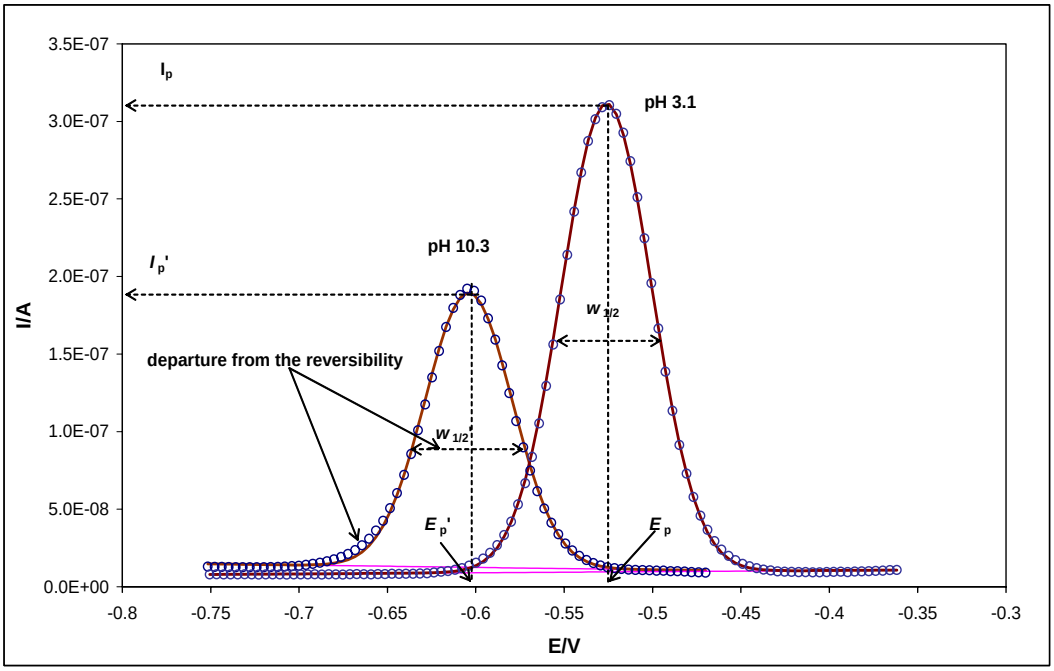

Figure 4.5: Example showing how the system became less reversible when the pH increased for Cd–Cyp_2EN system. L_T:M_T ratio 200 studied by DPP at 25°C and ionic strength 0.1 M in $NaNO_3$. $[M_T] = 1.99 \times 10^{-5}$ M and $[L_T] = 3.98 \times 10^{-3}$ M. The circles and solid lines indicate experimental and fitted curves, respectively.

This is shown by the experimental peak at pH 10.3, which became a little bit wider ($w_{1/2}$ = 63.5 mV) when the pH increased. As a result, the experimental parameter E_p was observed at more negative potential than it would be expected for a fully reversible signal. This behaviour results in the computed stability constants which being larger than expected. It is important to stress that I_p decreases when $w_{1/2}$ increases. The decrease in I_p implies the additional uncertainty in the values of E_p, which would make the stability constants also uncertain. That is the reason why the data from DPP was not considered for the refinement of stability constants. As the limiting diffusion current I_d does not depend on the reversibility of the system under consideration, only DC_{tast} was used.

4.3.2. Modelling of experimental data from DC_{tast}

i. Variation in limiting current

The variation in limiting current versus pH is presented in Figure 4.6. The experiment was performed from pH 4 to pH 10.5. In region I which correspond to the pH values between 4 and 6, there is almost no change in the limiting diffusion current. The dashed line indicates that the normalised limiting diffusion current in that pH range is almost equal to 1. This can suggest that either no complex was formed or if it was formed, it is a minor species in the solution.

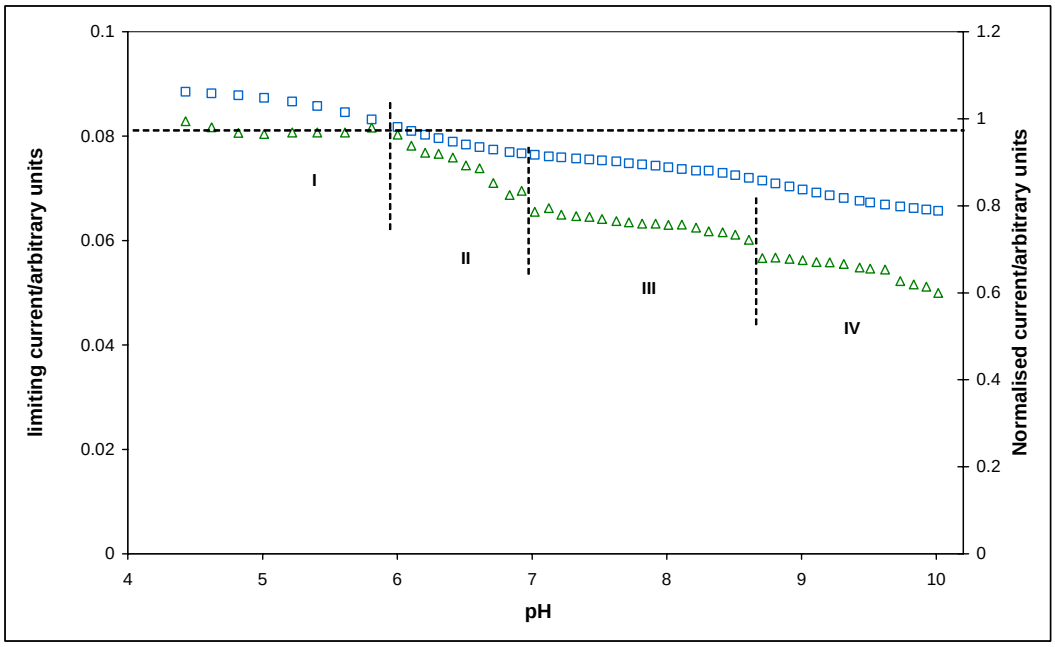

Figure 4.6: Variation in limiting diffusion current for Cd–Cyp_2EN system studied by DC_{tast} at L_T:M_T ratio 200, initial $[M_T] = 1.99 \times 10^{-5}$ M and $[L_T] = 3.98 \times 10^{-3}$ M, at 25 °C and ionic strength 0.1 M in $NaNO_3$. The dashed line and triangles indicate the normalised limiting diffusion current; the squares indicate the expected current when complexes are not formed.

At the pH values above 6, there is a small gradual decrease in the normalised current which reaches the value of about 0.6. This indicates the formation of consecutive labile complexes and three different labile complexes are predicted.

In region II between pH 6 and 7, the first labile complex seems to form in solution. The second labile complex seems to form in region III, which correspond to the pH values between 7 and 8.7. In this region a further decrease in the normalised current is observed. Another labile seems to form in region IV, where the decrease in the normalised current is observed again. This region corresponds to the pH values above 8.7. It is also clear that nonlabile complexes are not formed at all as I_d in that case would decrease to the much smaller value.

ii. Variation in the virtual half-wave potential vs. pH

Metal-ligand complexes can be predicted using a plot of the observed half-wave potential ($E_{1/2}$) vs. pH. When labile complexes are formed, a Nernstian slope is expected. The interpretation is that the dominance of a particular form of the ligand and metal species at a particular pH range generates a slope of $m\frac{(RT/nF)}{x}$ mV per pH unit where m is the number of protons involved; x is the number of metal ions in the complex and n is the number of electrons taking part in the electrochemical reaction [65]. Note that the observed slope is close to the Nernstian value only if one metal species is formed in the region where only one protonated form of the ligand is predominant. Otherwise, if many species are formed or if the complex is predominant in the region where two different forms of the ligand are present, the calculated slope will be slightly different to the Nernstian value. The observed slope is also due to species mainly reduced at the DME when several complexes are formed.

The form of the ligand in the pH range between 4 and 6 is H_2L. This is the region where M(HL) might be formed, but the slope observed is close to 0. The

slope expected for M(HL) formation in this region would be close to 30 mV per pH unit as shown by the following electrochemical process where one proton is involved at the DME:

$Cd(HL)^{3+} + H^{+} + 2e^{-} = Cd(Hg) + H_2L^{2+}$

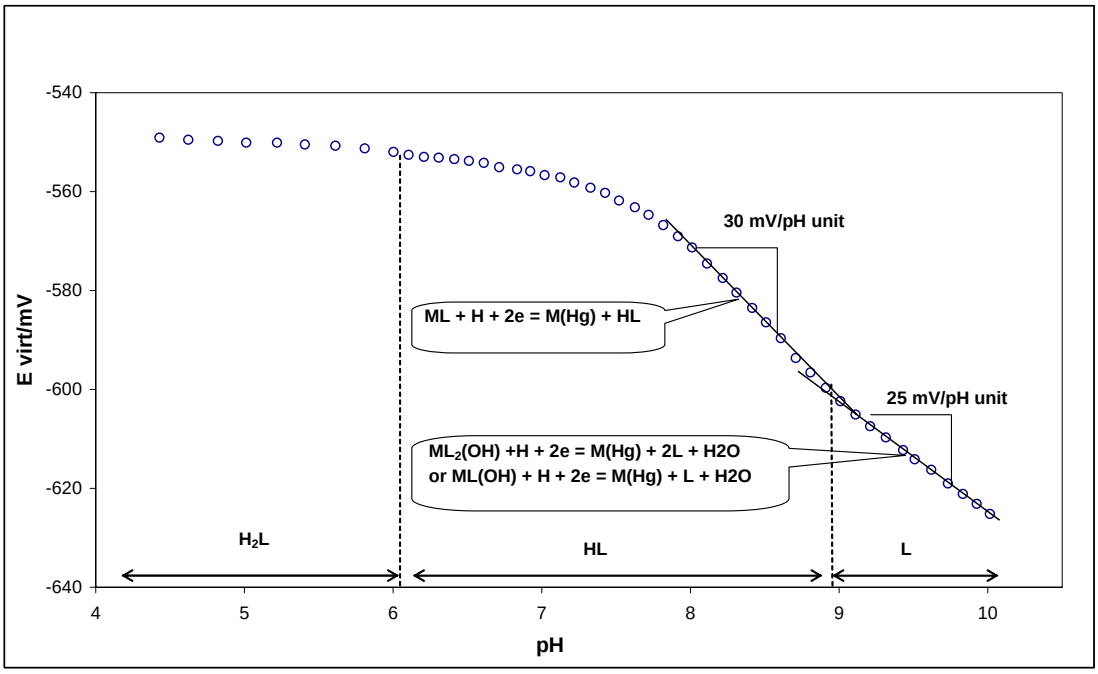

Figure 4.7: Variation in half–wave potential vs. pH for Cd–Cyp_2EN system studied by DC_{tast} at L_T:M_T ratio 200, initial $[M_T] = 1.99 \times 10^{-5}$ M and $[L_T] = 3.98 \times 10^{-3}$ M, at 25 °C and ionic strength 0.1 M in $NaNO_3$.

The slope of the value close to 0 is also observed in the pH range 6 and 7.5, where the predominant form of the ligand is HL^{+}. This can indicate the formation of the complex M(HL) following the electrochemical process where no proton is involved at the DME:

$Cd(HL)^{3+} + 2e^{-} = Cd(Hg) + HL^{+}$

Between pH 7.5 and 9 a slope of about 30 mV per pH unit is observed. This slope can be considered as close to the theoretical value when one proton is involved in

electrochemical reaction. In this pH range the HL^+ form of the ligand Cyp_2EN is predominant. Hence one can suggest the formation of ML, which undergoes the following reaction at the DME:

$CdL^{2+} + H^+ + 2e^- = Cd(Hg) + HL^+$

However, the marked slope can also indicate the presence of another metal complex. For instance, the complex $Cd(OH)^+$ also requires one proton when reduced at the DME as indicated by the following electrochemical reaction:

$Cd(OH)^+ + H^+ + 2e^- = Cd(Hg) + H_2O$

Another slope of about 25 mV per pH unit is observed in the region where the predominant form of the ligand is L. This might indicate the formation of hydroxospecies in the solution for which the electrochemical processes at the DME would be:

$CdL(OH)^+ + H^+ + 2e^- = Cd(Hg) + L + H_2O$

or

$CdL_2(OH)^+ + H^+ + 2e^- = Cd(Hg) + 2L + H_2O$

However, the reduction of ML_2 complex also involves one proton with the formation of both form of the ligand as indicated by the following electrochemical process at the DME:

$CdL_2^{2+} + H^+ + 2e^- = Cd(Hg) + L + HL^+$

The slope observed is less than the one predicted when one proton is involved. This strongly suggests that metal species ML_x still remain in the solution at a significant level. If hydroxospecies were the only species reduced at the DME, then the observed slope would be at least 30 mV per pH unit.

From the above, the formation of ML and ML_2 has been confirmed. In addition, complexes M(HL) and $ML_j(OH)$ should be tested in the refinement operations.

iii. Variation in the virtual half-wave potential vs. log [L]

The relationship between log [L] and variation in half-wave potential can also predict which species is formed in the solution (see Figure 4.8). Same Equation used in section (*ii*) to calculate slopes is also used in this section, but the number of protons *m* involved in the electrochemical process is replaced by the number of the ligands *j*. Then Equation becomes $j\frac{(RT/nF)}{x}$ [65].

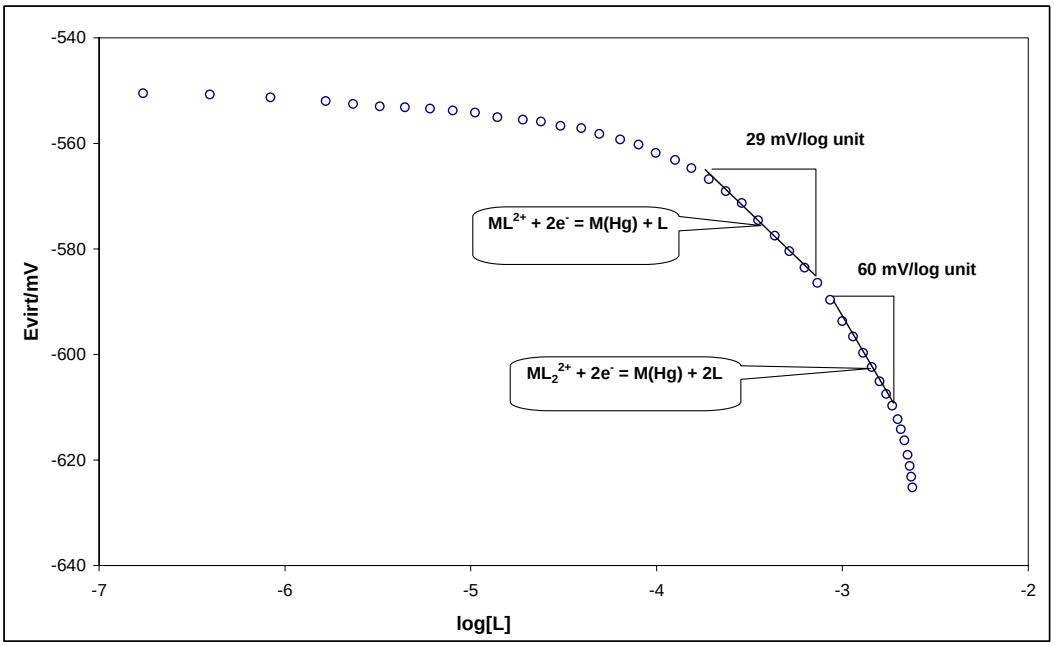

Figure 4.8: Variation in half–wave potential vs. log [L] for Cd–Cyp_2EN system studied by DC_{tast} at L_T:M_T ratio 200, initial $[M_T] = 1.99 \times 10^{-5}$ M and $[L_T] = 3.98 \times 10^{-3}$ M, at 25°C and ionic strength 0.1 M in $NaNO_3$.

In Figure 4.8, a slope of 29 mV per log unit is observed. This slope can confirm the presence of ML complex predicted in Figure 4.7. The reaction involved is

$CdL^{2+} + 2e^{-} = Cd(Hg) + L$

Another slope of 60 mV per log unit is also observed. This slope suggests the formation of ML_2 complex, which was also predicted in Figure 4.7. This complex is formed as indicated by the following reaction

$CdL_2^{2+} + 2e^{-} = Cd(Hg) + 2L$

iv. Virtual half-wave potential vs. log [M]

The use of virtual potential [64, 71] helped in the determination of a potentiometric sensor E^o. This E^o was used in the refinement of the data from polarography by ESTA software. Instead of the observed half-wave potential, the virtual half–wave potential was used. This is illustrated in Figure 4.9. The slope obtained was close to the Nernstian slope, which supported the proposed model and refined stability constants.

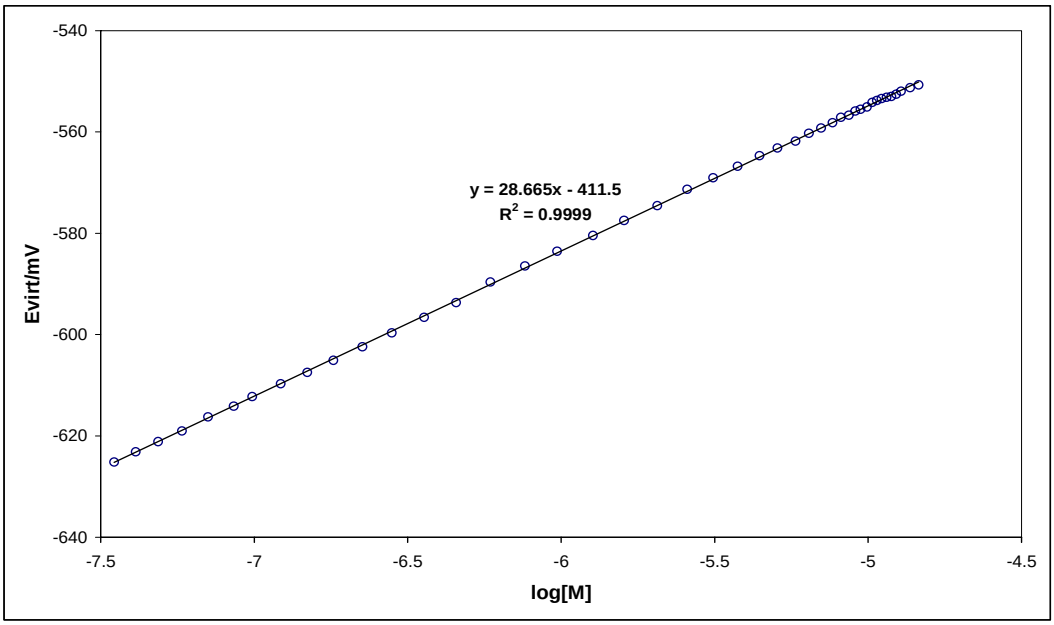

Figure 4.9: Virtual half-wave potential as a function of log [M] for Cd–Cyp_2EN system studied by DC_{tast} at L_T:M_T ratio 200, initial $[M_T] = 1.99 \times 10^{-5}$ M and $[L_T] = 3.98 \times 10^{-3}$ M, at 25°C and ionic strength 0.1 M in $NaNO_3$.

v. Corrected shift in half–wave potential vs. pH

The complex formation curves for the proposed model are shown in Figure 4.10. The ECFC is shown as circles. The CCFC (solid line) for the model M(HL), ML, ML_2 and ML(OH) is the same as for the model M(HL), ML, ML_2 and ML_2(OH). Refined stability constants for both models are presented in Table 4.4.

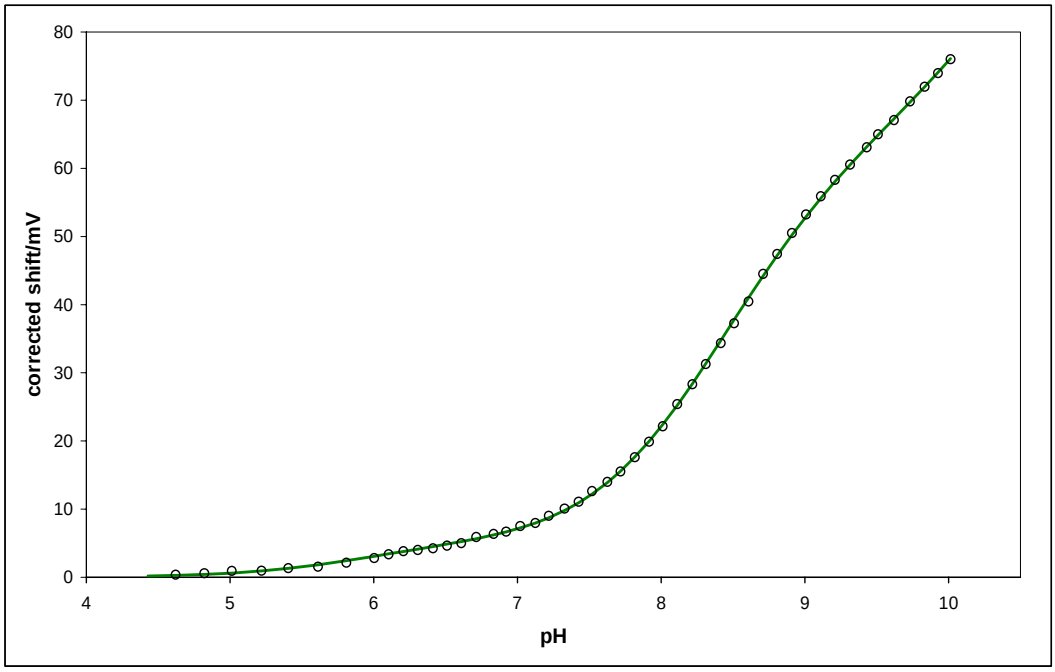

Figure 4.10: Experimental and calculated complex formation curves for Cd–Cyp_2EN system studied by DC_{tast} at L_T:M_T ratio 200, initial $[M_T] = 1.99 \times 10^{-5}$ M and $[L_T] = 3.98 \times 10^{-3}$ M, at 25°C and ionic strength 0.1 M in $NaNO_3$. The circles indicate the experimental corrected shift in DC_{tast} half-wave potential calculated for each data point. The solid line represents the CCFC for the optimised M–L model.

During refinement operation, software 3D–CFC [73] could not distinguish between ML(OH) and ML_2(OH) complexes. The computed log β of ML(OH) (log β = 8.8) is much larger than the one expected for simple hydrolysis of a ML complex.

$$\log \beta_{ML(OH)} = \log K_{ML} + \log K_{M(OH)}; \log \beta_{ML(OH)} = 4 + 3.9 = 7.9$$

The computed log β of $ML_2(OH)$ complex with a value of 11.4 is close to the theoretical value which is 11.2 as shown by the following reaction:

$$\log \beta_{ML_2(OH)} = \log K_{ML_2} + \log K_{M(OH)}; \log \beta_{ML_2(OH)} = 7.3 + 3.9 = 11.2$$

This can suggest that the more appropriate interpretation for Cd–Cyp_2EN system is given by the model M(HL), ML, ML_2 and $ML_2(OH)$. But, as these two complexes (ML(OH) and $ML_2(OH)$) are predicted to form in the pH range where the ligand is fully deprotonated (see Figure 4.7), one cannot really distinguish which one is formed. Either one of them is formed or both are present in solution.

vi. Species distribution diagram

The species distribution diagram is presented in Figure 4.11. It shows that the complex M(HL) is present in the pH range between 5 and 8. The small shift observed in Figure 4.9 between pH 5 and 6.5 is due to the formation of M(HL), because, at that pH, only M(HL) complex is present. At pH about 6.8, M(HL) complex is at its maximum concentration. In this pH range, the predominant form of the ligand is HL. This can explain the reason why, in Figure 4.7, the slope observed in the pH range between 6 and 7.5 was so small. Below pH 6 the concentration of M(HL) complex was not high enough to cause a significant shift. The Figure 4.11 shows that the complex ML_2 presents a significant amount above pH 9. This is in a good agreement with the slope of 25 mV per pH unit observed in Figure 4.7 above pH 9. If the complex $ML_2(OH)$ (or ML(OH)) was a major species in the solution, a slope of about 30 mV per pH unit was supposed to be observed. Then, the slope of 25 mV per pH unit suggests that the species mainly reduced at the DME was ML_2. The complex ML also was still remaining in that

pH range, but at much smaller concentration than ML_2 complex. The same Figure shows that the formation of hydroxospecies occurs when the ligand is fully deprotonated. This can explain the reason why the refinement operations could not distinguish between ML(OH) and $ML_2(OH)$ (see Table 4.4) since according to the following reactions

$$ML(OH)^+ + H^+ + 2e^- = M(Hg) + L + H_2O$$

and

$$ML_2(OH)^+ + H^+ + 2e^- = M(Hg) + 2L + H_2O,$$

one proton is involved for both electrochemical reactions for which the free ligand is generated.

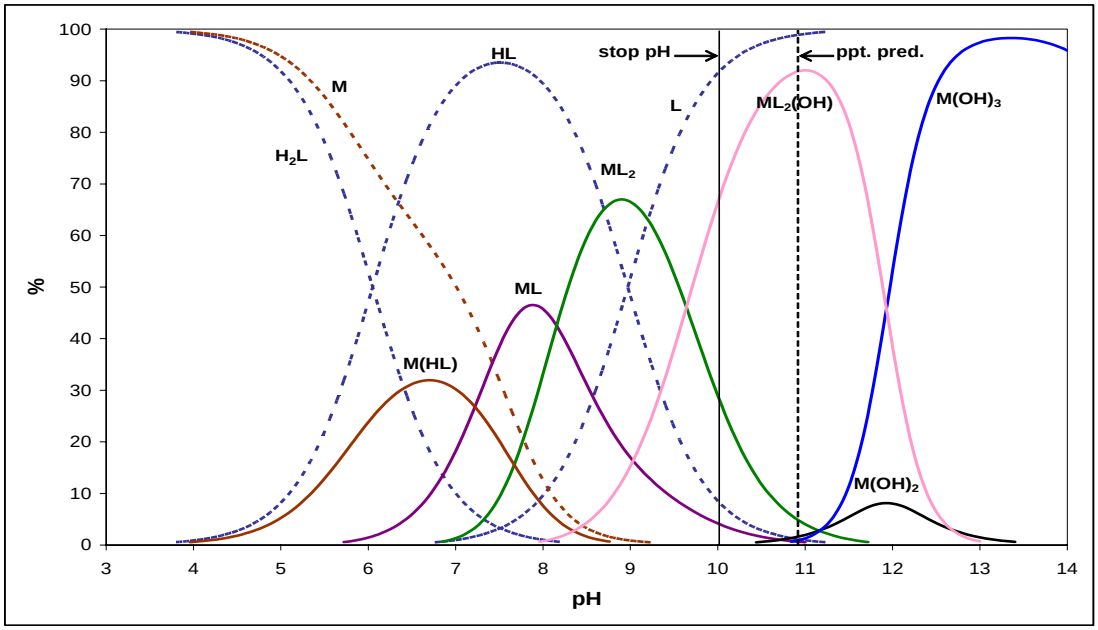

Figure 4.11: Species distribution diagram for Cd–Cyp_2EN system ratio L_T:M_T 200 studied by DC_{tast} at 25°C and ionic strength 0.1 M in $NaNO_3$. $[L_T] = 3.98 \times 10^{-3}$ M and $[M_T] = 1.99 \times 10^{-5}$ M.

From the above, one can suggest that the model from polarography is M(HL), ML, ML_2 and $ML_2(OH)$. Refined stability constants from DC_{tast} are presented in Table 4.4.

Table 4.4: Model and stability constants obtained for Cd–Cyp_2EN system studied by DC_{tast}, L_T:M_T ratio 200

M(HL)	ML	ML_2	ML(OH)	$ML_2(OH)$	R-Factor
11.20 (04)	3.98 (04)	7.26 (03)	excluded	11.40(03)	0.0529
11.18 (04)	3.98 (04)	7.18(04)	8.8 (03)	excluded	0.0531

4.4. Study of Cd-Cyp_2EN by potentiometry + polarography

Another approach used in the refinement of stability constants for Cd–Cyp_2EN involved the refinement of GEP data combined with polarographic data using ESTA software package. This approach involved the use of virtual potential data. Another approach of refinement was adopted where only data from polarography (using virtual potential) were entered into ESTA software. The stability constants obtained in this regard were comparable with those obtained from GEP and DC_{tast}. All the results obtained for Cd–Cyp_2EN system are presented in Table 4.5. The refinement operations using GEP + VP–DC support the model for Cd–Cyp_2EN system obtained from the DC_{tast} experiment. As discussed before, the complex $ML_2(OH)$ will be considered instead of ML(OH) complex in the final model, but one cannot confirm that ML(OH) does not exist in solution. If the species distribution diagram is calculated for potentiometric conditions, one can see that it was impossible to refine $ML_2(OH)$ by GEP because of the precipitation that occurred when $ML_2(OH)$ just started to be present in the solution (see Figure 4.12). From this, one can conclude that GEP could not generate a full model for Cd–Cyp_2EN system. The use of DC_{tast} helped to get the final model by including hydroxospecies in this model.

Table 4.5: Model and stability constants obtained for Cd–Cyp_2EN system at 25°C and ionic strength 0.1 M in $NaNO_3$.

Technique	Equilibrium	Log β	R-Factor
GEP	M + H + L = M(HL)	11.31(01)	0.00412
	M + L = ML	3.96(01)	
	M + 2L = ML_2	7.24(01)	
DC_{tast}	M + H + L = M(HL)	11.20(04)	0.0529
	M + L = ML	3.98(04)	
	M + 2L = ML_2	7.26(03)	
	M + 2L + OH = ML_2(OH)	11.40(04)	
VP-DC	M + L + H = M(HL)	11.10(04)	0.0012
	M + L = ML	3.86(04)	
	M + 2L = ML_2	7.20(03)	
	M + 2L + OH = ML_2(OH)	11.28(02)	
GEP + VP-DC (Final model)	M + H + L = M(HL)	11.35(01)	0.00154
	M + L = ML	3.98(01)	
	M + 2L = ML_2	7.28(02)	
	M + 2L + OH = ML_2(OH)	11.49(01)	

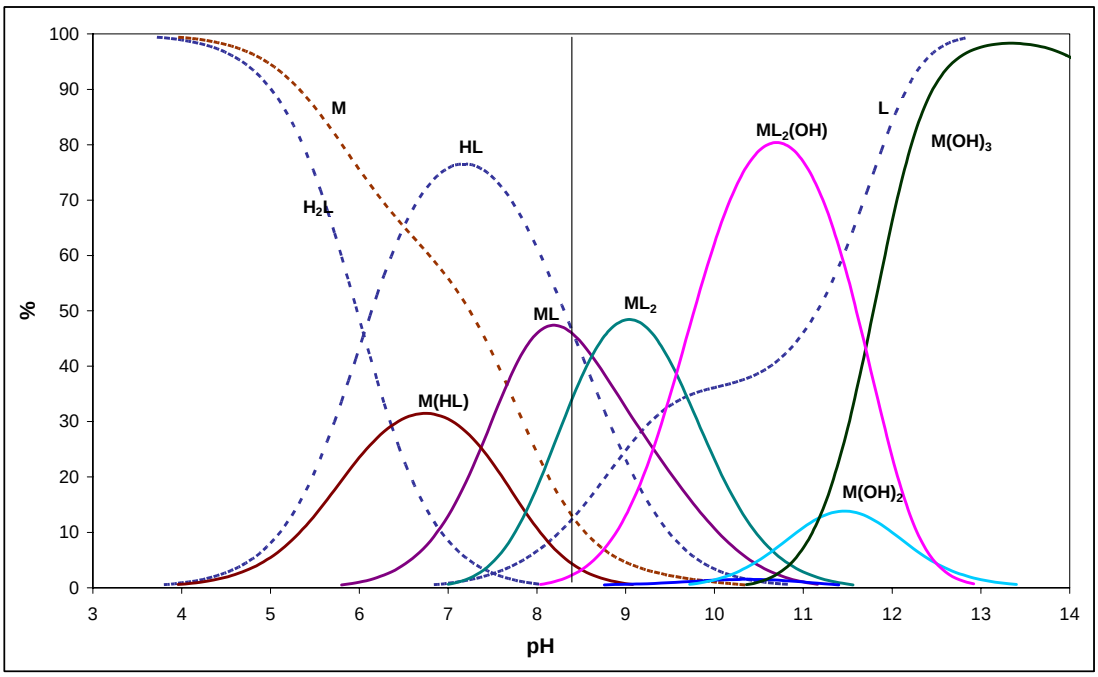

Figure 4.12: Species distribution diagram for Cd–Cyp_2EN system using the results from GEP + VP-DC and conditions from potentiometry. $[L_T] = 3.00 \times 10^{-3}$ M and $[M_T] = 1.00 \times 10^{-3}$ M.

In order to investigate further whether the complex ML(OH) was formed, the stability constant of ML(OH) complex was fixed at 7.9 (theoretical value) in the refinement of the data by ESTA (GEP + VP/DC). It was observed that the stability constants for M(HL) and ML did not change, and the stability constants for ML_2 and $ML_2(OH)$ changed only slightly. The values of stability constants obtained were 11.35, 3.98, 7.27, and 11.45 for M(HL), ML, ML_2 and $ML_2(OH)$, respectively. The species distribution generated using this model with fixed stability constant for ML(OH) complex at 7.9 (see Figure 4.13) showed that the complex ML(OH) was a minor species and formed under $ML_2(OH)$ complex. This can explain the reason why it was not possible to fit ML(OH) in the presence of $ML_2(OH)$ complex.

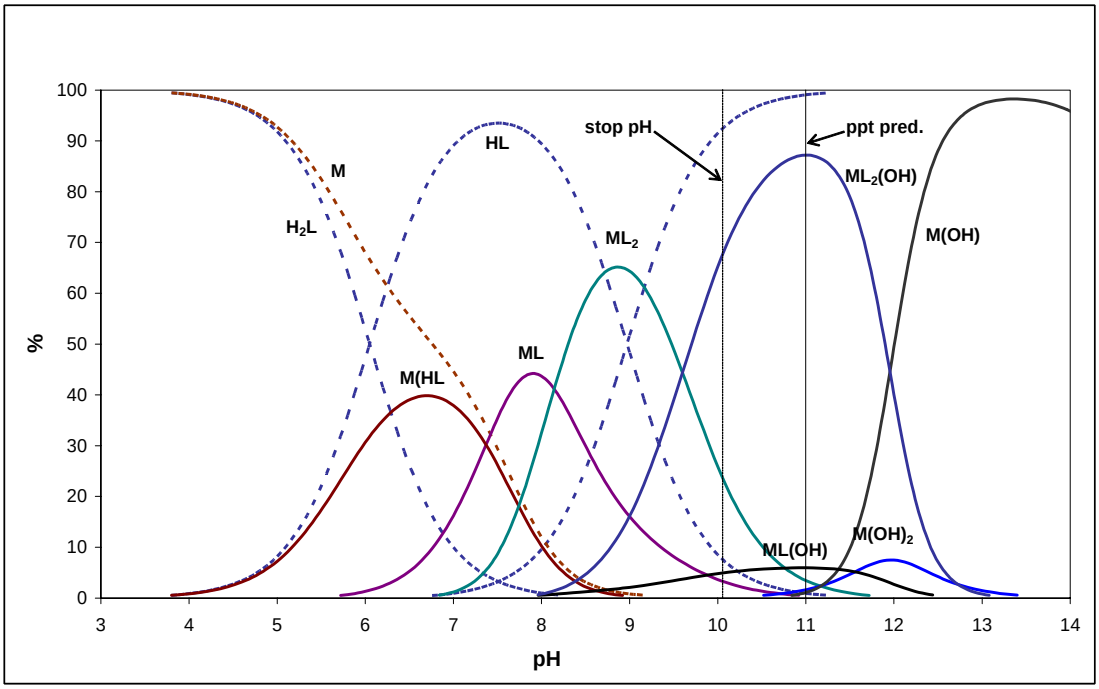

Figure 4.13: Species distribution diagram for Cd–Cyp_2EN system by GEP + VP-DC calculated using polarographic conditions and the model obtained when the stability constant of ML(OH) was fixed at 7.9. $[L_T] = 3.98 \times 10^{-3}$ M and $[M_T] = 1.99 \times 10^{-5}$ M.

4.5. Study of Pb–Cyp$_2$EN system by GEP

4.5.1. Data refinement

Three titrations were performed from pH 3 to pH 8.5, at 25 ± 0.1 ° C and ionic strength of 0.1 M in $NaNO_3$. The pK_w was fixed at 13.78 [74]. Precipitation was observed for all ratios studied. The precipitation occurred at pH 7.8, 8.3, and 8.7 for ratios 1, 2, and 3, respectively. The results obtained are presented in Table 4.6.

Table 4.6: Model and stability constants obtained for Pb–Cyp$_2$EN system studied by GEP at 25°C and ionic strength 0.1 M in $NaNO_3$.

L_T:M_T ratio	M(HL)	ML	ML(OH)	ML(OH)$_2$	R-Factor	Remarks
1 $[L_T]$ =2.01 × 10^{-3}M $[M_T]$ =1.99 × 10^{-3}M	11.57(01)	4.93(01)	10.74(02)	Rejected	0.01372	base refined 0.0101M⇒0.0100685 M
	11.58(01)	4.94(01)	10.78(02)	Rejected	0.01365	acid refined 0.0103M⇒0.0103194 M
	excluded	4.89(02)	10.42(07)	Rejected	0.05450	acid refined 0.0103M⇒0.0103308 M
	excluded	4.88(03)	10.32(09)	Rejected	0.05381	base refined 0.0101M⇒0.0099493 M
2 $[L_T]$ =2.67 × 10^{-3}M $[M_T]$ =1.34 × 10^{-3}M	11.78(01)	5.03(01)	10.89(01)	Rejected	0.01021	base refined 0.0101M⇒0.009982 M
	11.80(01)	5.08(01)	11.00(01)	Rejected	0.01184	acid refined 0.0103M⇒0.0103194 M
	excluded	4.79(03)	10.52(03)	Rejected	0.05359	acid refined 0.0103M⇒0.010375 M
		4.72(03)	10.32(05)	Rejected	0.05162	base refined 0.0101M⇒0.0098506 M
3 $[L_T]$= 2.99 × 10^{-3}M $[M_T]$ =1.00 × 10^{-3}M	11.88(01)	5.12(01)	10.77(01)	15.17(02)	0.00494	base refined 0.0101M⇒0.0099817 M
	11.91(01)	5.205 (005)	10.91(01)	15.41(01)	0.00530	acid refined 0.0103M⇒0.0103483 M
	excluded	4.83(03)	10.19(06)	15.10(08)	0.04379	acid refined 0.0103 M⇒0.010373 M
	excluded	4.71(03)	9.64(20)	14.97(09)	0.04185	base refined 0.0101 M⇒0.009826 M
Combined refinement	**11.73(01)**	**5.05(01)**	**10.81(02)**	**14.96(07)**	**0.02007**	**Base refined** **R1: 0.0101 M⇒0.01004 M** **R2: 0.0101 M⇒0.00997 M** **R3: 0.0101 M⇒0.00998 M**
	11.74(01)	**5.06(01)**	**10.82(01)**	**14.98(06)**	**0.01873**	**Acid refined** **R1: 0.0103 M⇒0.01033 M** **R2: 0.0103 M⇒0.01036 M** **R3: 0.0103 M⇒0.01036 M**
	excluded	**4.78(02)**	**10.06(07)**	**15.09(08)**	**0.04880**	**Base refined** **R1: 0.0101 M⇒0.00993 M** **R2: 0.0101 M⇒0.00984 M** **R3: 0.0101 M⇒0.00986 M**
	excluded	**4.85(02)**	**10.32(04)**	**15.18(02)**	**0.04976**	**Acid refined** **R1: 0.0103 M⇒0.01034 M** **R2: 0.0103 M⇒0.01038 M** **R3: 0.0103 M⇒0.01037 M**

As for Cd–Cyp_2EN system, three titrations were combined and refined simultaneously by ESTA software. Generally, the acid and/or base concentrations have also been optimised during the refinement operations. This caused a small variation in the optimised model and calculated stability constants. The complex $ML(OH)_2$ was rejected by the software for L_T:M_T ratios 1 and 2. This can be explained by the fact that there were not enough experimental points to compute the stability constant for $ML(OH)_2$ complex due to the precipitation that was observed at pH 7.8 and 8.2 for L_T:M_T ratios 1 and 2, respectively.

4.5.2. Complex formation function $\overline{Z}_M$

The complex formation function $\overline{Z}_M$ showed a better fit for three titrations when they were combined and refined simultaneously as shown by Figure 4.14. It was calculated for the model M(HL), ML, ML(OH), and $ML(OH)_2$.

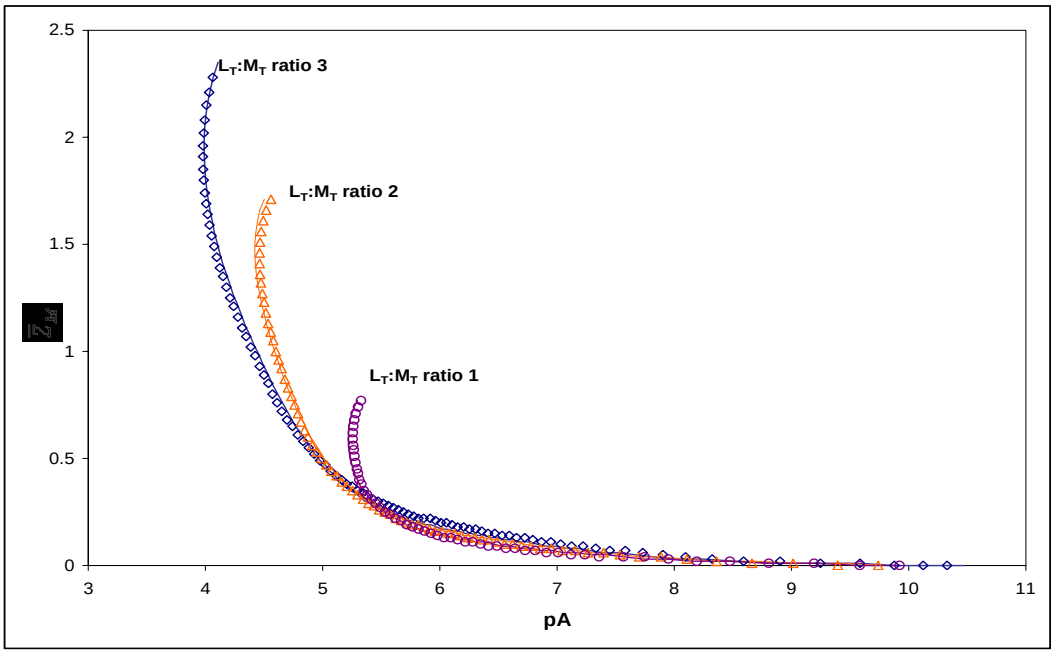

Figure 4.14: Complex formation curves for Pb–Cyp_2EN system studied by potentiometry at 25°C and ionic strength 0.1 M in $NaNO_3$. Circles, triangles and diamonds represent experimental points for L_T:M_T ratio 1, 2, and 3, respectively. The solid lines represent the fitted curves.

A slight change of $\overline{Z}_M$ observed between pA 6 and 8 can suggest the formation of M(HL) complex and a visible change of $\overline{Z}_M$ between pA 4 and 6 might confirm the presence of ML complex. The presence of ML(OH) and $ML(OH)_2$ can be confirmed by the observed back-fanning feature in Figure 4.14, but it is not pronounced because of the precipitation that occurred early.

4.5.2. Species distribution diagram

The species distribution diagram in Figure 4.15 was calculated using the stability constants from the combined refinement and potentiometric conditions for L_T:M_T ratio 1.

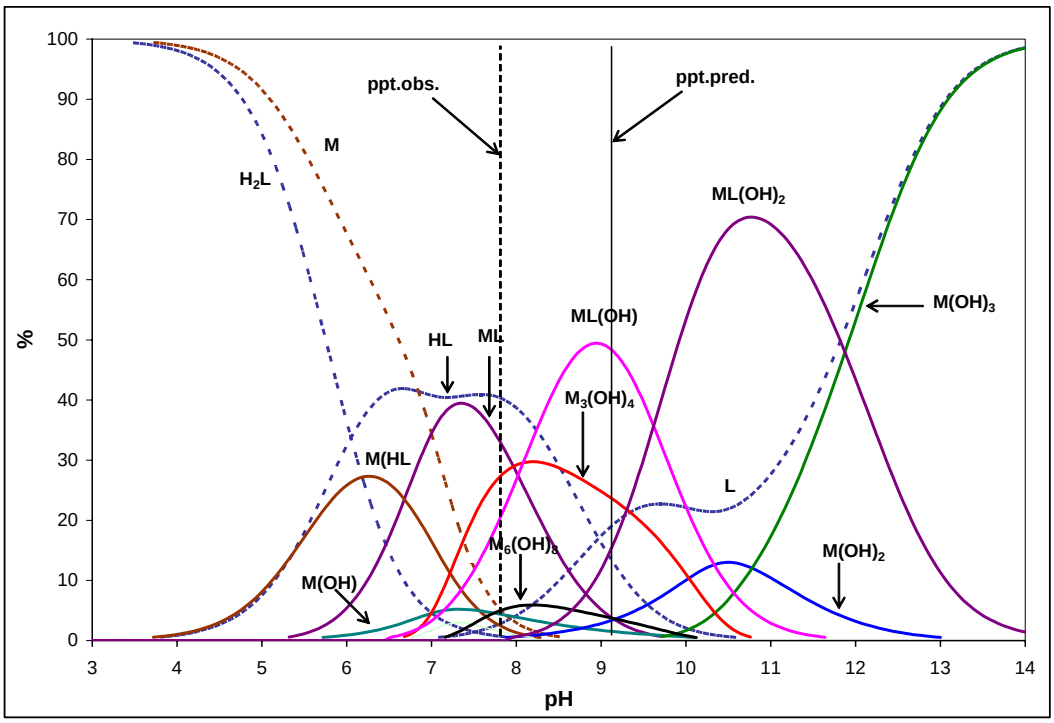

Figure 4.15: Species distribution diagram for Pb–Cyp_2EN system calculated using the results from the combined refinement and potentiometric conditions for L_T:M_T ratio 1. $[L_T] = 2.00 \times 10^{-3}$ M and $[M_T] = 2.00 \times 10^{-3}$ M.

This Figure shows that, at very low ratios as those used in potentiometry, the polynuclear species ($M_3(OH)_4$ and $M_6(OH)_8$) constitute a significant percentage of lead species. The predicted precipitation using the solubility product of $Pb(OH)_2$ [74] for ratios 1 and 2 was at pH 9 and 9.3, respectively. The precipitation was observed at pH 7.8 and 8.2 for these ratios. This can justify the reason why the complex $ML(OH)_2$ was not refined for L_T:M_T ratios 1 and 2. This is clearly observed in Figure 4.15, which shows that the complex $ML(OH)_2$ started to be present in solution only above pH 8. The few points recorded after pH 8 for L_T:M_T ratio 2 were not enough to compute $ML(OH)_2$ complex. Note that the data recorded for L_T:M_T ratio 3 could refine $ML(OH)_2$. The precipitation appeared at pH 8.7 when $ML(OH)_2$ was already present from pH 8. From GEP, one can propose the following model for Pb–Cyp_2EN system: M(HL), ML, ML(OH) and $ML(OH)_2$.

4.6. Polarographic study of Pb–Cyp_2EN system

4.6.1. Data treatment

For fully reversible system, the DPP polarograms are characterised by a peak width ($w_{1/2}$) of approximately 62 mV throughout the experiment. The fitting of this kind of polarograms is a straightforward matter and this was the case for Pb–Cyp_2EN system. The fitting of the data showed that the system was fully reversible; the value of $w_{1/2}$ was between 59 and 62 mV for all DPP polarograms. Two different L_T:M_T ratios were investigated for Pb–Cyp_2EN system, ratio 50 and ratio 83, the model obtained from them is ML, ML(OH) and $ML(OH)_2$ for ratio 50 and M(HL), ML, ML(OH) and $ML(OH)_2$ for ratio 83.

4.6.2. Modelling of experimental data from DPP ratio L_T:M_T 50

The peak width was close to 62 mV up to pH 8.8 followed by a slight decrease to a value of 59 mV up to pH 10.7. Hence, for a fully reversible electrochemical reduction process studied by DPP, the peak width is expected to be 62 mV, the Pb–Cyp_2EN system could be regarded as a reversible. The variation in the peak width observed could be attributed to the change in the diffusion coefficients rather than to a significant change in electron transfer rate. Similar observations were made for DC_{tast} where the value of δ varied between 1 and 0.89.

i. The variation in the DPP peak height with pH

The variation in the peak height contributes to the interpretation of a model and to the calculated overall stability constants. The plot in Figure 4.16 provides significant information about the system Pb–Cyp_2EN.

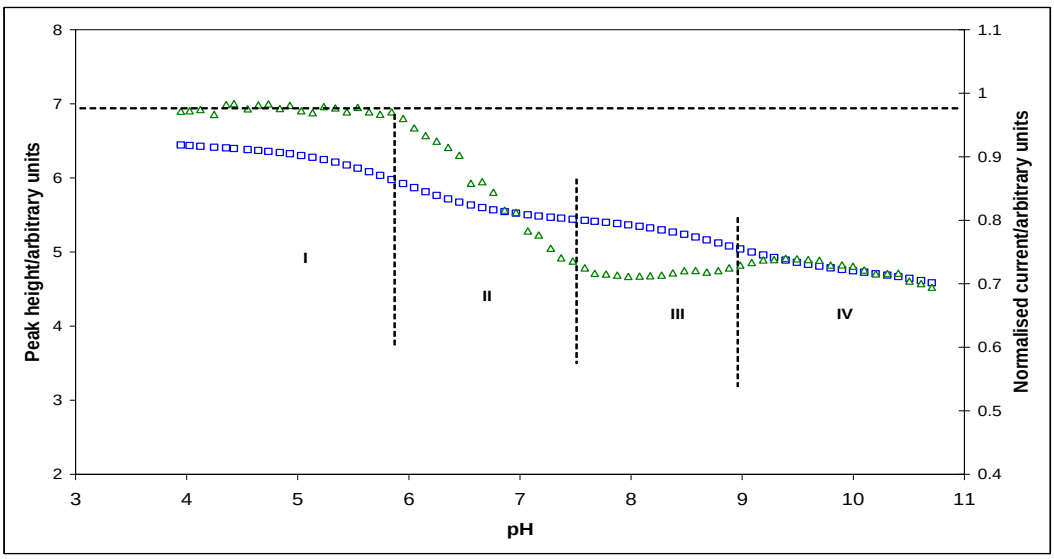

Figure 4.16: Pb–Cyp_2EN system studied by DPP at L_T:M_T ratio 50. The dashed line indicates the normalised peak height (triangles). Squares represent expected peak height if the metal complexes were not formed (if the observed decrease at high pH is only caused by dilution of the sample). $[M_T] = 8.01 \times 10^{-5}$ M and $[L_T] = 4.029 \times 10^{-3}$ M.

Initially the normalised I_p (triangles) has a constant value of about 0.99 in the pH range 4-6. In this pH range, there is no complex formed or if it is formed it could be a minor species (region I). Between pH 6 and pH 7.5 (region II) a notable decrease in the normalised peak current is observed. This can suggest that there is a formation of a labile complex. In region III, another labile complex seems to form. This region corresponds to the pH range between 7.5 and 9. Above pH 9 (region IV), a slight increase in the peak height is observed followed by a small decrease which reaches a value of 0.7 of the normalised current. This suggests the formation of successive labile complexes.

ii. Variation in the virtual peak potential with pH

As shown in Figure 4.17, there is no shift in the peak potential up to pH 6. A visible shift is observed in the pH range where HL is the predominant form of the ligand. In this pH range a slope of about 30 mV per pH unit is observed. This slope suggests the formation of PbL^{2+} complex according to the following reaction at the DME:

$PbL^{2+} + H^+ + 2e^- = Pb(Hg) + HL^+$

The marked slope can also indicate the presence of $Pb(OH)^+$ complex which require one proton when reduced at the DME as shown by the following electrochemical process:

$Pb(OH)^+ + H^+ + 2e^- = Pb(Hg) + H_2O$

The variation in the virtual peak potential vs. pH also shows a slope of about 40 mV in the pH range between 8 and 10, where the complex $PbL(OH)^+$ is supposed to be formed. As the electrochemical process predicts, a slope of about 30 mV or

60 mV is observed if ML(OH) complex is formed in the region where the predominant form of the ligand is L or HL, respectively. Then the electrochemical process at the DME for the formation of ML(OH) complex involves one or two proton(s) and is presented as follows:

$PbL(OH)^{+} + H^{+} + 2e^{-} = Pb(Hg) + H_2O + L$

or

$PbL(OH)^{+} + 2H^{+} + 2e^{-} = Pb(Hg) + H_2O + HL^{+}$

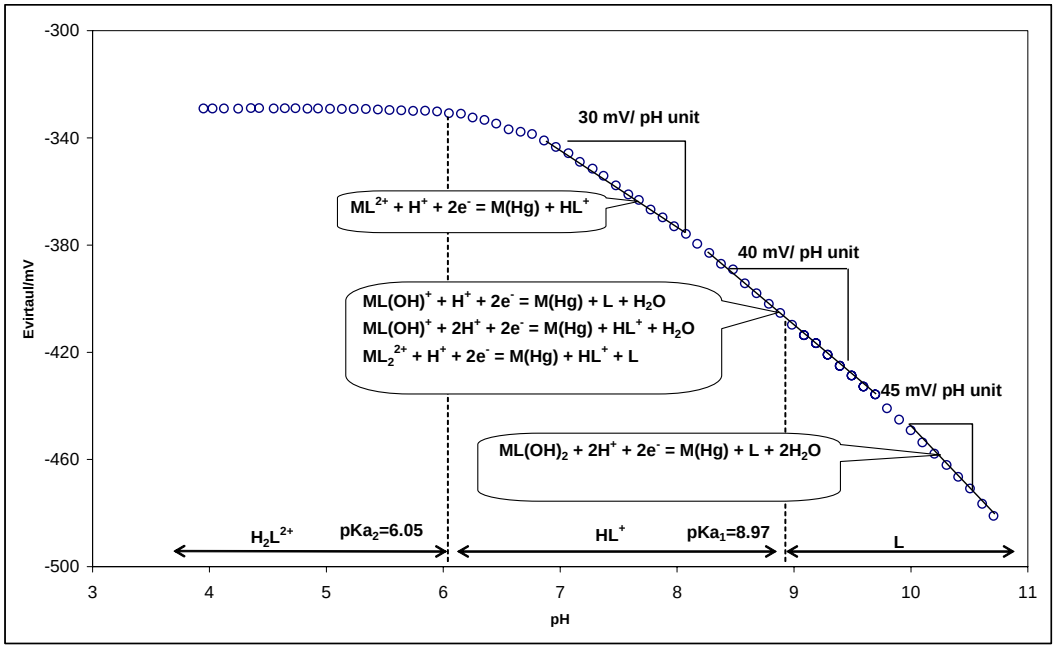

Figure 4.17: Variation in virtual peak potential versus pH for Pb–Cyp_2EN system L_T:M_T 50 ratio studied by DPP at 25°C and ionic strength 0.1 M in $NaNO_3$. $[M_T] = 8.01 \times 10^{-5}$ M and $[L_T] = 4.029 \times 10^{-3}$ M.

According to Figure 4.17, the formation of $PbL(OH)^{+}$ might start its formation in the region where HL is the predominant form of the ligand, and continues in the region where the deprotonated ligand is predominant. This can justify the intermediate slope of about 40 mV observed. The same slope can also predict the formation of ML_2 complex. The reduction of this complex at the DME would

involve one proton and produce HL^+ and L as indicated by the following electrochemical process:

$CdL_2^{2+} + H^+ + 2e^- = Cd(Hg) + HL^+ + L$

In the pH range above 10, a slope of 45 mV/ pH unit is observed. This slope predicts a formation of another species. The complex suspected to form in the solution is $PbL(OH)_2$, but the slope observed is lower than the slope predicted for its formation, which is close to 60 mV/pH unit, assuming that $ML(OH)_2$ is the only and major metal species. The slope of 45 mV observed suggests that the complex $PbL(OH)^+$ still remains in a solution. The electrochemical process for the formation of $PbL(OH)_2$ complex involves two protons at the DME and is presented by the following reaction:

$PbL(OH)_2 + 2H^+ + 2e^- = Pb(Hg) + 2H_2O + L$

iii. Variation in virtual potential with Log [*L*]

The variation in virtual peak potential can also predict which species is formed in the solution. This is seen in Figure 4.18. A slope of about 30 mV per log unit seen in Figure 4.18 supports the formation of ML complex which is involved in the following reaction at the DME:

$PbL^{2+} + 2e^- = Pb(Hg) + L$

where one ligand is liberated (hence slope of about 30 mV per log unit). A further increase in the slope is observed at – log of about 3.4–2.9 (about 70 mV/log unit). This could be either due to the ML_2 formation or due to the deprotonation of the ligand. If ML_2 is reduced at the DME, then the following electrochemical process takes place:

$PbL_2^{2+} + 2e^- = Pb(Hg) + 2L$

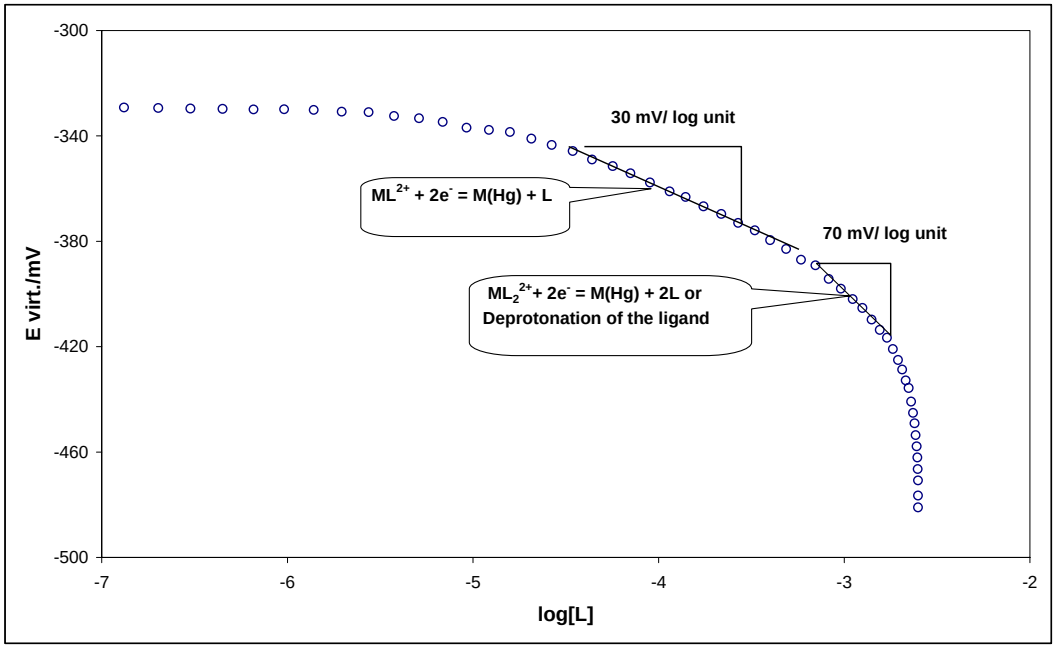

Figure 4.18: Variation in virtual peak potential versus log [L] for Pb–Cyp_2EN system at 25°C and ionic strength 0.1 M in $NaNO_3$. $[M_T] = 8.01 \times 10^{-5}$ M, and $[L_T] = 4.029 \times 10^{-3}$ M.

iv. Complex formation curves (ECFC, CCFC)

The experimental and calculated complex formation curves are illustrated in Figure 4.19. One can observe that a good fit was obtained for the model ML, ML(OH) and $ML(OH)_2$. The Figure 4.19 shows that there is no shift in the pH range between 4 and 6. A visible shift starts at about pH 6, and continues up to pH 10.7. This suggests a successive formation of labile complexes. For L_T:M_T ratio 83, it was possible to refine M(HL), but the standard deviation was rather high. This suggests that M(HL) is a minor species in the solution. The values of refined stability constants obtained are presented in Table 4.7.

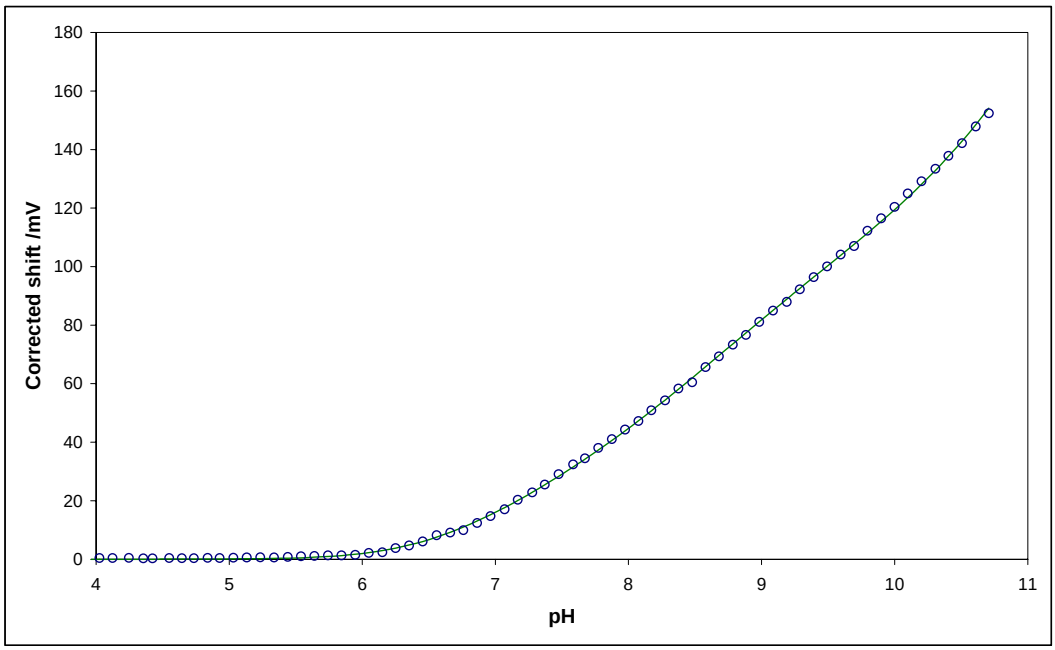

Figure 4.19: Experimental (circles) and calculated (solid line) complex formation curves for Pb–Cyp_2EN system for the model ML, ML(OH) and $ML(OH)_2$ derived from this work. $[M_T] = 8.01 \times 10^{-5}$ M and $[L_T] = 4.029 \times 10^{-3}$ M.

Table 4.7: Model obtained for Pb–Cyp_2EN system studied at different ratios by DPP and DC_{tast}.

L_T:M_T ratio	M(HL)	ML	ML(OH)	$ML(OH)_2$	R-Factor
50 (DPP) $[M_T]=8.01\times10^{-5}$ M $[L_T]=4.03\times10^{-3}$ M	Rejected	4.89(01)	10.30(01)	13.36(08)	0.3388
50(DC) $[M_T]=8.01\times10^{-5}$ M $[L_T]=4.03\times10^{-3}$ M	Rejected	4.89(01)	10.33(01)	12.32(69)	0.5840
83 (DPP) $[M_T]=5.35\times10^{-5}$ M $[L_T]=4.45\times10^{-3}$ M	10.82(10)	4.76(02)	10.30(02)	13.86(08)	0.293
83 (DC) $[M_T]=5.35\times10^{-5}$ M $[L_T]=4.45\times10^{-3}$ M	10.66(14)	4.76(02)	10.25(02)	13.51(14)	0.4061

v. Observed and virtual potentials vs. log [M]

The Figure 4.20 indicates the slope obtained when the virtual peak potential was plotted versus log [M]. When the slope obtained is close to the Nernstian slope,

the proposed model and fitting procedures are reliable. The theory of virtual potential [64, 71] can be used instead of observed potential if one wishes to determine the value of E^o. The value of E^o is used in the refinement of polarographic data using ESTA program. In Figure 4.20, one can see that the plot of virtual potential vs. log[M] gave a slope closer to the Nernstian value if it is compared to the plot of observed potential vs. log[M]. In this case, the difference in these two slopes is small because the decrease in I_d was also small.

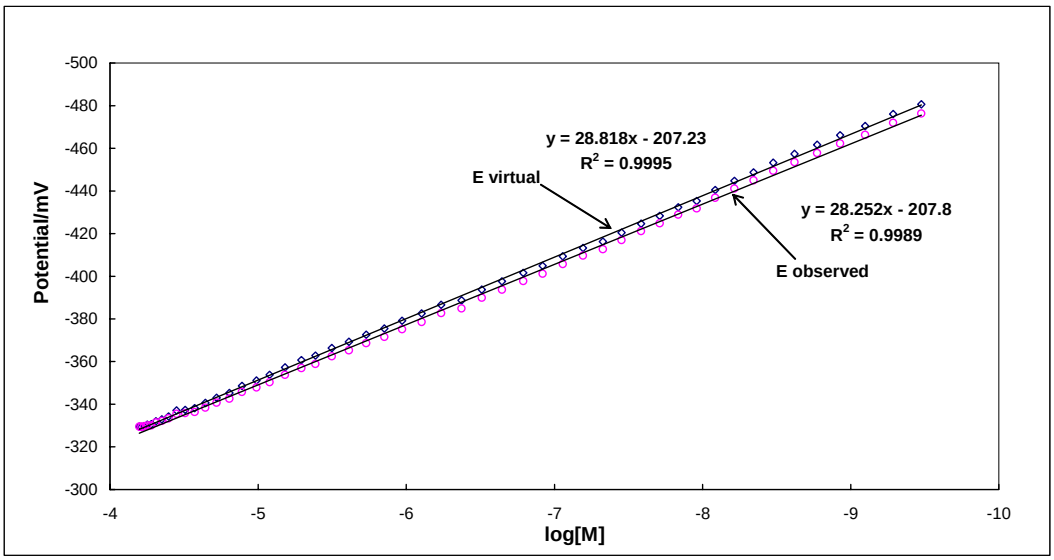

Figure 4.20: Observed potential compared to the virtual potential in terms of slope and E^o for Pb-Cyp_2EN system. The experimental conditions are 25°C and ionic strength 0.1 M in $NaNO_3$. $[M_T] = 8.01 \times 10^{-5}$ M and $[L_T] = 4.029 \times 10^{-3}$ M.

vi. Species distribution diagram

The species distribution diagram in Figure 4.21 was calculated for the model ML, ML(OH), and $ML(OH)_2$. It shows that the major species ML and ML(OH) are formed in a consecutive manner with large fraction for each species. The complex ML is at its maximum between pH 6.5 and 8. This is in agreement with the slope

of about 30 mV per pH unit observed in Figure 4.17 in that pH range. The complex ML(OH) starts to form at about pH 7 and its maximum is above pH 9. This can also confirm the fact that the complex ML(OH) is at its maximum concentration in the region where the forms of the ligand are HL and L. This is in a good agreement with the slope of 40 mV per pH unit observed in Figure 4.17. Figure 4.21 shows clearly that $ML(OH)_2$ complex started to form when ML(OH) complex was still present in solution. Maximum concentration of $ML(OH)_2$ is at about pH 11. At this pH, the concentration of ML(OH) and $ML(OH)_2$ is almost the same in the solution. This is in a good agreement with the slope of about 45 mV per pH unit observed in Figure 4.17.

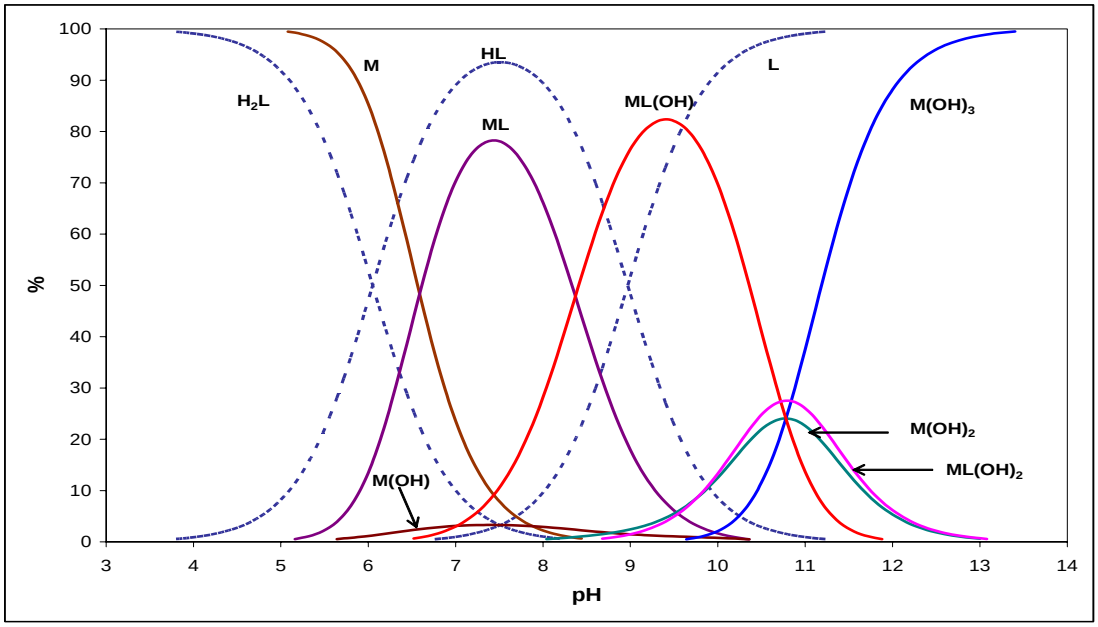

Figure 4.21: Species distribution diagram for Pb–Cyp_2EN system L_T:M_T ratio 50 studied by DPP at 25°C and ionic strength 0.1 M in $NaNO_3$. $[M_T] = 8.01 \times 10^{-5}$ M and $[L_T] = 4.029 \times 10^{-3}$ M.

4.7. Study of Pb-Cyp$_2$EN by polarography + potentiometry

Another approach used in the refinement of the data for Pb–Cyp$_2$EN system was the combined refinement of GEP and polarographic data. This approach involved the use of virtual potential data as it was performed for Cd–Cyp$_2$EN system. Data refined in this way is termed GEP + VP-DP/DC in this work. Another approach used was the refinement of the data from DC$_{tast}$ and DPP by ESTA for two ratios studied. This is termed VP-DP/DC and presented in Table 4.8.

Table 4.8: Stability constants obtained for Pb–Cyp$_2$EN system using the concept of virtual potentiometry

L_T:M_T ratio	ML	ML(OH)	ML(OH)$_2$	R-Factor	Remarks
50 (VP-DP)	4.90(01)	10.10(02)	13.94(04)	0.00450	E^o not refined
$[M_T]=8.01 \times 10^{-5}$ M $[L_T]= 4.03 \times 10^{-3}$ M	5.00(01)	10.15(02)	14.05(03)	0.00313	E^o refined 207.23 ⇒ 205.221
50 (VP-DC)	4.93(01)	10.15(02)	13.86(04)	0.00368	E^o not refined
$[M_T]=8.01\times10^{-5}$ M $[L_T]=4.03 \times10^{-3}$ M	4.99(01)	10.19(02)	13.94(03)	0.00309	E^o refined 229.29 ⇒ 227.984
83 (VP-DP)	4.96(01)	10.12(02)	13.31(19)	0.00335	E^o not refined
$[M_T]=5.35 \times 10^{-5}$ M $[L_T]=4.45 \times 10^{-3}$ M	5.01(01)	10.15(01)	13.44(14)	0.00291	E^o refined 220.18 ⇒ 219.18
83 (VP-DC)	5.05(02)	10.04(04)	13.59(18)	0.00468	E^o not refined
$[M_T]=5.35 \times 10^{-5}$ M $[L_T]=4.45 \times 10^{-3}$ M	5.10(02)	10.07(04)	13.71(14)	0.00418	E^o refined 243.78 ⇒ 242.443
50 + 83 **(VP-DP/DC)**	5.00(01)	10.09(02)	13.90(03)	0.00511	E^o not refined
	5.07(01)	10.12(01)	14.01(02)	0.00420	E^o refined: 207.23 ⇒ 204.933 229.29 ⇒ 227.585 220.18 ⇒ 219.808 243.78 ⇒ 242.347

When M(HL) was excluded from the potentiometric model, the stability constant of ML complex becomes very close to that from polarography (see Table 4.6). Note that in potentiometry the L_T:M_T ratio is much lower allowing for hydrolysis of lead species, which results in a relatively higher concentration of

hydrolysed complexes relative to those observed in polarography. As a result, the log β data for the hydrolysed complexes shows increased deviations with increasing the degree of hydrolysis. This can explain the reason why the computed stability constant for $ML(OH)_2$ complexes is larger in GEP than in polarography.

As the ligand was very basic, the metal and ligand were mixed in the beginning of the experiment and were prepared in acidic medium. This means that there was no peak for the metal only for comparison with the first polarograms recorded in polarography. This can explain the reason why polarography could not fit M(HL) complex properly.

Table 4.9: Final model proposed for Pb-Cyp_2EN system at 25°C and ionic strength 0.1 M $NaNO_3$.

Technique	Equilibrium	Log β	R-Factor
GEP	M + H + L = M(HL)	11.74 (01)	0.01873
	M + L = ML	5.06 (01)	
	M + L + OH= ML(OH)	10.82 (01)	
	M + L + 2OH = $ML(OH)_2$	14.98 (06)	
VP- DP/DC	M + L = ML	5.07(01)	0.00420
	M + L + OH = ML(OH)	10.12(01)	
	M + L + 2OH = $ML(OH)_2$	14.01(02)	
GE+VP-DP/DC	M + H + L = M(HL)	11.57(09)	0.04868
(Final model)	M + L = ML	4.97(05)	
	M + L = ML(OH)	10.62(05)	
	M + L + 2OH = $ML(OH)_2$	13.53(57)	

As polarography can operate at the very low total metal concentration, it is more efficient in a situation when one is dealing with easily hydrolysable ions.

The precipitation of solid hydroxide will then occur at much higher pH values and the formation of polynuclear species can be either avoided or minimised. This means that, for kinetic reasons, one can also study by polarography the complexes of metal ions that should not exist at all from the thermodynamic point of view because of hydrolysis [5]. Advantage of using polarography was reported previously, for example, complexes of Pb^{2+} with EN. Only ML complex was observed by GEP, and in polarographic study, the additional complexes, M(HL), ML(OH), ML_2, and $ML_2(OH)$ complexes were observed as well [75]. The final model proposed for Pb–Cyp_2EN system is M(HL), ML, ML(OH) and $ML(OH)_2$. It is from the combined refinement of GEP and polarographic data by ESTA as it is seen in Table 4.9.

4.8. Study of Cu–Cyp_2EN, Ni–Cyp_2EN and Zn–Cyp_2EN by GEP

Other systems were studied with the ligand Cyp_2EN by GEP. These included Cu-Cyp_2EN, Ni-Cyp_2EN and Zn-Cyp_2EN systems. They were studied under the same conditions as those used for Cd-Cyp_2EN and Pb-Cyp_2EN systems: 25°C and ionic strength 0.1 M in $NaNO_3$.

4.8.1. Cu–Cyp_2EN system

i. Refinement of the data

The system Cu–Cyp_2EN was studied at four ratios, and no precipitation was observed during the experiment. The Table 4.10 shows the results obtained for different ratios performed. For the L_T:M_T ratios 0.98, 1.45 and 2.3, M(HL) complex was rejected when the unmodified experiment data were refined, it was accepted when acid or base concentrations were refined. This can suggest that the

complex M(HL) is a minor species in the solution. For the final model, one can consider the complexes M(HL), ML, ML(OH) and $ML(OH)_2$.

Different optimisation procedures were used in the refinement of the data, and it was observed that all procedures gave almost the same results. The final model was obtained by simultaneous refinement of acid and base concentration.

Table 4.10: Proposed model and stability constants for Cu–Cyp_2EN system studied by GEP at 25°C and ionic strength 0.1M in $NaNO_3$.

L_T:M_T ratio	M(HL)	ML	ML(OH)	$ML(OH)_2$	R-factor	Remarks
0.98	Rejected	6.10(09)	11.99(08)	15.27(13)	0.08938	Raw data
$[M_T]=1.90\times10^{-3}$M $[L_T]=1.86\times10^{-3}$M	11.72 (02)	6.71 (01)	13.34 (01)	17.33 (01)	0.00879	acid and base refined
1 $[M_T]=2.10\times10^{-3}$M	12.59 (02)	6.93 (01)	13.77 (01)	18.05 (02)	0.0227	Raw data
$[L_T]=2.05\times10^{-3}$M	12.00 (01)	6.73 (01)	13.37 (01)	17.42 (01)	0.01364	acid and base refined
1.45 $[M_T]=1.49\times10^{-3}$M	Rejected	6.82 (01)	13.39 (01)	17.37 (01)	0.05315	Raw data
$[L_T]=2.16\times10^{-3}$M	11.77 (02)	6.798 (003)	13.41 (01)	17.46 (01)	0.0047	acid and base refined
2.3 $[M_T]=1.14\times10^{-3}$M	Rejected	6.94 (09)	11.42 (11)	14.43 (22)	0.3186	Raw data
$[L_T]=2.67\times10^{-3}$M	11.72 (02)	6.774 (004)	13.36 (01)	17.51 (01)	0.00586	acid and base refined
Combined refinement	11.87 (01)	6.747 (003)	13.363 (003)	17.395 (004)	0.01276	Acid and base refined for all ratios
	excluded	6.734 (004)	13.343 (004)	17.40 (01)	0.01672	Acid and base refined for all ratios

The acid or base concentrations generally varied by approximately ± 5 %. As an example, the Table 4.11 shows the concentration of base and acid before and after their refinement.

Table 4.11: Change in acid and base concentrations for Cu–Cyp_2EN system studied by GEP at different L_T:M_T ratios

L_T:M_T ratio	$[H^+]$ before	$[H^+]$ after	% change	$[OH^-]$ before	$[OH^-]$ after	% change
0.98	0.009978 M	0.00942 M	- 5.6 %	0.0102 M	0.01001 M	- 1.9 %
1	0.009978 M	0.01029 M	+ 3.1%	0.0098 M	0.009765 M	-0.4 %
1.45	0.009978 M	0.00993 M	-0.5 %	0.0098 M	0.009911 M	+ 1.1 %
2.3	0.009978 M	0.00994 M	-0.4 %	0.0102 M	0.010266 M	+ 0.6 %

ii. Complex formation function $\overline{Z}_M$

The potentiometric complex formation curve is presented in Figure 4.22. Its analysis suggests that (MHL) complex exists in solution. This is confirmed by the small shift observed from about pA 8.

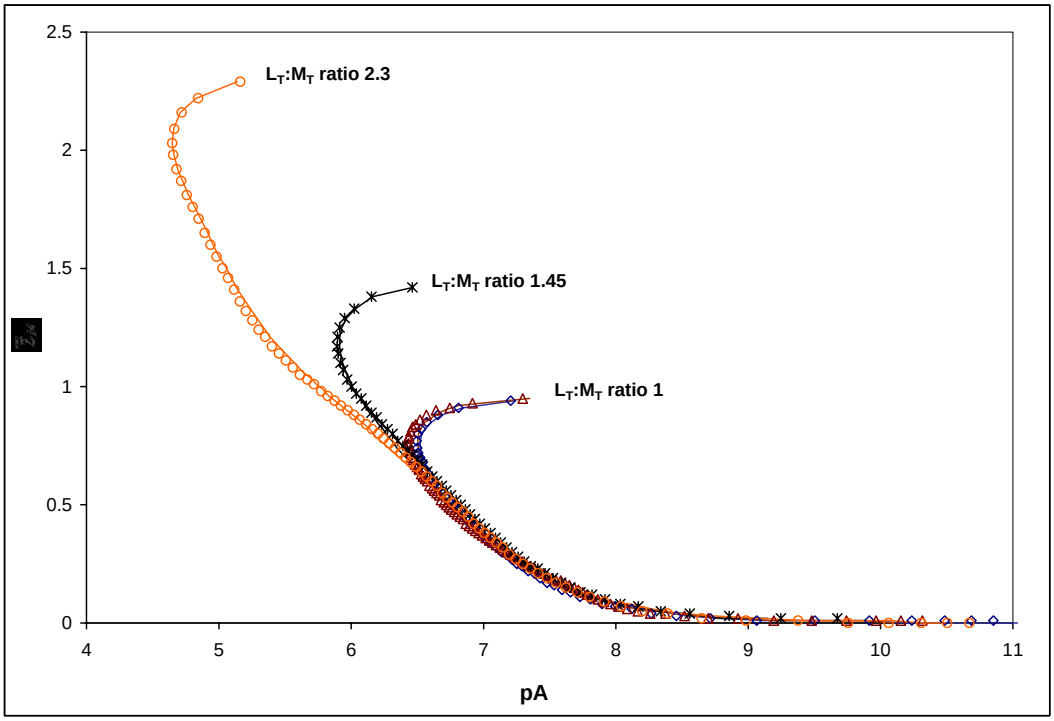

Figure 4.22: Complex formation curves for Cu–Cyp_2EN system studied at different ratios by GEP at 25° C and ionic strength 0.1 M in $NaNO_3$. Model M(HL), ML, ML(OH), and $ML(OH)_2$.

The analysis of $\overline{Z}_M$ curves also shows that there is a formation of hydroxo species. In this case, the complexes predicted to form are ML(OH) and $ML(OH)_2$. The back–fanning feature observed for all ratios studied confirms the presence of these complexes, especially ML(OH) complex in L_T:M_T ratio 1.

iii. Species distribution diagram

The species distribution diagram in Figure 4.23 was calculated for the model M(HL), ML, ML(OH) and $ML(OH)_2$. This Figure indicates that the complex M(HL) will be up to 15 % of all species in solution. The hydroxo–complexes, ML(OH) and $ML(OH)_2$ seem to be the predominant species in the solution. The complex M(HL) is formed under ML complex. This supports the fact that M(HL) complex was rejected during refinement operation.

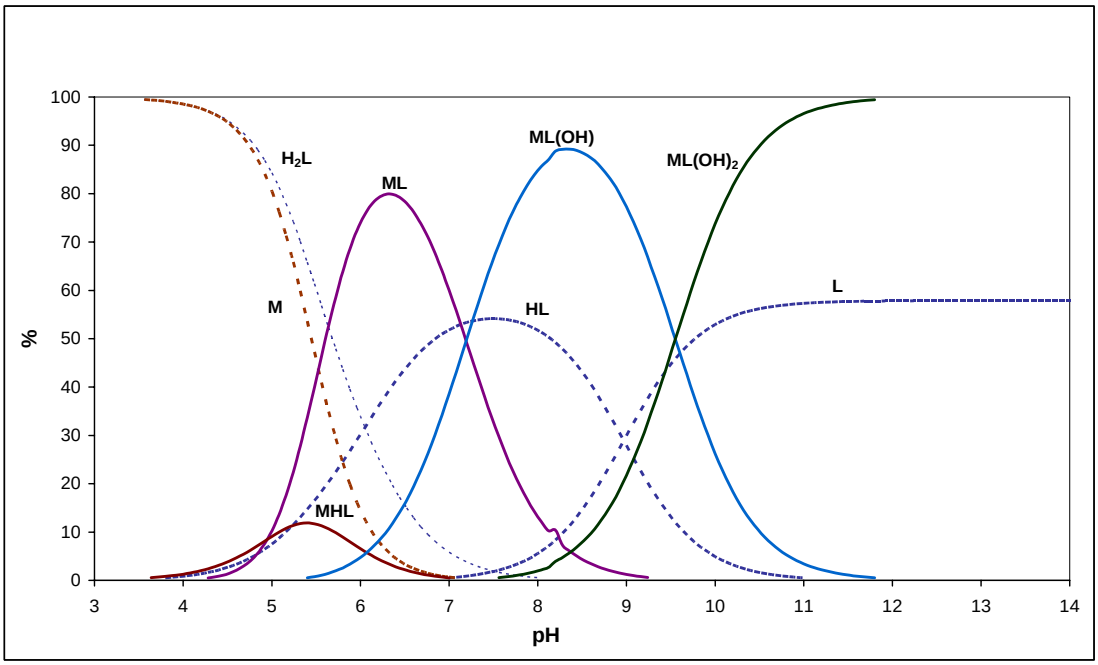

Figure 4.23: Species distribution diagram for Cu–Cyp_2EN system studied at 25° C and ionic strength 0.1 M in $NaNO_3$. The model used is from the combined refinement and conditions for L_T:M_T ratio 2.3. $[L_T] = 2.67 \times 10^{-3}$ M, $[M_T] = 1.14 \times 10^{-3}$ M.

If one wishes to study Cu–Cyp_2EN by polarography, a slope of about 30 mV per pH unit must be observed in the pH range between 5.5 and 7 (plot of virtual potential versus pH). One proton would be involved in the electrochemical process at the DME. The Figure 4.23 shows that the complex ML(OH) has a maximum in the pH range between 7 and 9.5. The same study would confirm the presence of ML(OH) complex by observing a slope of about 60 mV per pH units, because this complex would be formed in the region where the predominant form of the ligand would be HL. This would involve two protons in electrochemical process at the DME. The same slope would be observed above pH 10. In this region $ML(OH)_2$ seems to be a major species. Its formation also would involve two protons because the deprotonated form of the ligand is predominant in that pH–range.

4.8.2. Study of Ni–Cyp_2EN system

i. Data refinement

As for Cd^{2+} and Pb^{2+}, three titrations were performed for Ni–Cyp_2EN system, at 25°C and ionic strength 0.1 M in $NaNO_3$. The overall stability constants for Ni–Cyp_2EN system were obtained by simultaneous refinement of three different titrations and are presented in Table 4.12. The model obtained for this system is M(HL), ML, ML(OH) and $ML(OH)_2$. During refinement operation, it was observed that the complex ML(OH) was rejected in the presence of $ML(OH)_2$ for L_T:M_T ratio 2. When $ML(OH)_2$ was excluded from the model, the complex ML(OH) was then accepted. For L_T:M_T ratio 3, the complex ML(OH) was accepted in the model in the presence of $ML(OH)_2$ complex but with a small

value of stability constant and large standard deviation. The refinement involving the combination of three titrations accepted two models, one with M(HL), ML and ML(OH) and another with M(HL), ML and $ML(OH)_2$.

Table 4.12: Model and stability constants for Ni–Cyp_2EN system studied by GEP at 25°C and ionic strength 0.1 M in $NaNO_3$.

L_T:M_T ratio	M(HL)	ML	ML(OH)	$ML(OH)_2$	R-factor	Remarks
1 $[M_T] = 2.03 \times 10^{-3}$M $[L_T] = 2.01 \times 10^{-3}$M	rejected	3.37 (07)	8.01(20)	rejected	0.07299	Raw data
	11.38 (02)	3.88 (01)	8.06(06)	rejected	0.01499	acid refined
2 $[M_T] = 1.34 \times 10^{-3}$M $[L_T] = 2.70 \times 10^{-3}$M	10.62 (06)	3.65 (01)	7.60(23)	12.81(09)	0.00593	Raw data
	11.04 (02)	3.71 (01)	8.31(01)	excluded	0.01201	acid or base refined
	11.06 (02)	3.760 (004)	excluded	13.06(01)	0.00847	acid or base refined
3 $[M_T] = 1.02 \times 10^{-3}$M $[L_T] = 2.99 \times 10^{-3}$M	10.68 (01)	3.65 (02)	8.10(13)	12.62(25)	0.00907	Raw data
	11.36 (01)	3.87 (01)	7.98(09)	13.10(04)	0.00734	acid or base refined
Combined refinement of 3 titrations	11.25 (01)	3.79 (01)	8.26(01)	excluded	0.01467	acid or base refined
	11.25 (01)	3.832 (003)	excluded	13.15(01)	0.01175	acid or base refined

As for Cu–Cyp_2EN system, the formation of the complex M(HL) is now of interest. For L_T:M_T ratio 1, when the raw data was treated, the M(HL) complex was rejected from the model; it was accepted after the refinement of the base or acid concentrations. The same explanation given to Cu–Cyp_2EN system is also valid here. The difference between two systems is that nickel is kinetically slow, and the complex ML also is formed slowly. As the L_T:M_T ratio increased, the software could refine M(HL) complex. This complex had enough time to form. The complex $ML(OH)_2$ was also rejected for L_T:M_T ratio 1 because of the precipitation that appeared at pH 8.6. The points recorded up to that pH were not enough to incorporate $ML(OH)_2$ complex. The complex ML(OH) was rejected in

the presence of $ML(OH)_2$. This can be justified by the fact that they are formed in a consecutive manner and $ML(OH)_2$ is a major species when compared to ML(OH) complex.

Table 4.13 Change in acid and base concentrations for Ni–Cyp_2EN system at different L_T:M_T ratios

L_T:M_T ratio	$[H^+]$ before	$[H^+]$ after	% change	$[OH^-]$ before	$[OH^-]$ after	% change
1	0.0103 M	0.010162 M	– 1.3 %	0.0099 M	0.010119 M	+ 2.2 %
2	0.0103 M	0.010183 M	– 1.1 %	0.0099 M	0.009704 M	– 1.9 %
3	0.0103 M	0.010191 M	– 1.1 %	0.0099 M	0.009745 M	– 1.6 %

ii. Complex formation curve $\overline{Z}_M$

The complex formation curve in Figure 4.24 shows a small change in the shape of the curve between pA 5 and pA 9. This suggests the formation of M(HL) complex.

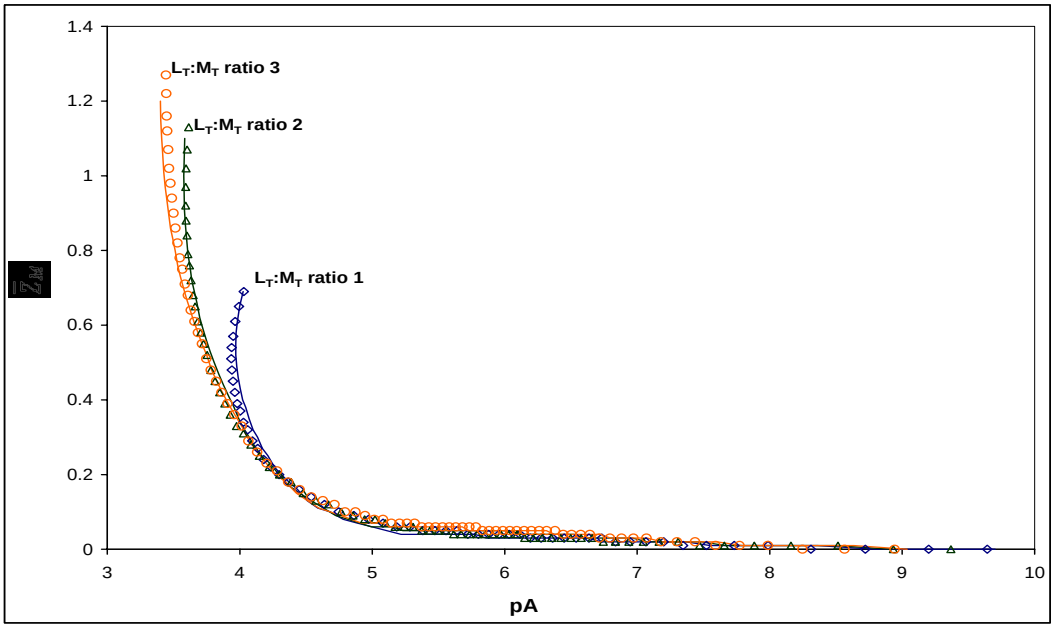

Figure 4.24: Experimental (points) and calculated (solid lines) complex formation curves for Ni-Cyp_2EN system studied at different ratios by GEP at 25°C and ionic strength 0.1 M in $NaNO_3$. Model M(HL), ML, ML(OH) and $ML(OH)_2$.

Below pA 5, there is a significant change in the shape of the curves for all ratios studied. This can confirm the presence of the complex ML. The computed stability constants for hydroxospecies are somewhat questionable because of the back-fanning feature, which is not well pronounced.

iii. Species distribution diagram

The species distribution diagram in Figure 4.25 suggests that the complex M(HL) is a major species in the solution below pH 7 even if it was rejected in L_T:M_T ratio 1. According to the same diagram, one cannot trust the stability constants of hydroxo species in the solution. The number of points recorded before the precipitation occurred were insufficient to get a low standard deviation for the species ML(OH) and $ML(OH)_2$. For ratios 1 and 2, the predicted precipitations were at pH 8.3 and pH 8.5 respectively, but we could see it only at pH 8.8 and 8.9. If hydroxo-species were formed, ML(OH) and $ML(OH)_2$ started to form almost at the same pH of about 8, and $ML(OH)_2$ was the major species when compared with ML(OH) complex. This can explain the reason why ML(OH) complex was rejected in the presence of $ML(OH)_2$ complex. As a result of precipitation of the hydroxospecies, an inadequate number of data points was acquired. This resulted in a larger deviation in calculated formation constants for the ML(OH) and $ML(OH)_2$ complexes. In order to confirm the formation and stability constants of ML(OH) and $ML(OH)_2$, other speciation techniques must be used. From GEP, one can only trust the stability constants of ML and M(HL) complexes which are about 3.8 and 11.3, respectively. The following equilibrium shows their formation:

$Ni^{2+} + Cyp_2EN \rightleftharpoons Ni(Cyp_2EN)^{2+}$

$Ni^{2+} + Cyp_2EN + H^+ \rightleftharpoons Ni(HCyp_2EN)^{3+}$

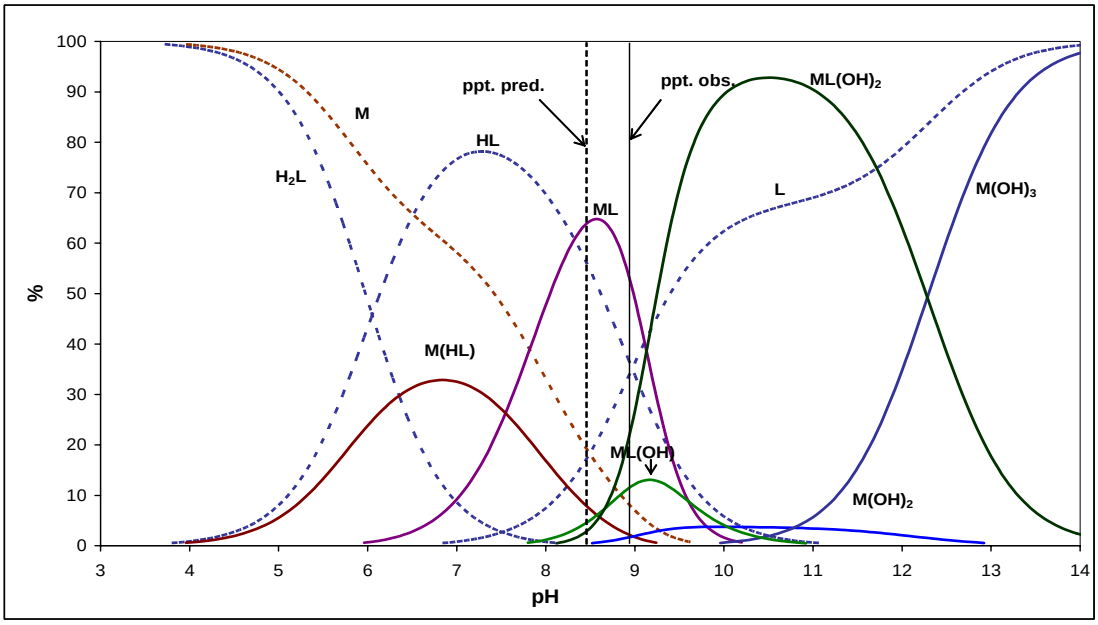

Figure 4.25: Species distribution diagram for Ni–Cyp_2EN system L_T:M_T ratio 3 at 25°C and ionic strength 0.1 M in $NaNO_3$. $[L_T] = 2.99 \times 10^{-3}$ M, $[M_T] = 1.00 \times 10^{-3}$ M. The model used is from the combined refinement.

4.8.3. Study of Zn–Cyp_2EN system

i. Data fitting

The potentiometric study of Zn–Cyp_2EN was performed at 25°C and ionic strength 0.1 M in $NaNO_3$. To establish stability constants, three titrations were performed at different L_T:M_T ratios. The model from GEP for Zn–Cyp_2EN system is M(HL), ML, ML(OH) and $ML(OH)_2$ as indicated in Table 4.14. During refinement operations, it was observed that the complex ML(OH) was rejected when the unmodified data were fitted. This was observed for L_T:M_T ratios 1 and 2. The complex ML(OH) was accepted by ESTA when acid or base concentrations were refined, but its standard deviation was large. Also, when the

complex ML(OH) was included in the model, the value of stability constant of ML complex decreased for L_T:M_T ratios 0.5 and 1.

Table 4.14: Model and stability constants for Zn–Cyp_2EN system studied by GEP at 25°C and ionic strength 0.1 M in $NaNO_3$.

L_T:M_T ratio	M(HL)	ML	ML(OH)	$ML(OH)_2$	R-factor	Remarks
0.5 $[M_T] = 2.66 \times 10^{-3}$ M $[L_T] = 1.33 \times 10^{-3}$ M	11.65 (04)	4.57 (04)	9.35(88)	16.70(03)	0.02279	Raw data
	11.62 (01)	4.62 (01)	excluded	16.58	0.01982	acid or base refined
	11.64 (05)	4.25 (06)	10.79(03)	excluded	0.05021	acid or base refined
1 $[M_T] = 1.98 \times 10^{-3}$ M $[L_T] = 1.99 \times 10^{-3}$ M	11.37 (06)	4.32 (03)	rejected	15.80(03)	0.03436	Raw data
	11.63 (05)	4.46 (03)	excluded	15.92(03)	0.01824	acid or base refined
	11.66 (04)	4.32 (03)	10.01(04)	15.82(02)	0.02589	acid or base refined
2 $[M_T] = 1.33 \times 10^{-3}$ M $[L_T] = 2.67 \times 10^{-3}$ M	12.46 (03)	5.19 (04)	rejected	16.67(04)	0.04207	Raw data
	11.89 (01)	4.62 (02)	8.49(76)	16.07(02)	0.01500	acid or base refined
	11.89 (02)	4.63 (01)	excluded	16.07(01)	0.01501	acid or base refined
Combined refinement	11.73 (02)	4.52 (02)	9.97(05)	16.03(01)	0.04550	Acid and base refined

For L_T:M_T ratio 2, the value of ML did not change if ML(OH) was or not included. Note that the precipitation was observed during the experiment. It was observed at pH 8, 8.6 and 9 for L_T:M_T ratios 0.5, 1 and 2, respectively. The precipitation was predicted at pH 8 and 8.3 for L_T:M_T 0.5 and 1, respectively, and no precipitation was predicted using solubility the product of $Zn(OH)_2$ [74] for L_T:M_T ratio 2.

ii. Complex formation curve $\overline{Z}_M$

In Figure 4.26, a plot of complex formation curves is presented. It is from the refinement of the data for L_T:M_T ratio 2, where the model for Zn–Cyp_2EN system includes M(HL), ML, ML(OH) and $ML(OH)_2$. This plot presents a significant

back-fanning feature which tells us that the hydroxospecies are present in solution. In this case the species predicted to be formed are ML(OH) and $ML(OH)_2$.

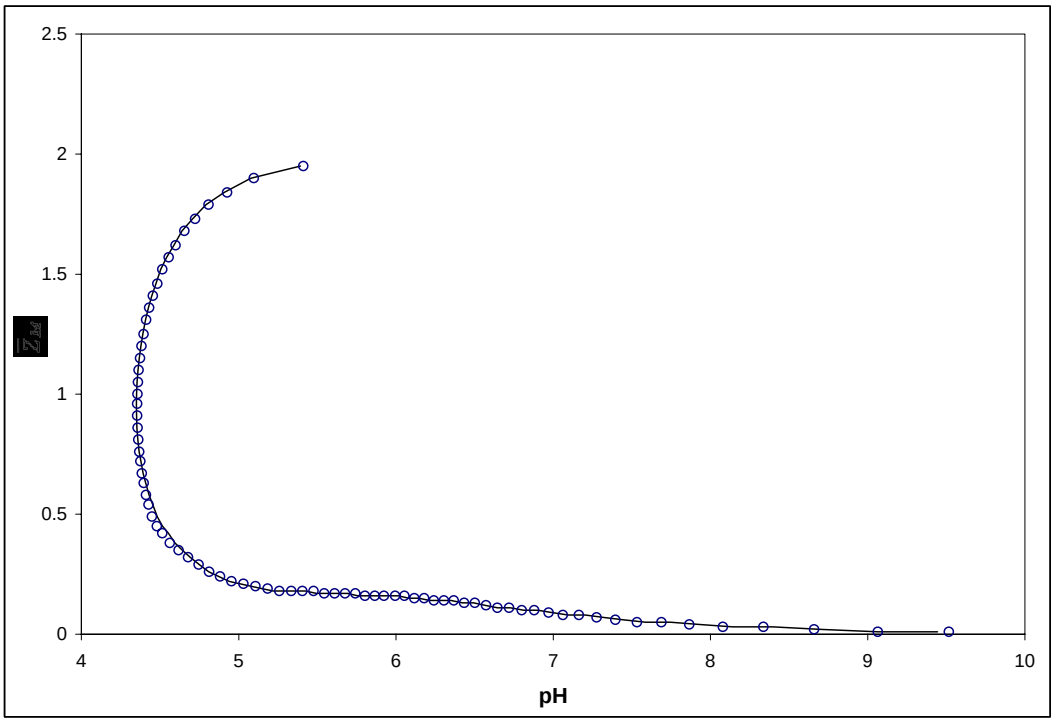

Figure 4.26: Experimental (circles) and calculated (solid line) complex formation curves for Zn–Cyp_2EN system studied at 25°C and ionic strength 0.1 M in $NaNO_3$. Model M(HL), ML, ML(OH) and $ML(OH)_2$.

A small change in the region between pA 5 and pA 9 could be attributed to the complex M(HL). The complex formation curve using combined refinement of all titrations did not show a good fit, and it was decided to take one titration as an example.

iii. Species distribution diagram

In Figure 4.27, a species distribution diagram is plotted. It was calculated for the refined Zn–Cyp_2EN model for which the best fit was obtained (the thick solid line

in Figure 4.26). It is seen that the complexes start to form above pH of about 4. In the pH range of 7 to 9, a number of zinc complexes is formed simultaneously. The major zinc species formed with Cyp_2EN is the complex $ML(OH)_2$ which starts to form at around pH 7. By analysing the species distribution diagram in Figure 4.27, one can observe that ML(OH) complex is formed under $ML(OH)_2$ complex. This can explain the reason why, during the refinement of the data, the complex ML(OH) was rejected by ESTA. The hydroxo–complex ML(OH) appears to be minor species for both Zn–Cyp_2EN and Ni-Cyp_2EN systems. The $ML(OH)_2$ species however are the dominant forms at higher pH values for the above systems. The complex M(HL) also seems to be major component for these systems if compared with Cu-Cyp_2EN system. The use of other speciation techniques is highly recommended to establish best β values and full model for Cu–Cyp_2EN, Ni–Cyp_2EN and Zn–Cyp_2EN systems.

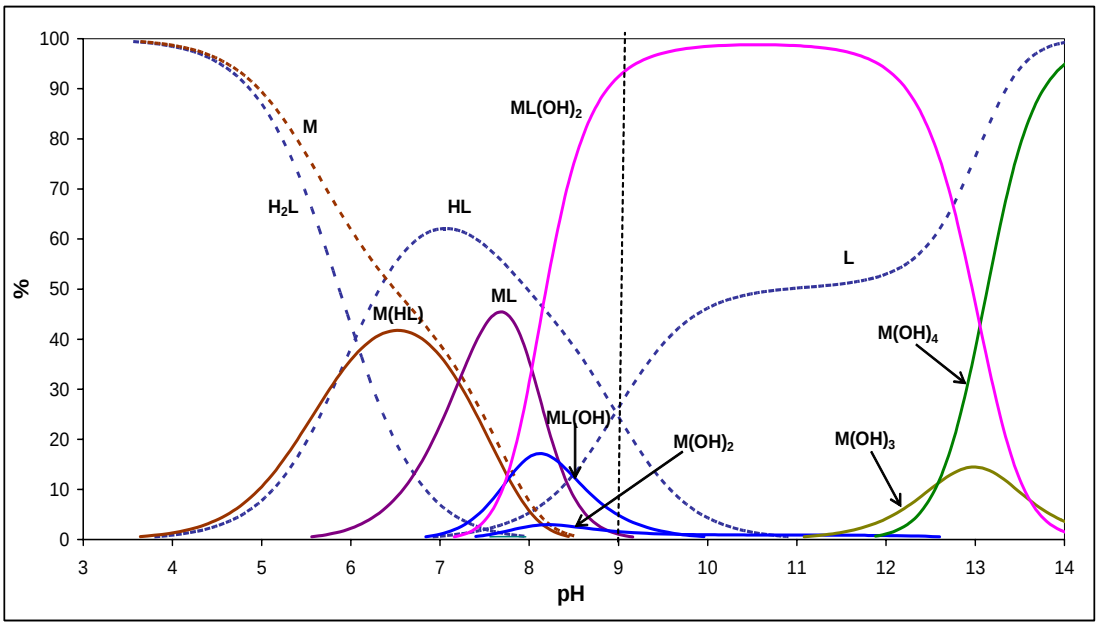

Figure 4.27: Species distribution diagram for Zn–Cyp_2EN system studied at 25°C and ionic strength 0.1 M in $NaNO_3$. The values of stability constants used are from the refinement of L_T:M_T ratio 2. $[M_T] = 1.332 \times 10^{-3}$ M and $[L_T] = 2.667 \times 10^{-3}$ M.

4.9. Polarographic study of Cd-Cy_2EN system

4.9.1. Data fitting

The polarographic study of Cd–Cy_2EN system was performed by DC_{tast}. The following discussion is focussed on L_T:M_T ratio 47. Initially, the recorded DC_{tast} curves showed one wave. As the pH increased, the behaviour of the waves changed and DC_{tast} curves started to show two overlapping waves. At highest pH values the curves showed again one wave. In the beginning of the experiment, the second wave was not pronounced. As the pH increased, the second wave became more and more pronounced. As the pH went on increasing, the first wave started to be negligible and the second became pronounced. The Figure 4.28 shows the behaviour of different waves recorded at different pH. Most of DC_{tast} curves showed two overlapping waves.

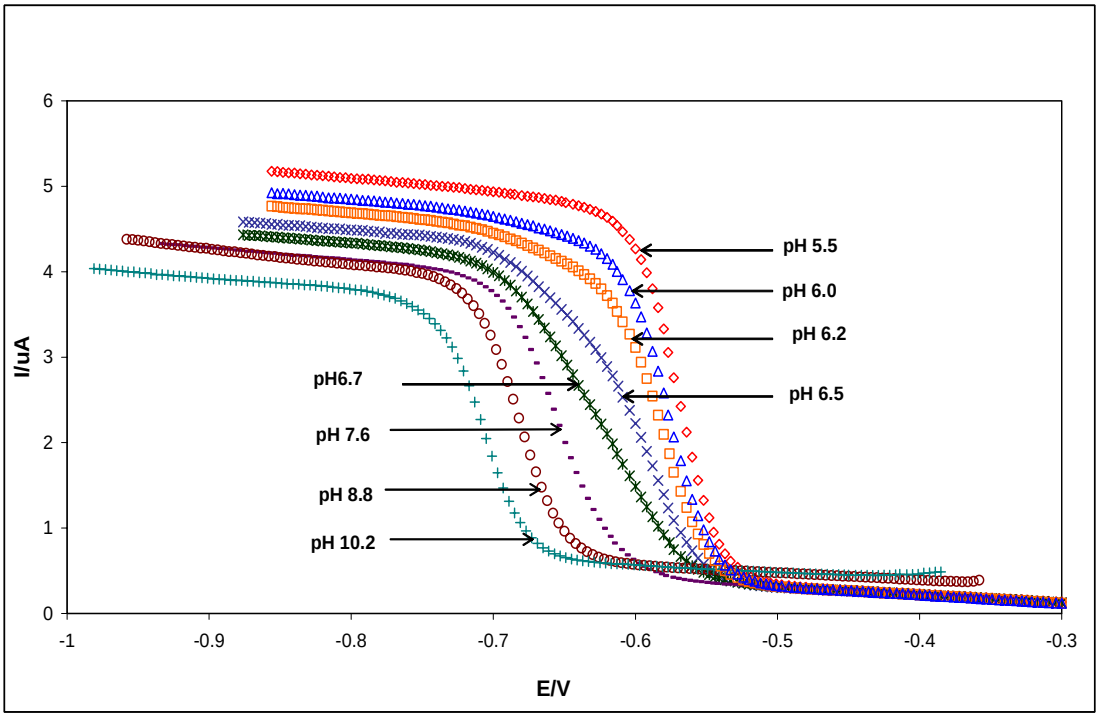

Figure 4.28: Behaviour of some of DC–waves recorded for Cd–Cy_2EN system ratio 47 studied at 25°C and ionic strength 0.1 M in $NaNO_3$. $[M_T] = 1.05 \times 10^{-4}$M and $[L_T] = 4.98 \times 10^{-3}$M.

By simple fitting, the waves at lower pH values appeared to be reversible, with a parameter δ computed between 0.89 and 0.91. From pH 6 to pH 8.9, some of the waves seemed to be quasi reversible and others irreversible. The parameter δ decreased down to 0.35 between pH 6 and pH 6.5. From pH 6.6, δ started to increase gradually. From pH 9, the waves seemed to become again reversible with δ between 0.82 and 0.89. From the above, it was impossible to analyse the recorded curves in a rigorous way. As theory allows analysis of the labile part of the M–L system, one has to evaluate and use $E_{1/2}$ and I_d related to the first wave. This was done in two different steps as indicated below:

- Firstly, the background was fitted. For this purpose, all data points from about a quarter height to the end of the wave were deleted. The remaining points were then used to fit parameters *a* and *b*.
- Secondly, the parameter δ was fixed at 1 (for fully reversible system) and parameters *a* and *b* were fixed at the values obtained from the fitting of the background with points towards the end of the wave marked (A) allowed. Thus it was possible to predict I_d and $E_{1/2}$.

The Figure 4.29 is an example showing how different waves were fitted. The solid line in pink represents the background current; the solid line in green represents the fitted curve without deleting any point and fixing any parameter and the solid line in red represents the fitted curve obtained when δ, *a* and *b* were fixed. The circles in blue represent the experimental points used while the circles in orange represent the experimental points deleted during the fitting of the DC_{tast} wave in order to predict $E_{1/2}$ (rev).

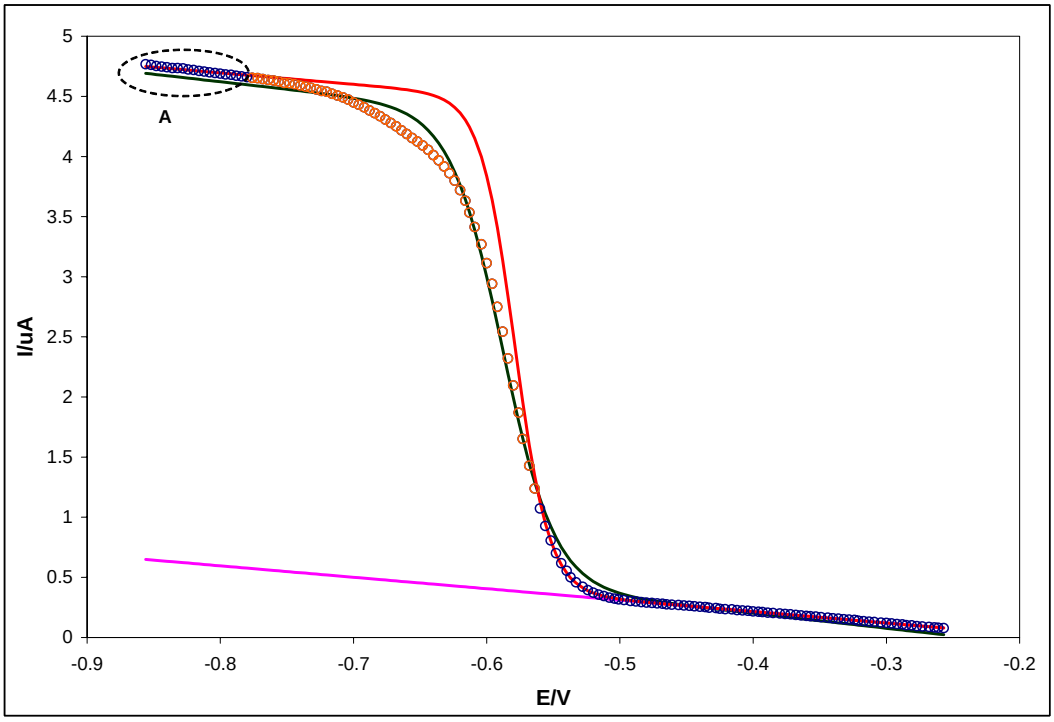

Figure 4.29: Example showing how DC–waves were fitted for Cd–Cy_2EN ratio 47 system studied at 25°C and ionic strength 0.1 M in $NaNO_3$, $[M_T] = 1.05 \times 10^{-4}$ M and $[L_T] = 4.98 \times 10^{-3}$ M. This wave was recorded at pH 6.2.

By trying to estimate the limiting current only for the first wave, one can see that the estimated I_d are too large and the half–wave potential ($E_{1/2}$) is observed at more negative potential than it would be expected. This is shown in Figure 4.30. As the very first and last waves seemed to be reversible, one could estimate the limits in corrected shift. From this, the computed stability constants for the first and last complex might be considered. It is known that this way of fitting is not correct. It would be a useful tool in the prediction of species formed in the solution, but one cannot trust the computed stability constants for these species. The use of another technique is highly recommended in order to confirm the model predicted by this way of fitting.

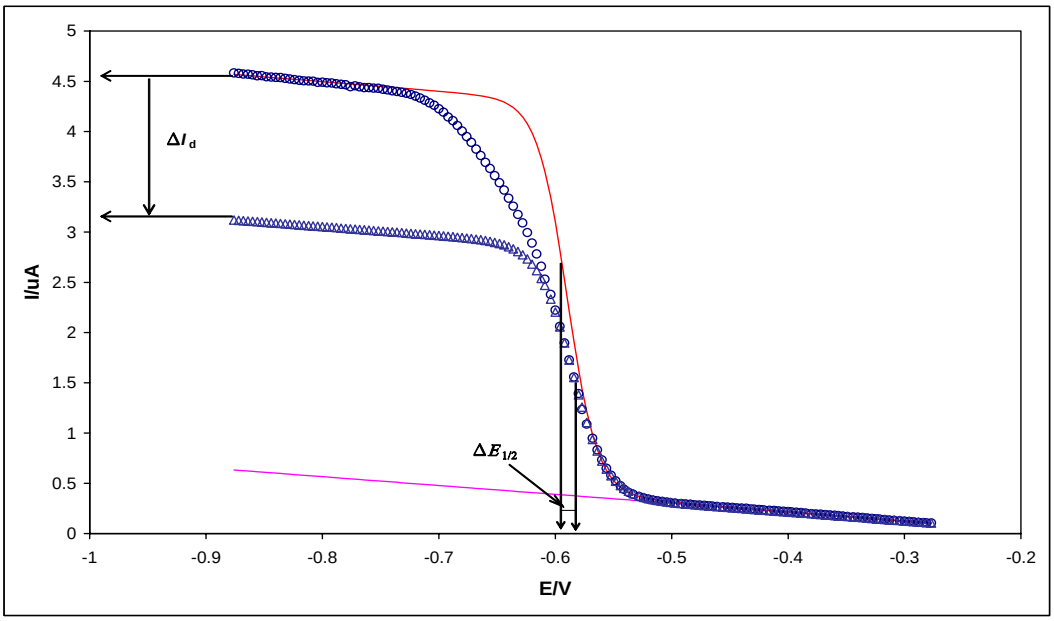

Figure 4.30: Example showing the difference in limiting current (ΔI_d) and half wave potential ($\Delta E_{1/2}$) when one tries to estimate the limiting current for one wave. The circles indicate the observed points, the triangle indicates the estimated one wave, the solid line in red indicates the fitted curve, and the solid line in pink indicates the background current.

4.9.2. Modelling for experimental data from DC-tast

i. Variation in the observed half-wave potential vs. pH

The procedure fitting described in Figure 4.29 was used to obtain $E_{1/2}(virt)$. A plot of E_{virt} vs. pH can be used in the prediction of the species formed in the solution. This is shown in Figure 4.31. A slope of about 31 mV per pH unit is observed in the pH range between 4 and 5.5. The predominant form of the ligand in this pH range is H_2L. This is the region where M(HL) might be formed. The slope observed is close to the theoretical value, which predict the formation of M(HL). This is represented by the following electrochemical process at DME and involves one proton:

$Cd(HL)^{3+} + H^+ + 2e^- = Cd(Hg) + H_2L^{2+}$

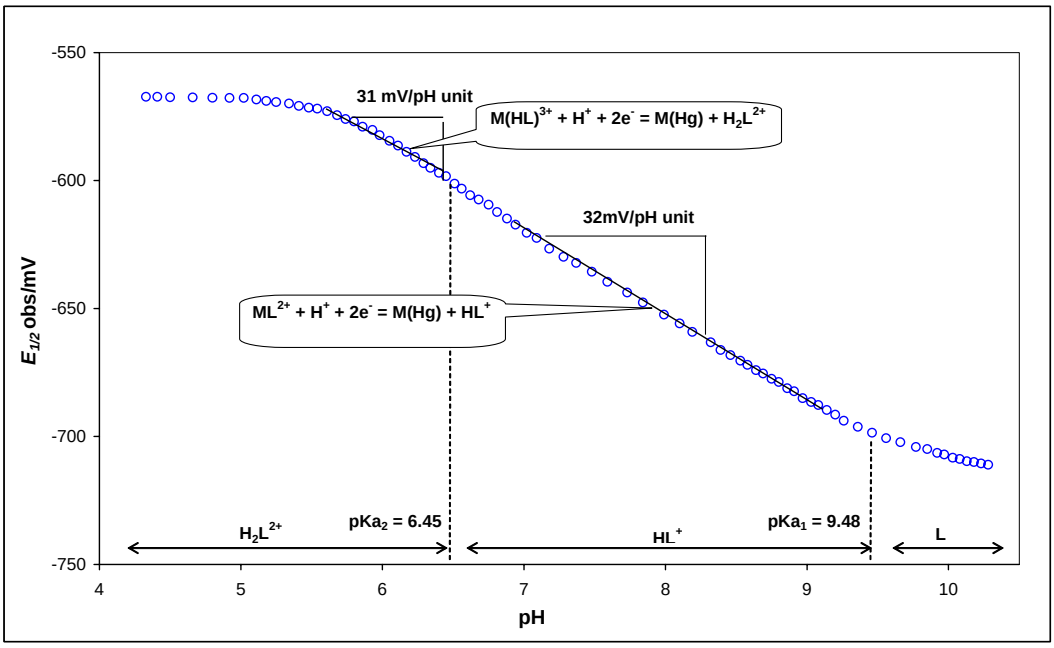

Figure 4.31: Variation in virtual half–wave potential vs. pH for Cd–Cy_2EN system studied by DC_{tast} at L_T: M_T ratio 47, $[M_T] = 1.05 \times 10^{-4}$ M and $[L_T] = 4.98 \times 10^{-3}$ M, at 25°C and ionic strength 0.1 M in $NaNO_3$.

Another slope of 32 mV per pH unit is observed in the pH range where the predominant form of the ligand is HL. This suggests the formation of ML complex as indicated by the following electrochemical process at the DME:

$CdL^{2+} + H^+ + 2e^- = Cd(Hg) + HL^+$

The same slope can also predict the formation of M(OH) complex. This involves one proton and can be presented by the following electrochemical process at the DME:

$Cd(OH)^+ + H^+ + 2e^- = Cd(Hg) + H_2O$

This slope is observed in the pH range where two overlapping waves were recorded. From this, one can explain why the slope observed is slightly higher than the predicted slope of about 30 mV per pH unit. The shift observed is slightly larger than the one expected in the case of one wave. The absence of the slope in the region where the ligand is fully deprotonated suggests that there is no evidence

of $ML_x(OH)_y$ complexes. From this relationship, one can only predict the formation of M(HL) and ML complexes.

ii. Variation in the observed half-wave potential vs. log [L]

The relationship between half-wave potential and log [L] can also predict which kind of species is formed in the solution. This is shown in Figure 4.32. By analysing the plot presented in this Figure, one can see that a slope of 29 mV per log unit is observed. This slope indicates the formation of ML complex and it is very close to the theoretical value. This supports the conclusion from the first relationship in Figure 4.31 on the presence of ML complex.

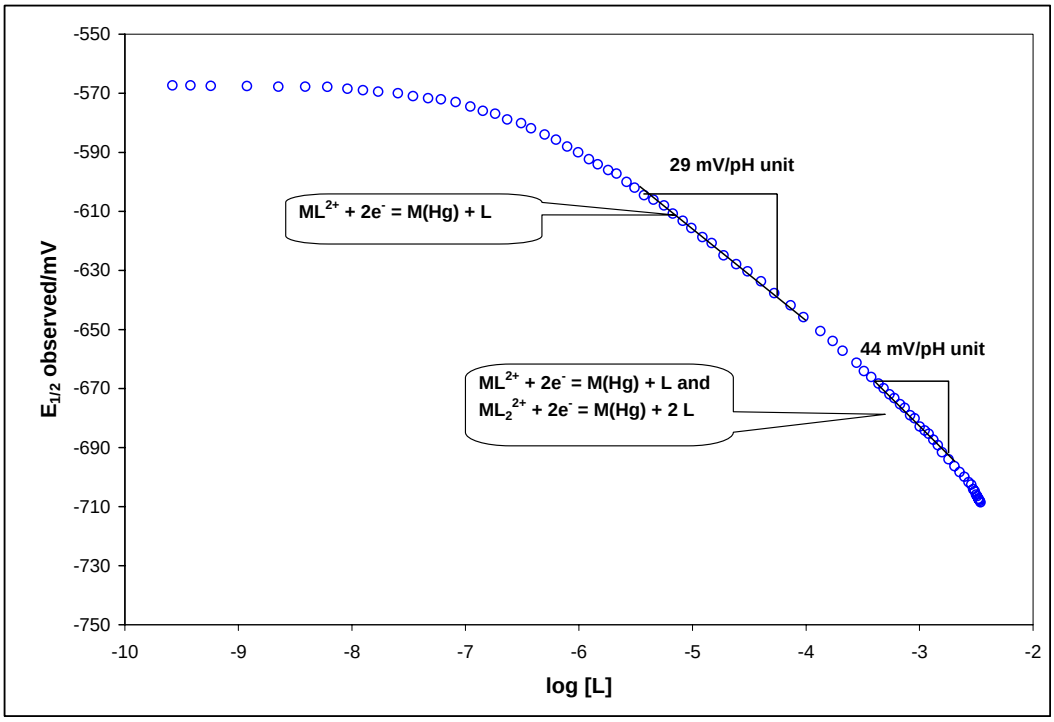

Figure 4.32: Variation in virtual half–wave potential vs. log [L] for Cd–Cy_2EN system studied by DC_{tast} at L_T:M_T ratio 47, initial $[M_T] = 1.05 \times 10^{-3}$M and $[L_T] = 4.98 \times 10^{-3}$M, at 25°C and ionic strength 0.1 M in $NaNO_3$.

Another slope of 44 mV per log unit is observed in Figure 4.32. This slope suggests the formation of ML_2 complex but it is lower than the one predicted (about 60 mV per log unit). From this one can suggest that ML complex still remain in the solution. But as indicated before, the way the curves were fitted was not totally correct. This can also explain the reason why the observed slope is lower than the theoretical slope. If the waves were reversible, a slope of about or slightly lower than 60 mV was supposed to be observed in the region where the predominant form of the ligand is HL. From the relationship in Figure 4.32, one can predict the formation of ML and ML_2 complexes.

iii. Complex formation curve

The experimental and calculated complex formation curves for Cd–Cy_2EN system are presented in Figure 4.33. Different models refined (see Table 4.15) present the same fit. During the fitting operation, the software could not distinguish which hydroxospecies was formed in the solution. Either ML(OH) was accepted in the model and $ML_2(OH)$ rejected, or $ML_2(OH)$ was accepted when ML(OH) was excluded or $ML(OH)_2$ was accepted when ML(OH) and $ML_2(OH)$ were excluded, or $ML_2(OH)_2$ was accepted when all the above hydroxospecies were excluded. These complexes were added in the model, but one cannot trust their stability constants, because they are formed in the region where the ligand is fully deprotonated. Any technique cannot distinguish which one is really present in solution. They were included into the model for a better fit.

The region (I) in Figure 4.34 shows that there is no shift up to pH 5. From pH 5 a small shift is observed. As the waves recorded in this pH range seemed to be

single and reversible, one can confirm the presence of M(HL) complex predicted in Figure 4.31.

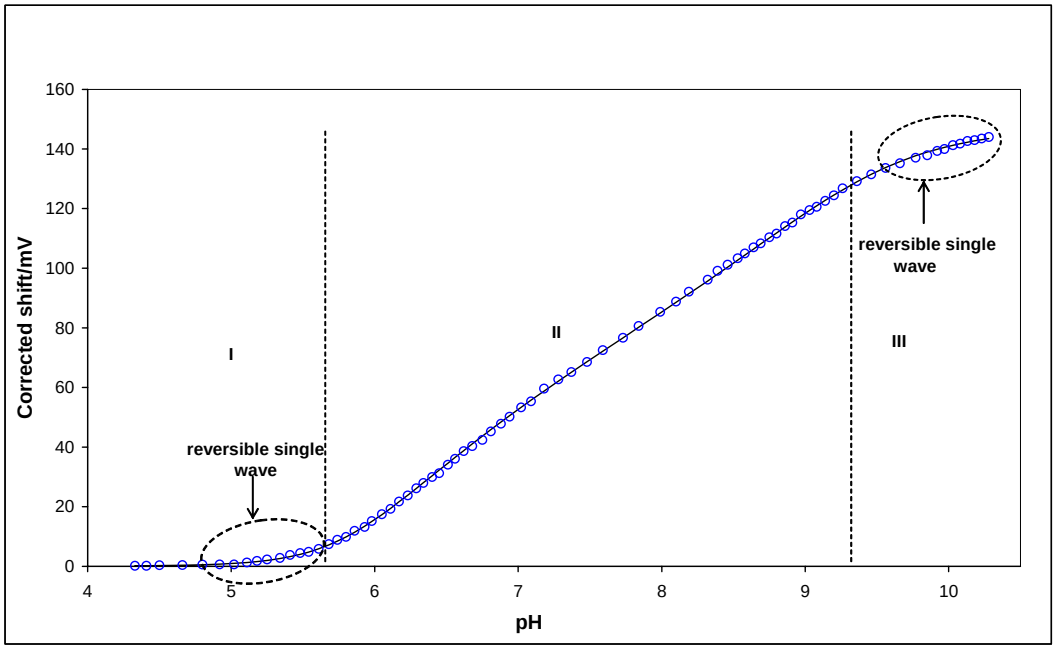

Figure 4.33: Experimental (circles) and calculated (solid line) complex formation curves for Cd–Cy_2EN system ratio 47 studied by DC tast. $[M_T] = 1.05 \times 10^{-3}$M and $[L_T] = 4.98 \times 10^{-3}$M, at 25°C and ionic strength 0.1 M in $NaNO_3$.

In region (II) there is a continuous shift up to about pH 9.5. This suggests a consecutive formation of a number of complexes proposed in Figure 4.32. This is the region where two overlapping waves were recorded and one cannot trust the shift observed. In region (III), a small shift is observed. This is the region where hydroxo-species are predicted. The shift observed in this region could be trusted because it was calculated from one reversible wave. As a conclusion, one can predict the formation of M(HL), ML and ML_2 complexes. Hydroxo–complexes are also predicted but one cannot distinguish which one was formed.

Table 4.15 Stability constants obtained from DC_{tast} for Cd–Cy_2EN system L_T:M_T ratio 47

M(HL)	ML	ML_2	ML(OH)	$ML_2(OH)$	$ML(OH)_2$	$ML_2(OH)_2$	R-Factor
11.91 (09)	6.70 (01)	9.63 (03)	9.50(61)	rejected	excluded	rejected	0.1978
11.91 (09)	6.70 (01)	9.63 (02)	excluded	11.92(61)	rejected	Excluded	0.1978
11.91 (09)	6.70 (01)	9.63 (02)	rejected	rejected	13.15(39)	Excluded	0.1886
11.91 (09)	6.70 (01)	9.63 (02)	rejected	excluded	excluded	15.65(38)	0.1871

4.10. Glass electrode potentiometric study of Cd–Cy_2EN system

4.10.1. Data refinement

In order to confirm the model predicted by polarography, GEP was used in the study of Cd-Cy_2EN system. For this purpose, four titrations were performed at different L_T:M_T ratios, at 25°C and ionic strength 0.1 M in $NaNO_3$. The L_T:M_T ratio 1 was performed twice. Complexes stability constants were calculated from titration data which were analysed by ESTA library program. Stability constants obtained for different titrations are presented in Table 4.16. The L_T:M_T ratio 1(I) was excluded in the combined refinement of different ratios. This ratio generated higher stability constants for M(HL), if compared with other ratios. The complex ML_2 was rejected in the refinement of L_T:M_T ratio 1. It was then decided to fix the stability constant of ML_2 complex using the value from the combined refinement. This decreased a little bit the stability constants of ML and $ML(OH)_2$ complexes while the stability constant of $ML(OH)_2$ increased. For L_T:M_T ratios 2 and 3, ESTA could refine ML_2 complex with its hydroxo–complexes $ML_2(OH)$ and $ML_2(OH)_2$. From this, hydroxo species could not be identified accurately and ESTA could not distinguish which one was really formed in the solution. They were formed in the region where the ligand was fully deprotonated. This can

explain the reason why the L_T:M_T ratios 2 and 3 gave different models as seen in Table 4.16.

Table 4.16: Stability constants for Cd-Cy_2EN system studied by GEP at different L_T:M_T ratios

L_T:M_T ratio	M(HL)	ML	ML_2	ML(OH)	$ML(OH)_2$	$ML_2(OH)$	$ML_2(OH)_2$	R-F
1(I)	12.42 (01)	6.26 (01)	rejected	9.97 (01)	12.61 (06)	excluded	excluded	0.0118
	12.41 (02)	6.25 (02)	9.35 (fixed)	9.92 (02)	13.04 (06)	excluded	excluded	0.0081
1(II)	12.00 (02)	6.264 (003)	rejected	9.90 (01)	12.49 (06)	excluded	excluded	0.0076
	12.03 (01)	6.111 (002)	9.35 (fixed)	9.87 (01)	12.68 (04)	excluded	excluded	0.0033
2	12.00 (01)	6.149 (002)	9.327 (007)	9.867 (004)	11.85 (02)	excluded	excluded	0.0016
	12.00 (01)	6.147 (002)	9.410 (006)	excluded	excluded	13.32 (01)	15.41 (02)	0.0015
	12.01 (01)	6.141 (002)	9.36 (01)	9.32(07)	excluded	13.12(03)	excluded	0.0020
	12.00 (01)	6.147 (002)	9.41 (01)	excluded	11.68(02)	13.32 (01)	excluded	0.0015
	11.997 (007)	6.149 (002)	9.36 (01)	9.869 (004)	excluded	excluded	15.12(03)	0.0016
3	12.02 (01)	6.291 (002)	9.50 (01)	10.33 (01)	12.62(02)	excluded	excluded	0.0017
	12.02 (01)	6.291 (002)	9.626 (007)	excluded	excluded	13.49 (01)	15.79(02)	0.0017
	12.02 (01)	6.291 (002)	9.62 (01)	excluded	12.47(02)	13.49 (01)	excluded	0.0016
1(II), 2 and 3	12.01 (01)	6.151 (004)	9.35 (01)	10.00 (01)	12.31(03)	excluded	excluded	0.0072
	12.01 (01)	6.150 (004)	9.35 (01)	10.004 (005)	Excluded	excluded	15.55(02)	0.0075
	12.00 (01)	6.152 (004)	9.33 (01)	9.98 (01)	Excluded	12.67(03)	excluded	0.0077

Let us focus on L_T:M_T ratios 1(II) and 2. The presence of ML_2 complex in L_T:M_T ratio 2 decreased a little bit the stability constants of M(HL) and ML(OH) complexes. This suggests that ML_2 was also present in L_T:M_T ratio 1 but the degree of its formation was not high enough to compute its stability constant. This was the reason why the stability constant of ML_2 complex was fixed in the refinement of L_T:M_T ratio 1 data. The results in Table 4.16 were obtained after

refinement of acid and base concentrations. The change in the concentration was not major as indicated in Table 4.17.

Table 4.17: Change in acid and base concentrations for Cd–Cy_2EN system at different L_T:M_T ratios

L_T:M_T ratio	$[H^+]$ before	$[H^+]$ after	% change	$[OH^-]$ before	$[OH^-]$ after	% change
1(I)	0.0106 M	0.0106246 M	+ 0.23 %	0.010 M	0.0099757 M	- 0.25 %
1(II)	0.0106 M	0.0106025 M	+ 0.03 %	0.010 M	0.0099938 M	- 0.06 %
2	0.0106 M	0.010608 M	+ 0.08 %	0.010 M	0.0099211 M	- 0.79 %
3	0.0106 M	0.010625 M	+ 0.24 %	0.010 M	0.0098915 M	- 1.09 %

4.10.2. Complex formation curve

Three different metal-ligand models resulted in the lowest standard deviation and Hamilton R-factor as well as better fit for both experimental and calculated potentiometric formation $\overline{Z}_M$ curves. Plots of $\overline{Z}_M$ vs. values of pA = $-\log_{10}$ A are presented below in Figure 4.34. The model used in the calculation was M(HL), ML, ML_2, ML(OH) and ML $(OH)_2$. The small shift observed between pA 6 and 8 suggests the formation of M(HL) complex. The observed plateau in the pA range 4–5 and at $\overline{Z}_M = 1$ confirms that the complex ML is formed and it seems to be a predominant species in the solution. The absence of the plateau at $\overline{Z}_M = 2$ suggests that the complex ML_2 is not major as ML complex. The presence of ML(OH) complex is indicated by the pronounced back-fanning feature observed for L_T:M_T ratio 1. The back–fanning feature observed for other ratios suggest that there is a formation of other hydroxospecies but, as explained before, one cannot distinguish which one was formed.

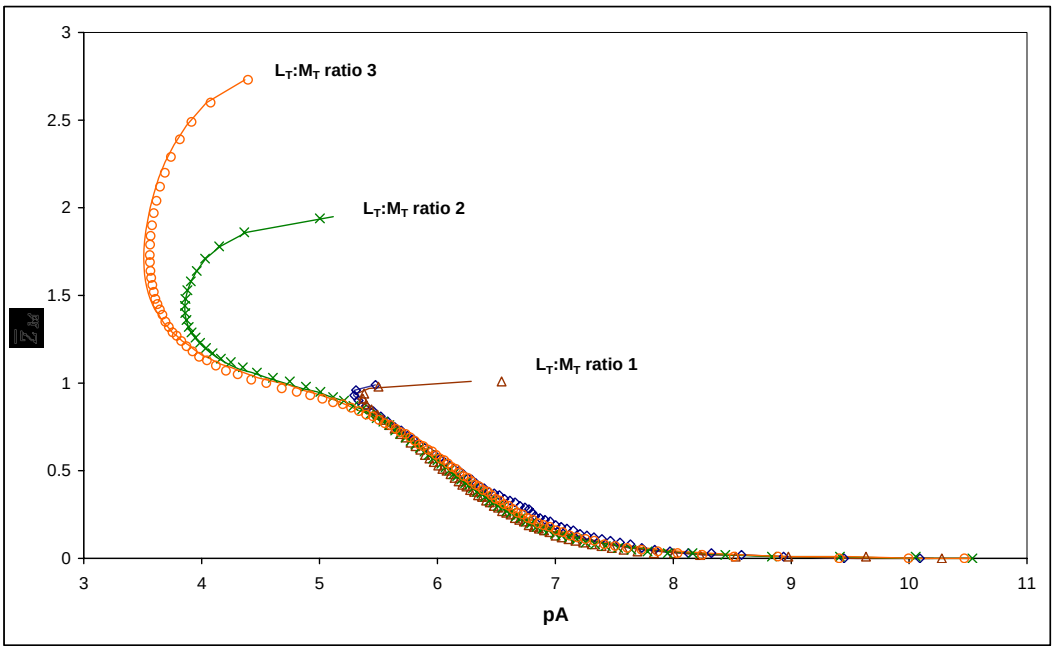

Figure 4.34: Experimental (points) and calculated (solid line) potentiometric complex formation curves for Cd–Cy_2EN system studied at 25°C and ionic strength 0.1 M in $NaNO_3$. Model M(HL), ML, ML_2, ML(OH) and ML $(OH)_2$.

4.10.3. Species distribution diagram

The species distribution diagrams are presented in Figures 4.35, 4.36, and 4.37. They were calculated for different models obtained from the combined refinement (see Table 4.16). According to the species distribution diagram in Figures 4.35 and 4.36, one can see that the precipitation of $Cd(OH)_2$ is predicted at pH about 10, when the complexes $ML_x(OH)_2$ start to form in solution. However, precipitation was noted only at pH 11, one pH unit above the predicted precipitation of $Cd(OH)_2$. Either the precipitate could not be seen at the beginning of its formation and, as the pH increased, the quantity of precipitate became significant and it could be seen at a later stage, or the precipitation of $ML_x(OH)_2$ took place at significant concentration of the complex. If the latter case is correct, then the formation of $ML_x(OH)_2$ must be seen as kinetically slow.

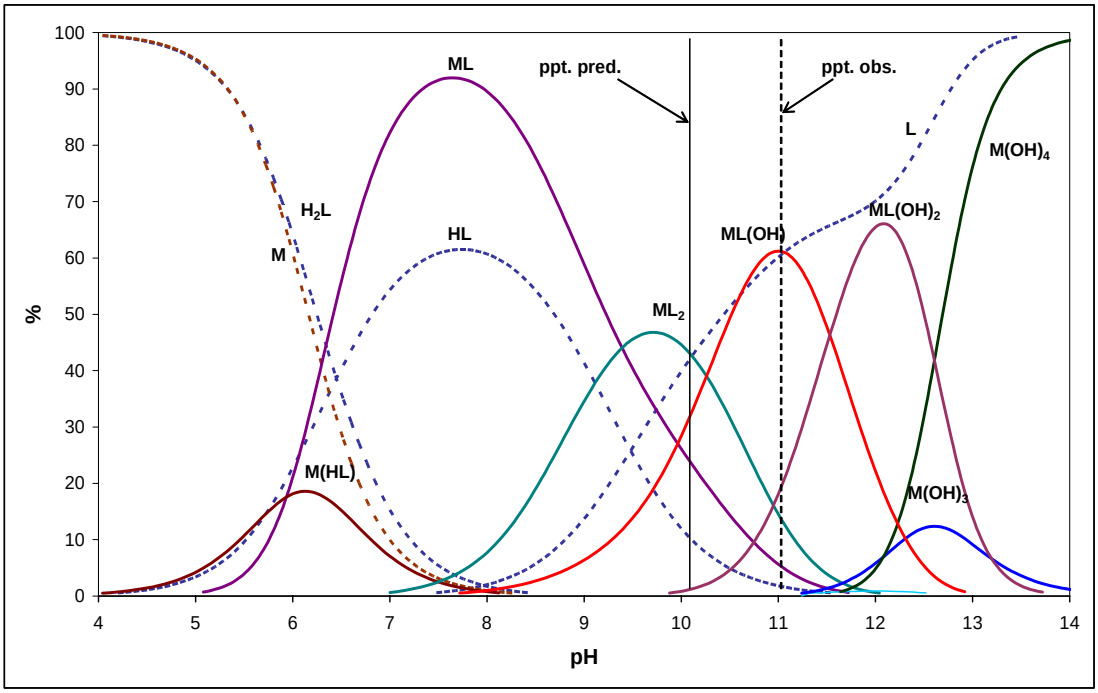

Figure 4.35: Species distribution diagram for Cd–Cy_2EN system studied by potentiometry at 25°C and ionic strength 0.1 M in $NaNO_3$. $[M_T] = 1 \times 10^{-3}$ M and $[L_T] = 3 \times 10^{-3}$ M. Model M(HL), ML, ML_2, ML(OH) and $ML(OH)_2$ from combined refinement.

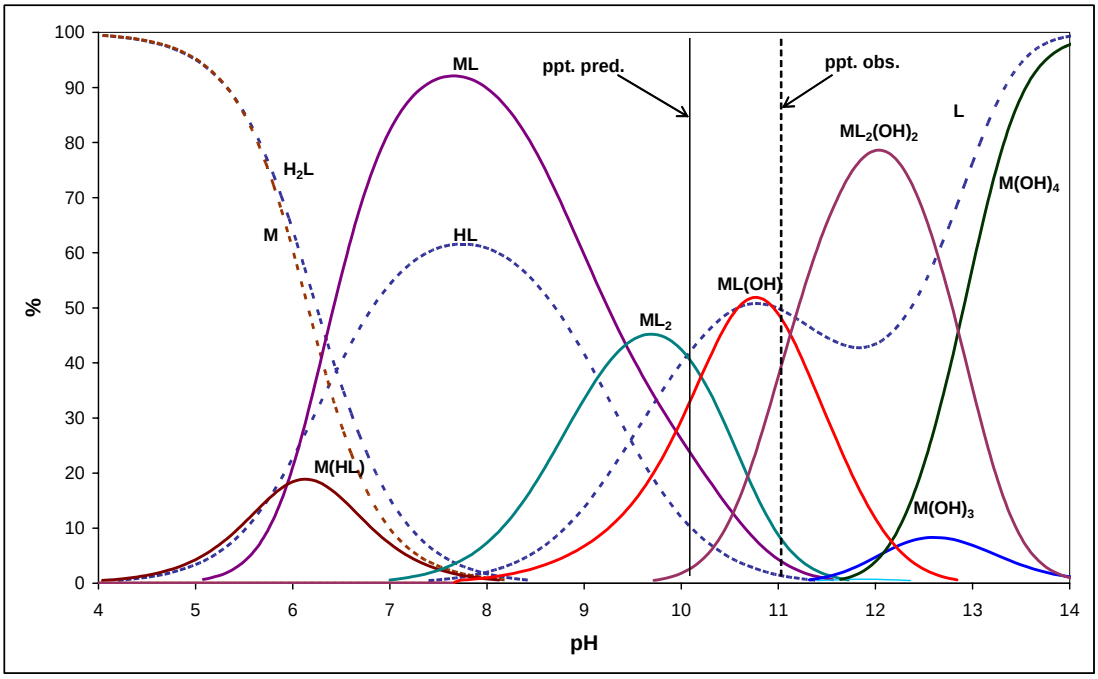

Figure 4.36: Species distribution diagram for Cd–Cy_2EN system studied by potentiometry at 25 ° C and ionic strength 0.1 M in $NaNO_3$. $[M_T] = 1 \times 10^{-3}$ M and $[L_T] = 3 \times 10^{-3}$ M. Model M(HL), ML, ML_2, ML(OH) and $ML_2(OH)_2$ from combined refinement.

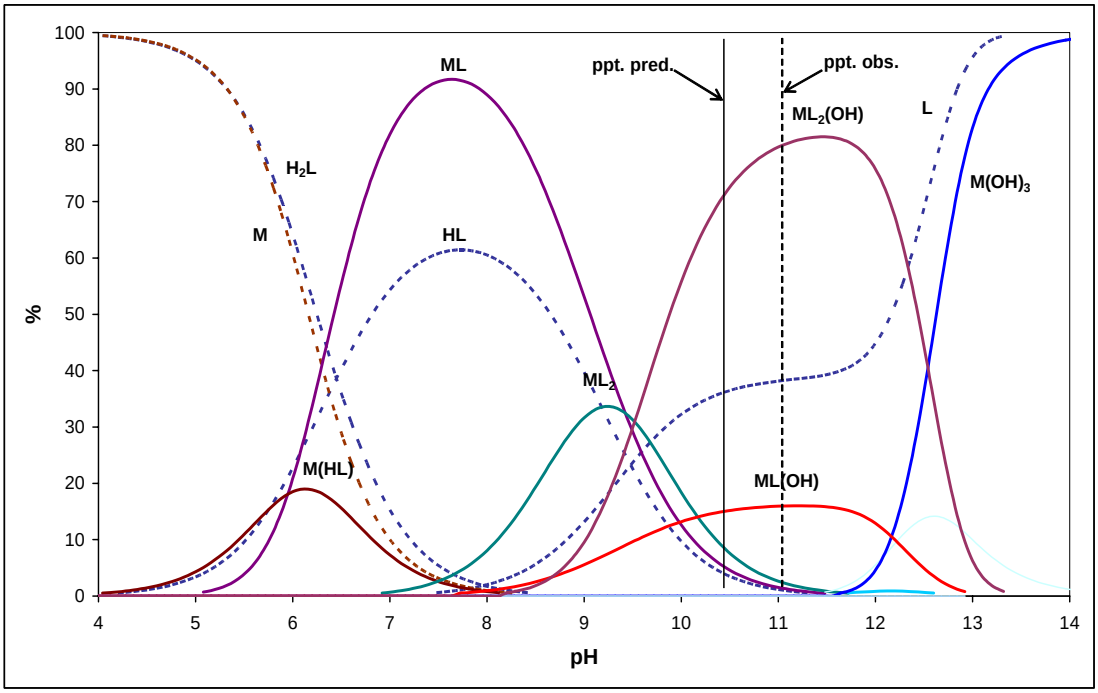

Figure 4.37: Species distribution diagram for Cd–Cy_2EN system studied by GEP at 25°C and ionic strength 0.1 M in $NaNO_3$. $[M_T] = 1 \times 10^{-3}$ M and $[L_T] = 3 \times 10^{-3}$ M. Model M(HL), ML, ML_2, ML(OH) and $ML_2(OH)$ from combined refinement.

The species distribution diagram in Figure 4.37 was calculated using the model M(HL), ML, ML_2, ML(OH) and $ML_2(OH)$. It shows that the predicted precipitation for $Cd(OH)_{2(s)}$ was at pH 10; 0.5 pH unit below the observed precipitation. The complexes ML(OH) and $ML_2(OH)$ are formed in the same pH range, but the complex ML(OH) is formed under the complex $ML_2(OH)$. For this model and all others (Figures 4.35 and 4.36), the complex ML seems to be a major species in the solution. This is confirmed by the plateau observed at $\overline{Z}_M = 1$ in Figure 4.34.

From Figures 4.35, 4.36, and 4.37 one cannot distinguish which hydroxospecies was formed in the solution. They are all fully formed in the region where the ligand is fully deprotonated. As the complex ML(OH) was refined in different models obtained for Cd–Cy_2EN system, one can confirm that this complex exists

in the solution. This is in accordance with the back–fanning feature observed in Figure 4.34 for L_T:M_T ratio 1. From GEP one can confirm the presence of M(HL), ML, ML_2 and ML(OH) complexes.

4.11. Comparison between GEP and DC_{tast} for Cd–Cy_2EN system

Even if the curves from polarography were not fitted properly (it appeared to be an impossible task), it was observed that the predicted M–L–OH model from GEP and DC_{tast} were in a good agreement. The computed stability constant of M(HL) complex from GEP is in good agreement with the one obtained from DC_{tast} (see Tables 4.15 and 4.16). This is not surprising because M(HL) complex was formed in the pH range where one DC–waves were recorded. This is confirmed by the shape of complex formation curves in Figures 4.38, 4.39, and 4.40. These Figures show the same small shift that is observed for both DC_{tast} experimental points and computed curves using potentiometric results in the pH range between 4 and 5.5. For ML and ML_2 complexes, the computed stability constants from GEP were smaller than the ones obtained from DC_{tast}. This could be attributed to the error made during the fitting of the polarographic waves as these complexes are formed in the region where the double DC–waves were observed. The difference observed for the ML_2 complex is smaller than the one observed for the ML complex. The fact that ML_2 is formed when the observed shift in half–wave potential is large made the errors in estimated $E_{1/2}$ less significant when compared with the errors made for ML complex. This complex also is at its maximum of formation when mainly one DC–wave was observed. According to the species distribution diagram in Figure 4.35, the maximum formation of ML complex is at

pH 8. At this pH, the difference in corrected shift between observed (DC_{tast}) and computed (GEP) curves is about 14 mV, which makes an error of 17 %. At about pH 9.5 when ML_2 complex is at its maximum of formation, the difference in corrected shift is about 9 mV. The error made was about 7 %. This can explain the reason why the difference between stability constants from GEP and DC_{tast} for ML_2 complex is not that significant.

The plots in Figures 4.38, 4.39 and 4.40 are calculated using the observed points from DC_{tast} experiment and computed CFC curves from GEP results. These results are for three models obtained when all titrations were combined and refined simultaneously (see Table 4.16).

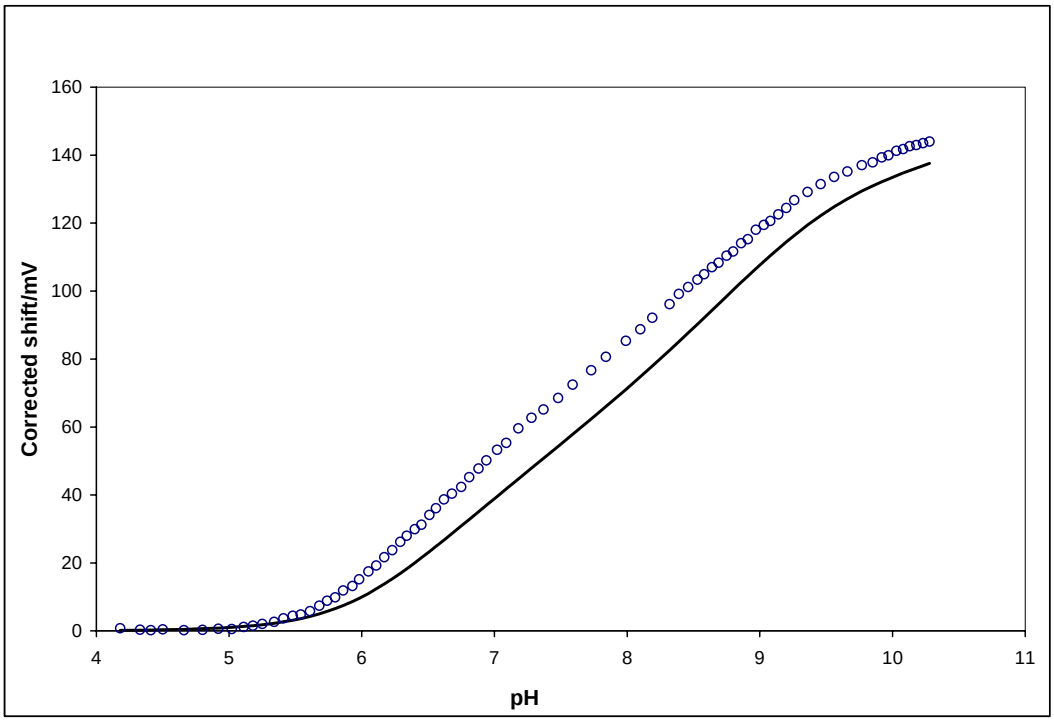

Figure 4.38: Complex formation curves using the model from GEP, and polarographic conditions for L_T:M_T ratio 47. $[M_T] = 1.05 \times 10^{-4}$ M and $[L_T] = 4.98 \times 10^{-3}$ M. Circles represent experimental points from DC_{tast} and solid line indicates the fitted curve for the model M(HL), ML, ML_2, ML(OH) and $ML(OH)_2$ from GEP.

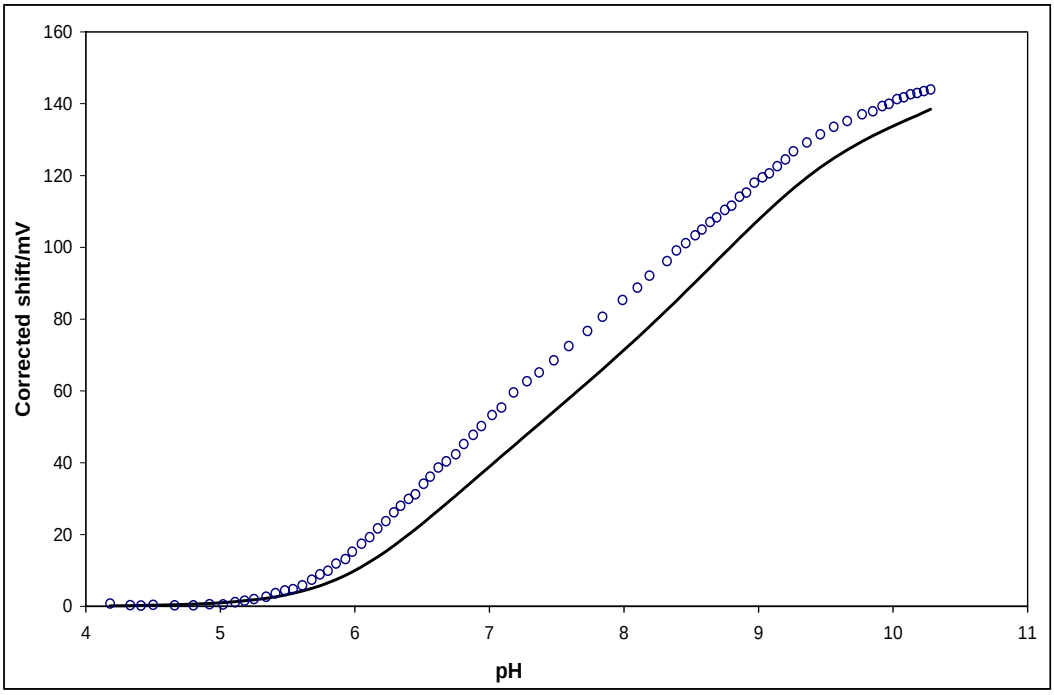

Figure 4.39: Complex formation curves using the model from GEP, and polarographic conditions for L_T:M_T ratio 47. $[M_T] = 1.05 \times 10^{-4}$ M and $[L_T] = 4.98 \times 10^{-3}$ M. Circles represent experimental points from DC_{tast} and solid line indicates the fitted curve for the model M(HL), ML, ML_2, ML(OH) and $ML_2(OH)_2$ from GEP.

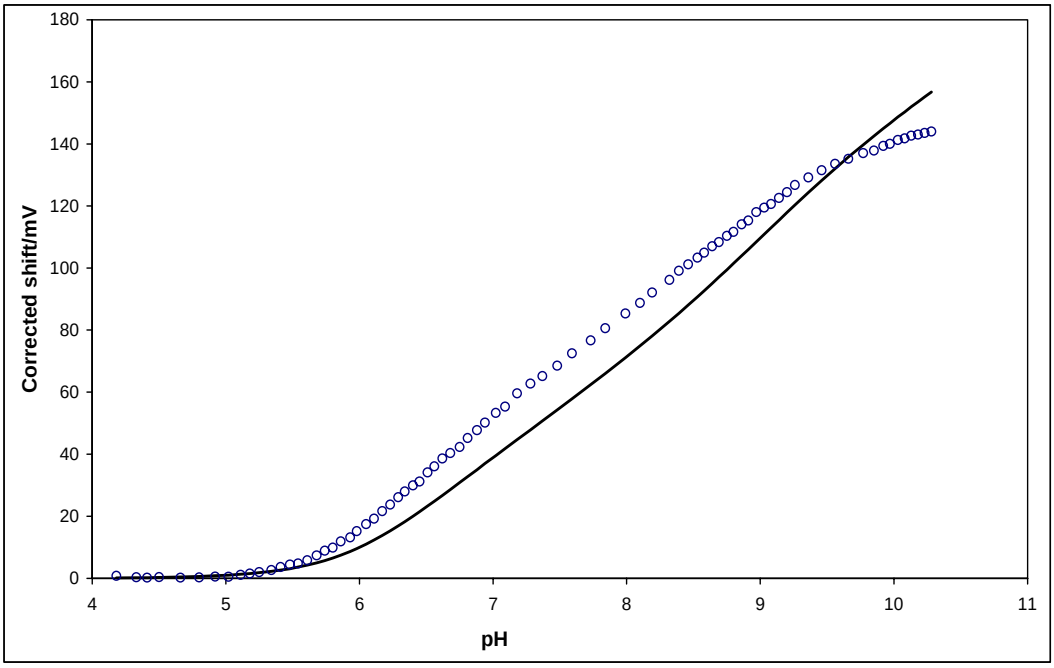

Figure 4.40: Complex formation curves using the model from GEP, and polarographic conditions for L_T:M_T ratio 47. $[M_T] = 1.05 \times 10^{-4}$ M and $[L_T] = 4.98 \times 10^{-3}$ M. Circles represent experimental points from DC_{tast} and solid line indicates the fitted curve for the model M(HL), ML, ML_2, ML(OH) and $ML_2(OH)$ from GEP.

By analysing these Figures, one can reject immediately the model presented in Figure 4-40. This Figure shows a shift much higher than the one observed as well as incorrect trend in the CCFC. The Figures 4.38 and 4.39 present the same shape and one cannot distinguish which one was the right model. Also one cannot trust the presence of $ML(OH)_2$ and $ML_2(OH)_2$ complexes. They start to form at pH of about 10 (see Figures 4.35 and 4.36) where the precipitation of $Cd(OH)_2$ complex is predicted. Even though the precipitation was observed at around pH 11, it could start to form early.

As a conclusion, the proposed model for Cd–Cy_2EN system must include M(HL), ML, ML_2 and ML(OH). Two different techniques predicted $ML_x(OH)_2$ complexes, but their stability constants are uncertain. Since the formation of ML(OH) was positively identified (see back–fanning feature for L_T:M_T ratio 1 in Figure 4.34), it seems to be reasonable also to propose $ML(OH)_2$ as more certain than $ML_2(OH)_2$. The model and stability constants proposed for Cd–Cy_2EN system are seen in Table 4.18. Note that DC_{tast} data are included mainly for comparison.

Table 4.18: Proposed model and stability constants for Cd–Cy_2EN system

Equilibrium	**Log β**	
Certain	**GEP**	**DC_{tast}**
M + L + H = M(HL)	12.01(01)	11.91(09)
M + L = ML	6.151(003)	6.70 (01)
M + 2L = ML_2	9.35(01)	9.63 (02)
M + L + OH = ML(OH)	10.000(005)	9.48 (61)
Uncertain		
M + L + 2OH = $ML(OH)_2$	12.31(03)	13.15(39)
M + 2 L + 2 OH = $ML_2(OH)_2$	15.55(02)	15.65(38)

4. 12. Study of Pb–Cy_2EN system by GEP

4.12.1. Data treatment

As for Cd–Cy_2EN system, three L_T:M_T ratios were investigated in the study of the Pb–Cy_2EN system. The L_T:M_T ratio 1 was performed twice, and the final model and stability constants were obtained when all ratios were combined and refined simultaneously. Different models and stability constants proposed are presented in Table 4.19.

Table 4.19: Model and stability constants for Pb–Cy_2EN system studied by GEP at 25°C and ionic strength 0.1 M in $NaNO_3$.

L_T:M_T ratio	M(HL)	ML	ML_2	ML(OH)	$ML_2(OH)$	$ML(OH)_2$	$ML_2(OH)_2$	R-factor
1(I)	12.24 (01)	6.724 (004)	12.04 (04)	12.87 (01)	Rejected	Rejected	Rejected	0.00552
	12.14 (02)	6.749 (003)	excluded	12.928 (004)	rejected	Rejected	Rejected	0.00732
1(II)	12.22 (01)	6.761 (003)	11.63 (01)	12.857 (002)	Rejected	Rejected	Rejected	0.00502
	12.18 (01)	6.770 (002)	excluded	12.886 (002)	Rejected	Rejected	Rejected	0.00502
2	12.10 (01)	6.785 (001)	11.67 (01)	12.89 (01)	Rejected	17.10 (01)	Rejected	0.0024
	12.21 (02)	6.772 (01)	11.96 (01)	rejected	16.82 (01)	rejected	Rejected	0.00591
	12.01 (02)	6.790 (003)	excluded	12.885 (004)	Rejected	16.80 (02)	Rejected	0.00591
3	11.98 (02)	6.813 (003)	excluded	12.888 (004)	Rejected	17.03 (01)	Rejected	0.0064
	12.05 (02)	6.816 (003)	11.664 (004)	rejected	16.325 (0.005)	rejected	19.96(02)	0.008
	12.06 (01)	6.816 (003)	11.668 (004)	rejected	16.20 (01)	16.73 (02)	rejected	0.00475
1(I) 1(II) 2 and 3	12.08 (01)	6.780 (002)	rejected	12.885 (002)	Rejected	16.952 (008)	Rejected	0.00860
	excluded	6.758 (003)	rejected	12.777 (004)	Rejected	16.34 (01)	Rejected	0.016

During refinement operation, it was observed that ML_2 complex was accepted and stability constants refined for L_T:M_T ratios 1 and 2 using the raw data, but this complex was accepted for L_T:M_T ratio 3 only when acid or base concentration was refined. Numerous models were tested as is indicated in Table 4.19. When all four

titrations were combined and refined simultaneously, ML_2 was rejected by ESTA. This can suggest that either ML_2 complex is a minor or unlikely species.

As for the previous systems, the acid or base concentrations were also refined. The change in their concentrations was rather small (less than ± 2 %) as shown in Table 4.20.

Table 4.20: Change in acid and base concentrations for Pb–Cy_2EN system at different L_T:M_T ratios

L_T:M_T ratio	$[H^+]$ before	$[H^+]$ after	% change	$[OH^-]$ before	$[OH^-]$ after	% change
1(I)	0.0106 M	0.0105959 M	– 0.04 %	0.010 M	0.0100062 M	+ 0.06 %
1(II)	0.0106 M	0.0106337 M	+ 0.32 %	0.010 M	0.0099487 M	- 0.51 %
2	0.0106 M	0.0106514 M	+ 0.48 %	0.010 M	0.0099022 M	- 0. 98 %
3	0.0106 M	0.0106701 M	+ 0.66 %	0.010 M	0.0098504 M	+ 1.50 %

4.12.2. Complex formation curve

The following metal-ligand model M(HL), ML, ML(OH) and $ML(OH)_2$ resulted in the lowest standard deviation as well as better fit for both calculated and experimental complex formation curves. Plots of $\overline{Z}_M$ vs. values of pA are seen in Figure 4.41. This Figure shows a back-fanning feature for all ratios studied. This confirms that hydroxo-species are formed. The smooth continuation of the curves up to $\overline{Z}_M$ equal to 2 suggests the formation of ML_2 complex. Even if this complex was rejected by the combined refinement, several refinement operations could get it as seen in Table 4.19.

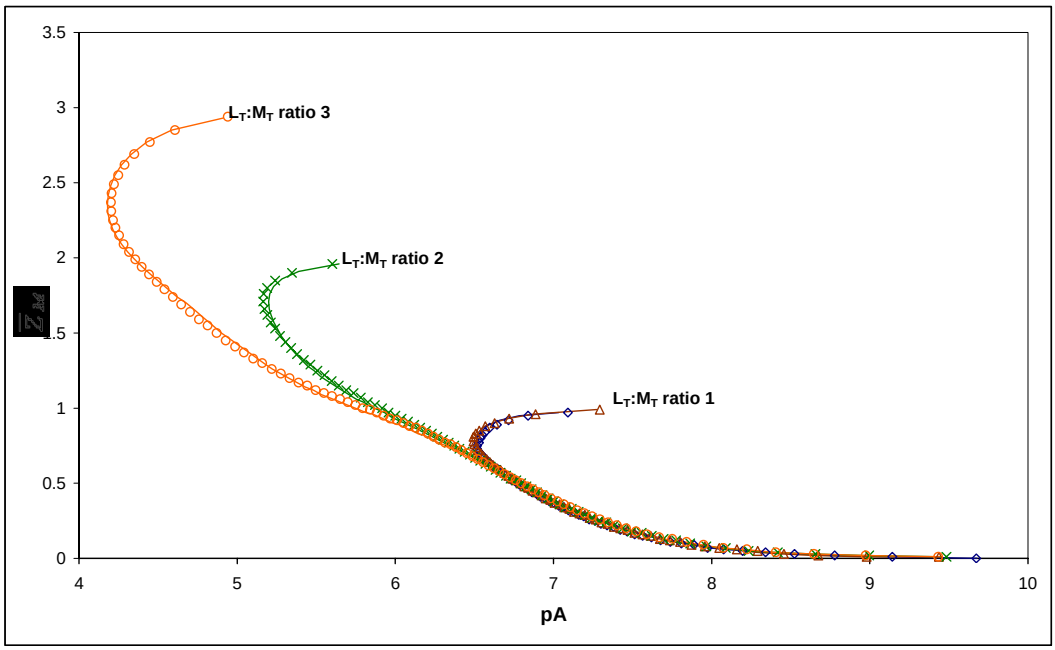

Figure 4.41: Experimental (points) and fitted (solid lines) potentiometric complex formation curves for Pb–Cy_2EN system studied at 25°C and ionic strength 0.1 M in $NaNO_3$. Model M(HL), ML, ML(OH) and $ML(OH)_2$.

4.12.3. Species distribution diagram

The plot of species distribution diagram presented in Figure 4.42 was calculated using the stability constants from the refinement of the data for L_T:M_T ratio 2. It shows that the complex M(HL) is a minor species in the solution, and when it was excluded from the model, the behaviour of the complex formation curve did not change. In addition, one can observe that (see Table 4.19) the values of stability constants of complexes ML and ML(OH) changed a little bit but R–factor became higher. This confirms that M(HL) complex exists in solution. The Figure 4.42 also shows that ML_2 complex was formed under ML(OH) complex. This can explain the reason why ML_2 was rejected in the combined refinement of all titrations. The same Figure also shows that no precipitation was predicted using solubility product of $Pb(OH)_2$. During the experiment, the precipitation was observed at pH

8.9 for L_T:M_T ratio 2. This can suggest that either it was $ML(OH)_2$) complex or the excess of the ligand that precipitated out.

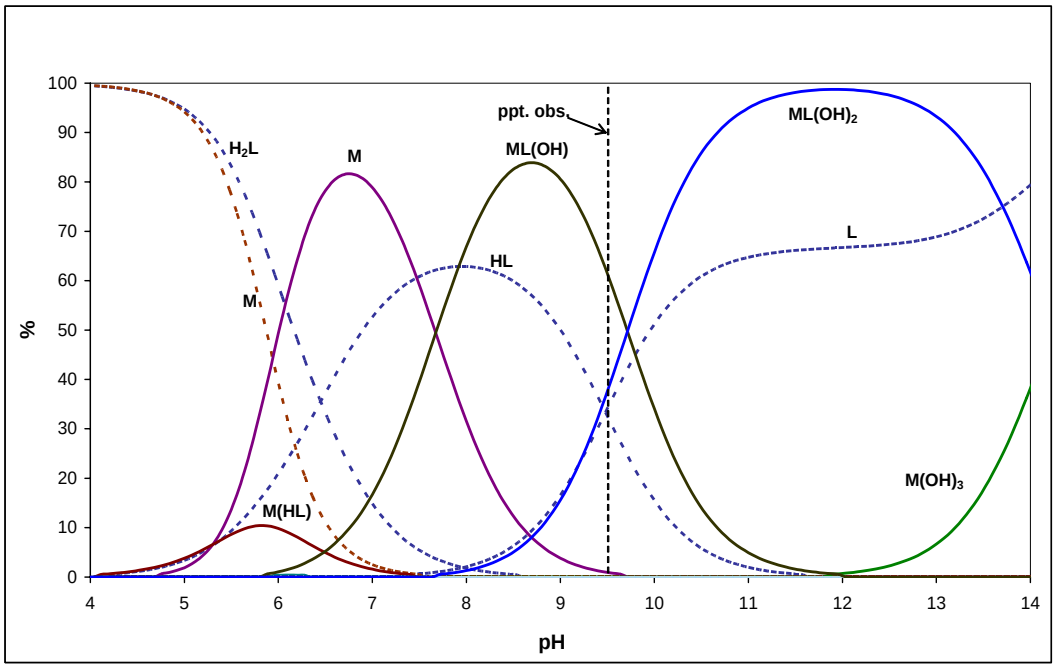

Figure 4.42: Species distribution diagram for Pb–Cy_2EN system studied by GEP at 25°C and ionic strength 0.1 M in $NaNO_3$. The model used is M(HL), ML, ML(OH) and $ML(OH)_2$ from the combined refinement and conditions for L_T:M_T ratio 3. $[M_T] = 1.01 \times 10^{-3}$ M and $[L_T] = 3.00 \times 10^{-3}$ M.

To know exactly which model is the correct one for the system Pb–Cy_2EN, some other speciation techniques must be used. It was tried to study this system by DC_{tast} polarography; unfortunately, the behaviour of the waves recorded did not allow the fitting of the data properly. This is fully explained in section 4.13.

4.13. DC_{tast} polarographic study of Pb-Cy_2EN

The experiment involving the system Pb–Cy_2EN have been performed by DC_{tast} at two L_T:M_T ratios: 49 and 29. The waves recorded during the experiment showed the same behaviour as those recorded in the study of Cd–Cy_2EN system. Selected

DC–waves recorded at different pH values are presented in Figure 4.43. By simple fitting, the first waves seemed to be fully reversible; delta was between 1 and 0.9. As the pH increased (from pH 6 to pH 10 for ratio 29), the DC–waves recorded split (two waves could be seen), and became less reversible. Between pH 6 and 7.5, delta decreased down to 0.44 and the system seemed to be irreversible. From pH 7.5, delta started increasing up to pH 10. At pH 10, alpha was about 0.7.

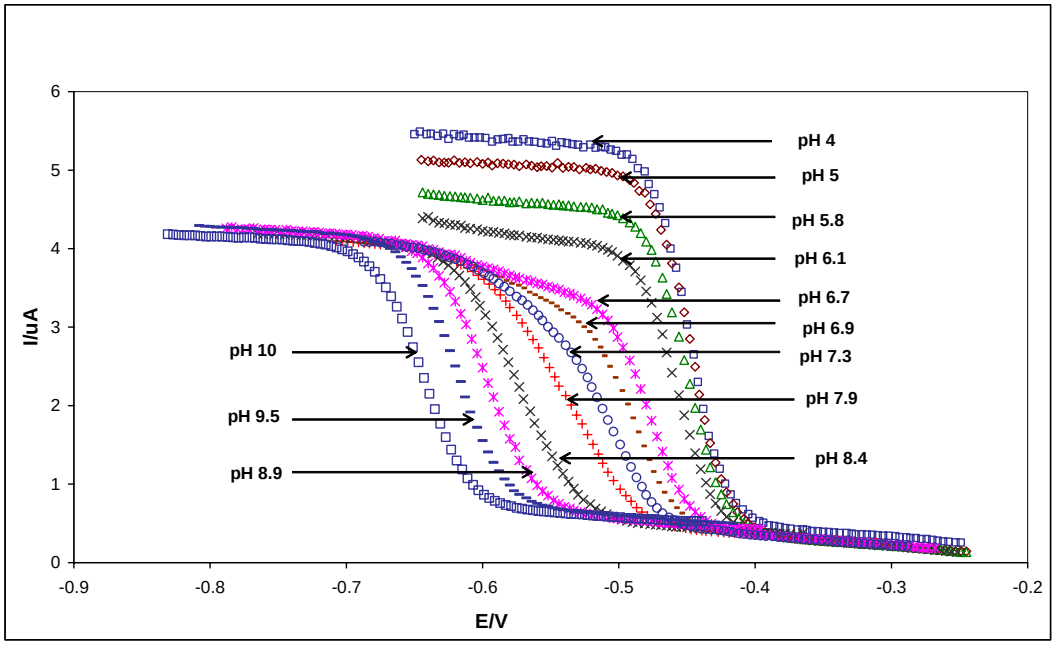

Figure 4.43: Behaviour of different waves recorded for Pb–Cy_2EN system L_T:M_T ratio 29 studied by DC_{tast} at 25 ° C and ionic strength 0.1 M in $NaNO_3$. $[M_T] = 1.017 \times 10^{-4}$ M and $[L_T] = 2.989 \times 10^{-3}$ M.

It was then decided to fit the initial and last waves where the system appeared to be more or less reversible, i.e. from pH 4 to pH 6, and from pH 8 to pH 10. In these pH ranges, only one wave was observed. Unfortunately the results obtained were not correlating with those from GEP. Figure 4.44 shows clearly the error made during the fitting procedure. This Figure was plotted using the model from GEP (solid line) and experimental points from DC_{tast} polarography. At about pH

8.1, the difference between experimental (DC_{tast}) and computed (GEP) shift was about 66 mV and at pH 10 the difference was about 47 mV.

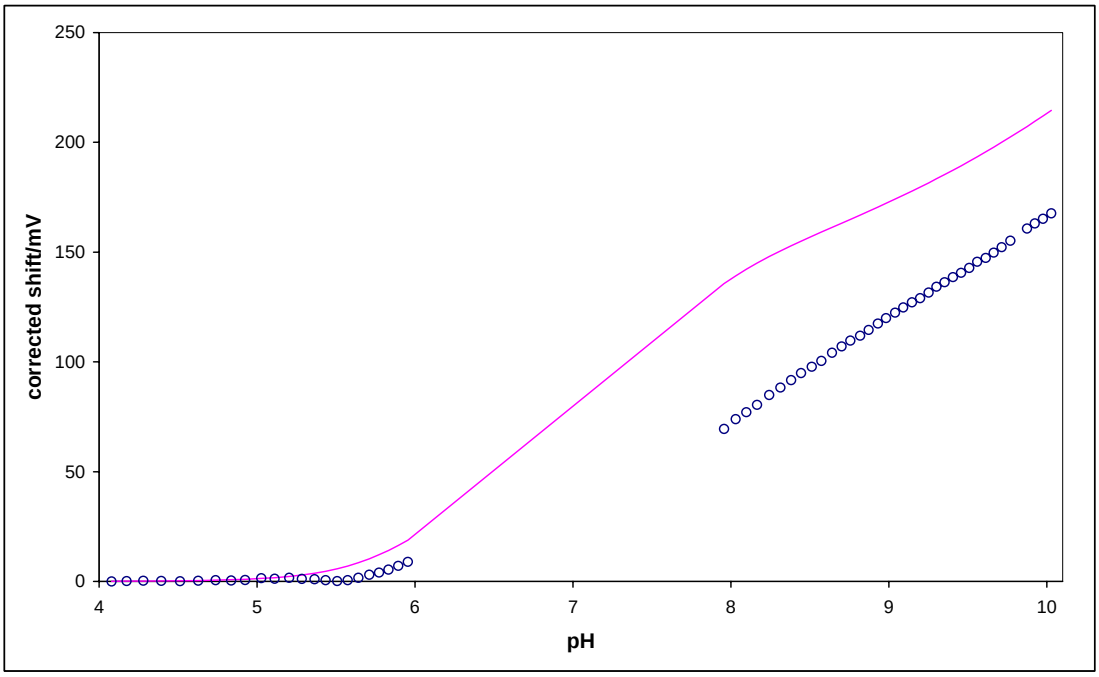

Figure 4.44: Experimental (circles) and calculated (solid line) complex formation curves obtained using the model from potentiometry (MHL, ML, ML(OH) and $ML(OH)_2$) and polarographic conditions. $[M_T] = 1.017 \times 10^{-4}$ M and $[L_T] = 2.989 \times 10^{-3}$ M.

Another observation made during the experiment was that the precipitation occurred earlier in polarography than it did in GEP. For example, the precipitation occurred at pH 9.6 in GEP at L_T:M_T ratio 3, but in DC_{tast} at L_T:M_T ratio 49 the precipitation occurred at pH 9.2. Note that the metal concentration used in polarography was 10 times smaller than the one used in potentiometry. Furthermore, using the solubility product of $Pb(OH)_2$, no precipitation was predicted for the conditions used in potentiometry at L_T:M_T ratio 3 and $[L_T] = 3 \times 10^{-3}$ M. This can suggest that it was not $Pb(OH)_2$ that precipitated out but the excess of the ligand. This is confirmed by the fact that the precipitation

occurred later (at higher pH) when the ligand concentration was decreased, At L_T:M_T ratio 29, the precipitation occurred at pH 10 ($L_T = 2.99 \times 10^{-3}$ M) while the precipitation occurred at pH 9.2 at L_T:M_T ratio 49 ($L_T = 4.98 \times 10^{-3}$ M).It is rather unusual and unexpected to observe polarographic ECFC (points) so much below GEP–computed CFC. The only reasonable explanation at this stage could be that since the total metal concentration [M_T] was low and the formation of complexes did not decrease the total ligand concentration [L_T] significantly, the experiment was conducted in oversaturated solution and possibly partly precipitated the ligand. This in turn would decrease the total ligand concentration resulting in much smaller corrected shift. If this assumption is correct, one can explain the behaviour of the DC–waves recorded for Pb–Cy_2EN system as said by Crow [50]: "If the ligand is not in sufficient excess, the reversible wave becomes distorted and may even split into two or more parts". An example of such behaviour was discovered by Koryota [75] who studied Cadmium in the presence of low concentrations of free cyanide. In the discharge of complex cadmium cyanide the wave divided into two sections. The same explanation can be given to the behaviour of DC–waves recorded for Cd–Cy_2EN system.

4.14. Study of Cu–Cy_2EN, Ni–Cy_2EN and Zn–Cy_2EN by GEP

4.14.1. Cu–Cy_2EN system

i. Data fitting

The GEP study of Cu–Cy_2EN system was performed at 25 ° C and ionic strength 0.1 M in $NaNO_3$. Three L_T:M_T ratios were performed: 1, 2 and 3. The L_T:M_T ratio 1 was done twice. During the refinement operation by ESTA software

(L_T:M_T ratio 1) it was possible to refine M(HL) complex but with a high standard deviation when compared with the standard deviations of other complexes. For other ratios M(HL) complex was rejected during the refinement and optimisation operations. Also it was observed that, when all ratios were refined simultaneously, ESTA could refine ML_2 complex, but with a large standard deviation when compared with other complexes. Note that each individual titration rejected ML_2 complex. From this, the presence of ML_2 complex is questionable. Different stability constants obtained are shown in Table 4.21.

Table 4.21: Models and stability constants for Cu–Cy_2EN system studied by GEP at different L_T:M_T ratios.

L_T:M_T ratio	M(HL)	ML	ML_2	ML(OH)	$ML(OH)_2$	R-Factor
1(I)	14.56(03)	11.400 (004)	rejected	18.27 (01)	23.54(01)	0.00595
1(II)	14.17(03)	11.343 (004)	Rejected	18.24(01)	23.49 (01)	0.00571
2	rejected	11.210 (002)	Rejected	18.060(003)	23.897(004)	0.00300
3	rejected	11.232 (005)	Rejected	18.16(01)	23.19 (01)	0.00655
Combined titrations	14.19(05)	11.286 (005)	Excluded	18.16(01)	23.23 (01)	0.01268
	14.04(06)	11.296 (004)	16.35(04)	18.17 (01)	23.30 (01)	0.01197
	excluded	11.285 (005)	16.34(04)	18.16 (01)	23.29 (01)	0.01222
	excluded	11.279 (004)	excluded	18.18(01)	23.24 (01)	0.01309

During refinement operation, acid and base concentrations were refined. The change in concentration was less than 4 % for all titrations as indicated in Table 4.22.

Table 4.22: Change in acid and base concentrations for Cu–Cy_2EN system at different L_T:M_T ratios

L_T:M_T ratio	$[H^+]$ before	$[H^+]$ after	% change	$[OH^-]$ before	$[OH^-]$ after	%Change
1(I)	0.0106 M	0.010828 M	+ 2.15 %	0.00993 M	0.010257 M	+ 3.32 %
1(II)	0.0106 M	0.010789 M	+ 1.79 %	0.00993 M	0.010193 M	+ 2.65 %
2	0.0106 M	0.010806 M	+ 1.95 %	0.00993 M	0.010005 M	+ 0.76 %
3	0.0106 M	0.010737 M	+ 0.13 %	0.00993 M	0.009909 M	– 0.20 %

ii. Complex formation curve

The plot of complex formation curves is presented in Figure 4.45. It shows a broad range of free ligand concentration where the complex formation function is equal to 1. This clearly indicates the involvement of one ligand molecule per one metal ion, which confirms the formation of ML complex. The complex ML seems to be very strong. This is be explained by the plateau observed at $\overline{Z}_M$ equal to 1 over approximately four pA units.

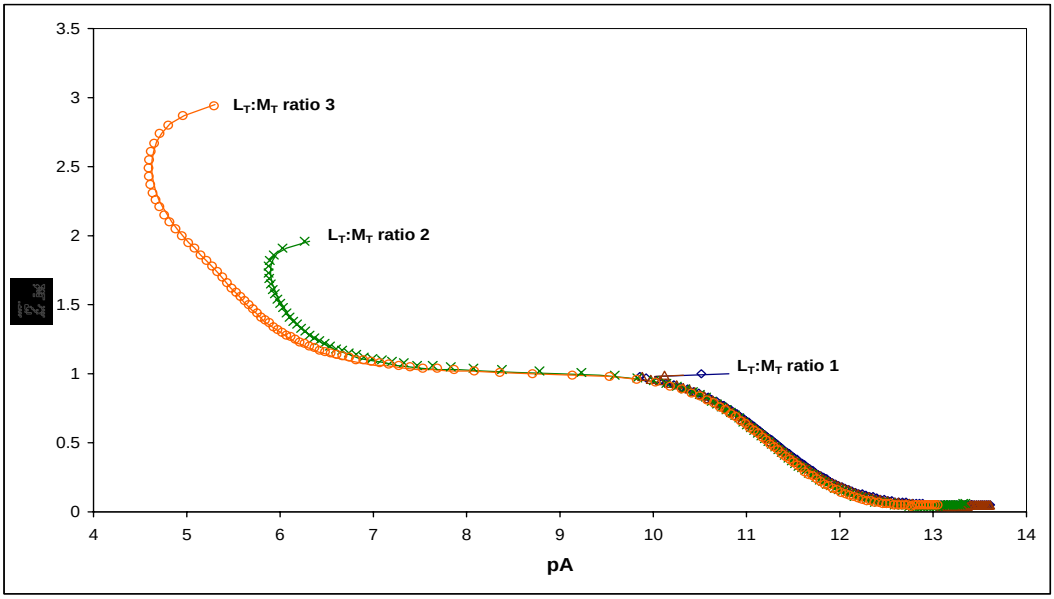

Figure 4.45: Experimental (points) and calculated (solid line) potentiometric complex formation curves for Cu–Cy_2EN system studied by GEP at 25°C and ionic strength 0.1 M in $NaNO_3$. The model used is M(HL), ML, ML(OH) and $ML(OH)_2$ from the combined refinement.

The same Figure shows a pronounced back-fanning feature which confirms the formation of hydroxospecies. In this study, it could be ML(OH) and $ML(OH)_2$. The shape of the plot in Figure 4.45 suggests the formation of ML_2 complex, but as it was discussed before, its presence is questionable.

iii. Species distribution diagram

The species distribution diagram is presented in Figure 4.46. This Figure shows that the complex ML starts to form already at about pH 3 and remains in solution up to pH 9. This confirms the fact that ML complex is strong as it was mentioned in section *ii* of this chapter. The complexes ML(OH) and $ML(OH)_2$ are formed in the region where the predominant form of the ligand is HL.

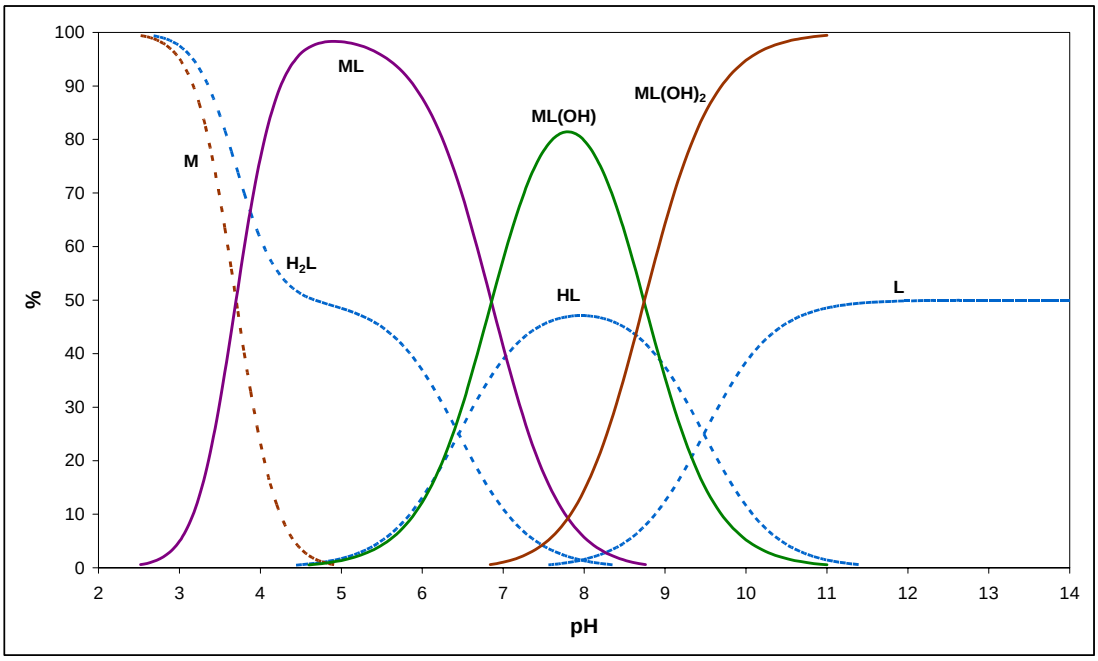

Figure 4.46: Species distribution diagram for Cu–Cy_2EN system studied by GEP at 25° C and ionic strength 0.1 M in $NaNO_3$. The model used is from the refinement of L_T:M_T ratio 3: ML, ML(OH) and $ML(OH)_2$. $[M_T] = 1.01 \times 10^{-3}$ M and $[L_T] = 2.99 \times 10^{-3}$ M.

If one could study this system by polarography, a plot of observed (or virtual) potential versus pH would show the slopes of 60 mV and 90 mV per pH unit. These slopes should then confirm the formation of ML(OH) and $ML(OH)_2$, respectively. Their formation would involve two and three protons, respectively, as indicated by the following electrochemical process at the DME:

$$ML(OH)^+ + 2\,H^+ + 2e^- = M(Hg) + HL^+ + H_2O$$

$$ML(OH)_2 + 3\,H^+ + 2e^- = M(Hg) + HL^+ + 2\,H_2O$$

The species distribution diagram potted using the model from the combination of all titrations and containing M(HL) and ML_2 complexes is shown in Figure 4.47.

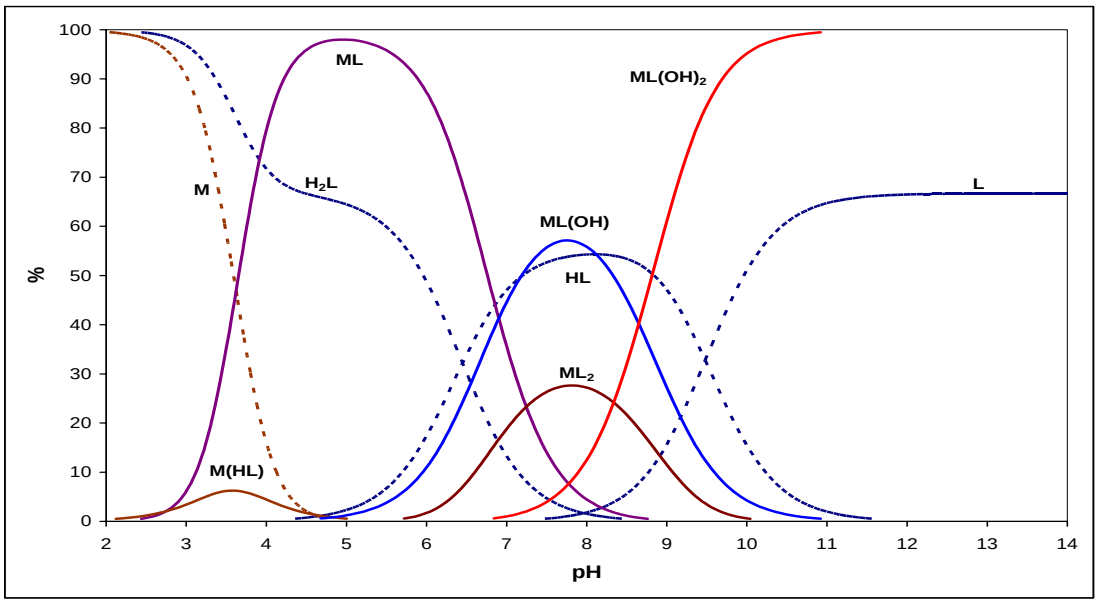

Figure 4.47: Species distribution diagram for Cu–Cy_2EN system studied by GEP at 25°C and ionic strength 0.1 M in $NaNO_3$. The model used is from the combined refinement and potentiometric conditions for L_T:M_T ratio 3: M(HL), ML, ML_2, ML(OH) and $ML(OH)_2$. $[M_T] = 1.01 \times 10^{-3}$ M and $[L_T] = 3.00 \times 10^{-3}$ M.

Figure 4.47 shows that the complex M(HL) is present at very low concentration, less than 10 % of all species present in solution. Due to the strong ML complex, the M(HL) complex is a very minor species, and ESTA software was unable to

identify this complex accurately. The same Figure also shows that ML_2 (if it is formed) is under ML(OH) complex. Note that the formation of ML_2 involves the same number of protons according to the following reactions:

$$M^{2+} + HL^{+} + H_2O \rightleftharpoons ML(OH)^{+} + 2H^{+}$$

$$M^{2+} + 2HL^{+} \rightleftharpoons ML_2 + 2H^{+}$$

This can explain the reason why the complex ML_2 was rejected during refinement operation. Other speciation techniques are needed to confirm if M(HL) and ML_2 complexes are formed.

4.14.2. Ni–Cy_2EN system

i. Data treatment

Four titrations were performed in the study of Ni–Cy_2EN system, the L_T:M_T ratio 1 was performed twice. During refinement operation, it was observed that many models could be generated. Due to the hydrolysis of the complexes ML and ML_2, several hydroxo-species were formed and the software could not distinguish which one was really in the solution. Different models obtained are presented in Table 4.23. It was also observed that the complex M(HL) had a higher standard deviation if compared with the standard deviations of other complexes. At L_T:M_T ratio 1 ESTA rejected ML_2 complex and only one model was obtained. The complex $ML(OH)_2$ also could not be refined at this ratio because of the precipitation that occurred before its formation. The complex ML(OH) was rejected by software in the presence of $ML(OH)_2$ complex at L_T:M_T ratio 2.

The complex $ML_2(OH)$ was also rejected in the presence of the complex $ML_2(OH)_2$ at the same ratio.

Table 4.23: Models and stability constants for Ni–Cy_2EN system studied by GEP at 25°C and ionic strength 0.1 M in $NaNO_3$.

L_T:M_T ratio	M(HL)	ML	ML_2	ML(OH)	$ML(OH)_2$	$ML_2(OH)$	$ML_2(OH)_2$	R-Factor
1(I)	12.76 (03)	7.81 (01)	rejected	11.78(01)	excluded	excluded	excluded	0.02207
1(II)	12.40 (03)	7.760 (003)	rejected	11.829 (006)	excluded	excluded	excluded	0.00721
2	12.27 (16)	7.80 (01)	exclude d	11.70(03)	15.34 (03)	excluded	excluded	0.01734
	11.65 (13)	7.747 (003)	10.96 (01)	rejected	15.36 (01)	rejected	rejected	0.00523
	11.69 (13)	7.748 (004)	10.98 (01)	rejected	rejected	rejected	18.90 (01)	0.00611
3	11.98 (04)	7.695 (003)	10.45 (01)	11.599 (007)	14.87 (01)	rejected	rejected	0.00318
	11.98 (04)	7.695 (003)	10.67 (01)	rejected	rejected	14.75 (01)	18.04 (01)	0.00306
	11.99 (05)	7.696 (003)	10.48 (01)	11.595 (008)	excluded	excluded	18.01 (01)	0.00366
	11.98 (05)	7.694 (003)	10.67 (01)	excluded	14.81 (01)	14.73 (01)	excluded	0.00321
Combined refinement	12.34 (04)	7.748 (004)	10.51 (03)	11.636 (008)	15.03 (02)	rejected	rejected	0.01439
	12.08 (21)	7.59 (01)	10.84 (06)	excluded	excluded	15.00 (06)	18.39 (06)	0.05490

At L_T:M_T ratio 3 $ML_x(OH)$ complexes could be refined in the presence of $ML_x(OH)_2$ complexes. Four different models were obtained as shown in Table 4.23. When all titrations were combined and refined simultaneously, only two models were obtained. The first model was M(HL), ML, ML_2, ML(OH) and $ML(OH)_2$; and the second was M(HL), ML, ML_2, $ML_2(OH)$ and $ML_2(OH)_2$. The first model had a lower R-factor than the second and it was taken as the right model from GEP. During refinement operation, acid or base concentrations were calculated. As for the previous systems, the change in their concentration was very small as seen in Table 4.24.

Table 4.24: Change in acid and base concentrations for Ni–Cy_2EN system studied by GEP at different L_T:M_T ratios

L_T:M_T ratio	$[H^+]$ before	$[H^+]$ after	% change	$[OH^-]$ before	$[OH^-]$ after	% change
1(I)	0.0106	0.0104968	– 0.97 %	0.00993	0.0099438	+ 0.14 %
1(II)	0.0106	0.0104892	– 1.05 %	0.00993	0.0099292	+ 0.008 %
2	0.0106	0.0106344	+ 0.32 %	0.00993	0.0098830	– 0.47 %
3	0.0106	0.0106412	+ 0.39 %	0.00993	0.0098683	– 0.62 %

ii. Complex formation curve

The complex formation curves for Ni–Cy_2EN system are shown in Figure 4.48. They were calculated for the model M(HL), ML, ML_2, ML(OH) and $ML(OH)_2$. As for the Cu–Cy_2EN system, the complex ML seems to be very strong. This is confirmed by the plateau observed over a range of three pA units (from pA 4 to pA 7) at $\overline{Z}_M$ equal to one.

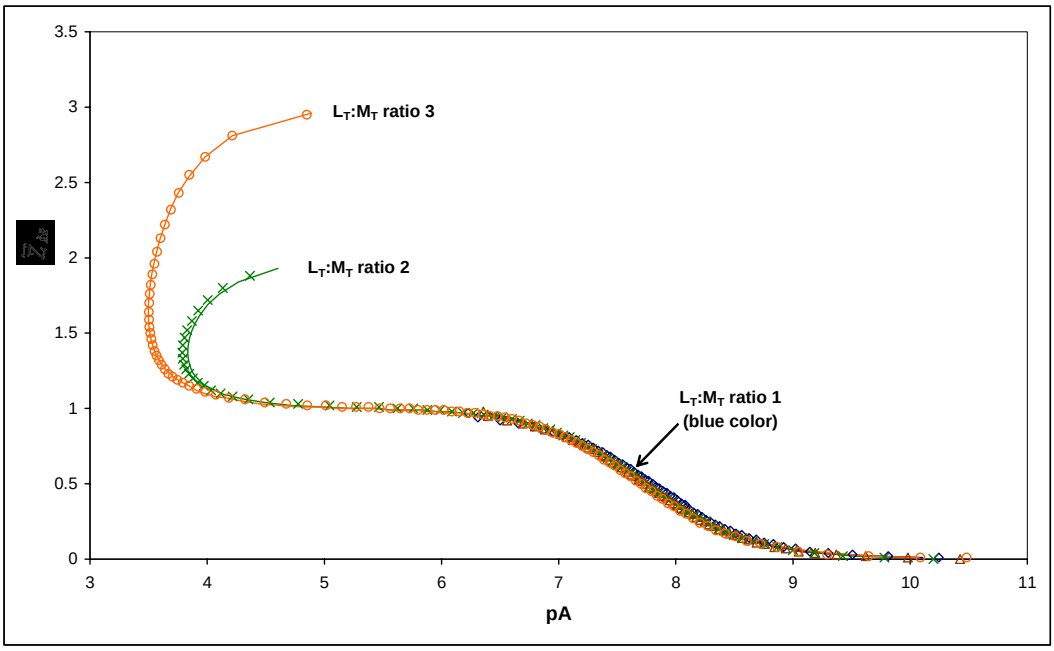

Figure 4.48: Experimental (points) and calculated (solid lines) complex formation curves for Ni–Cy_2EN system studied by GEP at 25°C and ionic strength 0.1 M in $NaNO_3$. The model used is M(HL), ML, ML_2, ML(OH) and $ML(OH)_2$ from the combined refinement

The formation of hydroxo-species is suggested by a pronounced back-fanning feature. Note that complex formation curves do not show the formation of ML_2 even if this complex was refined without a problem. This might indicate that ML_2 is a minor metal containing species when compared with ML and $ML(OH)_x$ complexes.

iii. Species distribution diagram

The precipitation was noted at pH 9.3 for L_T:M_T ratio 1, but for other L_T:M_T ratios, no precipitation was observed. This is in a good agreement with the species distribution diagram in Figure 4.49.

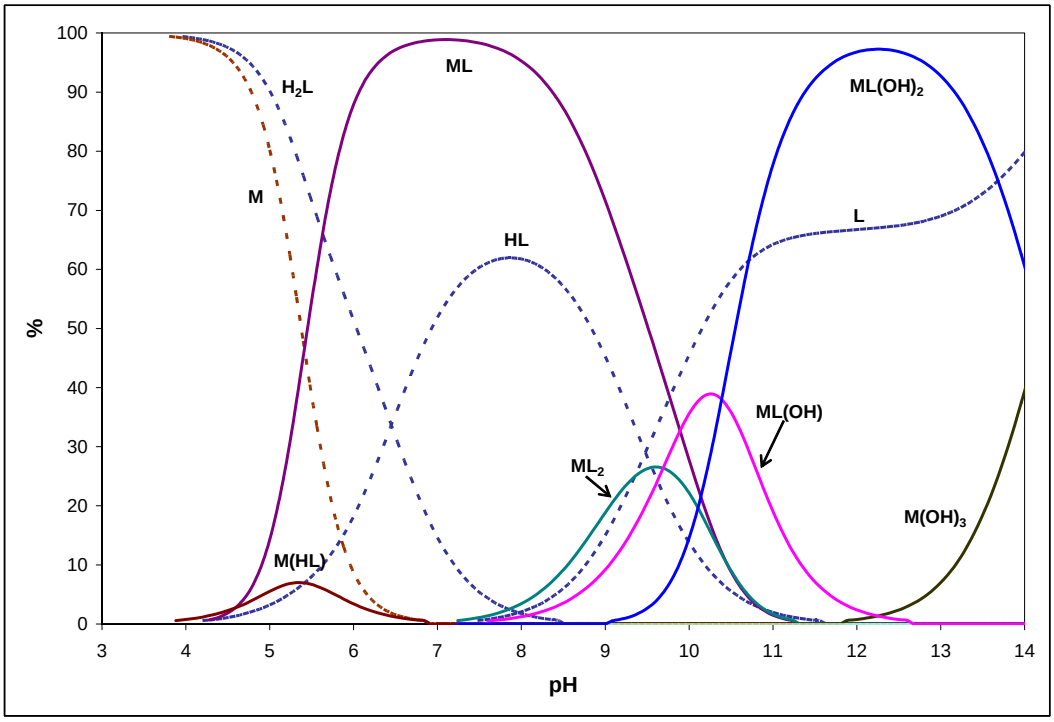

Figure 4.49: Species distribution diagram for Ni–Cy_2EN system studied by GEP at 25°C and ionic strength 0.1 M in $NaNO_3$. The model used is M(HL), ML_2, ML, ML(OH) and $ML(OH)_2$ from the refinement of L_T:M_T ratio 3. $[M_T] = 1.01 \times 10^{-3}$ M and $[L_T] = 2.99 \times 10^{-3}$ M.

By use of solubility product of $Ni(OH)_2$ the precipitation was predicted at pH 9 for L_T:M_T ratio 1 and no precipitation was predicted for higher L_T:M_T ratios. The

species distribution diagram confirms that the complex ML is very strong and dominates in a solution. It was present from the beginning (at about pH 4) until the end of the experiment. (For L_T:M_T ratio 3, the experiment was stopped at pH 10.8). The complex M(HL) is a minor metal containing species and it is formed under the ML complex. Its fraction in a solution does not reach 10 % of all species. Due to the precipitation that appeared at pH 9.3 at L_T:M_T ratio 1, the complex $ML(OH)_2$ was not refined at this ratio 1. The species distribution in Figure 4.49 shows that this complex starts to form in the solution at around pH 9 and it appears to be a major species above pH 10.5.

4.14.3. Zn–Cy_2EN system

i. Data treatment

The system Zn–Cy_2EN was studied under the same conditions as those used for the preceding metal-ligand systems. The L_T:M_T ratio 1 was repeated twice. The other ratios, 2 and 3, were performed only once. During refinement operation, one could not refine ML_2 complex for L_T:M_T ratio 1 and the refinement resulted in only one model, M(HL), ML, ML(OH) and $ML(OH)_2$. In case of L_T:M_T ratios 2 and 3, one could refine ML_2 and two models resulted. The first and second model contained $ML(OH)_x$ and $ML_2(OH)_x$ as hydroxo-species, respectively. The values of stability constants for different models are included in Table 4.25. The suggested final model for Zn–Cy_2EN system was M(HL), ML, ML_2, ML(OH) and $ML(OH)_2$ because the Hamilton R-factor was significantly lower than the one obtained for the model containing $ML_2(OH)_x$ species.

Table 4.25: Models and stability constants for Zn–Cy_2EN system studied by GEP at 25°C and ionic strength 0.1 M in $NaNO_3$.

L_T:M_T ratio	M(HL)	ML	ML_2	ML(OH)	$ML(OH)_2$	$ML_2(OH)$	$ML_2(OH)_2$	R-Factor
1(I)	12.00 (01)	6.300 (003)	rejected	11.834 (004)	16.61(01)	rejected	rejected	0.00662
1(II)	12.02 (02)	6.269 (003)	rejected	11.790 (006)	16.57(01)	rejected	rejected	0.01086
2	11.87 (01)	6.238 (002)	10.69 (02)	11.51 (02)	16.628 (003)	rejected	rejected	0.00292
	11.92 (01)	6.232 (002)	10.907 (004)	rejected	rejected	16.003 (004)	20.06(01)	0.00366
3	11.83 (01)	6.237 (002)	10.59 (02)	11.14 (07)	16.606 (003)	rejected	rejected	0.00303
	11.85 (01)	6.236 (002)	10.676 (003)	excluded	excluded	15.508 (004)	19.746 (005)	0.00366
Combined refinement	11.94 (01)	6.271 (002)	10.23 (02)	11.782 (004)	16.615 (004)	rejected	rejected	0.00817
	11.91 (09)	6.15 (02)	11.09 (04)	excluded	excluded	16.17(04)	20.08(09)	0.07563

As for the previous systems, the acid and base concentrations were refined. The following Table shows how the change in their concentrations was very small. This can suggest that the refinement and stability constants were reliable.

Table 4.26: Change in acid and base concentrations for Ni–Cy_2EN system at different L_T:M_T ratios

L_T:M_T ratio	$[H^+]$ before	$[H^+]$ after	% change	$[OH^-]$ before	$[OH^-]$ after	% change
1(I)	0.0106 M	0.010587 M	– 0.12 %	0.00993 M	0.009949 M	+ 0.20 %
1(II)	0.0106 M	0.010605 M	+ 0.05 %	0.00993 M	0.009923 M	– 0.07 %
2	0.0106 M	0.010675 M	+ 0.70 %	0.00993 M	0.009790 M	+ 1.41 %
3	0.0106 M	0.010726 M	+ 1.19 %	0.00993 M	0.009668 M	– 2.64 %

ii. Complex formation function $\overline{Z}_M$

The potentiometric complex formation curves are presented in Figure 4.50. They were calculated for the model M(HL), ML, ML_2, ML(OH) and $ML(OH)_2$. A pronounced back-fanning feature is observed for all ratios studied. This supports

the formation of hydroxo-species (ML(OH) and $ML(OH)_2$ for the model considered). At $\overline{Z}_M = 1$, the plateau is not large as it was observed in Figures 4.45 and 4.48. This can suggest that ML complex is not as predominant as it was for example CuL and NiL complexes. The formation of ML_2 also is no obvious. This suggests that this complex is a minor species in the solution.

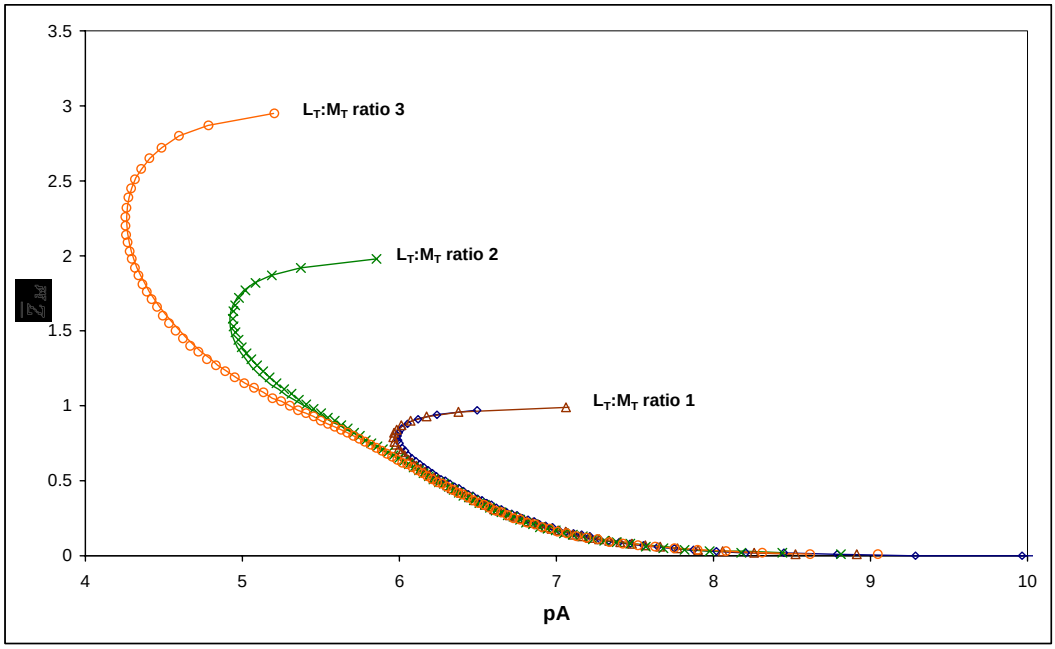

Figure 4.50: Experimental (points) and calculated (solid line) complex formation curves for Zn–Cy_2EN system studied by GEP at 25°C and ionic strength 0.1 M in $NaNO_3$. The model used is M(HL), ML, ML_2, ML(OH) and $ML(OH)_2$ from the combined refinement.

iii. Species distribution diagram

The species distribution diagram in Figure 4.51 shows how different complexes are formed with a change in pH of a solution. The complex M(HL) accounts for low percentage of the total metal ion in a solution (about 10 %). The complex ML presents 80 % of all metal species in the solution, but it is not dominant as ML complexes for Cu–Cy_2EN and Ni–Cy_2EN systems. This supports the suggestion

made before in section *ii* of this chapter. The similarity between Cu–Cy_2EN and Zn–Cy_2EN is in that the complex ML_2 is formed under ML(OH) complex and the complex $ML(OH)_2$ seems to be a major species in the solution. In polarographic study, a slope of about 60 mV per pH unit would be observed in the pH range above 9 when the observed (or virtual) potential is plotted versus pH. This slope would confirm the formation of $ML(OH)_2$ complex which involves two protons in the electrochemical process.

$$ML(OH)_2 + 2\,H^+ + 2e^- = M(Hg) + L + 2\,H_2O$$

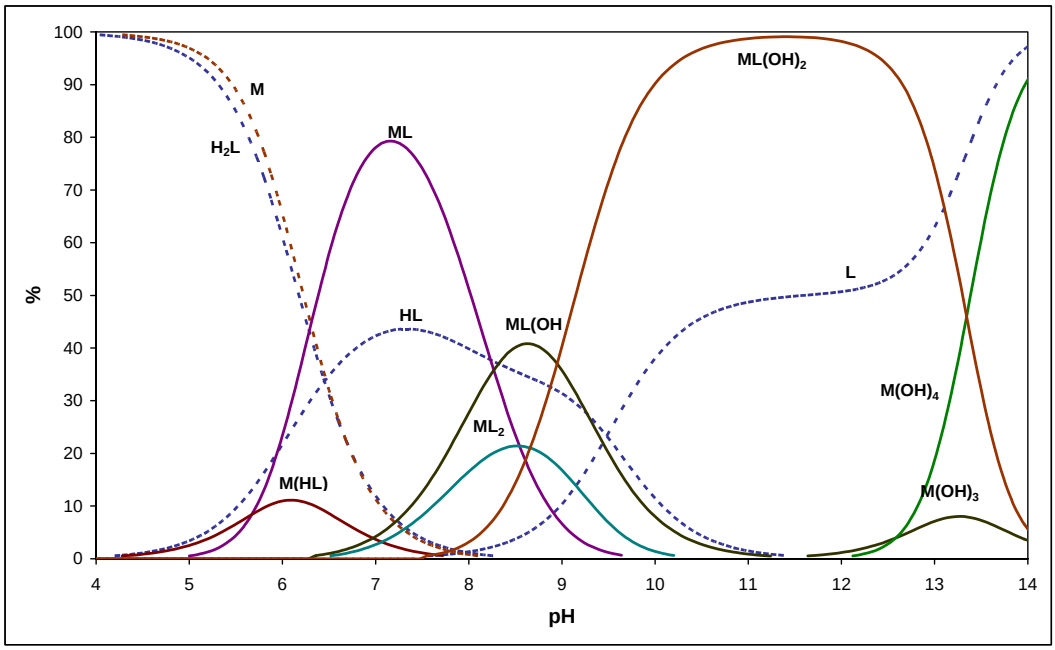

Figure 4.51: Species distribution diagram for Zn–Cy_2EN system studied by GEP at 25°C and ionic strength 0.1 M in $NaNO_3$. The model used is M(HL), ML_2, ML, ML(OH) and $ML(OH)_2$ from the refinement of L_T:M_T ratio 2. $[M_T] = 1.34 \times 10^{-3}$ M and $[L_T] = 1.67 \times 10^{-3}$ M.

From the above, the stability constants of ML, ML(OH) and $ML(OH)_2$ complexes which are 6.3, 1.8, and 16.6, respectively, can be regarded as reliable. To complete different models with Cy_2EN ligand, the use of other speciation techniques is highly recommended.

4.15. Effect of the addition of cyclic moiety in the pendant donor groups of diamine

A comparison will be established between the open chain diamine of N,N'-2-hydroxyethylenediamine (DHEEN) and N,N'–bis(2–hydroxycyclopentyl)–ethylenediamine (Cyp_2EN) or N,N'–bis(2–hydroxycyclohexyl)ethylenediamine (Cy_2EN). The comparison will also be established between the ligands Cyp_2EN and Cy_2EN. The ligand DHEEN was chosen because it has the same donor atoms as the ligands Cyp_2EN and Cy_2EN; these ligands can be seen as derived from DHEEN. In addition the ligand DHEEN might be regarded as being derived from ethylenediamine (EN) and, as it was explained by Hancock et al [12], the addition of groups containing neutral oxygen donor atoms (EN → DHEEN) to an existing ligand leads to an increase in selectivity of the ligand for large metal ions over small metal ions. The same comparison will be then focused on what is observed when the cyclopentyl and cyclohexyl moieties are added in the pendant donor groups (neutral oxygen) of DHEEN in terms of metal ions size.

4.15.1. Comparison of Cyp_2EN with DHEEN

The stability constants for the ligand Cyp_2EN and DHEEN are compared in Table 4.27 where $\log K_1$ values for complexes of Cyp_2EN and DHEEN are shown. From this Table, one can see that the introduction of the cyclopentyl bridges on the pendant arms resulted in a decrease in complex stability for all the metal studied. The small metal ions such as Cu and Ni are disfavoured over the large metal ions as shown in Figure 4.52. This can be explained by the fact that the chelate ring formed by the cyclopentyl bridge and its trans donor atoms is a five–membered ring, and five–membered rings should favour larger metal ions [12].

Table 4.27: Formation constants of ML complexes for Cyp_2EN and DHEEN showing the effect of cyclopentyl bridges on complex stability in relation to metal ion size.

Metal ion	Ionic radius*	DHEEN $\log K_1$*	Cyp_2EN $\log K_1$	$\Delta\log K_1$
Cu^{2+}	0.57	9.68	6.75	– 2.93
Ni^{2+}	0.69	6.67	3.79	– 2.88
Zn^{2+}	0.74	4.79	4.52	– 0.27
Cd^{2+}	0.95	5.07	3.98	– 1.09
Pb^{2+}	1.18	6.12	4.85	– 1.27

* Data from reference [10]

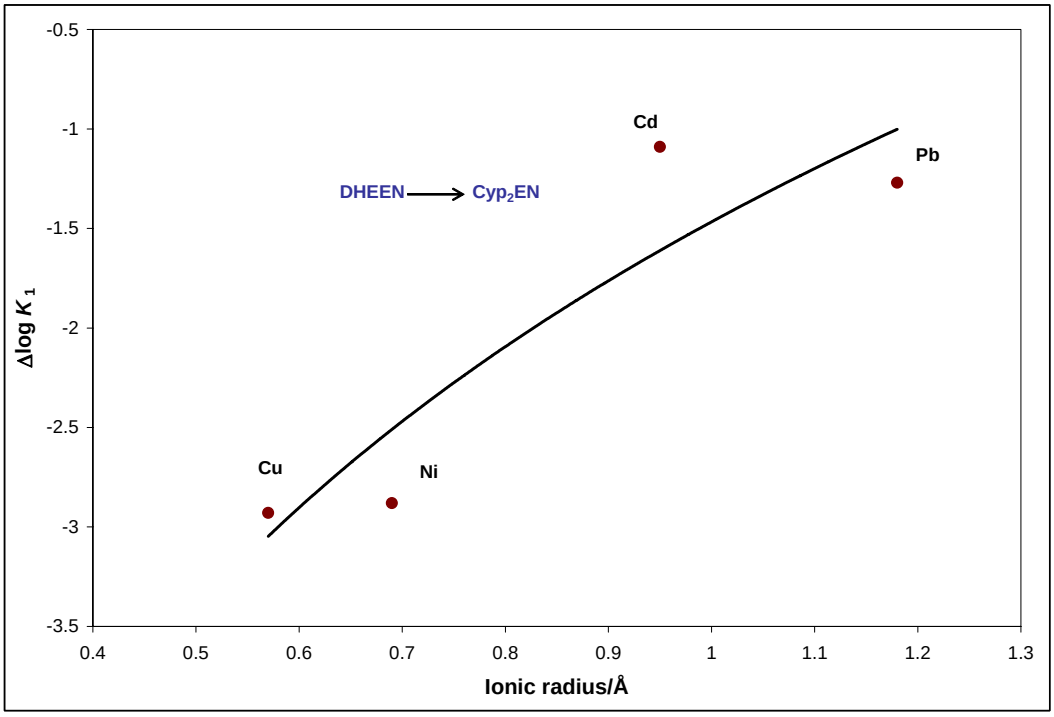

Figure 4.52: Plot of change in complex stability relating to metal ion size when passing from DHEEN to Cyp_2EN.

Note that, in Figure 4.52, Zn metal ion was not included because it showed a large deviation. This deviation can be explained by the fact that Zn^{2+} is flexible and has variable coordination geometry with four (tetrahedral), five (trigonal bipyramidal, axial H_2O) and six (octahedral) coordination number [76]. At this stage, one cannot precise which geometry has the metal ion Zn^{2+}. Other metal ions were considered as being octahedral.

4.15.2. Comparison of Cy_2EN with DHEEN

Contrarily to the ligand Cyp_2EN, the introduction of the trans-cyclohexyl pendant group on the pendant arms resulted in an increase in complex stability for all the metal studied. This is seen in Table 4.28. The small metal ions such as Cu and Zn are favoured by the more rigid bridging over the larger metal ions such as Pb^{2+} as shown in Figure 4.53.

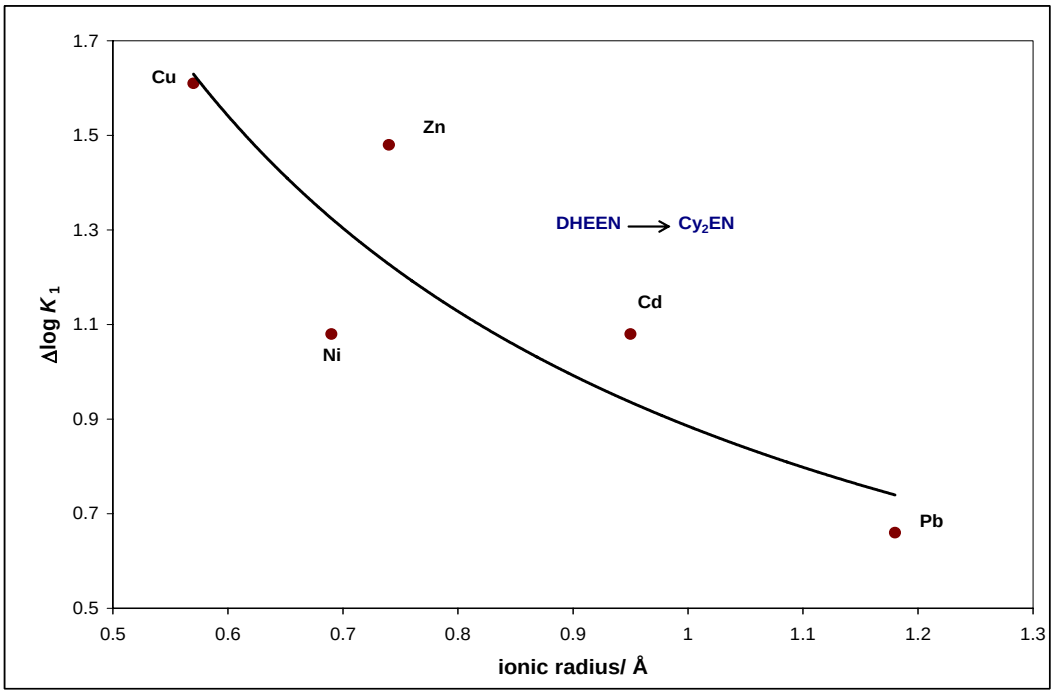

Figure 4.53: Plot of change in complex stability relating to metal ion size when passing from DHEEN to Cy_2EN.

The chelate ring formed by the cyclohexyl bridge and its trans donor atoms is also a five–membered ring and five membered rings should favour larger metal ions [12] and the extra rigidity imparted to the chelate ring by the cyclohexyl bridge might even expect to enhance the preference for larger metal ions by inhibiting the distortion of the chelate ring that are necessary to allow for complexation of small

metal ions. The fact that the inverse is observed can be explained by the greater curvature of the ligand when it is coordinated to a small metal ion, which relieves steric crowding on the outside of the ligand caused by the bulky cyclohexyl bridges [21].

Table 4.28: Formation constants of ML complexes for Cy_2EN and DHEEN showing the effect of cyclohexyl bridges on complex stability in relation to metal ion size.

Metal ion	Ionic radius*	DHEEN log K_1*	Cy_2EN log K_1	$\Delta\log K_1$
Cu^{2+}	0.57	9.68	11.29	1.61
Ni^{2+}	0.69	6.67	7.75	1.08
Zn^{2+}	0.74	4.79	6.27	1.48
Cd^{2+}	0.95	5.07	6.15	1.08
Pb^{2+}	1.18	6.12	6.78	0.66

* Data from reference [10]

4.15.3. Comparison of Cyp_2EN with Cy_2EN

The change of cyclopentyl to cyclohexyl bridges resulted in an increase in complex stability for all metals studied. This is presented in Table 4.29. As for the previous comparison, the smaller metal ions such as, Cu and Ni, are more favoured as seen in Figure 4.54. Once again, the metal ion Zn^{2+} was not included as it showed a large deviation.

Table 4.29: Formation constants of ML complexes for Cyp_2EN and Cy_2EN showing the effect of changing the cyclopentyl to cyclohexenyl bridges on complex stability in relation to metal ion size.

Metal ion	Ionic radius	Cyp_2EN/ logK_1	Cy_2EN /logK_1	$\Delta\log K_1$
Cu^{2+}	0.57	6.75	11.29	4.54
Ni^{2+}	0.69	3.79	7.75	3.96
Zn^{2+}	0.74	4.52	6.27	1.75
Cd^{2+}	0.95	3.98	6.15	2.17
Pb^{2+}	1.18	4.85	6.78	1.93

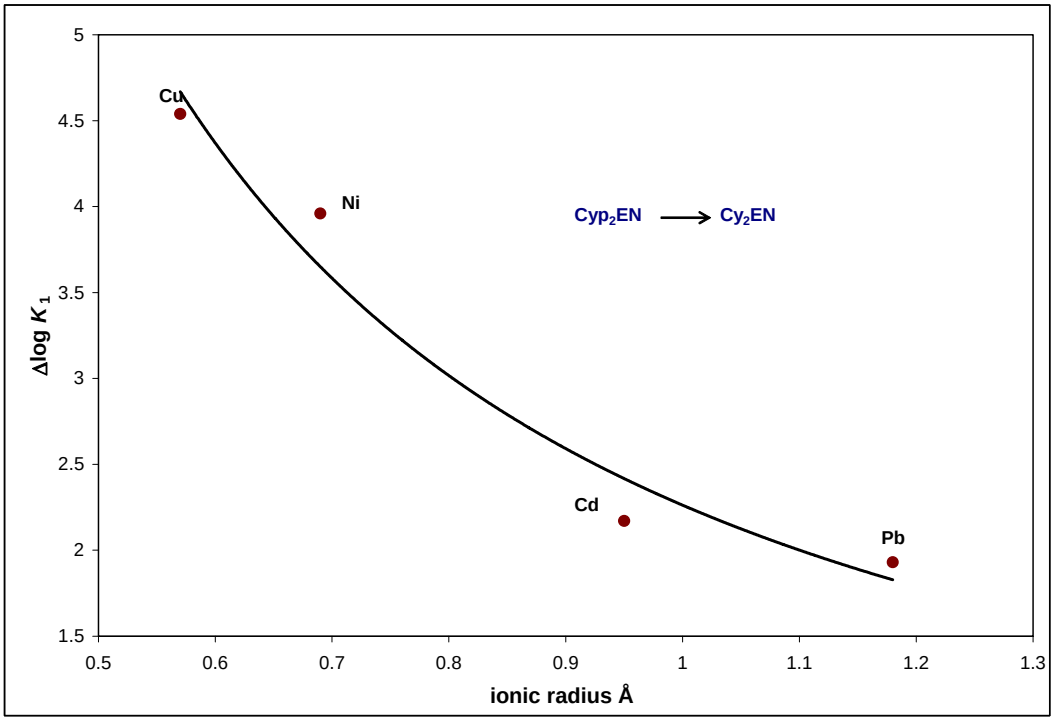

Figure 4.54: Plot of change in complex stability relating to metal ion size when passing from Cyp_2EN to Cy_2EN.

From all the above comparisons, one can suggest that the introduction of the cyclopentyl group on the pendant arms of DHEEN results in a more rigid pendant donor, while the introduction of cyclohexyl results in a more flexible donor. In terms of selectivity for metal ion, the large metal ions are favoured by the addition of cyclopentyl bridge on the pendant arms of DHEEN whereas the small metal ions are favoured when cyclohexyl bridge are added. As suggested before, the greater curvature of the ligand Cy_2EN when it is coordinated to small metal ions relieves steric crowding on the outside of the ligand caused by the bulky cyclohexyl bridges. As the cyclopentyl bridges seem to be less flexible than cyclohexyl bridges, the curvature of the ligand Cyp_2EN is difficult and large metal ions (such as Pb^{2+}) are more favoured than small metal ions (such as Cu^{2+}).

Note that all the above suggestions have to be confirmed by getting crystal structures of ML complexes formed by the ligands Cyp_2EN and Cy_2EN with different metals studied in this work. Molecular modelling computation (calculation) can also be useful if one wishes to explain the effect of the addition of cyclopentyl and cyclohexyl bridges in the pendant donors of DHEEN. Neutron diffraction studies are currently being done to evaluate these arguments.

Chapter 5: Conclusion

The aim of this work was the modelling of complexation of metal ions with chelating ligands Cyp_2EN and Cy_2EN. This modelling should make a useful contribution towards ligand design strategies as stability constants are among the required parameters. Glass Electrode Potentiometry was used in the determination of protonation and stability constants of all systems studied. Polarography and Virtual Potentiometry were only successful in the study of Cd–Cyp_2EN and Pb–Cyp_2EN systems. It was observed that the ligands Cyp_2EN and Cy_2EN had almost similar pK_a values as open–chain amines with the same donor atoms. The small difference observed was explained in terms of inductive effect which is slightly high in open–chain amines. The difference between pK_a values for the ligands Cyp_2EN and Cy_2EN was also found minimum (ΔpKa_1 = 0.5 and ΔpKa_2 = 0.4).

For all systems studied, it was observed that different complexes were formed. The common complexes obtained were M(HL) and ML. Compared to ML, the complex M(HL) seemed to be a minor species, especially for the systems Cu–Cyp_2EN and for all systems studied with the ligand Cy_2EN. It was also observed that the complex ML_2 was found in all systems studied with the ligand Cy_2EN while this complex was only obtained in the study of Cd–Cyp_2EN system. The complex ML_2 also seems to be a minor species when compared to the complex ML. In several systems studied, potentiometric (ESTA) and voltammetric (3D–CFC) software could not distinguish which hydroxo–complexes ($M_xL_y(OH)_z$) were present in the solution as these species were formed in the pH range where the ligand was fully deprotonated. To decide which species

was formed in the solution, the Hamilton R–factor was considered. In all cases, the model containing ML(OH) and $ML(OH)_2$ complexes was taken as the correct or most likely one as it had a slightly lower R–factor.

The complexes ML formed with the ligand Cy_2EN were found more stable than the complexes formed with the ligand Cyp_2EN. The difference in log β values for the complex ML was between 2 and 4.5 log units. When the maximum concentration of ML complexes was calculated for all systems studied using species distribution diagrams, it was observed that the increase in the concentration was between 26 and 52 % when passing from Cyp_2EN to Cy_2EN. This large difference cannot only be attributed to the difference in the first pK_a value ($\Delta pKa_1 = 0.5$) but also to the structures of the ligands. It was then suggested that cyclopentyl bridges are more rigid than cyclohexyl bridges and the flexibility of cyclohexyl bridges allows the formation of more stables complexes.

GEP could determine different species formed in different systems studied. The complex M(HL), which was inaccessible by polarographic study of Pb–Cyp_2EN system, was determined by GEP . Different models obtained for all systems studied with the ligand Cy_2EN were also determined by GEP as polarography failed in the study of these systems. But it was observed that GEP could not be fully reliable, especially for the system Cd–Cyp_2EN where hydroxo–complexes $M_xL_y(OH)_z$ could not be identified due to the precipitation that occurred early. The refinement of potentiometric data obtained for the system Pb–Cyp_2EN also generated a high value of stability constant of $ML(OH)_2$ complex due to the lower ratio used in GEP allowing for hydrolysis of lead species.

Polarography was used in the study of Cd–Cyp_2EN and Pb–Cyp_2EN systems. Polarographic study could get $ML_2(OH)$ complex which was not found by potentiometric study of Cd–Cyp_2EN. As polarography is more efficient in a situation when one is dealing with hydrolysable ions, it could refine properly the stability constant of the complex $ML(OH)_2$ in Pb–Cyp_2EN system. Polarography also was not successful for all the system studied. It could not determine the complex M(HL) which was refined by GEP in Pb–Cyp_2EN system. The behaviour of the DC–waves recorded in the study of Cd–Cy_2EN and Pb–Cy_2EN also did not allow the fitting of data properly. This was mainly due to the ligand which was not easily soluble. When the pH was increased, the ligand started to precipitate and this decreased the ligand total concentration. As a result the ligand was not in sufficient excess and the reversible wave became distorted and split into two parts. It was tried to predict the species formed by the system Cd–Cy_2EN, but the values of stability constants were not considered.

The use of a new concept termed virtual potentiometry (VP) in the study of Cd–Cyp_2EN and Pb–Cyp_2EN assisted in obtaining a final model for these systems when potentiometric and polarographic data were combined and refined using ESTA software. VP could refine M(HL) complex inaccessible via polarographic study of Pb–Cyp_2EN system and refined the hydroxo–complex $ML_2(OH)$ that in turn was inaccessible using GEP for Cd–Cyp_2EN system.

Compared to the ligand DHEEN, it was observed that the large metal ions were favoured by the addition of cyclopentyl bridge while the small metal ions were favoured when cyclohexyl bridge were added. This was explained in terms of greater curvature of the ligand Cy_2EN when it is coordinated to small metal

ions (such as Cu^{2+}), which relieves steric crowding on the outside of the ligand caused by the bulky cyclohexyl bridges. As cyclopentyl bridges seem to be less flexible than cyclohexyl bridges, the curvature of the ligand Cyp_2EN is difficult and large metal ions (such as Pb^{2+}) are more favoured than small metal ions.

In order to confirm the model proposed for all the systems studied, the use of other speciation techniques is highly recommended, especially for the systems Cu–Cyp_2EN, Ni–Cyp_2EN, Zn–Cyp_2EN and all systems formed with the ligand Cy_2EN as polarography failed in their study. The suggestions made before on the effect of the addition of cyclic moieties must be verified by the determination of crystal structures in order to understand well the effect of the addition of cyclopentyl and cyclohexyl moieties in the pendant donor groups of diamine.

References

1. F. R. Hartley, C. Burgess, R. Alcock, *Solution equilibria* (1980), pp15–30,123–129, 267
2. R. G. Pearson, *J. Am. Chem. Soc*.(1963), 85, 3533
3. T. N. Mali, *Lewis acid behavior of metal ions with macrocyclic ligands* (1996) Thesis
4. M. T. Beck, I. Nagypál, *Chemistry of complex equilibria* (1990), pp. 7, 192, 220
5. A. E Martell, R.D. Hancock, *Metal Complexes in aqueous Solutions*, Modern Inorganic Chemistry Series, Plenum Press, New York (1996), pp.40–55, 63, 74, 217
6. B. P. Hay, J. R. Rustad, C. Hostetler, *J. Am. Chem. Soc.* (1993) , 115, 158
7. J. P. Hunt, *Metal ions in aqueous solution* (1963), p. 69
8. E. C. Constable, *Metal and ligand reactivity*, Weinheim, New York (1996), p 135
9. R. D. Hancock, *The recognition of metal ions by ligands* (1990), Thesis
10. A. S. de Sousa, *Coordinating properties of more highly preorganised ligands*, (1995), Thesis
11. G. Shwarzenbach, *Helv. Chim. Acta*; (1952), 35, 2344
12. R. D. Hancock, A. E. Martell, *Chem. Rev.,*(1989), 89, 1875–1914
13. A. E. Martell and R. M. Smith, *Critical Stability constants* (1974–1988), Plenum, New York, , Vols. 1–6
14. R. D. Shannon, *Acta. Cryst, Sect. A* (1976), A32, 751
15. T. E. Chantson, *A molecular mechanics study of ligands for selective complexation of metal ions in medical applications* (1994), Thesis
16. E. M. V. M. Casimiro, *Newly synthesized chelating agents as possible antidotes for heavy metal ion poisoning, with special reference to cadmium* (2000), Thesis
17. M. M. Hayward, J. C. Adrian, A. Schepartz, *J. Org. Chem.* (1995), 60, 3924–3927
18. http://pages.prodigy.net/naturedoctor/chelation.html#One

19. http://www.sci.u-szeged.hu/kkk/vanadium4/Makinen.pdf

20. R. V. Khadikar, B. D. Heda, R. Saxena, T. Khaddar, *Indian Journal of Pharmaceutical Sciences* (1995); 57(4); 157-61

21. R.D. Hancock, H. Maumela, A.S.de Sousa, *Coord. Chem. Rev.,* 148 (1996) 315–347

22. R. D. Hancock, R. Bhavan, M. S. Shaikjee, P. W. Wade, A. Hearn, *Inorg. Chim. Acta*, 112 (1986)L23–L25

23. V. J. Thom, M. S. Shaikejee, R. D. Hancock, *Inorg. Chem.,* 25 (1986), 2992

24. R. D. Hancock, M. S. Shaikejee, S. M. Dobson, J. C. A. Boeyens, *Inorg. Chim. Acta*, 154 (1988) 229–238

25. A. S. de Sousa, G. J. B. Croft, C. A. Wagner, J. P. Michael, R. D. Hancock, *Inorg. Chem*. (1991), 30, 3525–3529

26. R. D. Hancock, *Pure Appl.Chem*., 58 (1986) 1445

27. M. P. Ngwenya, *Chelating ring size as a means of controlling ligand selectivity for metal ions* (1989), Thesis

28. R. D. Hancock, P. W. Wade, M. P. Ngwenya, A. S. de Sousa, K. V. Damu, *Inorg.Chem*., 29 (1990) 1968–1974

29. A. W. Adamson, *J. Am. Chem. Soc.* (1954), 76, 1578

30. R. D. Hancock, F. Marsicano, *Journal of Chemical Society*; Dalton Transaction, (1976); 1096–1098,

31. R. R. Corderman, J. L. Beauchamp, *J. Am. Chem. Soc*., 98, (1976) 3998

32. B. S. Nakani, J. J. B. Wels, R. D. Hancock, *Inorg. Chem.*, 22, (1983), 2956

33. M. Gerloch, *Ligands–field parameters*, (1973), Cambridge University Press,

34. A. E. Martell, R. J. Motekaitis, *Determination and use of Stability constants* (1988), p 9

35. R. B., Lauffer, *Chem. Rev.,* (1987), 87, 901

36. H. Freiser and Q. Fernando, *Ionic equilibria in analytical chemistry*, John Wiley & sons, New York (1963), p144.

37. F. J. C Rossoti and H. Rossoti, *The Determination of Stability Constants* (1961), p 127

38. D. C. Harris, *Quantitative Chemical Analysis* (1995), Fourth edition, W.H. Freeman, New York, pp 390-393, 497
39. G. Eisenman, *Glass electrode for hydrogen and other cations* (1967), E. Arnold, London,
40. G. Svehla, *Automatic Potentiometric Titrations* (1978) Pergamon Press, p. 113.
41. R. C. Luckay, *Factors that control selectivity of ligands for metal ions* (1997), Thesis
42. I. Cukrowski, *Analyst,* (1997), vol.122, pp827-833.
43. J. Bjerrum, *Stability constant for metal ions complexes, with solubility product of inorganic substances* (1957), Chemical society, London,
44. K. Murray and P. M. May, *ESTA Users Manual,* University of Wales Institute of Science and Technology (1984) pp.2, 8, 16, and 17
45. P. M. May, K. Murray and D. R. Williams, *Talanta* (1985), vol.32, No 6, pp. 483-489
46. P. M. May, K. Murray and D. R. Williams, *Talanta* (1988), 35 No11, pp. 825–830
47. P. M. May and K. Murray, *Talanta*, (1988), 35, No 12, pp. 933-941
48. I. S. Longmuir, *Advances in Polarography*, Volume 1, (1960)
49. A. J. Bard and L. R. Faulkner, *Electrochemical Methods*, John Wiley & Sons, New York, (2001), pp. 261–301
50. D. R. Crow, *Polarography of Metal Complexes,* Academic Press, London and new York, (1969), pp. 22–24, 66, 67, 72, 73
51. C. H. Hamann, A. Hamnett and W. Vielstich, *Electrochemistry*, WILEY-VCH Verlag GmbH, Germany (1998), pp. 391-396.
52. J. Heyroský, J. Kůta, *Principles of Polarography* (1966), pp. 17, 46
53. server.ccl.net/cca/software/MS-WIN95-NT/Polarograms/old/v4.3/polar.doc.htm
54. www.epsilon-web.net/Ec/manual/Techniques/Pulse/pulse.html#sampled
55. www.chemistry.adelaide.edu.au/external/soc-rel/content/dpp.htm
56. J. J. Lingane, *Chem. Rev*. (1941) 29, p1.
57. D. D. DeFord and D. N. Hume, *J. Am. Chem. Soc.,* 73 (1951), 5321
58. W. B. Schaap, D. L. McMasters, *J. Am. Chem. Soc*., 83, (1961), 4699

59. I. Cukrowski, *Electroanal* (1997), 9, N° 15, pp. 1167-1173.
60. I. Cukrowski, *Journal of Electroanaly. Chem*. 460 (1999), pp. 197-206.
61. I. Cukrowski, *Anal. Chim. Acta* 336 (1996), pp. 23-36.
62. I. Cukrowski, *Electroanal.* (1999), 11, N° 9, pp. 606-612
63. I. Cukrowski, M. Adsetts, *Journal of Electroanaly. Chem.* 429(1997) pp. 129-137
64. I Cukrowski, J. M. Zhang, A.V. Aswegen, *Helv. Chim. Acta*, Vol.87 (2004), pp. 2135–2158
65. I. Cukrowski, J.R. Zeevaart, N.V. Jarvis, *Anal. Chim. Acta* 379 (1999) pp. 217 -226.
66. I. Cukrowski, R. C. Luckay, *Anal. Chim. Acta* 372 (1998) pp. 323-331
67. I. Cukrowski, S. A. Loader, *Electroanal.* (1998), 10, N° 13, pp. 877-885.
68. I. Cukrowski, *Electroanal.* (1997), 9, No 9, pp. 699-705
69. I. Cukrowski, *Electroanal*. (2001), 13, No. 15, pp. 1242-1252
70. I. Cukrowski, R. D. Hancock, R. C. Luckay, *Anal. Chim. Acta* 319 (1996) pp.39-48,
71. I. Cukrowski, J. M. Zhang, *Electroanalysis*, (2004), 16, No 8, pp. 612–624
72. A. S. De Sousa, R. D. Hancock and J. H. Reibenspies, *J.Chem.Soc.*Dalton Trans.(1997), pp. 2831-2835,
73. I. Cukrowski, *dedicated to polarography program 3D–CFC*, unpublished work
74. A. E. Martell and R. M. Smith, *NIST Critically selected stability constants of metal complexes* (2004), NIST Standard Reference Database 46 Version 8.0
75. I. Cukrowski, F. Marsicano, R. D. Hancock, P .T . Tshetlho and W. A. L. Van Otterlo, *Polyhedron* Vol.14, No12 (1995), pp1661-1674,
76. J. Koryta, *Z. Elektrochem.*, 61, 423 (1957)
77. D. T. Richens, *The Chemistry of Aqua Ions*, (1997), John Wiley and Sons, p. 540

Appendix

1. Formation constants for the metal ions complexes with hydroxide ion used in this work [74]

1.1. Formation constants for Cd^{2+} complexes with hydroxide ion

Equilibrium	log β	Temperature/	Ionic strength
$Cd^{2+} + OH^- \rightleftharpoons Cd(OH)^+$	3.9	25° C	0
$Cd^{2+} + 2\ OH^- \rightleftharpoons Cd(OH)_2$	7.7	25° C	0 and 3
$Cd^{2+} + 3\ OH^- \rightleftharpoons Cd(OH)_3^-$	10.3	25° C	3
$Cd^{2+} + 4\ OH^- \rightleftharpoons Cd(OH)_4^{2-}$	12.0	25° C	3
$2\ Cd^{2+} + OH^- \rightleftharpoons Cd_2(OH)^{3+}$	5.06	25° C	3
$4Cd^{2+} + 4\ OH^- \rightleftharpoons Cd_4(OH)^{4+}$	23.7	25° C	3
$Cd^{2+} + 2\ OH^- \rightleftharpoons Cd(OH)_{2\ (s)}$	– 14.3	25° C	3

1.2. Formation constants for Pb^{2+} complexes with hydroxide ion

Equilibrium	log β	Temperature	Ionic strength
$Pb^{2+} + OH^- \rightleftharpoons Pb(OH)^+$	5.9	25° C	0.1
$Pb^{2+} + 2\ OH^- \rightleftharpoons Pb(OH)_2$	10.9	25° C	3
$Pb^{2+} + 3\ OH^- \rightleftharpoons Pb(OH)_3^-$	13.9	25° C	0
$2\ Pb^{2+} + OH^- \rightleftharpoons Pb_2(OH)^{3+}$	7.6	25° C	0
$3\ Pb^{2+} + 4\ OH^- \rightleftharpoons Pb_3(OH)_4^{2+}$	32.1	25° C	0
$4\ Pb^{2+} + 4\ OH^- \rightleftharpoons Pb_4(OH)^{4+}$	34.7	25° C	0.1
$6\ Pb^{2+} + 8\ OH^- \rightleftharpoons Pb_6(OH)_8^{4+}$	66.9	25° C	0.1
$Pb^{2+} + 2\ OH^- \rightleftharpoons Pb(OH)_{2\ (s)}$	– 15.0	25° C	0

1.3. Formation constants for Zn^{2+} complexes with hydroxide ion

Equilibrium	log β	Temperature	Ionic strength
$Zn^{2+} + OH^- \rightleftharpoons Zn(OH)^+$	4.6	25° C	0.1
$Zn^{2+} + 2\ OH^- \rightleftharpoons Zn(OH)_2$	11.1	25° C	0
$Zn^{2+} + 3\ OH^- \rightleftharpoons Zn(OH)_3^-$	13.6	25° C	0
$Zn^{2+} + 4\ OH^- \rightleftharpoons Zn\ (OH)_4^{3+}$	14.8	25° C	0
$2\ Zn^{2+} +\ OH^- \rightleftharpoons Zn_2(OH)^{3+}$	5.0	25° C	0
$4\ Zn^{2+} + 4\ OH^- \rightleftharpoons Zn_4(OH)_4^{4+}$	27.9	25° C	3
$Zn^{2+} + 2\ OH^- \rightleftharpoons Zn(OH)_{2\ (s)}$	– 14.84	25° C	0.1

1.4. Formation constants for Cu^{2+} complexes with hydroxide ion

Equilibrium	log β	Temperature	Ionic strength
$Cu^{2+} + OH^- \rightleftharpoons Cu(OH)^+$	6.1	25° C	0.1
$2\ Cu^{2+} + OH^- \rightleftharpoons Cu_2(OH)^{3+}$	7.7	25° C	3
$2\ Cu^{2+} + 2\ OH^- \rightleftharpoons Cu_2(OH)_2^{2+}$	16.8	25° C	0.1
$3\ Cu^{2+} + 4\ OH^- \rightleftharpoons Pb_3(OH)_4^{2+}$	33.7	25° C	0.1
$Cu^{2+} + 2\ OH^- \rightleftharpoons Cu(OH)_{2\ (s)}$	-18.9	25° C	1

1.5. Formation constants for Ni^{2+} complexes with hydroxide ion

Equilibrium	log β	Temperature	Ionic strength
$Ni^{2+} + OH^- \rightleftharpoons Ni(OH)^+$	4.1	25° C	0
$Ni^{2+} + 2\ OH^- \rightleftharpoons Ni\ (OH)_2$	9	25° C	0
$Ni^{2+} + 3\ OH^- \rightleftharpoons Ni(OH)_3^-$	12	25° C	0
$4\ Ni^{2+} + 4\ OH^- \rightleftharpoons Ni_4(OH)_4^{4+}$	28.3	25° C	0
$Ni^{2+} + 2\ OH^- \rightleftharpoons Ni\ (OH)_{2\ (s)}$	- 15.1	25° C	0

2. GEP data for protonation constants of Cyp_2EN

TASK	ZBAR	1	HPD0	PROTONATION			
MODL	HPD0	H	1				
CPLX	0	0	-13.78	H	+1(	-1)	
CPLX	1	0	8.966	HPD0(	1)	H	+1(1)
CPLX	1	0	15.02	HPD0(	1)	H	+1(2)
CONC							
VESL	IVOL	20	0	0			
VESL	H + 1	0.01037	0	0			
VESL	HPD0	0.00498	0	0			
BUR1	H + 1	-0.0102	0	0			
ELEC							
ZERO	H + 1	405.29	0	0			
GRAD	H + 1	58.321	0	0			
DATA							

EMF	PH			ZBAR(H)			POINT	PA			ZBAR(M)			POINT
OBS	OBS	CALC	RESID	OBS	CALC	RESID	RESID	OBS	CALC	RESID	OBS	CALC	RESID	RESID
204.2	3.448	3.379	0.069	2.01	2	0.012	0.07	0	0	0	0	0	0	0
201.4	3.496	3.436	0.06	2.01	2	0.009	0.061	0	0	0	0	0	0	0
198	3.554	3.501	0.054	2	2	0.007	0.054	0	0	0	0	0	0	0
194	3.623	3.575	0.048	2	2	0.006	0.049	0	0	0	0	0	0	0
189.3	3.703	3.661	0.043	2	2	0.004	0.043	0	0	0	0	0	0	0
183.9	3.796	3.763	0.033	2	1.99	0.003	0.033	0	0	0	0	0	0	0
177.4	3.908	3.885	0.022	1.99	1.99	0.001	0.022	0	0	0	0	0	0	0
169.8	4.038	4.031	0.007	1.99	1.99	0	0.007	0	0	0	0	0	0	0
161.4	4.182	4.195	-0.013	1.99	1.99	0	0.013	0	0	0	0	0	0	0
152.7	4.331	4.359	-0.028	1.98	1.98	-0.001	0.028	0	0	0	0	0	0	0
144.7	4.468	4.505	-0.036	1.97	1.97	-0.001	0.036	0	0	0	0	0	0	0
137.6	4.59	4.627	-0.037	1.96	1.96	0	0.037	0	0	0	0	0	0	0
131.5	4.695	4.73	-0.036	1.95	1.95	0	0.036	0	0	0	0	0	0	0
126.2	4.785	4.818	-0.032	1.94	1.95	0	0.032	0	0	0	0	0	0	0
121.6	4.864	4.893	-0.029	1.94	1.94	0	0.029	0	0	0	0	0	0	0
117.5	4.935	4.96	-0.025	1.93	1.93	0	0.025	0	0	0	0	0	0	0
113.9	4.996	5.019	-0.023	1.92	1.92	0	0.023	0	0	0	0	0	0	0
110.6	5.053	5.072	-0.02	1.91	1.91	0	0.02	0	0	0	0	0	0	0
107.6	5.104	5.121	-0.017	1.9	1.9	0	0.017	0	0	0	0	0	0	0
104.8	5.152	5.166	-0.014	1.89	1.89	0	0.014	0	0	0	0	0	0	0
102.3	5.195	5.208	-0.013	1.88	1.88	0	0.013	0	0	0	0	0	0	0
99.9	5.236	5.247	-0.011	1.87	1.87	0	0.011	0	0	0	0	0	0	0
97.6	5.276	5.284	-0.008	1.85	1.85	0	0.008	0	0	0	0	0	0	0
95.5	5.312	5.318	-0.006	1.84	1.84	0	0.006	0	0	0	0	0	0	0
93.5	5.346	5.351	-0.005	1.83	1.83	0	0.005	0	0	0	0	0	0	0
91.5	5.38	5.382	-0.002	1.82	1.82	0	0.002	0	0	0	0	0	0	0
89.7	5.411	5.412	-0.001	1.81	1.81	0	0.001	0	0	0	0	0	0	0
87.9	5.442	5.441	0.001	1.8	1.8	0	0.001	0	0	0	0	0	0	0
86.2	5.471	5.468	0.003	1.79	1.79	0	0.003	0	0	0	0	0	0	0
84.6	5.499	5.495	0.004	1.78	1.78	0	0.004	0	0	0	0	0	0	0
83	5.526	5.521	0.005	1.77	1.77	0	0.005	0	0	0	0	0	0	0
81.5	5.552	5.546	0.006	1.76	1.76	0	0.006	0	0	0	0	0	0	0
80	5.578	5.57	0.008	1.75	1.75	0	0.008	0	0	0	0	0	0	0
78.6	5.602	5.593	0.008	1.74	1.74	0	0.008	0	0	0	0	0	0	0
77.2	5.626	5.616	0.009	1.73	1.73	0	0.009	0	0	0	0	0	0	0

75.8	5.65	5.639	0.011	1.72	1.72	0	0.011	0	0	0	0	0	0	0
74.5	5.672	5.661	0.011	1.71	1.71	0	0.011	0	0	0	0	0	0	0
73.2	5.694	5.682	0.012	1.7	1.7	0	0.012	0	0	0	0	0	0	0
71.9	5.716	5.703	0.013	1.69	1.69	0	0.013	0	0	0	0	0	0	0
70.6	5.739	5.724	0.015	1.68	1.68	0	0.015	0	0	0	0	0	0	0
69.4	5.759	5.744	0.015	1.67	1.67	0	0.015	0	0	0	0	0	0	0
68.2	5.78	5.764	0.016	1.66	1.66	0	0.016	0	0	0	0	0	0	0
67	5.8	5.784	0.017	1.65	1.65	0	0.017	0	0	0	0	0	0	0
65.8	5.821	5.803	0.018	1.64	1.64	0	0.018	0	0	0	0	0	0	0
64.6	5.842	5.822	0.02	1.63	1.63	0	0.02	0	0	0	0	0	0	0
63.5	5.86	5.841	0.02	1.62	1.62	0	0.02	0	0	0	0	0	0	0
62.3	5.881	5.86	0.021	1.61	1.61	0	0.021	0	0	0	0	0	0	0
61.2	5.9	5.878	0.022	1.6	1.6	0	0.022	0	0	0	0	0	0	0
60.1	5.919	5.897	0.022	1.59	1.59	0	0.022	0	0	0	0	0	0	0
59	5.938	5.915	0.023	1.58	1.58	0	0.023	0	0	0	0	0	0	0
57.9	5.957	5.933	0.023	1.57	1.57	0	0.023	0	0	0	0	0	0	0
56.7	5.977	5.951	0.026	1.56	1.56	0	0.026	0	0	0	0	0	0	0
55.7	5.994	5.969	0.025	1.55	1.55	0	0.025	0	0	0	0	0	0	0
54.6	6.013	5.987	0.026	1.54	1.54	0	0.026	0	0	0	0	0	0	0
53.6	6.03	6.005	0.026	1.53	1.53	0	0.026	0	0	0	0	0	0	0
52.5	6.049	6.023	0.027	1.52	1.52	0	0.027	0	0	0	0	0	0	0
51.4	6.068	6.04	0.028	1.51	1.51	0	0.028	0	0	0	0	0	0	0
50.3	6.087	6.058	0.029	1.5	1.5	0	0.029	0	0	0	0	0	0	0
49.4	6.102	6.076	0.027	1.49	1.49	0	0.027	0	0	0	0	0	0	0
48.7	6.114	6.093	0.021	1.48	1.48	0	0.021	0	0	0	0	0	0	0
47.9	6.128	6.111	0.017	1.47	1.47	0	0.017	0	0	0	0	0	0	0
47	6.143	6.129	0.014	1.46	1.46	0	0.014	0	0	0	0	0	0	0
46	6.161	6.147	0.014	1.45	1.45	0	0.014	0	0	0	0	0	0	0
45.1	6.176	6.165	0.011	1.44	1.44	0	0.011	0	0	0	0	0	0	0
44	6.195	6.183	0.012	1.43	1.43	0	0.012	0	0	0	0	0	0	0
43	6.212	6.201	0.011	1.41	1.41	0	0.011	0	0	0	0	0	0	0
42	6.229	6.219	0.01	1.4	1.4	0	0.01	0	0	0	0	0	0	0
40.9	6.248	6.238	0.01	1.39	1.39	0	0.01	0	0	0	0	0	0	0
39.8	6.267	6.256	0.011	1.38	1.38	0	0.011	0	0	0	0	0	0	0
38.7	6.286	6.275	0.011	1.37	1.37	0	0.011	0	0	0	0	0	0	0
37.5	6.306	6.294	0.013	1.36	1.36	0	0.013	0	0	0	0	0	0	0
36.4	6.325	6.313	0.012	1.35	1.35	0	0.012	0	0	0	0	0	0	0
35.2	6.346	6.332	0.013	1.34	1.34	0	0.013	0	0	0	0	0	0	0
34	6.366	6.352	0.014	1.33	1.33	0	0.014	0	0	0	0	0	0	0
32.8	6.387	6.372	0.015	1.32	1.32	0	0.015	0	0	0	0	0	0	0
31.5	6.409	6.392	0.017	1.31	1.31	0	0.017	0	0	0	0	0	0	0
30.3	6.43	6.413	0.017	1.3	1.3	0	0.017	0	0	0	0	0	0	0
29.1	6.45	6.434	0.017	1.29	1.29	0	0.017	0	0	0	0	0	0	0
27.8	6.473	6.455	0.018	1.28	1.28	0	0.018	0	0	0	0	0	0	0
26.5	6.495	6.477	0.018	1.27	1.27	0	0.018	0	0	0	0	0	0	0
25.1	6.519	6.499	0.02	1.26	1.26	0	0.02	0	0	0	0	0	0	0
23.7	6.543	6.522	0.021	1.25	1.25	0	0.021	0	0	0	0	0	0	0
22.3	6.567	6.545	0.022	1.24	1.24	0	0.022	0	0	0	0	0	0	0
20.8	6.593	6.569	0.024	1.23	1.23	0	0.024	0	0	0	0	0	0	0
19.3	6.618	6.594	0.025	1.22	1.22	0	0.025	0	0	0	0	0	0	0
17.8	6.644	6.619	0.025	1.21	1.21	0	0.025	0	0	0	0	0	0	0
16.2	6.672	6.645	0.026	1.2	1.2	0	0.026	0	0	0	0	0	0	0
14.6	6.699	6.672	0.027	1.19	1.19	0	0.027	0	0	0	0	0	0	0
12.8	6.73	6.7	0.029	1.18	1.18	0	0.029	0	0	0	0	0	0	0

11	6.761	6.729	0.031	1.17	1.17	0	0.031	0	0	0	0	0	0	0
9.2	6.792	6.76	0.032	1.16	1.16	0	0.032	0	0	0	0	0	0	0
7.2	6.826	6.792	0.034	1.15	1.15	0	0.034	0	0	0	0	0	0	0
5.2	6.86	6.825	0.035	1.14	1.14	0	0.035	0	0	0	0	0	0	0
3	6.898	6.859	0.038	1.13	1.13	0	0.038	0	0	0	0	0	0	0
0.8	6.936	6.896	0.04	1.12	1.12	0	0.04	0	0	0	0	0	0	0
-1.6	6.977	6.935	0.042	1.11	1.11	0	0.042	0	0	0	0	0	0	0
-4.1	7.02	6.976	0.044	1.1	1.1	0	0.044	0	0	0	0	0	0	0
-6.8	7.066	7.019	0.047	1.09	1.09	0	0.047	0	0	0	0	0	0	0
-9.6	7.114	7.065	0.049	1.08	1.08	0	0.049	0	0	0	0	0	0	0
-12.6	7.165	7.115	0.051	1.07	1.07	0	0.051	0	0	0	0	0	0	0
-15.8	7.22	7.167	0.053	1.06	1.06	0	0.053	0	0	0	0	0	0	0
-19.1	7.277	7.223	0.053	1.05	1.05	0	0.053	0	0	0	0	0	0	0
-22.6	7.337	7.283	0.054	1.04	1.04	0	0.054	0	0	0	0	0	0	0
-26.2	7.399	7.346	0.053	1.03	1.03	0	0.053	0	0	0	0	0	0	0
-30	7.464	7.411	0.053	1.02	1.01	0	0.053	0	0	0	0	0	0	0
-33.8	7.529	7.478	0.05	1	1	0	0.05	0	0	0	0	0	0	0
-37.6	7.594	7.546	0.048	0.99	0.99	0	0.048	0	0	0	0	0	0	0
-41.3	7.657	7.613	0.044	0.98	0.98	0	0.044	0	0	0	0	0	0	0
-44.9	7.719	7.679	0.04	0.97	0.97	0	0.04	0	0	0	0	0	0	0
-48.3	7.777	7.741	0.036	0.96	0.96	0	0.036	0	0	0	0	0	0	0
-51.6	7.834	7.8	0.034	0.95	0.95	0	0.034	0	0	0	0	0	0	0
-54.7	7.887	7.856	0.031	0.94	0.94	0	0.031	0	0	0	0	0	0	0
-57.6	7.937	7.908	0.029	0.93	0.93	0	0.029	0	0	0	0	0	0	0
-60.3	7.983	7.957	0.026	0.92	0.92	0	0.026	0	0	0	0	0	0	0
-62.9	8.028	8.003	0.025	0.91	0.91	0	0.025	0	0	0	0	0	0	0
-65.3	8.069	8.046	0.023	0.9	0.9	0	0.023	0	0	0	0	0	0	0
-67.6	8.108	8.087	0.022	0.89	0.89	0	0.022	0	0	0	0	0	0	0
-69.8	8.146	8.125	0.021	0.88	0.88	0	0.021	0	0	0	0	0	0	0
-71.9	8.182	8.162	0.021	0.87	0.87	0	0.021	0	0	0	0	0	0	0
-73.9	8.216	8.196	0.02	0.86	0.86	0	0.02	0	0	0	0	0	0	0
-75.8	8.249	8.229	0.02	0.85	0.85	0	0.02	0	0	0	0	0	0	0
-77.6	8.28	8.26	0.019	0.84	0.84	0	0.019	0	0	0	0	0	0	0
-79.4	8.311	8.291	0.02	0.83	0.83	0	0.02	0	0	0	0	0	0	0
-81.1	8.34	8.32	0.02	0.82	0.82	0	0.02	0	0	0	0	0	0	0
-82.7	8.367	8.347	0.02	0.81	0.81	0	0.02	0	0	0	0	0	0	0
-84.3	8.395	8.374	0.02	0.8	0.8	0	0.02	0	0	0	0	0	0	0
-85.8	8.42	8.4	0.02	0.79	0.79	0	0.02	0	0	0	0	0	0	0
-87	8.441	8.426	0.016	0.78	0.78	0	0.016	0	0	0	0	0	0	0
-88.2	8.462	8.45	0.012	0.77	0.77	0	0.012	0	0	0	0	0	0	0
-89.4	8.482	8.474	0.008	0.76	0.76	0	0.008	0	0	0	0	0	0	0
-90.7	8.504	8.497	0.008	0.75	0.75	0	0.008	0	0	0	0	0	0	0
-91.9	8.525	8.52	0.006	0.74	0.74	0	0.006	0	0	0	0	0	0	0
-93.1	8.546	8.542	0.004	0.73	0.73	0	0.004	0	0	0	0	0	0	0
-94.3	8.566	8.563	0.003	0.72	0.72	0	0.003	0	0	0	0	0	0	0
-95.5	8.587	8.584	0.002	0.71	0.71	0	0.002	0	0	0	0	0	0	0
-96.7	8.607	8.605	0.002	0.7	0.7	0	0.002	0	0	0	0	0	0	0
-97.8	8.626	8.625	0.001	0.69	0.69	0	0.001	0	0	0	0	0	0	0
-98.9	8.645	8.646	0	0.68	0.68	0	0	0	0	0	0	0	0	0
-100.1	8.666	8.665	0	0.67	0.67	0	0	0	0	0	0	0	0	0
-101.2	8.685	8.685	0	0.66	0.66	0	0	0	0	0	0	0	0	0
-102.3	8.703	8.704	0	0.65	0.65	0	0	0	0	0	0	0	0	0
-103.4	8.722	8.723	-0.001	0.64	0.64	0	0.001	0	0	0	0	0	0	0
-104.5	8.741	8.742	0	0.63	0.63	0	0	0	0	0	0	0	0	0

-105.6	8.76	8.76	0	0.62	0.62	0	0	0	0	0	0	0	0	0
-106.7	8.779	8.778	0	0.61	0.61	0	0	0	0	0	0	0	0	0
-107.8	8.798	8.796	0.001	0.6	0.6	0	0.001	0	0	0	0	0	0	0
-108.8	8.815	8.814	0	0.59	0.59	0	0	0	0	0	0	0	0	0
-109.9	8.834	8.832	0.001	0.58	0.58	0	0.001	0	0	0	0	0	0	0
-110.9	8.851	8.85	0.001	0.57	0.57	0	0.001	0	0	0	0	0	0	0
-111.9	8.868	8.868	0	0.56	0.56	0	0	0	0	0	0	0	0	0
-113	8.887	8.885	0.001	0.55	0.55	0	0.001	0	0	0	0	0	0	0
-114	8.904	8.903	0.001	0.54	0.54	0	0.001	0	0	0	0	0	0	0
-115	8.921	8.92	0.001	0.53	0.53	0	0.001	0	0	0	0	0	0	0
-116	8.938	8.938	0.001	0.52	0.52	0	0.001	0	0	0	0	0	0	0
-117.1	8.957	8.955	0.002	0.51	0.51	0	0.002	0	0	0	0	0	0	0
-118.1	8.974	8.972	0.002	0.5	0.5	0	0.002	0	0	0	0	0	0	0
-119.1	8.991	8.99	0.002	0.49	0.49	0	0.002	0	0	0	0	0	0	0
-120.1	9.009	9.007	0.002	0.48	0.48	0	0.002	0	0	0	0	0	0	0
-121.1	9.026	9.024	0.001	0.47	0.47	0	0.001	0	0	0	0	0	0	0
-122.1	9.043	9.042	0.001	0.46	0.46	0	0.001	0	0	0	0	0	0	0
-123.2	9.062	9.059	0.003	0.45	0.45	0	0.003	0	0	0	0	0	0	0
-124.2	9.079	9.077	0.002	0.44	0.44	0	0.002	0	0	0	0	0	0	0
-125.2	9.096	9.094	0.002	0.43	0.43	0	0.002	0	0	0	0	0	0	0
-126.2	9.113	9.112	0.001	0.42	0.42	0	0.001	0	0	0	0	0	0	0
-127.3	9.132	9.129	0.003	0.41	0.41	0	0.003	0	0	0	0	0	0	0
-128.3	9.149	9.147	0.002	0.4	0.4	0	0.002	0	0	0	0	0	0	0
-129.3	9.166	9.165	0.001	0.39	0.39	0	0.001	0	0	0	0	0	0	0
-130.4	9.185	9.183	0.002	0.38	0.38	0	0.002	0	0	0	0	0	0	0
-131.4	9.202	9.202	0.001	0.37	0.37	0	0.001	0	0	0	0	0	0	0
-132.5	9.221	9.22	0.001	0.36	0.36	0	0.001	0	0	0	0	0	0	0
-133.5	9.238	9.238	0	0.35	0.35	0	0	0	0	0	0	0	0	0
-134.6	9.257	9.257	0	0.34	0.34	0	0	0	0	0	0	0	0	0
-135.7	9.276	9.276	0	0.33	0.33	0	0	0	0	0	0	0	0	0
-136.8	9.295	9.295	0	0.32	0.32	0	0	0	0	0	0	0	0	0
-137.9	9.314	9.315	-0.001	0.31	0.31	0	0.001	0	0	0	0	0	0	0
-139	9.333	9.334	-0.002	0.3	0.3	0	0.002	0	0	0	0	0	0	0
-140.1	9.352	9.354	-0.003	0.29	0.29	0	0.003	0	0	0	0	0	0	0
-141.3	9.372	9.375	-0.003	0.28	0.28	0	0.003	0	0	0	0	0	0	0
-142.3	9.389	9.395	-0.006	0.27	0.27	0	0.006	0	0	0	0	0	0	0
-143.5	9.41	9.416	-0.006	0.26	0.26	0	0.006	0	0	0	0	0	0	0
-144.7	9.43	9.438	-0.007	0.25	0.25	0	0.007	0	0	0	0	0	0	0
-145.9	9.451	9.459	-0.008	0.24	0.24	0	0.008	0	0	0	0	0	0	0
-147.1	9.472	9.481	-0.01	0.23	0.23	0	0.01	0	0	0	0	0	0	0
-148.3	9.492	9.504	-0.012	0.22	0.22	-0.001	0.012	0	0	0	0	0	0	0
-149.6	9.514	9.527	-0.012	0.22	0.22	-0.001	0.013	0	0	0	0	0	0	0
-150.9	9.537	9.55	-0.014	0.21	0.21	-0.001	0.014	0	0	0	0	0	0	0
-152.2	9.559	9.574	-0.015	0.2	0.2	-0.001	0.015	0	0	0	0	0	0	0
-153.5	9.581	9.599	-0.018	0.19	0.19	-0.001	0.018	0	0	0	0	0	0	0
-154.9	9.605	9.624	-0.018	0.18	0.18	-0.001	0.019	0	0	0	0	0	0	0
-156.2	9.628	9.649	-0.022	0.17	0.17	-0.001	0.022	0	0	0	0	0	0	0
-157.7	9.653	9.675	-0.022	0.16	0.16	-0.002	0.022	0	0	0	0	0	0	0
-159.1	9.677	9.702	-0.025	0.15	0.16	-0.002	0.025	0	0	0	0	0	0	0
-160.5	9.701	9.729	-0.028	0.14	0.15	-0.002	0.028	0	0	0	0	0	0	0
-162	9.727	9.757	-0.03	0.14	0.14	-0.003	0.03	0	0	0	0	0	0	0
-163.5	9.753	9.785	-0.033	0.13	0.13	-0.003	0.033	0	0	0	0	0	0	0
-165.1	9.78	9.814	-0.034	0.12	0.12	-0.003	0.034	0	0	0	0	0	0	0
-166.6	9.806	9.843	-0.038	0.11	0.12	-0.004	0.038	0	0	0	0	0	0	0

-168.2	9.833	9.873	-0.04	0.11	0.11	-0.004	0.04	0	0	0	0	0	0	0
-169.8	9.861	9.903	-0.042	0.1	0.1	-0.005	0.043	0	0	0	0	0	0	0
-171.5	9.89	9.933	-0.043	0.09	0.1	-0.005	0.044	0	0	0	0	0	0	0
-173.1	9.917	9.964	-0.046	0.09	0.09	-0.006	0.047	0	0	0	0	0	0	0
-174.8	9.947	9.994	-0.048	0.08	0.09	-0.007	0.048	0	0	0	0	0	0	0
-176.5	9.976	10.024	-0.049	0.07	0.08	-0.008	0.049	0	0	0	0	0	0	0
-178.2	10.01	10.055	-0.05	0.07	0.08	-0.008	0.05	0	0	0	0	0	0	0
-179.9	10.03	10.084	-0.05	0.06	0.07	-0.009	0.051	0	0	0	0	0	0	0
-181.6	10.06	10.114	-0.051	0.06	0.07	-0.01	0.052	0	0	0	0	0	0	0
-183.3	10.09	10.143	-0.05	0.05	0.06	-0.01	0.051	0	0	0	0	0	0	0
-185	10.12	10.171	-0.049	0.05	0.06	-0.011	0.051	0	0	0	0	0	0	0
-186.7	10.15	10.198	-0.048	0.04	0.06	-0.011	0.049	0	0	0	0	0	0	0
-188.4	10.18	10.225	-0.046	0.04	0.05	-0.011	0.047	0	0	0	0	0	0	0
-190.1	10.21	10.251	-0.042	0.04	0.05	-0.011	0.044	0	0	0	0	0	0	0
-191.7	10.24	10.277	-0.04	0.04	0.05	-0.011	0.042	0	0	0	0	0	0	0
-193.4	10.27	10.301	-0.036	0.03	0.04	-0.011	0.037	0	0	0	0	0	0	0
-194.9	10.29	10.325	-0.033	0.03	0.04	-0.011	0.035	0	0	0	0	0	0	0
-196.5	10.32	10.347	-0.029	0.03	0.04	-0.01	0.03	0	0	0	0	0	0	0
-198	10.34	10.369	-0.025	0.03	0.04	-0.009	0.027	0	0	0	0	0	0	0
-199.5	10.37	10.391	-0.021	0.03	0.04	-0.008	0.022	0	0	0	0	0	0	0
-200.9	10.39	10.411	-0.017	0.03	0.03	-0.007	0.018	0	0	0	0	0	0	0
-202.3	10.42	10.431	-0.013	0.03	0.03	-0.005	0.014	0	0	0	0	0	0	0
-203.6	10.44	10.45	-0.01	0.03	0.03	-0.004	0.01	0	0	0	0	0	0	0
-205	10.46	10.468	-0.004	0.03	0.03	-0.002	0.004	0	0	0	0	0	0	0
-206.2	10.49	10.486	-0.001	0.03	0.03	-0.001	0.001	0	0	0	0	0	0	0
-207.4	10.51	10.503	0.002	0.03	0.03	0.001	0.003	0	0	0	0	0	0	0
-208.6	10.53	10.52	0.006	0.03	0.03	0.004	0.007	0	0	0	0	0	0	0
-209.8	10.55	10.536	0.011	0.03	0.03	0.006	0.013	0	0	0	0	0	0	0
-210.9	10.57	10.551	0.015	0.03	0.03	0.009	0.017	0	0	0	0	0	0	0
-212	10.58	10.566	0.018	0.04	0.02	0.011	0.022	0	0	0	0	0	0	0
-213	10.6	10.58	0.021	0.04	0.02	0.013	0.025	0	0	0	0	0	0	0
-214	10.62	10.594	0.024	0.04	0.02	0.016	0.029	0	0	0	0	0	0	0
-215	10.64	10.608	0.028	0.04	0.02	0.019	0.034	0	0	0	0	0	0	0
-216	10.65	10.621	0.032	0.04	0.02	0.023	0.039	0	0	0	0	0	0	0
-216.9	10.67	10.634	0.035	0.05	0.02	0.026	0.043	0	0	0	0	0	0	0
-217.8	10.68	10.646	0.038	0.05	0.02	0.029	0.047	0	0	0	0	0	0	0
-218.6	10.7	10.658	0.039	0.05	0.02	0.031	0.05	0	0	0	0	0	0	0
-219.5	10.71	10.67	0.043	0.05	0.02	0.035	0.056	0	0	0	0	0	0	0
-220.3	10.73	10.681	0.045	0.06	0.02	0.038	0.059	0	0	0	0	0	0	0
-221.1	10.74	10.692	0.048	0.06	0.02	0.042	0.064	0	0	0	0	0	0	0
-221.8	10.75	10.703	0.049	0.06	0.02	0.044	0.066	0	0	0	0	0	0	0
-222.4	10.76	10.714	0.049	0.06	0.02	0.045	0.067	0	0	0	0	0	0	0
-223.1	10.78	10.724	0.051	0.07	0.02	0.048	0.07	0	0	0	0	0	0	0
-223.7	10.79	10.734	0.051	0.07	0.02	0.05	0.071	0	0	0	0	0	0	0

3. GEP data for protonation constants of the ligand Cy_2EN

TASK	ZBAR	1	HCH0	PROTONATION			
MODL	HCH0	H	1				
CPLX	0	0	-13.78	H	+1(	-1)	
CPLX	1	0	9.483	HCH0(1)	H	+1(	1)
CPLX	1	0	15.94	HCH0(1)	H	+1(	2)
CONC							
VESL	IVOL	12	0	0			
VESL	H + 1	0.011	0	0			
VESL	HCH0	0.005	0	0			
BUR1	H + 1	-0.01	0	0			
ELEC							
ZERO	H + 1	404.29	0	0			
GRAD	H + 1	58.971	0	0			
DATA							

EMF	PH	ZBAR(H	POINT	PA	ZBAR(N	POINT								
OBS	OBS	CALC	RESID	OBS	CALC	RESID	RESID	OBS	CALC	RESID	OBS	CALC	RESID	RESID
188.4	3.661	3.666	-0.005	2	2	-0.001	0.005	0	0	0	0	0	0	0
178.3	3.832	3.85	-0.018	2	2	-0.001	0.018	0	0	0	0	0	0	0
163.5	4.083	4.131	-0.047	1.99	2	-0.002	0.047	0	0	0	0	0	0	0
142.1	4.446	4.53	-0.084	1.99	1.99	-0.001	0.084	0	0	0	0	0	0	0
121.9	4.789	4.864	-0.075	1.97	1.98	-0.001	0.075	0	0	0	0	0	0	0
108.1	5.023	5.081	-0.058	1.96	1.96	0	0.058	0	0	0	0	0	0	0
98.4	5.187	5.234	-0.047	1.94	1.94	0	0.047	0	0	0	0	0	0	0
91	5.313	5.352	-0.039	1.93	1.93	0	0.039	0	0	0	0	0	0	0
85	5.414	5.448	-0.034	1.91	1.91	0	0.034	0	0	0	0	0	0	0
79.9	5.501	5.53	-0.029	1.89	1.89	0	0.029	0	0	0	0	0	0	0
75.5	5.575	5.601	-0.026	1.88	1.88	0	0.026	0	0	0	0	0	0	0
71.6	5.642	5.664	-0.023	1.86	1.86	0	0.023	0	0	0	0	0	0	0
68	5.703	5.722	-0.019	1.84	1.84	0	0.019	0	0	0	0	0	0	0
64.8	5.757	5.775	-0.018	1.83	1.83	0	0.018	0	0	0	0	0	0	0
61.8	5.808	5.823	-0.016	1.81	1.81	0	0.016	0	0	0	0	0	0	0
59	5.855	5.869	-0.014	1.79	1.79	0	0.014	0	0	0	0	0	0	0
56.4	5.899	5.912	-0.013	1.78	1.78	0	0.013	0	0	0	0	0	0	0
53.9	5.942	5.953	-0.011	1.76	1.76	0	0.011	0	0	0	0	0	0	0
51.6	5.981	5.991	-0.011	1.74	1.74	0	0.011	0	0	0	0	0	0	0
49.3	6.02	6.029	-0.009	1.73	1.73	0	0.009	0	0	0	0	0	0	0
47.1	6.057	6.064	-0.007	1.71	1.71	0	0.007	0	0	0	0	0	0	0
45	6.093	6.099	-0.006	1.69	1.69	0	0.006	0	0	0	0	0	0	0
43	6.127	6.133	-0.006	1.68	1.68	0	0.006	0	0	0	0	0	0	0
41	6.16	6.165	-0.005	1.66	1.66	0	0.005	0	0	0	0	0	0	0
39.1	6.193	6.197	-0.004	1.65	1.65	0	0.004	0	0	0	0	0	0	0
37.2	6.225	6.228	-0.003	1.63	1.63	0	0.003	0	0	0	0	0	0	0
35.3	6.257	6.259	-0.002	1.61	1.61	0	0.002	0	0	0	0	0	0	0
33.5	6.288	6.289	-0.001	1.6	1.6	0	0.001	0	0	0	0	0	0	0
31.7	6.318	6.319	-0.001	1.58	1.58	0	0.001	0	0	0	0	0	0	0
29.9	6.349	6.348	0.001	1.56	1.56	0	0.001	0	0	0	0	0	0	0
28.1	6.379	6.377	0.002	1.55	1.55	0	0.002	0	0	0	0	0	0	0
26.4	6.408	6.406	0.002	1.53	1.53	0	0.002	0	0	0	0	0	0	0
24.6	6.439	6.435	0.003	1.51	1.51	0	0.003	0	0	0	0	0	0	0
22.9	6.467	6.464	0.003	1.5	1.5	0	0.003	0	0	0	0	0	0	0
21.1	6.498	6.493	0.005	1.48	1.48	0	0.005	0	0	0	0	0	0	0

19.4	6.527	6.522	0.005	1.46	1.46	0	0.005	0	0	0	0	0	0	0
17.6	6.557	6.551	0.007	1.45	1.45	0	0.007	0	0	0	0	0	0	0
15.8	6.588	6.58	0.008	1.43	1.43	0	0.008	0	0	0	0	0	0	0
14	6.618	6.609	0.009	1.41	1.41	0	0.009	0	0	0	0	0	0	0
12.2	6.649	6.639	0.01	1.4	1.4	0	0.01	0	0	0	0	0	0	0
10.3	6.681	6.669	0.012	1.38	1.38	0	0.012	0	0	0	0	0	0	0
8.4	6.713	6.7	0.013	1.36	1.36	0	0.013	0	0	0	0	0	0	0
6.5	6.746	6.732	0.014	1.35	1.35	0	0.014	0	0	0	0	0	0	0
4.6	6.778	6.764	0.014	1.33	1.33	0	0.014	0	0	0	0	0	0	0
2.5	6.813	6.796	0.017	1.31	1.31	0	0.017	0	0	0	0	0	0	0
0.4	6.849	6.83	0.019	1.3	1.3	0	0.019	0	0	0	0	0	0	0
-1.7	6.885	6.865	0.02	1.28	1.28	0	0.02	0	0	0	0	0	0	0
-4	6.924	6.901	0.023	1.26	1.26	0	0.023	0	0	0	0	0	0	0
-6.3	6.963	6.938	0.024	1.25	1.25	0	0.024	0	0	0	0	0	0	0
-8.8	7.005	6.977	0.028	1.23	1.23	0	0.028	0	0	0	0	0	0	0
-11.4	7.049	7.018	0.031	1.21	1.21	0	0.031	0	0	0	0	0	0	0
-14.1	7.095	7.061	0.034	1.2	1.2	0	0.034	0	0	0	0	0	0	0
-17	7.144	7.106	0.038	1.18	1.18	0	0.038	0	0	0	0	0	0	0
-20.2	7.198	7.155	0.043	1.16	1.16	0	0.043	0	0	0	0	0	0	0
-23.6	7.256	7.207	0.049	1.15	1.15	0	0.049	0	0	0	0	0	0	0
-27.3	7.319	7.264	0.055	1.13	1.13	0	0.055	0	0	0	0	0	0	0
-31.4	7.388	7.325	0.063	1.11	1.11	0	0.063	0	0	0	0	0	0	0
-36	7.466	7.393	0.073	1.1	1.1	0	0.073	0	0	0	0	0	0	0
-41.1	7.553	7.468	0.084	1.08	1.08	0	0.084	0	0	0	0	0	0	0
-46.9	7.651	7.553	0.098	1.06	1.06	0	0.098	0	0	0	0	0	0	0
-53.2	7.758	7.649	0.109	1.05	1.05	0	0.109	0	0	0	0	0	0	0
-60.1	7.875	7.756	0.119	1.03	1.03	0	0.119	0	0	0	0	0	0	0
-67.2	7.995	7.874	0.122	1.01	1.01	0	0.122	0	0	0	0	0	0	0
-74.2	8.114	7.997	0.117	1	1	0	0.117	0	0	0	0	0	0	0
-80.5	8.221	8.118	0.103	0.98	0.98	0	0.103	0	0	0	0	0	0	0
-86.2	8.317	8.231	0.086	0.96	0.96	0	0.086	0	0	0	0	0	0	0
-91.2	8.402	8.332	0.07	0.95	0.95	0	0.07	0	0	0	0	0	0	0
-95.7	8.479	8.422	0.057	0.93	0.93	0	0.057	0	0	0	0	0	0	0
-99.8	8.548	8.502	0.047	0.91	0.91	0	0.047	0	0	0	0	0	0	0
-103.5	8.611	8.573	0.038	0.9	0.9	0	0.038	0	0	0	0	0	0	0
-106.9	8.668	8.637	0.032	0.88	0.88	0	0.032	0	0	0	0	0	0	0
-110	8.721	8.695	0.026	0.87	0.87	0	0.026	0	0	0	0	0	0	0
-112.9	8.77	8.749	0.021	0.85	0.85	0	0.021	0	0	0	0	0	0	0
-115.5	8.814	8.799	0.015	0.83	0.83	0	0.015	0	0	0	0	0	0	0
-118.1	8.858	8.845	0.013	0.82	0.82	0	0.013	0	0	0	0	0	0	0
-120.5	8.899	8.889	0.01	0.8	0.8	0	0.01	0	0	0	0	0	0	0
-122.7	8.936	8.931	0.006	0.78	0.78	0	0.006	0	0	0	0	0	0	0
-124.9	8.974	8.97	0.004	0.77	0.77	0	0.004	0	0	0	0	0	0	0
-127	9.009	9.007	0.002	0.75	0.75	0	0.002	0	0	0	0	0	0	0
-129	9.043	9.043	0	0.74	0.74	0	0	0	0	0	0	0	0	0
-130.9	9.075	9.078	-0.003	0.72	0.72	0	0.003	0	0	0	0	0	0	0
-132.8	9.108	9.112	-0.004	0.7	0.7	0	0.004	0	0	0	0	0	0	0
-134.6	9.138	9.144	-0.006	0.69	0.69	0	0.006	0	0	0	0	0	0	0
-136.4	9.169	9.175	-0.007	0.67	0.67	0	0.007	0	0	0	0	0	0	0
-138.1	9.198	9.206	-0.009	0.66	0.66	0	0.009	0	0	0	0	0	0	0
-139.8	9.226	9.236	-0.01	0.64	0.64	0	0.01	0	0	0	0	0	0	0
-141.4	9.254	9.266	-0.012	0.62	0.62	0	0.012	0	0	0	0	0	0	0
-143.1	9.282	9.294	-0.012	0.61	0.61	0	0.012	0	0	0	0	0	0	0
-144.7	9.309	9.323	-0.013	0.59	0.59	0	0.013	0	0	0	0	0	0	0

-146.2	9.335	9.351	-0.016	0.58	0.58	0	0.016	0	0	0	0	0	0	0
-147.8	9.362	9.378	-0.016	0.56	0.56	-0.001	0.016	0	0	0	0	0	0	0
-149.3	9.387	9.406	-0.018	0.54	0.55	-0.001	0.018	0	0	0	0	0	0	0
-150.9	9.415	9.433	-0.018	0.53	0.53	-0.001	0.018	0	0	0	0	0	0	0
-152.3	9.438	9.46	-0.021	0.51	0.51	-0.001	0.021	0	0	0	0	0	0	0
-153.9	9.465	9.487	-0.021	0.5	0.5	-0.001	0.021	0	0	0	0	0	0	0
-155.3	9.489	9.513	-0.024	0.48	0.48	-0.001	0.024	0	0	0	0	0	0	0
-156.9	9.516	9.54	-0.023	0.47	0.47	-0.001	0.023	0	0	0	0	0	0	0
-158.4	9.542	9.566	-0.024	0.45	0.45	-0.001	0.024	0	0	0	0	0	0	0
-159.9	9.567	9.593	-0.025	0.44	0.44	-0.001	0.025	0	0	0	0	0	0	0
-161.4	9.593	9.619	-0.026	0.42	0.42	-0.002	0.026	0	0	0	0	0	0	0
-162.8	9.616	9.646	-0.029	0.41	0.41	-0.002	0.029	0	0	0	0	0	0	0
-164.3	9.642	9.672	-0.03	0.39	0.39	-0.002	0.03	0	0	0	0	0	0	0
-165.8	9.667	9.699	-0.032	0.38	0.38	-0.002	0.032	0	0	0	0	0	0	0
-167.3	9.693	9.726	-0.033	0.36	0.36	-0.003	0.033	0	0	0	0	0	0	0
-168.8	9.718	9.753	-0.035	0.35	0.35	-0.003	0.035	0	0	0	0	0	0	0
-170.4	9.745	9.78	-0.035	0.33	0.34	-0.003	0.035	0	0	0	0	0	0	0
-171.9	9.771	9.808	-0.037	0.32	0.32	-0.003	0.037	0	0	0	0	0	0	0
-173.4	9.796	9.835	-0.039	0.3	0.31	-0.004	0.039	0	0	0	0	0	0	0
-175	9.823	9.863	-0.04	0.29	0.29	-0.004	0.04	0	0	0	0	0	0	0
-176.6	9.85	9.891	-0.041	0.28	0.28	-0.005	0.041	0	0	0	0	0	0	0
-178.2	9.878	9.919	-0.042	0.26	0.27	-0.005	0.042	0	0	0	0	0	0	0
-179.8	9.905	9.948	-0.043	0.25	0.26	-0.006	0.043	0	0	0	0	0	0	0
-181.4	9.932	9.976	-0.045	0.24	0.24	-0.006	0.045	0	0	0	0	0	0	0
-183	9.959	10.005	-0.046	0.22	0.23	-0.007	0.047	0	0	0	0	0	0	0
-184.7	9.988	10.034	-0.047	0.21	0.22	-0.007	0.047	0	0	0	0	0	0	0
-186.3	10.015	10.063	-0.049	0.2	0.21	-0.008	0.049	0	0	0	0	0	0	0
-188	10.044	10.093	-0.049	0.19	0.2	-0.009	0.05	0	0	0	0	0	0	0
-189.7	10.073	10.122	-0.049	0.18	0.19	-0.01	0.05	0	0	0	0	0	0	0
-191.4	10.101	10.151	-0.05	0.17	0.18	-0.01	0.051	0	0	0	0	0	0	0
-193.1	10.13	10.18	-0.05	0.16	0.17	-0.011	0.051	0	0	0	0	0	0	0
-194.8	10.159	10.209	-0.05	0.15	0.16	-0.012	0.051	0	0	0	0	0	0	0
-196.5	10.188	10.238	-0.05	0.14	0.15	-0.013	0.051	0	0	0	0	0	0	0
-198.2	10.217	10.266	-0.049	0.13	0.14	-0.014	0.051	0	0	0	0	0	0	0
-199.9	10.246	10.294	-0.048	0.12	0.13	-0.014	0.05	0	0	0	0	0	0	0
-201.5	10.273	10.321	-0.049	0.11	0.13	-0.015	0.051	0	0	0	0	0	0	0
-203.2	10.302	10.348	-0.047	0.1	0.12	-0.016	0.049	0	0	0	0	0	0	0
-204.8	10.329	10.374	-0.046	0.1	0.11	-0.017	0.049	0	0	0	0	0	0	0
-206.5	10.357	10.4	-0.042	0.09	0.11	-0.017	0.046	0	0	0	0	0	0	0
-208	10.383	10.425	-0.042	0.09	0.1	-0.017	0.045	0	0	0	0	0	0	0
-209.5	10.408	10.449	-0.041	0.08	0.1	-0.018	0.045	0	0	0	0	0	0	0
-211	10.434	10.473	-0.039	0.07	0.09	-0.018	0.043	0	0	0	0	0	0	0
-212.5	10.459	10.495	-0.036	0.07	0.09	-0.018	0.04	0	0	0	0	0	0	0
-213.9	10.483	10.518	-0.035	0.07	0.08	-0.018	0.039	0	0	0	0	0	0	0
-215.3	10.507	10.539	-0.032	0.06	0.08	-0.018	0.037	0	0	0	0	0	0	0
-216.6	10.529	10.56	-0.031	0.06	0.08	-0.018	0.036	0	0	0	0	0	0	0
-217.9	10.551	10.579	-0.029	0.06	0.07	-0.018	0.034	0	0	0	0	0	0	0
-219.2	10.573	10.599	-0.026	0.05	0.07	-0.017	0.031	0	0	0	0	0	0	0
-220.4	10.593	10.617	-0.024	0.05	0.07	-0.016	0.029	0	0	0	0	0	0	0
-221.5	10.612	10.635	-0.023	0.05	0.07	-0.017	0.029	0	0	0	0	0	0	0
-222.7	10.632	10.653	-0.02	0.05	0.06	-0.015	0.026	0	0	0	0	0	0	0
-223.7	10.649	10.669	-0.02	0.05	0.06	-0.016	0.026	0	0	0	0	0	0	0
-224.8	10.668	10.686	-0.018	0.04	0.06	-0.015	0.023	0	0	0	0	0	0	0
-225.8	10.685	10.701	-0.017	0.04	0.06	-0.014	0.022	0	0	0	0	0	0	0

-226.8	10.702	10.716	-0.015	0.04	0.06	-0.013	0.02	0	0	0	0	0	0	0
-227.7	10.717	10.731	-0.014	0.04	0.05	-0.013	0.019	0	0	0	0	0	0	0
-228.7	10.734	10.745	-0.011	0.04	0.05	-0.011	0.016	0	0	0	0	0	0	0
-229.5	10.747	10.759	-0.012	0.04	0.05	-0.011	0.016	0	0	0	0	0	0	0
-230.4	10.763	10.772	-0.01	0.04	0.05	-0.01	0.014	0	0	0	0	0	0	0
-231.2	10.776	10.785	-0.009	0.04	0.05	-0.009	0.013	0	0	0	0	0	0	0
-232	10.79	10.798	-0.008	0.04	0.05	-0.009	0.012	0	0	0	0	0	0	0
-232.8	10.803	10.81	-0.006	0.04	0.04	-0.007	0.01	0	0	0	0	0	0	0
-233.6	10.817	10.822	-0.005	0.04	0.04	-0.005	0.007	0	0	0	0	0	0	0
-234.3	10.829	10.833	-0.004	0.04	0.04	-0.005	0.007	0	0	0	0	0	0	0
-235	10.841	10.844	-0.003	0.04	0.04	-0.004	0.005	0	0	0	0	0	0	0
-235.7	10.853	10.855	-0.002	0.04	0.04	-0.003	0.004	0	0	0	0	0	0	0
-236.4	10.864	10.865	-0.001	0.04	0.04	-0.001	0.002	0	0	0	0	0	0	0
-237	10.875	10.876	-0.001	0.04	0.04	-0.001	0.002	0	0	0	0	0	0	0
-237.6	10.885	10.886	-0.001	0.04	0.04	-0.001	0.001	0	0	0	0	0	0	0
-238.3	10.897	10.895	0.001	0.04	0.04	0.002	0.003	0	0	0	0	0	0	0
-238.9	10.907	10.905	0.002	0.04	0.04	0.003	0.004	0	0	0	0	0	0	0
-239.4	10.915	10.914	0.002	0.04	0.04	0.002	0.003	0	0	0	0	0	0	0
-240	10.926	10.923	0.003	0.04	0.04	0.004	0.005	0	0	0	0	0	0	0
-240.6	10.936	10.932	0.004	0.04	0.03	0.007	0.008	0	0	0	0	0	0	0
-241.1	10.944	10.94	0.004	0.04	0.03	0.007	0.008	0	0	0	0	0	0	0
-241.6	10.953	10.948	0.004	0.04	0.03	0.007	0.008	0	0	0	0	0	0	0
-242.1	10.961	10.956	0.005	0.04	0.03	0.008	0.009	0	0	0	0	0	0	0
-242.6	10.97	10.964	0.005	0.04	0.03	0.009	0.011	0	0	0	0	0	0	0
-243.1	10.978	10.972	0.006	0.04	0.03	0.011	0.012	0	0	0	0	0	0	0
-243.6	10.987	10.98	0.007	0.04	0.03	0.013	0.014	0	0	0	0	0	0	0
-244.1	10.995	10.987	0.008	0.05	0.03	0.015	0.017	0	0	0	0	0	0	0
-244.5	11.002	10.994	0.008	0.04	0.03	0.014	0.016	0	0	0	0	0	0	0
-245	11.01	11.001	0.009	0.05	0.03	0.017	0.019	0	0	0	0	0	0	0

4. GEP data for Cd-Cyp$_2$EN system

```
TASK    ZBAR          1 HPD0    COMP WITH Cd(II)
MODL    Cd+2    HPD0    H            1
CPLX        0       0   -13.78 H      +1(    -1)
CPLX        0       0     8.97 HPD0( 1)     H        +1(        1)
CPLX        0       0    15.02 HPD0( 1)     H        +1(        2)
CPLX        0       0    -9.88 Cd+2( 1)     H        +1(       -1)
CPLX        0       0   -19.86 Cd+2( 1)     H        +1(       -2)
CPLX        0       0   -31.04 Cd+2( 1)     H        +1(       -3)
CPLX        0       0   -43.12 Cd+2( 1)     H        +1(       -4)
CPLX        0       0    -8.72 Cd+2( 2)     H        +1(       -1)
CPLX        0       0   -31.42 Cd+2( 4)     H        +1(       -4)
CPLX        1       0    11.46 Cd+2( 1)     HPD0(    1)       H        +1(        1)
CPLX        1       0    4.166 Cd+2( 1)     HPD0(    1)
CPLX        1       0     7.21 Cd+2( 1)     HPD0(    2)
CONC
VESL    IVOL       15       0       0
VESL    H + 1   0.0103       0       0
VESL    Cd + 2   0.002       0       0
VESL    HPD0     0.002       0       0
BUR1    H + 1    -0.01       0       0
ELEC
ZERO    H + 1   406.64       0       0
GRAD    H + 1   58.358       0       0
DATA
EMF             PH                      ZBAR(H)     POINT           PA                      ZBAR(M)     POINT
OBS     OBS     CALC    RESID   OBS     CALC RESID  RESID   OBS     CALC    RESID   OBS     CALC    RESID   RESID

  204.2   3.469   3.492  -0.023   1.98     2  -0.014   0.027  10.984  10.935   0.049     0     0   0.007   0.049
  200.6   3.531   3.554  -0.023   1.98     2  -0.012   0.026  10.863  10.814   0.048     0     0   0.006   0.049
  196.5   3.601   3.624  -0.023   1.98  1.99   -0.01   0.026  10.724  10.675   0.049     0     0   0.005   0.049
  191.6   3.685   3.707  -0.022   1.99  1.99  -0.008   0.024  10.558  10.511   0.047     0     0   0.004   0.047
  185.9   3.783   3.807  -0.025   1.98  1.99  -0.007   0.026  10.365  10.314   0.051     0     0   0.004   0.051
  178.7   3.906   3.931  -0.026   1.98  1.99  -0.006   0.026   10.12  10.068   0.052     0     0   0.003   0.052
  169.6   4.062   4.091  -0.029   1.98  1.99  -0.005    0.03   9.811   9.752    0.06     0     0   0.003    0.06
  157.9   4.262   4.296  -0.034   1.97  1.98  -0.003   0.034   9.415   9.347   0.069  0.01     0   0.002   0.069
  144.3   4.495   4.531  -0.036   1.96  1.96  -0.002   0.036   8.957   8.885   0.072  0.01  0.01   0.002   0.072
  131.5   4.715   4.747  -0.032   1.93  1.94  -0.001   0.032   8.529   8.465   0.064  0.01  0.01   0.002   0.064
    121   4.895   4.922  -0.027   1.91  1.91  -0.001   0.027   8.182   8.129   0.053  0.01  0.01   0.002   0.053
  112.6   5.039   5.062  -0.023   1.88  1.88       0   0.023   7.909   7.863   0.046  0.02  0.02   0.002   0.046
  105.6   5.159   5.178   -0.02   1.84  1.85       0    0.02   7.684   7.646   0.038  0.02  0.02   0.003   0.038
   99.6   5.261   5.278  -0.017   1.81  1.81       0   0.017   7.495   7.463   0.032  0.03  0.02   0.003   0.032
   94.2   5.354   5.366  -0.012   1.78  1.78       0   0.012   7.327   7.304   0.024  0.03  0.03   0.002   0.024
   89.5   5.434   5.446  -0.011   1.75  1.75       0   0.011   7.184   7.162   0.022  0.03  0.03   0.002   0.022
   85.2   5.508   5.519  -0.011   1.71  1.71       0   0.011   7.055   7.034   0.021  0.03  0.03   0.002   0.021
   81.2   5.577   5.588  -0.011   1.68  1.68       0   0.011   6.937   6.917    0.02  0.04  0.04   0.003   0.021
   77.4   5.642   5.652  -0.011   1.65  1.65       0   0.011   6.827   6.808    0.02  0.04  0.04   0.003    0.02
   73.8   5.703   5.714  -0.011   1.62  1.62       0   0.011   6.725   6.705    0.02  0.04  0.04   0.003    0.02
   70.3   5.763   5.774  -0.011   1.58  1.58       0   0.011   6.628   6.608   0.019  0.05  0.04   0.003    0.02
     67    5.82   5.833  -0.013   1.55  1.55       0   0.013   6.538   6.515   0.022  0.05  0.04   0.004   0.023
   63.7   5.876    5.89  -0.013   1.52  1.52       0   0.013   6.449   6.426   0.023  0.05  0.05   0.004   0.024
   60.5   5.931   5.947  -0.015   1.48  1.48       0   0.015   6.365   6.339   0.026  0.05  0.05   0.005   0.027
   57.3   5.986   6.003  -0.017   1.45  1.45       0   0.017   6.283   6.254   0.029  0.06  0.05   0.006   0.029
   54.1   6.041    6.06  -0.019   1.42  1.42       0   0.019   6.202   6.171   0.031  0.06  0.05   0.007   0.032
   50.9   6.096   6.117  -0.021   1.38  1.38       0   0.021   6.123   6.089   0.035  0.06  0.05   0.008   0.036
   47.6   6.152   6.175  -0.023   1.35  1.35       0   0.023   6.044   6.007   0.037  0.06  0.05   0.009   0.038
   44.3   6.209   6.235  -0.026   1.32  1.32       0   0.026   5.966   5.925   0.041  0.06  0.06    0.01   0.042
     41   6.265   6.297  -0.031   1.28  1.28       0   0.031    5.89   5.842   0.048  0.07  0.06   0.012   0.049
   37.5   6.325    6.36  -0.035   1.25  1.25       0   0.035   5.811   5.759   0.052  0.07  0.06   0.013   0.054
   33.9   6.387   6.427   -0.04   1.22  1.22       0    0.04   5.732   5.674   0.058  0.07  0.06   0.014    0.06
   30.1   6.452   6.496  -0.044   1.18  1.18       0   0.044   5.651   5.588   0.063  0.08  0.06   0.015   0.065
   26.2   6.519    6.57  -0.051   1.15  1.15       0   0.051    5.57   5.499    0.07  0.08  0.06   0.016   0.072
     22   6.591   6.647  -0.056   1.12  1.12       0   0.056   5.484   5.409   0.076  0.08  0.07   0.017   0.077
   17.6   6.666   6.728  -0.062   1.08  1.08       0   0.062   5.398   5.317   0.081  0.09  0.07   0.017   0.083
     13   6.745   6.813  -0.068   1.05  1.05       0   0.068    5.31   5.224   0.086   0.1  0.08   0.017   0.088
    8.1   6.829   6.901  -0.071   1.02  1.02       0   0.071   5.219   5.131   0.088   0.1  0.09   0.016    0.09
    2.9   6.918    6.99  -0.071   0.98  0.98       0   0.071   5.125    5.04   0.086  0.11   0.1   0.014   0.087
   -2.4   7.009   7.079   -0.07   0.95  0.95       0    0.07   5.033   4.952   0.081  0.13  0.11   0.012   0.082
   -7.7     7.1   7.166  -0.066   0.92  0.92       0   0.066   4.944   4.868   0.076  0.14  0.13   0.011   0.077
  -13.1   7.193   7.251  -0.059   0.88  0.88       0   0.059   4.857   4.791   0.066  0.16  0.15   0.008   0.066
  -18.3   7.282   7.333  -0.051   0.85  0.85       0   0.051   4.776   4.719   0.057  0.18  0.17   0.007   0.057
  -23.3   7.367   7.411  -0.044   0.82  0.82       0   0.044     4.7   4.653   0.048   0.2  0.19   0.005   0.048
  -28.2   7.451   7.487  -0.035   0.78  0.78       0   0.035   4.629   4.591   0.038  0.22  0.22   0.004   0.038
  -32.7   7.528   7.559  -0.031   0.75  0.75       0   0.031   4.567   4.535   0.032  0.25  0.24   0.004   0.033
  -37.1   7.604   7.629  -0.025   0.72  0.72       0   0.025   4.509   4.483   0.026  0.27  0.27   0.003   0.026
  -41.2   7.674   7.696  -0.022   0.68  0.68       0   0.022   4.457   4.434   0.023   0.3   0.3   0.003   0.023
```

-45.1	7.741	7.762	-0.021	0.65	0.65	0	0.021	4.411	4.388	0.022	0.32	0.32	0.003	0.022
-48.9	7.806	7.827	-0.021	0.62	0.62	0	0.021	4.368	4.346	0.022	0.35	0.35	0.003	0.022
-52.6	7.869	7.891	-0.021	0.58	0.58	0	0.021	4.328	4.305	0.022	0.38	0.38	0.003	0.022
-56.1	7.929	7.954	-0.025	0.55	0.55	0	0.025	4.293	4.267	0.025	0.41	0.4	0.003	0.026
-59.5	7.988	8.017	-0.029	0.52	0.52	0	0.029	4.262	4.231	0.03	0.43	0.43	0.004	0.03
-62.8	8.044	8.08	-0.036	0.49	0.49	0	0.036	4.234	4.197	0.037	0.46	0.46	0.006	0.037

5. DC_{tast} data for Cd-Cyp_2EN system

49 Experimental points

HCPE Cd [LT]/[MT 200

4-11-2 Date when experiment was performed

cdhcp Files recorded during the experiment

DPP DCT ISE

0 1 0 indicators for mode of experiment

DCT EXPERIMENT

OH-titr L-titran M-titrant

1 0 0 indicaters for mode of titration

Titratic with protons

No.:	pH	NaOH/n	L-so	M-so	Ip(obs)	Ip(exp)	Ip(corr)	Log[MF	Log[LF	Ep(obs)	Init Ep	Shift/mV	ECFC/m	CCFC/	[LT]	[MT]
1	4.429	3.266	0	0	0.088	8.85E-02	0.9944	-4.76	-8.625	-549	-549	-0.17	######	0.174	3.52E-03	1.76E-05
2	4.622	3.358	0	0	0.087	8.82E-02	0.9806	-4.765	-8.247	-549.3	-549	0.11005	0.3616	0.267	3.51E-03	1.76E-05
3	4.821	3.481	0	0	0.085	8.78E-02	0.9678	-4.771	-7.859	-549.3	-549	0.15002	0.5709	0.41	3.50E-03	1.75E-05
4	5.012	3.639	0	0	0.084	8.73E-02	0.9651	-4.781	-7.493	-549.6	-549	0.47003	0.9264	0.61	3.48E-03	1.74E-05
5	5.22	3.873	0	0	0.084	8.66E-02	0.9683	-4.795	-7.102	-549.7	-549	0.53003	0.9434	0.921	3.45E-03	1.72E-05
6	5.406	4.161	0	0	0.083	8.58E-02	0.9686	-4.812	-6.764	-550.1	-549	0.90002	1.3096	1.297	3.41E-03	1.71E-05
7	5.612	4.583	0	0	0.082	8.46E-02	0.9684	-4.836	-6.404	-550.3	-549	1.13001	1.5426	1.825	3.37E-03	1.68E-05
8	5.81	5.077	0	0	0.082	8.32E-02	0.9797	-4.863	-6.078	-551	-549	1.84003	2.1037	2.429	3.31E-03	1.66E-05
9	6.003	5.605	0	0	0.079	0.081761	0.9638	-4.893	-5.78	-551.5	-549	2.33002	2.8038	3.075	3.25E-03	1.63E-05
10	6.104	5.892	0	0	0.076	8.10E-02	0.9382	-4.908	-5.633	-551.7	-549	2.54999	3.3691	3.423	3.22E-03	1.61E-05
11	6.207	6.174	0	0	0.074	8.03E-02	0.9218	-4.924	-5.489	-551.9	-549	2.77002	3.8155	3.782	3.19E-03	1.60E-05
12	6.307	6.433	0	0	0.073	7.96E-02	0.9194	-4.94	-5.355	-552.1	-549	2.90002	3.9793	4.133	3.17E-03	1.58E-05
13	6.412	6.702	0	0	0.072	7.89E-02	0.9108	-4.956	-5.219	-552.2	-549	3.04004	4.2404	4.503	3.14E-03	1.57E-05
14	6.51	6.926	0	0	0.07	0.078391	0.893	-4.971	-5.097	-552.3	-549	3.16003	4.6144	4.858	3.12E-03	1.56E-05
15	6.61	7.137	0	0	0.069	0.077878	0.886	-4.987	-4.977	-552.6	-549	3.45001	5.0049	5.235	3.10E-03	1.55E-05
16	6.713	7.327	0	0	0.066	7.74E-02	0.8525	-5.003	-4.856	-553	-549	3.83002	5.8805	5.653	3.08E-03	1.54E-05
17	6.834	7.514	0	0	0.064	7.70E-02	0.8249	-5.024	-4.719	-553.1	-549	3.88001	6.3527	6.202	3.06E-03	1.53E-05
18	6.922	7.634	0	0	0.064	7.67E-02	0.8345	-5.041	-4.622	-553.5	-549	4.36005	6.6849	6.657	3.05E-03	1.53E-05
19	7.02	7.753	0	0	0.06	7.64E-02	0.7865	-5.063	-4.516	-553.6	-549	4.42999	7.5159	7.236	3.04E-03	1.52E-05
20	7.125	7.87	0	0	0.061	7.61E-02	0.7945	-5.089	-4.405	-554.2	-549	4.98999	7.9451	7.964	3.03E-03	1.52E-05
21	7.218	7.956	0	0	0.059	7.59E-02	0.7795	-5.116	-4.308	-555	-549	5.81	9.0107	8.726	3.02E-03	1.51E-05
22	7.328	8.054	0	0	0.059	7.57E-02	0.7765	-5.153	-4.196	-556	-549	6.82001	10.07	9.798	3.01E-03	1.51E-05
23	7.426	8.134	0	0	0.059	7.55E-02	0.7744	-5.193	-4.097	-557	-549	7.79004	11.075	10.94	3.01E-03	1.50E-05
24	7.519	8.21	0	0	0.058	7.54E-02	0.7695	-5.236	-4.005	-558.4	-549	9.27002	12.636	12.2	3.00E-03	1.50E-05
25	7.626	8.297	0	0	0.058	7.52E-02	0.7649	-5.295	-3.9	-559.7	-549	10.55	13.993	13.9	2.99E-03	1.50E-05
26	7.718	8.463	0	0	0.057	0.074804	0.762	-5.353	-3.812	-561.2	-549	12.03	15.522	15.56	2.98E-03	1.49E-05
27	7.817	8.564	0	0	0.057	7.46E-02	0.7589	-5.424	-3.719	-563.2	-549	14.06	17.604	17.61	2.97E-03	1.48E-05
28	7.916	8.675	0	0	0.056	7.43E-02	0.7587	-5.503	-3.627	-565.5	-549	16.33	19.877	19.91	2.96E-03	1.48E-05
29	8.011	8.806	0	0	0.056	7.40E-02	0.7563	-5.587	-3.542	-567.7	-549	18.55	22.139	22.33	2.95E-03	1.47E-05
30	8.112	8.958	0	0	0.056	0.073717	0.7569	-5.682	-3.453	-571	-549	21.81	25.387	25.11	2.93E-03	1.47E-05
31	8.217	9.119	0	0	0.055	7.34E-02	0.7496	-5.789	-3.363	-573.8	-549	24.6	28.302	28.19	2.92E-03	1.46E-05
32	8.31	9.119	0	0	0.054	7.34E-02	0.7414	-5.887	-3.285	-576.6	-549	27.41	31.253	31.11	2.92E-03	1.46E-05
33	8.415	9.318	0	0	0.054	7.29E-02	0.7389	-6.001	-3.203	-579.6	-549	30.47	34.357	34.39	2.90E-03	1.45E-05
34	8.508	9.518	0	0	0.053	7.25E-02	0.7335	-6.101	-3.135	-582.5	-549	33.29	37.271	37.29	2.89E-03	1.44E-05
35	8.608	9.758	0	0	0.052	7.20E-02	0.722	-6.208	-3.066	-585.5	-549	36.28	40.465	40.34	2.87E-03	1.43E-05
36	8.709	10.017	0	0	0.049	7.15E-02	0.6798	-6.311	-3.001	-588.7	-549	39.54	44.499	43.32	2.85E-03	1.42E-05
37	8.807	10.295	0	0	0.048	0.070935	0.6809	-6.407	-2.943	-591.7	-549	42.49	47.427	46.03	2.82E-03	1.41E-05
38	8.91	10.588	0	0	0.048	7.04E-02	0.678	-6.5	-2.889	-594.7	-549	45.51	50.502	48.68	2.80E-03	1.40E-05
39	9.008	10.88	0	0	0.047	6.98E-02	0.675	-6.581	-2.843	-597.3	-549	48.17	53.22	50.97	2.78E-03	1.39E-05
40	9.111	11.186	0	0	0.046	6.92E-02	0.6706	-6.657	-2.8	-599.9	-549	50.77	55.904	53.12	2.75E-03	1.38E-05
41	9.209	11.466	0	0	0.046	6.87E-02	0.6699	-6.721	-2.765	-602.3	-549	53.15	58.296	54.92	2.73E-03	1.37E-05

42	9.314	11.748	0	0	0.045	6.81E-02	0.6663	-6.781	-2.733	-604.5	-549	55.32	60.536	56.59	2.71E-03	1.36E-05
43	9.431	12.039	0	0	0.045	6.76E-02	0.6582	-6.837	-2.703	-606.9	-549	57.72	63.092	58.15	2.69E-03	1.35E-05
44	9.509	12.214	0	0	0.044	6.73E-02	0.6554	-6.869	-2.686	-608.7	-549	59.55	64.978	59.04	2.68E-03	1.34E-05
45	9.62	12.441	0	0	0.044	6.69E-02	0.6534	-6.908	-2.666	-610.8	-549	61.62	67.087	60.11	2.66E-03	1.33E-05
46	9.732	12.653	0	0	0.042	6.65E-02	0.627	-6.94	-2.65	-613	-549	63.84	69.837	60.98	2.65E-03	1.32E-05
47	9.833	12.822	0	0	0.041	6.62E-02	0.6192	-6.964	-2.639	-615	-549	65.8	71.957	61.64	2.64E-03	1.32E-05
48	9.926	12.974	0	0	0.041	6.59E-02	0.6141	-6.983	-2.63	-616.9	-549	67.71	73.973	62.14	2.62E-03	1.31E-05
49	10.01	13.114	0	0	0.039	6.57E-02	0.5996	-6.998	-2.624	-618.6	-549	69.44	76.01	62.56	2.62E-03	1.31E-05

13.79 Overall fit of CCFC in ECFC/mV

ini-VT/	ini-LT/M	ini-MT/M	ini-E	ini-Ip
25.13	0.004	2E-05	###	0.1

2 No. of protonation constants

LogKa:

8.97

6.05

3 No. of ML and M(HL) complexes

Log(Be	M	L	H	Refin	RefInd
3.977	1	1	0	0	0
7.264	1	2	0	0	0
11.19	1	1	1	0	0

6 No. of MOH and ML(OH) complexes

Log(Be	M	L	OH	Refin	RefInd
3.9	1	0	1	0	0
7.7	1	0	2	0	0
10.3	1	0	3	0	0
12	1	0	4	0	0
5.06	2	0	1	0	1
23.7	4	0	4	0	0

Temp.	I-strenc	pKw	SLC	n-ELECTRONS
25	0.1	13.78	30	2

AMAX	APOS	ANEG
4	1	4

Softwa indicators

1	1	1	1	1	1
0					

6. GEP data for Pb-Cyp$_2$EN system

TASK	ZBAR	1	HPD0	COMP	WITH	Pb(II)								
MODL	PB+2	HPD0	H	1										
CPLX	0	0	-13.78	H	+1(	-1)								
CPLX	0	0	8.97	HPD0(	1)	H	+1(	1)						
CPLX	0	0	15.02	HPD0(	1)	H	+1(	2)						
CPLX	0	0	-7.88	PB+2(	1)	H	+1(	-1)						
CPLX	0	0	-16.66	PB+2(	1)	H	+1(	-2)						
CPLX	0	0	-27.44	PB+2(	1)	H	+1(	-3)						
CPLX	0	0	-6.18	PB+2(	2)	H	+1(	-1)						
CPLX	0	0	-20.52	PB+2(	4)	H	+1(	-4)						
CPLX	0	0	-23.02	PB+2(	3)	H	+1(	-4)						
CPLX	0	0	-43.34	PB+2(	6)	H	+1(	-8)						
CPLX	1	0	5.075	PB+2(	1)	HPD0(	1)							
CPLX	1	0	11.75	PB+2(	1)	HPD0(	1)	H	+1(	1)				
CPLX	1	0	-2.968	PB+2(	1)	HPD0(	1)	H	+1(	-1)				
CPLX	1	0	-12.45	PB+2(	1)	HPD0(	1)	H	+1(	-2)				
CONC														
VESL	IVOL	16	0	0										
VESL	H + 1	0.0103	0	0										
VESL	PB+2	0.0011	0	0										
VESL	HPD0	0.003	0	0										
BUR1	H + 1	-0.01	0	0										
ELEC														
ZERO	H + 1		402.04	0										
GRAD	H + 1		58.187	0										
DATA														
EMF		pH			ZBAR(H)		POINT		pA			ZBAR(M)		POINT
OBS	OBS	CALC	RESID	OBS	CALC	RESID	RESID	OBS	CALC	RESID	OBS	CALC	RESID	RESID
192.7	3.598	3.607	-0.009	1.99	1.99	-0.002	0.009	10.498	10.479	0.019	0.01	0	0.004	0.019
187.7	3.684	3.69	-0.007	1.99	1.99	-0.001	0.007	10.328	10.314	0.014	0	0	0.002	0.014
181.7	3.787	3.79	-0.003	1.99	1.99	-0.001	0.003	10.124	10.118	0.006	0	0	0.001	0.006
174.5	3.91	3.911	-0.001	1.99	1.99	0	0.001	9.879	9.878	0.001	0	0	0	0.001
165.8	4.06	4.06	0	1.99	1.99	0	0	9.584	9.584	0	0.01	0.01	0	0
155.9	4.23	4.237	-0.007	1.98	1.98	0	0.007	9.248	9.234	0.014	0.01	0.01	0.001	0.014
145.7	4.405	4.424	-0.019	1.97	1.97	-0.001	0.019	8.903	8.866	0.038	0.02	0.01	0.002	0.038
136.4	4.565	4.596	-0.03	1.95	1.95	-0.001	0.03	8.591	8.531	0.06	0.02	0.02	0.004	0.061
128.4	4.703	4.74	-0.037	1.93	1.93	-0.001	0.037	8.325	8.251	0.073	0.03	0.03	0.006	0.074
121.5	4.821	4.86	-0.038	1.91	1.92	-0.001	0.038	8.096	8.021	0.076	0.04	0.03	0.008	0.076
115.6	4.923	4.961	-0.038	1.9	1.9	0	0.038	7.903	7.828	0.075	0.05	0.04	0.009	0.076
110.3	5.014	5.048	-0.034	1.88	1.88	0	0.034	7.731	7.664	0.067	0.06	0.05	0.01	0.068
105.7	5.093	5.125	-0.032	1.86	1.86	0	0.032	7.583	7.52	0.063	0.07	0.06	0.01	0.064
101.5	5.165	5.194	-0.029	1.84	1.84	0	0.029	7.45	7.393	0.057	0.07	0.06	0.011	0.058
97.7	5.23	5.257	-0.027	1.81	1.81	0	0.027	7.33	7.278	0.052	0.08	0.07	0.011	0.053
94.2	5.291	5.315	-0.025	1.79	1.79	0	0.025	7.221	7.174	0.047	0.09	0.08	0.011	0.049
91	5.346	5.369	-0.023	1.77	1.77	0	0.023	7.123	7.078	0.045	0.09	0.08	0.011	0.046
88	5.397	5.419	-0.022	1.75	1.75	0	0.022	7.031	6.989	0.042	0.1	0.09	0.012	0.044
85.2	5.445	5.467	-0.022	1.73	1.73	0	0.022	6.947	6.906	0.041	0.11	0.09	0.012	0.043
82.5	5.492	5.512	-0.021	1.71	1.71	0	0.021	6.867	6.828	0.039	0.11	0.1	0.013	0.041
80	5.535	5.556	-0.021	1.69	1.69	0	0.021	6.793	6.754	0.039	0.12	0.11	0.013	0.041
77.6	5.576	5.597	-0.021	1.67	1.67	0	0.021	6.724	6.684	0.039	0.13	0.11	0.014	0.042
75.2	5.617	5.637	-0.02	1.65	1.65	0	0.02	6.654	6.617	0.037	0.13	0.12	0.014	0.04

73	5.655	5.676	-0.021	1.63	1.63	0	0.021	6.592	6.554	0.039	0.14	0.12	0.016	0.042
70.8	5.693	5.714	-0.021	1.61	1.61	0	0.021	6.531	6.492	0.038	0.14	0.13	0.016	0.042
68.6	5.73	5.751	-0.02	1.59	1.59	0	0.02	6.469	6.433	0.036	0.15	0.13	0.016	0.04
66.5	5.767	5.787	-0.02	1.57	1.57	0	0.02	6.412	6.376	0.036	0.15	0.14	0.017	0.039
64.5	5.801	5.822	-0.021	1.54	1.54	0	0.021	6.358	6.321	0.037	0.16	0.14	0.018	0.041
62.5	5.835	5.857	-0.021	1.52	1.52	0	0.021	6.305	6.267	0.037	0.17	0.15	0.019	0.042
60.5	5.87	5.891	-0.021	1.5	1.5	0	0.021	6.252	6.215	0.037	0.17	0.15	0.019	0.042
58.6	5.902	5.925	-0.022	1.48	1.48	0	0.022	6.203	6.164	0.039	0.18	0.16	0.021	0.044
56.6	5.937	5.958	-0.022	1.46	1.46	0	0.022	6.151	6.114	0.037	0.18	0.16	0.021	0.042
54.7	5.969	5.992	-0.022	1.44	1.44	0	0.022	6.103	6.065	0.038	0.19	0.17	0.022	0.043
52.8	6.002	6.025	-0.023	1.42	1.42	0	0.023	6.056	6.018	0.038	0.2	0.17	0.022	0.044
50.9	6.035	6.058	-0.023	1.4	1.4	0	0.023	6.009	5.971	0.038	0.2	0.18	0.023	0.045
49	6.067	6.091	-0.023	1.38	1.38	0	0.023	5.963	5.924	0.038	0.21	0.19	0.024	0.045
47.1	6.1	6.124	-0.024	1.36	1.36	0	0.024	5.917	5.879	0.039	0.22	0.19	0.024	0.045
44.8	6.14	6.157	-0.017	1.34	1.34	0	0.017	5.861	5.834	0.028	0.22	0.2	0.018	0.033
42.9	6.172	6.19	-0.018	1.32	1.32	0	0.018	5.817	5.789	0.028	0.22	0.2	0.018	0.033
41.1	6.203	6.223	-0.02	1.29	1.29	0	0.02	5.776	5.745	0.032	0.23	0.21	0.021	0.038
39.1	6.237	6.257	-0.019	1.27	1.27	0	0.019	5.731	5.701	0.03	0.24	0.22	0.02	0.036
37.2	6.27	6.291	-0.02	1.25	1.25	0	0.02	5.689	5.658	0.031	0.25	0.23	0.021	0.038
35.2	6.305	6.325	-0.02	1.23	1.23	0	0.02	5.645	5.614	0.031	0.26	0.24	0.02	0.037
33.2	6.339	6.359	-0.02	1.21	1.21	0	0.02	5.602	5.571	0.031	0.27	0.25	0.02	0.037
31.2	6.373	6.394	-0.021	1.19	1.19	0	0.021	5.56	5.529	0.031	0.28	0.26	0.02	0.037
29.1	6.409	6.43	-0.02	1.17	1.17	0	0.02	5.516	5.486	0.03	0.29	0.27	0.019	0.036
27	6.445	6.466	-0.02	1.15	1.15	0	0.02	5.473	5.444	0.029	0.3	0.28	0.019	0.035
24.8	6.483	6.502	-0.019	1.13	1.13	0	0.019	5.428	5.401	0.027	0.31	0.29	0.017	0.032
22.6	6.521	6.539	-0.018	1.11	1.11	0	0.018	5.384	5.359	0.026	0.32	0.3	0.016	0.03
20.4	6.559	6.577	-0.018	1.09	1.09	0	0.018	5.342	5.316	0.025	0.34	0.32	0.015	0.03
18.1	6.598	6.616	-0.017	1.06	1.06	0	0.017	5.297	5.274	0.023	0.35	0.34	0.014	0.027
15.7	6.64	6.655	-0.015	1.04	1.04	0	0.015	5.252	5.232	0.02	0.37	0.35	0.012	0.023
13.2	6.683	6.694	-0.012	1.02	1.02	0	0.012	5.205	5.19	0.016	0.38	0.37	0.009	0.018
10.8	6.724	6.735	-0.011	1	1	0	0.011	5.162	5.147	0.014	0.4	0.39	0.008	0.016
8.2	6.769	6.776	-0.008	0.98	0.98	0	0.008	5.115	5.105	0.01	0.42	0.42	0.005	0.011
5.6	6.813	6.818	-0.005	0.96	0.96	0	0.005	5.069	5.063	0.006	0.44	0.44	0.003	0.007
2.9	6.86	6.861	-0.002	0.94	0.94	0	0.002	5.023	5.021	0.002	0.47	0.47	0.001	0.002
0.2	6.906	6.905	0.001	0.92	0.92	0	0.001	4.977	4.978	-0.002	0.49	0.49	-0.001	0.002
-2.7	6.956	6.949	0.007	0.9	0.9	0	0.007	4.928	4.936	-0.008	0.52	0.52	-0.004	0.009
-5.6	7.006	6.994	0.012	0.88	0.88	0	0.012	4.881	4.894	-0.014	0.55	0.55	-0.006	0.015
-8.5	7.056	7.04	0.016	0.86	0.86	0	0.016	4.834	4.853	-0.018	0.58	0.59	-0.007	0.02
-11.5	7.107	7.086	0.021	0.83	0.83	0	0.021	4.787	4.811	-0.024	0.61	0.62	-0.009	0.026
-14.5	7.159	7.133	0.025	0.81	0.81	0	0.025	4.741	4.769	-0.029	0.65	0.65	-0.01	0.03
-17.5	7.21	7.181	0.029	0.79	0.79	0	0.029	4.695	4.728	-0.033	0.68	0.69	-0.011	0.035
-20.5	7.262	7.229	0.033	0.77	0.77	0	0.033	4.651	4.687	-0.036	0.72	0.73	-0.011	0.038
-23.3	7.31	7.278	0.032	0.75	0.75	0	0.032	4.611	4.646	-0.035	0.76	0.77	-0.01	0.037
-26.1	7.358	7.327	0.031	0.73	0.73	0	0.031	4.572	4.606	-0.034	0.8	0.81	-0.01	0.035
-28.8	7.404	7.377	0.028	0.71	0.71	0	0.028	4.536	4.566	-0.03	0.85	0.85	-0.008	0.031
-31.6	7.453	7.426	0.026	0.69	0.69	0	0.026	4.499	4.527	-0.028	0.89	0.9	-0.008	0.029
-34.4	7.501	7.476	0.024	0.67	0.67	0	0.024	4.462	4.488	-0.026	0.93	0.94	-0.007	0.027
-37.3	7.55	7.526	0.024	0.65	0.65	0	0.024	4.424	4.45	-0.025	0.98	0.99	-0.007	0.026
-40.3	7.602	7.577	0.025	0.63	0.63	0	0.025	4.386	4.412	-0.027	1.02	1.03	-0.007	0.028
-43.3	7.654	7.627	0.027	0.6	0.6	0	0.027	4.348	4.376	-0.028	1.07	1.08	-0.007	0.029
-46.2	7.703	7.677	0.027	0.58	0.58	0	0.027	4.312	4.34	-0.028	1.11	1.12	-0.007	0.029
-49.2	7.755	7.727	0.028	0.56	0.56	0	0.028	4.276	4.306	-0.03	1.16	1.17	-0.008	0.031
-52.2	7.807	7.776	0.031	0.54	0.54	0	0.031	4.24	4.272	-0.032	1.21	1.22	-0.009	0.033
-55	7.855	7.825	0.03	0.52	0.52	0	0.03	4.209	4.24	-0.031	1.25	1.26	-0.009	0.032

-57.9	7.905	7.874	0.031	0.5	0.5	0	0.031	4.177	4.209	-0.032	1.3	1.31	-0.01	0.033
-60.7	7.953	7.922	0.031	0.48	0.48	0	0.031	4.148	4.18	-0.032	1.35	1.36	-0.01	0.034
-63.4	7.999	7.969	0.03	0.46	0.46	0	0.03	4.121	4.152	-0.031	1.39	1.4	-0.01	0.033
-66	8.044	8.015	0.028	0.44	0.44	0	0.028	4.097	4.126	-0.029	1.44	1.45	-0.01	0.031
-68.6	8.088	8.061	0.027	0.42	0.42	0	0.027	4.074	4.102	-0.028	1.49	1.5	-0.01	0.029
-71.2	8.133	8.106	0.027	0.4	0.4	0	0.027	4.052	4.079	-0.027	1.54	1.55	-0.01	0.029
-73.6	8.174	8.151	0.024	0.38	0.38	0	0.024	4.035	4.059	-0.024	1.59	1.6	-0.01	0.026
-76	8.216	8.194	0.021	0.35	0.35	0	0.021	4.019	4.041	-0.022	1.64	1.65	-0.009	0.023
-78.4	8.257	8.237	0.02	0.33	0.33	0	0.02	4.005	4.025	-0.02	1.69	1.7	-0.009	0.022
-80.7	8.296	8.279	0.017	0.31	0.31	0	0.017	3.994	4.012	-0.018	1.74	1.75	-0.008	0.019
-83	8.336	8.32	0.016	0.29	0.29	0	0.016	3.985	4.001	-0.016	1.8	1.8	-0.007	0.018
-85.2	8.374	8.361	0.013	0.27	0.27	0	0.013	3.981	3.994	-0.013	1.85	1.86	-0.006	0.015
-87.4	8.412	8.4	0.011	0.25	0.25	0	0.011	3.978	3.99	-0.011	1.91	1.91	-0.005	0.012
-89.6	8.449	8.439	0.01	0.23	0.23	0	0.01	3.979	3.989	-0.01	1.96	1.97	-0.005	0.011
-91.7	8.485	8.478	0.008	0.21	0.21	0	0.008	3.985	3.992	-0.008	2.02	2.03	-0.004	0.009
-93.9	8.523	8.515	0.008	0.19	0.19	0	0.008	3.993	4.001	-0.008	2.08	2.09	-0.004	0.009
-96	8.559	8.553	0.007	0.17	0.17	0	0.007	4.008	4.015	-0.007	2.15	2.15	-0.003	0.008
-98	8.594	8.589	0.005	0.15	0.15	0	0.005	4.031	4.036	-0.005	2.21	2.21	-0.002	0.005
-100.1	8.63	8.625	0.005	0.13	0.13	0	0.005	4.061	4.066	-0.005	2.28	2.28	-0.002	0.005
-102.1	8.664	8.661	0.004	0.11	0.11	0	0.004	4.104	4.108	-0.004	2.35	2.35	-0.001	0.004

7.1 DPP data for Pb-Cyp$_2$EN system

Experimental points
hc Pb [LT]/[M 50
Date when experiment was performed
pb Files recorded during the experiment
DF DCT ISE
1 0 0 indicators for mode of experiment
DPP EXPERIMENT
OH L-titrant M-titrant
1 0 0 indicaters for mode of titration
Titration with protons

Nc	pH	NaOH	L-so	M-sc	Ip(obs)	Ip(exp)	Ip(corr	Log[Ml	Log[LF]	Ep(obs	Init Ep/r	Shift/mV	ECFC/r	CCFC/mV	[LT]	[MT]	Evirt/mv
1			0	0	6.596	6.8153	0.968	-4.12	-11.63	-329	-328.6	2.00E-02	0.435	5.78E-04	3.81E-03	7.57E-05	-329.04
2			0	0	6.35	6.5424	0.971	-4.14	-10.63	-329	-328.6	3.00E-02	0.409	1.82E-03	3.66E-03	7.27E-05	-329.013
3	3.95	2.93	0	0	6.262	6.4442	0.972	-4.15	-9.568	-329	-328.6	5.00E-02	0.414	6.33E-03	3.61E-03	7.16E-05	-329.019
4	4.03	2.96	0	0	6.26	6.4368	0.972	-4.15	-9.416	-329	-328.6	5.00E-02	0.405	8.75E-03	3.60E-03	7.15E-05	-329.009
5	4.12	3.01	0	0	6.261	6.4272	0.974	-4.15	-9.221	-329	-328.6	7.00E-02	0.402	1.10E-02	3.60E-03	7.14E-05	-329.006
6	4.25	3.06	0	0	6.2	6.4148	0.966	-4.15	-8.978	-329	-328.6	7.00E-02	0.503	1.49E-02	3.59E-03	7.13E-05	-329.108
7	4.36	3.11	0	0	6.29	6.4041	0.982	-4.15	-8.764	-329	-328.6	8.00E-02	0.308	1.93E-02	3.58E-03	7.12E-05	-328.911
8	4.43	3.14	0	0	6.292	6.3968	0.984	-4.15	-8.626	-329	-328.6	0.100006	0.309	2.30E-02	3.58E-03	7.11E-05	-328.912
9	4.55	3.2	0	0	6.226	6.383	0.975	-4.15	-8.381	-329	-328.6	0.109985	0.427	3.14E-02	3.57E-03	7.09E-05	-329.031
#	4.65	3.25	0	0	6.254	6.371	0.982	-4.15	-8.195	-329	-328.6	0.130005	0.366	4.00E-02	3.57E-03	7.08E-05	-328.969
#	4.74	3.31	0	0	6.251	6.3584	0.983	-4.15	-8.017	-329	-328.6	0.149994	0.367	5.07E-02	3.56E-03	7.06E-05	-328.97
#	4.84	3.38	0	0	6.188	6.3416	0.976	-4.15	-7.818	-329	-328.6	0.160004	0.471	6.66E-02	3.55E-03	7.05E-05	-329.075
#	4.93	3.46	0	0	6.203	6.3249	0.981	-4.16	-7.645	-329	-328.6	0.179993	0.426	8.50E-02	3.54E-03	7.03E-05	-329.029
#	5.03	3.56	0	0	6.129	6.3027	0.972	-4.16	-7.448	-329	-328.6	0.179993	0.535	0.11309	3.53E-03	7.00E-05	-329.139
#	5.13	3.67	0	0	6.085	6.2775	0.969	-4.16	-7.258	-329	-328.6	0.199982	0.595	0.150619	3.51E-03	6.97E-05	-329.2
#	5.23	3.81	0	0	6.116	6.2476	0.979	-4.17	-7.07	-329	-328.6	0.369995	0.641	0.201852	3.50E-03	6.94E-05	-329.244
#	5.34	3.97	0	0	6.069	6.2131	0.977	-4.17	-6.88	-329	-328.6	0.299988	0.598	0.274492	3.48E-03	6.90E-05	-329.202
#	5.44	4.15	0	0	5.992	6.1741	0.971	-4.18	-6.695	-329	-328.6	0.410004	0.79	0.373848	3.45E-03	6.86E-05	-329.395
#	5.54	4.36	0	0	5.994	6.1312	0.978	-4.18	-6.522	-329	-328.6	0.699982	0.988	0.504296	3.43E-03	6.81E-05	-329.592
#	5.64	4.59	0	0	5.904	6.0833	0.971	-4.19	-6.349	-329	-328.6	0.75	1.129	0.684681	3.40E-03	6.76E-05	-329.734
#	5.74	4.84	0	0	5.831	6.0322	0.967	-4.21	-6.182	-329	-328.6	0.880005	1.31	0.927744	3.38E-03	6.70E-05	-329.915
#	5.85	5.11	0	0	5.802	5.9775	0.971	-4.22	-6.017	-330	-328.6	0.899994	1.279	1.258639	3.34E-03	6.64E-05	-329.884
#	5.95	5.39	0	0	5.687	5.9226	0.96	-4.24	-5.858	-330	-328.6	1	1.514	1.694905	3.31E-03	6.58E-05	-330.121
#	6.05	5.67	0	0	5.548	5.8687	0.945	-4.26	-5.708	-330	-328.6	1.440002	2.152	2.246902	3.28E-03	6.52E-05	-330.761
#	6.15	5.96	0	0	5.426	5.8145	0.933	-4.29	-5.562	-330	-328.6	1.48999	2.368	2.950668	3.25E-03	6.46E-05	-330.978
#	6.25	6.23	0	0	5.329	5.7644	0.925	-4.32	-5.425	-331	-328.6	2.820007	3.816	3.803216	3.23E-03	6.40E-05	-332.428
#	6.35	6.5	0	0	5.228	5.715	0.915	-4.36	-5.291	-332	-328.6	3.570007	4.701	4.853377	3.20E-03	6.35E-05	-333.315
#	6.45	6.73	0	0	5.119	5.6727	0.902	-4.41	-5.163	-333	-328.6	4.769989	6.073	6.08657	3.17E-03	6.30E-05	-334.689
#	6.56	6.95	0	0	4.835	5.6333	0.858	-4.46	-5.035	-335	-328.6	6.279999	8.219	7.576735	3.15E-03	6.26E-05	-336.843
#	6.66	7.15	0	0	4.819	5.5989	0.861	-4.52	-4.914	-336	-328.6	7.199982	9.104	9.22621	3.13E-03	6.22E-05	-337.727
#	6.76	7.32	0	0	4.701	5.57	0.844	-4.59	-4.801	-336	-328.6	7.769989	9.922	11.01274	3.12E-03	6.19E-05	-338.548
#	6.86	7.47	0	0	4.524	5.5441	0.816	-4.66	-4.686	-338	-328.6	9.790009	12.37	13.0556	3.10E-03	6.16E-05	-341.002
#	6.96	7.59	0	0	4.486	5.5225	0.812	-4.73	-4.575	-341	-328.6	12.10999	14.75	15.2294	3.09E-03	6.14E-05	-343.38
#	7.07	7.71	0	0	4.309	5.5022	0.783	-4.82	-4.462	-343	-328.6	13.97	17.07	17.67623	3.08E-03	6.11E-05	-345.711
#	7.17	7.82	0	0	4.261	5.4851	0.777	-4.9	-4.359	-346	-328.6	17.13	20.33	20.10135	3.07E-03	6.09E-05	-348.973
#	7.28	7.91	0	0	4.135	5.4691	0.756	-5	-4.247	-348	-328.6	19.29999	22.85	22.88972	3.06E-03	6.08E-05	-351.493
#	7.37	7.99	0	0	4.041	5.4559	0.741	-5.09	-4.152	-350	-328.6	21.70999	25.52	25.42669	3.05E-03	6.06E-05	-354.166
#	7.48	8.08	0	0	4.004	5.4418	0.736	-5.19	-4.047	-354	-328.6	25.16	29.05	28.37477	3.05E-03	6.05E-05	-357.701
#	7.58	8.17	0	0	3.935	5.4274	0.725	-5.3	-3.941	-357	-328.6	28.34	32.42	31.52613	3.04E-03	6.03E-05	-361.071
#	7.67	8.24	0	0	3.88	5.4152	0.716	-5.39	-3.854	-359	-328.6	30.26999	34.5	34.21132	3.03E-03	6.02E-05	-363.153
#	7.77	8.33	0	0	3.864	5.4004	0.715	-5.5	-3.758	-362	-328.6	33.82001	38.07	37.35376	3.02E-03	6.00E-05	-366.722
#	7.88	8.43	0	0	3.842	5.3841	0.714	-5.61	-3.663	-365	-328.6	36.72	41	40.62981	3.01E-03	5.98E-05	-369.655
#	7.98	8.54	0	0	3.818	5.3664	0.711	-5.73	-3.572	-369	-328.6	40.00998	44.33	43.90789	3.00E-03	5.96E-05	-372.984
#	8.08	8.67	0	0	3.807	5.3462	0.712	-5.85	-3.482	-372	-328.6	42.89999	47.21	47.35094	2.99E-03	5.94E-05	-375.862
#	8.17	8.81	0	0	3.795	5.3245	0.713	-5.96	-3.399	-375	-328.6	46.60001	50.9	50.71336	2.98E-03	5.92E-05	-379.552
#	8.28	8.97	0	0	3.781	5.2986	0.714	-6.09	-3.313	-379	-328.6	49.97998	54.26	54.41306	2.97E-03	5.89E-05	-382.916
#	8.38	9.16	0	0	3.778	5.2689	0.717	-6.22	-3.233	-383	-328.6	54.13	58.35	58.12019	2.95E-03	5.85E-05	-387.003
#	8.48	9.37	0	0	3.774	5.2377	0.721	-6.36	-3.155	-385	-328.6	56.29999	60.46	61.97584	2.93E-03	5.82E-05	-389.111
#	8.58	9.61	0	0	3.749	5.2016	0.721	-6.49	-3.084	-390	-328.6	61.5	65.66	65.80134	2.91E-03	5.78E-05	-394.307
#	8.68	9.87	0	0	3.708	5.1626	0.718	-6.62	-3.018	-394	-328.6	65.16	69.36	69.61807	2.89E-03	5.74E-05	-398.011
#	8.79	10.1	0	0	3.691	5.1215	0.721	-6.77	-2.955	-398	-328.6	69.13998	73.3	73.64141	2.87E-03	5.69E-05	-401.948
#	8.88	10.4	0	0	3.685	5.0817	0.725	-6.9	-2.902	-401	-328.6	72.59	76.67	77.34989	2.84E-03	5.65E-05	-405.32
#	8.98	10.7	0	0	3.677	5.0403	0.729	-7.03	-2.853	-406	-328.6	77.10999	81.11	81.19054	2.82E-03	5.60E-05	-409.763
#	9.09	11	0	0	3.666	4.999	0.733	-7.17	-2.808	-410	-328.6	81.04999	84.98	85.0758	2.80E-03	5.55E-05	-413.634
#	9.19	11.3	0	0	3.657	4.9599	0.737	-7.3	-2.77	-413	-328.6	84.09	87.96	88.92641	2.78E-03	5.51E-05	-416.604
#	9.29	11.6	0	0	3.634	4.9241	0.738	-7.43	-2.738	-417	-328.6	88.38998	92.24	92.59565	2.76E-03	5.47E-05	-420.892
#	9.39	11.8	0	0	3.619	4.8897	0.74	-7.57	-2.71	-421	-328.6	92.60001	96.42	96.42841	0.002736	5.43E-05	-425.066
#	9.49	12	0	0	3.593	4.8597	0.739	-7.69	-2.687	-425	-328.6	96.25	100.1	100.1443	2.72E-03	5.40E-05	-428.731
#	9.59	12.3	0	0	3.566	4.8321	0.738	-7.83	-2.668	-429	-328.6	100.27	104.1	103.8718	2.70E-03	5.37E-05	-432.773
#	9.7	12.4	0	0	3.544	4.8078	0.737	-7.96	-2.653	-432	-328.6	103.18	107.1	107.6378	2.69E-03	5.34E-05	-435.699
#	9.8	12.6	0	0	3.491	4.7853	0.729	-8.09	-2.64	-437	-328.6	108.24	112.2	111.4667	2.68E-03	5.32E-05	-440.892
#	9.9	12.8	0	0	3.477	4.7651	0.73	-8.23	-2.629	-441	-328.6	112.5	116.5	115.4706	2.67E-03	5.29E-05	-445.149
#	10	12.9	0	0	3.454	4.7461	0.728	-8.37	-2.621	-445	-328.6	116.41	120.4	119.4829	2.66E-03	5.27E-05	-449.094
#	10.1	13.1	0	0	3.412	4.7278	0.722	-8.51	-2.615	-449	-328.6	120.84	125	123.6526	2.65E-03	5.25E-05	-453.63

#	10.2	13.2	0	0	3.37	4.7088	0.716	-8.67	-2.61	-454	-328.6	124.93	129.2	128.1467	2.63E-03	5.23E-05	-457.827
#	10.3	13.4	0	0	3.358	4.6885	0.716	-8.83	-2.606	-458	-328.6	129.2	133.4	132.9238	2.62E-03	5.21E-05	-462.088
#	10.4	13.6	0	0	3.346	4.6678	0.717	-9	-2.604	-462	-328.6	133.63	137.9	137.7263	2.61E-03	5.19E-05	-466.508
#	10.5	13.8	0	0	3.27	4.6435	0.704	-9.18	-2.603	-466	-328.6	137.71	142.2	142.9063	2.60E-03	5.16E-05	-470.813
#	10.6	14	0	0	3.231	4.615	0.7	-9.37	-2.602	-472	-328.6	143.35	147.9	148.5595	2.58E-03	5.13E-05	-476.529
#	10.7	14.3	0	0	3.182	4.5831	0.694	-9.57	-2.603	-476	-328.6	147.76	152.4	154.1349	2.56E-03	5.09E-05	-481.046

0 Overall fit of CCFC in ECFC/mV

ini- ini-LT/ ini-MT ini-E ini-Ip
0 0 ### 7.2

2 No. of protonation constants
LogKa:
9
6

2 No. of ML and M(HL) complexes
Lo M L H Refir RefInd
5 1 1 0 1 1
Stand. deviation in Log(beta)
COVAR for this log
1 1 1 1 1
1 Stand. deviation in Log(beta)
0 COVAR for this log

9 No. of MOH and ML(OH) complexes
Lo M L OH Refir RefInd
6 1 0 1 0 0
1 0 2 0 0
1 0 3 0 0
8 2 0 1 0 0
4 0 4 0 0
3 0 4 0 1
6 0 8 0 1
1 1 1 1 1
Stand. deviation in Log(beta)
COVAR for this log
1 1 2 1 0
Stand. deviation in Log(beta)
COVAR for this log
Te I-stren pKw SLO n-ELECTRONS
0.1 13.8 29 2

AN APOS ANEG
6 1 6

Software indicators
1 1 1 1 1 1
1

8. GEP data for Cu-Cyp$_2$EN system

TASK	ZBAR		1	HPD0	COMPL	WITH	Cu(II)				
MODL	CU+2	HPD0	H		1						
CPLX		0	0	-13.78	H	+1(	-1)				
CPLX		0	0	8.97	HPD0(	1)	H	+1(	1)		
CPLX		0	0	15.02	HPD0(	1)	H	+1(	2)		
CPLX		0	0	-7.68	CU+2(	1)	H	+1(	-1)		
CPLX		0	0	-6.08	CU+2(	2)	H	+1(	-1)		
CPLX		0	0	-10.76	CU+2(	2)	H	+1(	-2)		
CPLX		0	0	-21.42	CU+2(	3)	H	+1(	-4)		
CPLX		1	0	11.87	CU+2(	1)	HPD0(	1)	H	+1(	1)
CPLX		1	0	6.747	CU+2(	1)	HPD0(	1)			
CPLX		1	0	-0.4174	CU+2(	1)	HPD0(	1)	H	+1(	-1)
CPLX		1	0	-10.16	CU+2(	1)	HPD0(	1)	H	+1(	-2)
CONC											
VESL	IVOL	13.9	0	0							
VESL	H + 1	0.0094	0	0							
VESL	CU+2	0.0019	0	0							
VESL	HPD0	0.0019	0	0							
BUR1	H + 1	-0.01	0	0							
ELEC											
ZERO	H + 1	398.84	0	0							
GRAD	H + 1	58.054	0	0							
DATA											

EMF	PH			ZBAR(H)			POINT	PA			ZBAR(M)			POINT
OBS	OBS	CALC	RESID	OBS	CALC	RESID	RESID	OBS	CALC	RESID	OBS	CALC	RESID	RESID
214.2	3.18	3.21	-0.029	1.96	2	-0.034	0.045	11.568	11.5	0.066	0.02	0	0.016	0.068
212	3.218	3.248	-0.029	1.97	2	-0.032	0.043	11.494	11.43	0.066	0.02	0	0.015	0.067
209.6	3.26	3.289	-0.029	1.97	2	-0.029	0.041	11.413	11.35	0.065	0.01	0	0.014	0.066
207	3.305	3.334	-0.029	1.97	2	-0.026	0.039	11.325	11.26	0.064	0.01	0	0.013	0.066
204.1	3.354	3.383	-0.029	1.97	2	-0.023	0.037	11.226	11.16	0.063	0.01	0	0.011	0.064
200.9	3.41	3.438	-0.029	1.97	1.99	-0.02	0.035	11.118	11.06	0.062	0.01	0	0.01	0.063
197.2	3.473	3.501	-0.027	1.98	1.99	-0.017	0.032	10.992	10.93	0.058	0.01	0	0.008	0.059
193.1	3.544	3.572	-0.028	1.98	1.99	-0.015	0.032	10.852	10.79	0.059	0.01	0	0.007	0.059
188.2	3.628	3.655	-0.027	1.98	1.99	-0.012	0.029	10.686	10.63	0.056	0.01	0	0.006	0.057
182.3	3.73	3.755	-0.025	1.98	1.99	-0.009	0.027	10.484	10.43	0.053	0.01	0	0.004	0.053
175	3.856	3.879	-0.023	1.98	1.99	-0.006	0.024	10.235	10.19	0.048	0.01	0	0.003	0.048
165.6	4.018	4.034	-0.017	1.98	1.98	-0.003	0.017	9.915	9.881	0.034	0.01	0.01	0.002	0.034
153.5	4.226	4.224	0.002	1.97	1.97	0	0.002	9.503	9.508	-0.005	0.01	0.01	0	0.005
140.5	4.45	4.423	0.027	1.95	1.95	0.002	0.027	9.064	9.118	-0.054	0.01	0.01	-0.002	0.054
130	4.631	4.594	0.037	1.92	1.92	0.002	0.037	8.713	8.788	-0.074	0.02	0.02	-0.002	0.074
122.2	4.765	4.727	0.039	1.89	1.88	0.001	0.039	8.457	8.534	-0.077	0.03	0.03	-0.003	0.077
116.3	4.867	4.831	0.036	1.85	1.85	0.001	0.036	8.267	8.338	-0.071	0.04	0.05	-0.003	0.071
111.6	4.948	4.916	0.032	1.81	1.81	0.001	0.032	8.119	8.182	-0.063	0.06	0.06	-0.003	0.063
107.6	5.017	4.988	0.029	1.77	1.77	0.001	0.029	7.995	8.052	-0.057	0.07	0.07	-0.003	0.057
104.3	5.074	5.05	0.024	1.74	1.74	0	0.024	7.896	7.942	-0.047	0.08	0.09	-0.002	0.047
101.3	5.125	5.104	0.021	1.7	1.7	0	0.021	7.807	7.847	-0.04	0.1	0.1	-0.002	0.04
98.6	5.172	5.154	0.018	1.66	1.66	0	0.018	7.728	7.762	-0.034	0.11	0.12	-0.002	0.034
96.1	5.215	5.2	0.015	1.62	1.62	0	0.015	7.657	7.686	-0.03	0.13	0.13	-0.002	0.03
93.8	5.254	5.242	0.013	1.58	1.58	0	0.013	7.593	7.617	-0.024	0.14	0.14	-0.002	0.025
91.6	5.292	5.281	0.011	1.54	1.54	0	0.011	7.533	7.554	-0.021	0.16	0.16	-0.001	0.021
89.6	5.327	5.319	0.008	1.5	1.5	0	0.008	7.48	7.495	-0.016	0.17	0.18	-0.001	0.016
87.6	5.361	5.354	0.007	1.47	1.47	0	0.007	7.427	7.44	-0.013	0.19	0.19	-0.001	0.013

85.8	5.392	5.388	0.004	1.43	1.43	0	0.004	7.382	7.389	-0.007	0.21	0.21	-0.001	0.007
84	5.423	5.421	0.002	1.39	1.39	0	0.002	7.337	7.34	-0.004	0.22	0.22	0	0.004
82.2	5.454	5.453	0.001	1.35	1.35	0	0.001	7.292	7.294	-0.002	0.24	0.24	0	0.002
80.5	5.484	5.484	-0.001	1.31	1.31	0	0.001	7.252	7.25	0.002	0.25	0.25	0	0.002
78.8	5.513	5.515	-0.002	1.27	1.27	0	0.002	7.212	7.208	0.004	0.27	0.27	0	0.004
77.1	5.542	5.545	-0.002	1.23	1.23	0	0.002	7.172	7.168	0.005	0.29	0.29	0	0.005
75.5	5.57	5.574	-0.004	1.19	1.19	0	0.004	7.137	7.129	0.008	0.3	0.3	0.001	0.008
73.8	5.599	5.603	-0.004	1.15	1.15	0	0.004	7.099	7.091	0.007	0.32	0.32	0.001	0.007
72	5.63	5.632	-0.002	1.12	1.12	0	0.002	7.058	7.055	0.003	0.34	0.34	0	0.003
70.4	5.657	5.66	-0.003	1.08	1.08	0	0.003	7.025	7.02	0.005	0.35	0.35	0	0.005
68.9	5.683	5.689	-0.006	1.04	1.04	0	0.006	6.996	6.985	0.01	0.37	0.37	0.001	0.01
67.2	5.713	5.717	-0.005	1	1	0	0.005	6.961	6.952	0.009	0.39	0.39	0.001	0.009
65.6	5.74	5.746	-0.006	0.96	0.96	0	0.006	6.93	6.92	0.01	0.41	0.41	0.001	0.01
63.9	5.769	5.775	-0.005	0.92	0.92	0	0.005	6.897	6.888	0.009	0.42	0.42	0.001	0.009
62.3	5.797	5.804	-0.006	0.88	0.88	0	0.006	6.869	6.857	0.012	0.44	0.44	0.001	0.012
60.6	5.826	5.833	-0.006	0.84	0.84	0	0.006	6.838	6.827	0.011	0.46	0.46	0.001	0.011
58.8	5.857	5.862	-0.005	0.8	0.8	0	0.005	6.806	6.797	0.009	0.48	0.48	0.001	0.009
57.1	5.887	5.892	-0.005	0.76	0.76	0	0.005	6.778	6.768	0.01	0.5	0.5	0.001	0.01
55.3	5.918	5.922	-0.005	0.72	0.72	0	0.005	6.748	6.74	0.008	0.51	0.51	0.001	0.008
53.4	5.95	5.953	-0.003	0.69	0.69	0	0.003	6.718	6.713	0.005	0.53	0.53	0	0.005
51.5	5.983	5.985	-0.002	0.65	0.65	0	0.002	6.689	6.686	0.003	0.55	0.55	0	0.003
49.6	6.016	6.017	-0.001	0.61	0.61	0	0.001	6.663	6.66	0.002	0.57	0.57	0	0.002
47.6	6.05	6.05	0	0.57	0.57	0	0	6.635	6.636	0	0.59	0.59	0	0
45.5	6.086	6.084	0.003	0.53	0.53	0	0.003	6.608	6.613	-0.004	0.61	0.61	0	0.004
43.4	6.123	6.118	0.004	0.49	0.49	0	0.004	6.584	6.591	-0.007	0.63	0.63	-0.001	0.007
41.2	6.16	6.154	0.006	0.45	0.45	0	0.006	6.56	6.571	-0.01	0.65	0.65	-0.001	0.01
39	6.198	6.191	0.008	0.41	0.41	0	0.008	6.541	6.553	-0.012	0.68	0.68	-0.001	0.012
36.6	6.24	6.228	0.011	0.37	0.37	0	0.011	6.521	6.538	-0.018	0.7	0.7	-0.001	0.018
34.2	6.281	6.267	0.014	0.33	0.33	0	0.014	6.506	6.528	-0.022	0.72	0.72	-0.001	0.022
31.8	6.322	6.307	0.015	0.29	0.29	0	0.015	6.499	6.522	-0.023	0.74	0.75	-0.001	0.023
29.2	6.367	6.348	0.019	0.26	0.26	0	0.019	6.495	6.523	-0.029	0.77	0.77	-0.001	0.029
26.7	6.41	6.39	0.02	0.22	0.22	0	0.02	6.505	6.534	-0.03	0.8	0.8	-0.001	0.03
24.1	6.455	6.433	0.022	0.18	0.18	0	0.022	6.528	6.559	-0.031	0.82	0.82	-0.001	0.031
21.4	6.502	6.477	0.024	0.14	0.14	0	0.024	6.571	6.605	-0.034	0.85	0.85	-0.001	0.034
18.8	6.546	6.522	0.024	0.1	0.1	0	0.024	6.654	6.687	-0.034	0.88	0.88	-0.001	0.034
16.2	6.591	6.568	0.023	0.06	0.06	0	0.023	6.811	6.843	-0.032	0.91	0.91	0	0.032
13.6	6.636	6.614	0.022	0.02	0.02	0	0.022	7.205	7.235	-0.03	0.94	0.94	0	0.03
11	6.681	6.661	0.02	-0.02	-0.02	0	0.02	0	0	0	0	0	0	0
8.4	6.725	6.708	0.018	-0.06	-0.06	0	0.018	0	0	0	0	0	0	0
5.8	6.77	6.755	0.015	-0.1	-0.1	0	0.015	0	0	0	0	0	0	0
3.3	6.813	6.802	0.011	-0.14	-0.14	0	0.011	0	0	0	0	0	0	0
0.8	6.856	6.85	0.007	-0.17	-0.17	0	0.007	0	0	0	0	0	0	0
-1.8	6.901	6.897	0.004	-0.21	-0.21	0	0.004	0	0	0	0	0	0	0
-4.3	6.944	6.945	-0.001	-0.25	-0.25	0	0.001	0	0	0	0	0	0	0
-6.8	6.987	6.993	-0.005	-0.29	-0.29	0	0.005	0	0	0	0	0	0	0
-9.3	7.03	7.041	-0.01	-0.33	-0.33	0	0.01	0	0	0	0	0	0	0
-11.9	7.075	7.089	-0.014	-0.37	-0.37	0	0.014	0	0	0	0	0	0	0
-14.5	7.12	7.138	-0.018	-0.41	-0.41	0	0.018	0	0	0	0	0	0	0
-17.2	7.166	7.187	-0.021	-0.45	-0.45	0	0.021	0	0	0	0	0	0	0
-19.9	7.213	7.238	-0.025	-0.49	-0.49	0	0.025	0	0	0	0	0	0	0
-22.7	7.261	7.29	-0.029	-0.53	-0.53	0	0.029	0	0	0	0	0	0	0
-25.7	7.313	7.343	-0.03	-0.57	-0.57	0	0.03	0	0	0	0	0	0	0
-28.7	7.365	7.398	-0.034	-0.6	-0.6	0	0.034	0	0	0	0	0	0	0
-32	7.421	7.456	-0.035	-0.64	-0.64	0	0.035	0	0	0	0	0	0	0

-35.4	7.48	7.517	-0.037	-0.68	-0.68	0	0.037	0	0	0	0	0	0	0
-39	7.542	7.581	-0.039	-0.72	-0.72	0	0.039	0	0	0	0	0	0	0
-43	7.611	7.649	-0.039	-0.76	-0.76	0	0.039	0	0	0	0	0	0	0
-47.4	7.687	7.724	-0.037	-0.8	-0.8	0	0.037	0	0	0	0	0	0	0
-52.1	7.768	7.805	-0.038	-0.84	-0.84	0	0.038	0	0	0	0	0	0	0
-57.5	7.861	7.896	-0.035	-0.88	-0.88	0	0.035	0	0	0	0	0	0	0
-63.6	7.966	7.998	-0.032	-0.92	-0.92	0	0.032	0	0	0	0	0	0	0
-70.7	8.088	8.114	-0.026	-0.95	-0.95	0	0.026	0	0	0	0	0	0	0
-78.8	8.228	8.246	-0.019	-0.99	-0.99	0	0.019	0	0	0	0	0	0	0
-87.8	8.383	8.393	-0.01	-1.03	-1.03	0	0.01	0	0	0	0	0	0	0
-97.1	8.543	8.545	-0.002	-1.07	-1.07	0	0.002	0	0	0	0	0	0	0
-105.9	8.694	8.692	0.003	-1.1	-1.1	0	0.003	0	0	0	0	0	0	0
-113.7	8.829	8.824	0.005	-1.14	-1.14	0	0.005	0	0	0	0	0	0	0
-120.5	8.946	8.94	0.006	-1.18	-1.18	0	0.006	0	0	0	0	0	0	0
-126.5	9.049	9.042	0.007	-1.21	-1.21	0	0.007	0	0	0	0	0	0	0
-131.7	9.139	9.132	0.007	-1.24	-1.24	0	0.007	0	0	0	0	0	0	0
-136.5	9.221	9.213	0.008	-1.28	-1.28	0.001	0.008	0	0	0	0	0	0	0
-140.8	9.295	9.287	0.009	-1.31	-1.31	0.001	0.009	0	0	0	0	0	0	0
-144.8	9.364	9.355	0.009	-1.34	-1.34	0.001	0.01	0	0	0	0	0	0	0
-148.5	9.428	9.418	0.01	-1.37	-1.38	0.001	0.01	0	0	0	0	0	0	0
-152	9.488	9.477	0.011	-1.41	-1.41	0.002	0.011	0	0	0	0	0	0	0
-155.3	9.545	9.534	0.012	-1.44	-1.44	0.002	0.012	0	0	0	0	0	0	0
-158.4	9.599	9.587	0.012	-1.47	-1.47	0.002	0.012	0	0	0	0	0	0	0
-161.4	9.65	9.638	0.012	-1.49	-1.5	0.002	0.013	0	0	0	0	0	0	0
-164.3	9.7	9.687	0.013	-1.52	-1.53	0.003	0.013	0	0	0	0	0	0	0
-167.1	9.749	9.735	0.014	-1.55	-1.55	0.004	0.014	0	0	0	0	0	0	0
-169.8	9.795	9.78	0.015	-1.58	-1.58	0.004	0.015	0	0	0	0	0	0	0
-172.5	9.842	9.825	0.017	-1.6	-1.61	0.005	0.018	0	0	0	0	0	0	0
-175	9.885	9.868	0.017	-1.62	-1.63	0.006	0.018	0	0	0	0	0	0	0
-177.5	9.928	9.909	0.018	-1.65	-1.65	0.007	0.019	0	0	0	0	0	0	0
-180	9.971	9.95	0.021	-1.67	-1.68	0.009	0.023	0	0	0	0	0	0	0
-182.4	10.012	9.989	0.023	-1.69	-1.7	0.011	0.025	0	0	0	0	0	0	0
-184.7	10.052	10.027	0.024	-1.71	-1.72	0.013	0.027	0	0	0	0	0	0	0
-187	10.091	10.064	0.027	-1.72	-1.74	0.015	0.031	0	0	0	0	0	0	0
-189.3	10.131	10.1	0.031	-1.74	-1.75	0.019	0.036	0	0	0	0	0	0	0
-191.5	10.169	10.135	0.034	-1.75	-1.77	0.023	0.041	0	0	0	0	0	0	0
-193.6	10.205	10.168	0.037	-1.76	-1.79	0.027	0.046	0	0	0	0	0	0	0
-195.7	10.241	10.2	0.041	-1.77	-1.8	0.032	0.052	0	0	0	0	0	0	0
-197.7	10.276	10.232	0.044	-1.78	-1.82	0.038	0.058	0	0	0	0	0	0	0
-199.7	10.31	10.261	0.049	-1.78	-1.83	0.045	0.066	0	0	0	0	0	0	0
-201.6	10.343	10.29	0.053	-1.79	-1.84	0.053	0.074	0	0	0	0	0	0	0
-203.4	10.374	10.318	0.056	-1.79	-1.85	0.06	0.082	0	0	0	0	0	0	0
-205.2	10.405	10.345	0.06	-1.79	-1.86	0.069	0.092	0	0	0	0	0	0	0
-206.9	10.434	10.37	0.064	-1.79	-1.87	0.079	0.102	0	0	0	0	0	0	0

9. GEP data for Ni-Cyp$_2$EN system

```
TASK    ZBAR        1 HPD0    COMPL WITH   Ni(II)
MODL    Ni+2    HPD0  H              1
CPLX        0       0   -13.78 H       +1(     -1)
CPLX        0       0     8.97 HPD0(  1)      H      +1(      1)
CPLX        0       0    15.02 HPD0(  1)      H      +1(      2)
CPLX        0       0    -9.68 Ni+2(  1)      H      +1(     -1)
CPLX        0       0   -18.58 Ni+2(  1)      H      +1(     -2)
CPLX        0       0   -29.34 Ni+2(  1)      H      +1(     -3)
CPLX        0       0   -26.82 Ni+2(  4)      H      +1(     -4)
CPLX        1       0    11.23 Ni+2(  1)      HPD0(  1)      H      +1(      1)
CPLX        1       0    3.786 Ni+2(  1)      HPD0(  1)
CPLX        1       0   -5.523 Ni+2(  1)      HPD0(  1)      H      +1(     -1)
CONC
VESL    IVOL       15       0       0
VESL    H + 1    0.01       0       0
VESL    Ni+2    0.002       0       0
VESL    HPD0    0.002       0       0
BUR1    H + 1   -0.01       0       0
ELEC
ZERO    H + 1   401.9       0       0
GRAD    H + 1   58.18       0       0
DATA
EMF             PH                      ZBAR(H)      POINT          PA                      ZBAR(M)      POINT
OBS     OBS     CALC   RESID   OBS     CALC   RESID RESID   OBS     CALC     RESID OBS     CALC RESID   RESID

194.7   3.562   3.562       0     2       2       0     0   10.794   10.794       0     0     0     0       0
190.4   3.636   3.634   0.002     2       2   0.001 0.002   10.649   10.653      -0     0     0     0   0.004
185.2   3.725   3.718   0.007     2    1.99   0.002 0.007   10.472   10.486   -0.01     0     0-0.001   0.014
178.9   3.833   3.821   0.013     2    1.99   0.003 0.013   10.257   10.283   -0.03     0     0-0.002   0.026
171.1   3.967   3.949   0.018  1.99    1.99   0.004 0.019    9.992   10.029   -0.04     0     0-0.002   0.038
160.8   4.144   4.116   0.029  1.99    1.99   0.004 0.029    9.642      9.7   -0.06     0     0-0.002   0.058
147.8   4.368   4.332   0.036  1.98    1.98   0.003 0.036      9.2    9.272   -0.07     0     0-0.002   0.072
133.6   4.612   4.578   0.034  1.96    1.96   0.002 0.034    8.721    8.789   -0.07     0     0-0.002   0.068
121.3   4.823   4.798   0.025  1.94    1.94   0.001 0.025    8.311    8.361   -0.05     0  0.01-0.002    0.05
111.5   4.992   4.972   0.019  1.91    1.91       0 0.019    7.988    8.027   -0.04  0.01  0.01-0.002   0.038
103.6   5.128   5.111   0.016  1.88    1.88       0 0.016    7.732    7.764   -0.03  0.01  0.01-0.002   0.032
   97   5.241   5.226   0.015  1.85    1.85       0 0.015    7.522     7.55   -0.03  0.01  0.01-0.002   0.029
 91.4   5.337   5.325   0.013  1.81    1.81       0 0.013    7.346     7.37   -0.02  0.01  0.02-0.002   0.024
 86.6    5.42   5.412   0.008  1.78    1.78       0 0.008    7.199    7.214   -0.02  0.02  0.02-0.002   0.015
 82.2   5.495    5.49   0.005  1.75    1.75       0 0.005    7.066    7.075   -0.01  0.02  0.02-0.001   0.009
 78.2   5.564   5.563   0.001  1.72    1.72       0 0.001    6.947     6.95      -0  0.02  0.02     0   0.003
 74.4   5.629    5.63  -0.001  1.68    1.68       0 0.001    6.836    6.835   0.002  0.02  0.02     0   0.002
 70.8   5.691   5.694  -0.003  1.65    1.65       0 0.003    6.733    6.728   0.006  0.03  0.02 0.001   0.006
 67.3   5.751   5.756  -0.004  1.62    1.62       0 0.004    6.635    6.627   0.007  0.03  0.03 0.001   0.008
 63.8   5.812   5.815  -0.003  1.59    1.59       0 0.003    6.538    6.532   0.006  0.03  0.03 0.001   0.006
 60.5   5.868   5.873  -0.004  1.55    1.55       0 0.004    6.449    6.441   0.007  0.03  0.03 0.001   0.008
 57.2   5.925   5.929  -0.004  1.52    1.52       0 0.004    6.361    6.353   0.008  0.03  0.03 0.002   0.008
 53.9   5.982   5.986  -0.004  1.49    1.49       0 0.004    6.275    6.268   0.007  0.03  0.03 0.001   0.007
 50.7   6.037   6.042  -0.005  1.45    1.45       0 0.005    6.193    6.185   0.009  0.03  0.03 0.002   0.009
 47.5   6.092   6.099  -0.007  1.42    1.42       0 0.007    6.114    6.102   0.011  0.04  0.03 0.003   0.012
 44.2   6.148   6.156  -0.008  1.39    1.39       0 0.008    6.033    6.021   0.012  0.04  0.03 0.003   0.012
   41   6.203   6.215  -0.011  1.36    1.36       0 0.011    5.957    5.939   0.018  0.04  0.03 0.004   0.018
 37.6   6.262   6.275  -0.013  1.32    1.32       0 0.013    5.878    5.858    0.02  0.04  0.03 0.005   0.021
 34.2    6.32   6.338  -0.017  1.29    1.29       0 0.017    5.801    5.775   0.026  0.04  0.04 0.006   0.027
 30.6   6.382   6.403  -0.021  1.26    1.26       0 0.021    5.721     5.69   0.031  0.04  0.04 0.008   0.032
 26.9   6.446   6.472  -0.026  1.22    1.22       0 0.026    5.641    5.603   0.038  0.05  0.04 0.009   0.039
 22.9   6.515   6.546  -0.031  1.19    1.19       0 0.031    5.556    5.513   0.043  0.05  0.04  0.01   0.045
 18.8   6.585   6.624  -0.039  1.16    1.16       0 0.039    5.472    5.419   0.054  0.05  0.04 0.012   0.055
 14.3   6.662   6.709  -0.047  1.13    1.13       0 0.047    5.382     5.32   0.062  0.05  0.04 0.014   0.063
  9.3   6.748   6.801  -0.053  1.09    1.09       0 0.053    5.284    5.217   0.067  0.06  0.04 0.014   0.069
  4.1   6.838     6.9  -0.062  1.06    1.06       0 0.062    5.186    5.109   0.077  0.06  0.05 0.015   0.078
 -1.6   6.936   7.005  -0.069  1.03    1.03       0 0.069    5.081    4.998   0.083  0.07  0.06 0.014   0.084
 -7.7    7.04   7.113  -0.073  0.99    0.99       0 0.073    4.972    4.888   0.084  0.08  0.07 0.013   0.085
-14.2   7.152   7.222   -0.07  0.96    0.96       0  0.07     4.86    4.781   0.079  0.09  0.08 0.011   0.079
-20.9   7.267   7.327   -0.06  0.93    0.93       0  0.06    4.747    4.681   0.066   0.1   0.1 0.008   0.067
-27.6   7.382   7.427   -0.044  0.9     0.9       0 0.044    4.638     4.59   0.048  0.12  0.11 0.006   0.048
-33.9   7.491    7.52   -0.029 0.86    0.86       0 0.029    4.539    4.509   0.031  0.14  0.13 0.004   0.031
-39.9   7.594   7.606   -0.012 0.83    0.83       0 0.012    4.448    4.436   0.013  0.16  0.16 0.002   0.013
-45.5    7.69   7.686    0.004  0.8     0.8       0 0.004    4.366    4.371      -0  0.18  0.18-0.001   0.004
-50.5   7.776   7.761    0.015 0.76    0.76       0 0.015    4.297    4.312   -0.02   0.2   0.2-0.002   0.016
-55.1   7.855   7.831    0.024 0.73    0.73       0 0.024    4.236     4.26   -0.03  0.22  0.22-0.004   0.025
-59.4   7.929   7.897    0.032  0.7     0.7       0 0.032    4.181    4.213   -0.03  0.24  0.25-0.005   0.033
-63.3   7.996    7.96    0.036 0.67    0.67       0 0.036    4.135    4.171   -0.04  0.27  0.27-0.006   0.037
-66.9   8.058    8.02    0.038 0.63    0.63       0 0.038    4.095    4.134   -0.04  0.29   0.3-0.007   0.039
```

-70.3	8.116	8.077	0.039	0.6	0.6	0	0.039	4.06	4.1	-0.04	0.32	0.32	-0.008	0.041
-73.6	8.173	8.132	0.041	0.57	0.57	0	0.041	4.028	4.07	-0.04	0.34	0.35	-0.009	0.043
-76.6	8.225	8.184	0.04	0.54	0.54	0	0.04	4.003	4.044	-0.04	0.37	0.38	-0.009	0.042
-79.5	8.274	8.235	0.04	0.5	0.5	0	0.04	3.981	4.021	-0.04	0.39	0.4	-0.009	0.041
-82.3	8.323	8.284	0.039	0.47	0.47	0	0.039	3.963	4.003	-0.04	0.42	0.43	-0.01	0.041
-85	8.369	8.331	0.038	0.44	0.44	0	0.038	3.949	3.988	-0.04	0.45	0.46	-0.01	0.04
-87.5	8.412	8.376	0.036	0.41	0.41	0	0.036	3.94	3.977	-0.04	0.48	0.49	-0.009	0.038
-89.9	8.453	8.42	0.033	0.37	0.37	0	0.033	3.936	3.97	-0.03	0.51	0.52	-0.009	0.035
-92.1	8.491	8.462	0.029	0.34	0.34	0	0.029	3.939	3.969	-0.03	0.54	0.55	-0.008	0.03
-94.1	8.525	8.503	0.022	0.31	0.31	0	0.022	3.95	3.972	-0.02	0.57	0.58	-0.006	0.023
-96	8.558	8.543	0.015	0.28	0.28	0	0.015	3.966	3.982	-0.02	0.61	0.61	-0.004	0.016
-97.7	8.587	8.581	0.006	0.24	0.24	0	0.006	3.993	3.999	-0.01	0.65	0.65	-0.002	0.007
-99.2	8.613	8.618	-0.005	0.21	0.21	0	0.005	4.03	4.026	0.005	0.69	0.69	0.001	0.005

10. GEP data for Zn-Cyp$_2$EN system

TASK	ZBAR	1	HPD0	COMPLE	WITH	Zn(II)									
MODL	ZN+2	HPD0	H	1											
CPLX	0	0	-13.78	H	+1(	-1)									
CPLX	0	0	8.97	HPD0(	1)	H	+1(	1)							
CPLX	0	0	15.02	HPD0(	1)	H	+1(	2)							
CPLX	0	0	-9.18	ZN+2(	1)	H	+1(	-1)							
CPLX	0	0	-16.46	ZN+2(	1)	H	+1(	-2)							
CPLX	0	0	-27.74	ZN+2(	1)	H	+1(	-3)							
CPLX	0	0	-40.32	ZN+2(	1)	H	+1(	-4)							
CPLX	0	0	-8.78	ZN+2(	2)	H	+1(	-1)							
CPLX	0	0	-27.22	ZN+2(	4)	H	+1(	-4)							
CPLX	1	0	11.9	ZN+2(	1)	HPD0(	1)	H	+1(	1)					
CPLX	1	0	4.626	ZN+2(	1)	HPD0(	1)								
CPLX	1	0	-11.49	ZN+2(	1)	HPD0(	1)	H	+1(	-2)					
CONC															
VESL	IVOL	15	0	0											
VESL	H + 1	0.0104	0	0											
VESL	ZN+2	0.0013	0	0											
VESL	HPD0	0.0027	0	0											
BUR1	H + 1	-0.0101	0	0											
ELEC															
ZERO	H + 1	392.58	0	0											
GRAD	H + 1	58.836	0	0											
DATA															
EMF		PH			ZBAR(H)		POINT		PA			ZBAR(M)		POINT	
OBS	OBS	CALC	RESID	OBS	CALC	RESID	RESID	OBS	CALC	RESID	OBS	CALC	RESID	RESID	
149.6	4.13	4.165	-0.036	1.97	1.98	-0.003	0.036	9.517	9.445	0.072	0.01	0.01	0.004	0.072	
136.1	4.359	4.357	0.002	1.97	1.97	0	0.002	9.064	9.068	-0.005	0.01	0.01	0	0.005	
124	4.565	4.542	0.023	1.95	1.95	0.001	0.023	8.66	8.707	-0.046	0.02	0.02	-0.002	0.046	
114.2	4.731	4.701	0.03	1.93	1.93	0.001	0.03	8.337	8.397	-0.06	0.03	0.03	-0.004	0.061	
106.3	4.866	4.834	0.032	1.91	1.91	0.001	0.032	8.079	8.142	-0.063	0.03	0.03	-0.005	0.063	
99.7	4.978	4.946	0.032	1.88	1.88	0	0.032	7.866	7.929	-0.062	0.04	0.04	-0.006	0.063	
94.1	5.073	5.043	0.03	1.86	1.86	0	0.03	7.688	7.746	-0.059	0.05	0.05	-0.006	0.059	
89.2	5.156	5.128	0.028	1.84	1.83	0	0.028	7.533	7.588	-0.054	0.05	0.05	-0.007	0.055	
84.8	5.231	5.205	0.026	1.81	1.81	0	0.026	7.396	7.447	-0.05	0.06	0.06	-0.007	0.051	
80.9	5.297	5.275	0.022	1.79	1.79	0	0.022	7.277	7.319	-0.043	0.07	0.07	-0.007	0.043	
77.2	5.36	5.34	0.02	1.76	1.76	0	0.02	7.164	7.203	-0.039	0.08	0.08	-0.007	0.039	
73.8	5.418	5.401	0.017	1.74	1.74	0	0.017	7.062	7.095	-0.033	0.08	0.08	-0.007	0.034	
70.7	5.471	5.458	0.013	1.71	1.71	0	0.013	6.971	6.995	-0.024	0.09	0.09	-0.005	0.025	
67.6	5.523	5.512	0.011	1.69	1.69	0	0.011	6.88	6.901	-0.021	0.1	0.1	-0.005	0.021	
64.8	5.571	5.564	0.007	1.66	1.66	0	0.007	6.8	6.812	-0.012	0.1	0.1	-0.003	0.013	
62	5.619	5.615	0.004	1.64	1.64	0	0.004	6.72	6.728	-0.007	0.11	0.11	-0.002	0.007	
59.3	5.665	5.663	0.001	1.61	1.61	0	0.001	6.645	6.647	-0.002	0.11	0.11	-0.001	0.002	
56.7	5.709	5.711	-0.002	1.59	1.59	0	0.002	6.573	6.569	0.004	0.12	0.12	0.001	0.004	
54.1	5.753	5.757	-0.004	1.56	1.56	0	0.004	6.502	6.494	0.008	0.13	0.13	0.003	0.008	
51.6	5.795	5.803	-0.008	1.54	1.54	0	0.008	6.434	6.421	0.014	0.13	0.13	0.005	0.014	
49.1	5.838	5.848	-0.01	1.51	1.51	0	0.01	6.368	6.35	0.018	0.14	0.14	0.007	0.019	
46.7	5.879	5.893	-0.014	1.48	1.48	0	0.014	6.305	6.281	0.025	0.14	0.14	0.009	0.026	
44.2	5.921	5.937	-0.016	1.46	1.46	0	0.016	6.241	6.213	0.028	0.14	0.14	0.011	0.03	
41.8	5.962	5.982	-0.02	1.43	1.43	0	0.02	6.18	6.146	0.034	0.15	0.15	0.014	0.037	
39.3	6.004	6.026	-0.022	1.41	1.41	0	0.022	6.117	6.08	0.037	0.15	0.15	0.016	0.04	

36.8	6.047	6.071	-0.024	1.38	1.38	0	0.024	6.055	6.015	0.04	0.16	0.16	0.018	0.044
34.3	6.089	6.117	-0.027	1.36	1.36	0	0.027	5.995	5.95	0.045	0.16	0.16	0.02	0.049
31.4	6.139	6.163	-0.024	1.33	1.33	0	0.024	5.924	5.886	0.038	0.16	0.16	0.018	0.042
28.9	6.181	6.209	-0.028	1.31	1.31	0	0.028	5.866	5.821	0.045	0.16	0.16	0.021	0.049
26.2	6.227	6.257	-0.03	1.28	1.28	0	0.03	5.803	5.757	0.047	0.16	0.16	0.022	0.052
23.5	6.273	6.306	-0.033	1.26	1.26	0	0.033	5.742	5.692	0.05	0.17	0.17	0.024	0.056
20.6	6.322	6.356	-0.034	1.23	1.23	0	0.034	5.677	5.626	0.051	0.17	0.17	0.024	0.056
17.6	6.373	6.408	-0.034	1.21	1.21	0	0.034	5.611	5.56	0.051	0.17	0.17	0.024	0.056
14.5	6.426	6.461	-0.035	1.18	1.18	0	0.035	5.544	5.494	0.051	0.17	0.17	0.024	0.056
11.3	6.48	6.516	-0.036	1.16	1.16	0	0.036	5.477	5.426	0.051	0.18	0.18	0.024	0.056
7.8	6.54	6.574	-0.034	1.13	1.13	0	0.034	5.405	5.358	0.047	0.18	0.18	0.022	0.052
4.3	6.599	6.633	-0.034	1.11	1.11	0	0.034	5.334	5.288	0.046	0.18	0.18	0.02	0.05
0.5	6.664	6.695	-0.031	1.08	1.08	0	0.031	5.259	5.219	0.04	0.18	0.18	0.017	0.044
-3.4	6.73	6.758	-0.028	1.06	1.06	0	0.028	5.184	5.148	0.036	0.19	0.19	0.015	0.039
-7.5	6.8	6.823	-0.023	1.03	1.03	0	0.023	5.107	5.078	0.029	0.2	0.2	0.011	0.031
-11.7	6.871	6.889	-0.018	1.01	1.01	0	0.018	5.03	5.008	0.022	0.21	0.21	0.008	0.024
-16	6.944	6.956	-0.012	0.98	0.98	0	0.012	4.954	4.94	0.014	0.22	0.22	0.005	0.015
-20.2	7.016	7.023	-0.008	0.96	0.96	0	0.008	4.882	4.873	0.009	0.24	0.24	0.003	0.009
-24.4	7.087	7.089	-0.002	0.93	0.93	0	0.002	4.812	4.81	0.002	0.26	0.26	0.001	0.003
-28.5	7.157	7.154	0.003	0.9	0.9	0	0.003	4.746	4.75	-0.004	0.29	0.29	-0.001	0.004
-32.7	7.228	7.216	0.012	0.88	0.88	0	0.012	4.679	4.693	-0.014	0.32	0.32	-0.004	0.014
-36.7	7.296	7.275	0.021	0.85	0.85	0	0.021	4.618	4.642	-0.023	0.35	0.35	-0.006	0.024
-40.5	7.361	7.331	0.03	0.83	0.83	0	0.03	4.562	4.595	-0.033	0.38	0.38	-0.007	0.033
-43.9	7.419	7.383	0.035	0.8	0.8	0	0.035	4.515	4.553	-0.038	0.42	0.42	-0.008	0.039
-46.7	7.466	7.432	0.034	0.78	0.78	0	0.034	4.479	4.515	-0.036	0.45	0.45	-0.008	0.037
-49.2	7.509	7.478	0.031	0.75	0.75	0	0.031	4.449	4.482	-0.033	0.49	0.49	-0.007	0.034
-51.3	7.544	7.52	0.025	0.73	0.73	0	0.025	4.428	4.454	-0.026	0.54	0.54	-0.005	0.027
-53.2	7.577	7.558	0.018	0.7	0.7	0	0.018	4.411	4.43	-0.019	0.58	0.58	-0.004	0.02
-54.9	7.606	7.594	0.011	0.68	0.68	0	0.011	4.397	4.409	-0.012	0.63	0.63	-0.002	0.012
-56.6	7.634	7.628	0.007	0.65	0.65	0	0.007	4.385	4.392	-0.007	0.67	0.67	-0.001	0.007
-58.2	7.662	7.659	0.003	0.63	0.63	0	0.003	4.375	4.378	-0.003	0.72	0.72	-0.001	0.003
-59.7	7.687	7.688	-0.001	0.6	0.6	0	0.001	4.368	4.367	0.001	0.76	0.76	0	0.001
-61.2	7.713	7.715	-0.002	0.58	0.58	0	0.002	4.362	4.359	0.002	0.81	0.81	0	0.002
-62.6	7.736	7.741	-0.004	0.55	0.55	0	0.004	4.358	4.353	0.004	0.86	0.86	0.001	0.004
-64	7.76	7.765	-0.005	0.53	0.53	0	0.005	4.355	4.35	0.005	0.91	0.91	0.001	0.005
-65.3	7.782	7.788	-0.006	0.5	0.5	0	0.006	4.355	4.349	0.006	0.96	0.96	0.001	0.006
-66.6	7.804	7.81	-0.005	0.48	0.48	0	0.005	4.356	4.35	0.006	1	1	0.001	0.006
-67.8	7.825	7.831	-0.006	0.45	0.45	0	0.006	4.36	4.354	0.006	1.05	1.05	0.001	0.006
-69.1	7.847	7.851	-0.004	0.43	0.43	0	0.004	4.364	4.36	0.004	1.1	1.1	0.001	0.004
-70.2	7.866	7.87	-0.005	0.4	0.4	0	0.005	4.373	4.368	0.005	1.15	1.15	0.001	0.005
-71.3	7.884	7.889	-0.005	0.38	0.38	0	0.005	4.383	4.378	0.005	1.2	1.2	0.001	0.005
-72.4	7.903	7.907	-0.005	0.35	0.35	0	0.005	4.396	4.391	0.005	1.25	1.25	0.001	0.005
-73.4	7.92	7.925	-0.005	0.32	0.32	0	0.005	4.412	4.407	0.005	1.31	1.31	0.001	0.005
-74.4	7.937	7.943	-0.006	0.3	0.3	0	0.006	4.431	4.426	0.006	1.36	1.36	0.001	0.006
-75.3	7.952	7.959	-0.007	0.27	0.27	0	0.007	4.455	4.448	0.007	1.41	1.41	0.001	0.007
-76.2	7.968	7.976	-0.008	0.25	0.25	0	0.008	4.483	4.474	0.009	1.46	1.46	0.001	0.009
-77.1	7.983	7.992	-0.01	0.22	0.22	0	0.01	4.515	4.505	0.01	1.52	1.52	0.001	0.01
-77.9	7.996	8.008	-0.012	0.2	0.2	0	0.012	4.555	4.542	0.012	1.57	1.57	0.001	0.012
-78.8	8.012	8.024	-0.013	0.17	0.17	0	0.013	4.599	4.587	0.013	1.62	1.62	0.001	0.013
-79.6	8.025	8.04	-0.015	0.15	0.15	0	0.015	4.655	4.64	0.015	1.68	1.68	0.001	0.015
-80.4	8.039	8.056	-0.017	0.12	0.12	0	0.017	4.724	4.707	0.017	1.73	1.73	0.001	0.017
-81.3	8.054	8.071	-0.017	0.1	0.1	0	0.017	4.809	4.792	0.018	1.79	1.79	0.001	0.018
-82.1	8.068	8.087	-0.019	0.07	0.07	0	0.019	4.927	4.907	0.02	1.84	1.84	0.001	0.02
-83.1	8.085	8.103	-0.018	0.05	0.05	0	0.018	5.096	5.077	0.019	1.9	1.9	0.001	0.019

-84	8.1	8.118	-0.018	0.02	0.02	0	0.018	5.412	5.392	0.02	1.95	1.95	0	0.02
-85	8.117	8.134	-0.017	0	0	0	0.017	0	0	0	0	0	0	0
-86	8.134	8.15	-0.016	-0.03	-0.03	0	0.016	0	0	0	0	0	0	0
-87	8.151	8.166	-0.014	-0.05	-0.05	0	0.014	0	0	0	0	0	0	0
-88	8.168	8.182	-0.014	-0.08	-0.08	0	0.014	0	0	0	0	0	0	0
-89	8.185	8.198	-0.013	-0.1	-0.1	0	0.013	0	0	0	0	0	0	0
-90.1	8.204	8.215	-0.011	-0.13	-0.13	0	0.011	0	0	0	0	0	0	0
-91.2	8.223	8.232	-0.009	-0.15	-0.15	0	0.009	0	0	0	0	0	0	0
-92.4	8.243	8.249	-0.006	-0.18	-0.18	0	0.006	0	0	0	0	0	0	0
-93.6	8.263	8.267	-0.004	-0.2	-0.2	0	0.004	0	0	0	0	0	0	0
-94.9	8.285	8.286	0	-0.23	-0.23	0	0	0	0	0	0	0	0	0
-96.2	8.307	8.305	0.003	-0.25	-0.25	0	0.003	0	0	0	0	0	0	0
-97.5	8.33	8.324	0.005	-0.28	-0.28	0	0.005	0	0	0	0	0	0	0
-98.9	8.353	8.345	0.009	-0.3	-0.3	0	0.009	0	0	0	0	0	0	0
-100.4	8.379	8.366	0.013	-0.33	-0.33	0	0.013	0	0	0	0	0	0	0
-101.9	8.404	8.388	0.016	-0.35	-0.36	0	0.016	0	0	0	0	0	0	0
-103.5	8.432	8.412	0.02	-0.38	-0.38	0	0.02	0	0	0	0	0	0	0
-105.1	8.459	8.437	0.022	-0.41	-0.41	0	0.022	0	0	0	0	0	0	0
-106.8	8.488	8.463	0.025	-0.43	-0.43	0	0.025	0	0	0	0	0	0	0
-108.5	8.517	8.491	0.026	-0.45	-0.46	0	0.026	0	0	0	0	0	0	0
-110.3	8.547	8.521	0.026	-0.48	-0.48	0	0.026	0	0	0	0	0	0	0
-112.1	8.578	8.553	0.025	-0.5	-0.51	0	0.025	0	0	0	0	0	0	0
-113.9	8.608	8.588	0.021	-0.53	-0.53	0	0.021	0	0	0	0	0	0	0
-115.8	8.641	8.625	0.016	-0.55	-0.55	0	0.016	0	0	0	0	0	0	0
-117.8	8.675	8.665	0.009	-0.58	-0.58	0	0.009	0	0	0	0	0	0	0
-119.7	8.707	8.709	-0.002	-0.6	-0.6	0	0.002	0	0	0	0	0	0	0
-121.7	8.741	8.755	-0.014	-0.63	-0.63	0	0.015	0	0	0	0	0	0	0
-123.8	8.777	8.806	-0.029	-0.65	-0.65	-0.001	0.029	0	0	0	0	0	0	0

AVERA OF SUM OF SQUARES
OF RESIDU ###### ###### ####### ##### ###### ######

NUMBE OF TITRATI = 1

TOTAL NUMBE OF POINTS = 107

11. DC_{tast} data for Cd-Cy_2EN system

80 Experimental points

HCH Cadm [LT]/[MT 48

Date when experiment was performed

CDH Files recorded during the experiment

DPP DCT ISE

0 1 0 indicators for mode of experiment

DCT EXPERIMENT

OH-ti L-titra M-titrant

1 0 0 indicaters for mode of titration

Titration with protons

No.:	pH	NaOH/m	L-sol	M-sc	Ip(obs)	Ip(exp)	Ip(corr)	Log[Ml	Log[LF]	Ep(obs)/n	Init Ep/r	Shift/m	ECFC/	CCFC/n	[LT]	[MT]
1	4.33	0.179	0	0	4.43	4.399	1.0071	-3.99	-9.58	-567.33	-567.1	0.26	0.169	0.151	4.94E-03	1.04E-04
2	4.41	0.189	0	0	4.428	4.397	1.0071	-3.99	-9.421	-567.33	-567.1	0.26	0.169	0.185	4.94E-03	1.04E-04
3	4.5	0.199	0	0	4.425	4.394	1.007	-3.99	-9.242	-567.53	-567.1	0.46	0.371	0.2334	4.93E-03	1.04E-04
4	4.66	0.219	0	0	4.423	4.39	1.0075	-4	-8.924	-567.58	-567.1	0.51	0.414	0.3568	4.93E-03	1.04E-04
5	4.8	0.239	0	0	4.419	4.386	1.0076	-4	-8.648	-567.77	-567.1	0.7	0.603	0.5247	4.92E-03	1.04E-04
6	4.92	0.259	0	0	4.416	4.381	1.0079	-4.01	-8.411	-567.79	-567.1	0.72	0.619	0.7385	4.92E-03	1.03E-04
7	5.02	0.279	0	0	4.411	4.377	1.0077	-4.02	-8.215	-567.83	-567.1	0.76	0.661	0.9897	4.91E-03	1.03E-04
8	5.11	0.299	0	0	4.411	4.373	1.0087	-4.03	-8.039	-568.45	-567.1	1.38	1.268	1.2955	4.91E-03	1.03E-04
9	5.18	0.319	0	0	4.408	4.369	1.009	-4.04	-7.903	-568.99	-567.1	1.92	1.805	1.6019	4.91E-03	1.03E-04
10	5.25	0.339	0	0	4.404	4.364	1.0091	-4.05	-7.768	-569.45	-567.1	2.38	2.264	1.9849	4.90E-03	1.03E-04
11	5.34	0.369	0	0	4.4	4.358	1.0097	-4.08	-7.595	-570	-567.1	2.93	2.806	2.6179	4.89E-03	1.03E-04
12	5.41	0.399	0	0	4.398	4.351	1.0107	-4.1	-7.461	-571	-567.1	3.93	3.793	3.2445	4.89E-03	1.03E-04
13	5.48	0.429	0	0	4.395	4.345	1.0115	-4.12	-7.328	-571.66	-567.1	4.59	4.443	4.0135	4.88E-03	1.03E-04
14	5.54	0.459	0	0	4.389	4.339	1.0116	-4.15	-7.216	-572.04	-567.1	4.97	4.822	4.8021	4.87E-03	1.02E-04
15	5.61	0.499	0	0	4.369	4.33	1.0089	-4.19	-7.085	-573.01	-567.1	5.94	5.826	5.8914	4.86E-03	1.02E-04
16	5.68	0.539	0	0	4.345	4.322	1.0053	-4.23	-6.956	-574.55	-567.1	7.48	7.412	7.1801	4.85E-03	1.02E-04
17	5.74	0.579	0	0	4.326	4.314	1.0029	-4.28	-6.847	-576	-567.1	8.93	8.893	8.4505	4.84E-03	1.02E-04
18	5.8	0.619	0	0	4.289	4.305	0.9962	-4.33	-6.738	-576.9	-567.1	9.83	9.879	9.8779	4.83E-03	1.02E-04
19	5.86	0.669	0	0	4.268	4.295	0.9938	-4.38	-6.632	-578.88	-567.1	11.81	11.89	11.456	4.82E-03	1.01E-04
20	5.93	0.719	0	0	4.232	4.285	0.9877	-4.45	-6.508	-580.1	-567.1	13.03	13.19	13.486	4.81E-03	1.01E-04
21	5.98	0.769	0	0	4.15	4.274	0.9709	-4.5	-6.422	-581.88	-567.1	14.81	15.19	15.042	4.80E-03	1.01E-04
22	6.05	0.829	0	0	4.093	4.262	0.9604	-4.58	-6.302	-584	-567.1	16.93	17.45	17.362	4.79E-03	1.01E-04
23	6.11	0.889	0	0	4.071	4.25	0.9579	-4.66	-6.202	-585.76	-567.1	18.69	19.24	19.455	4.77E-03	1.00E-04
24	6.17	0.949	0	0	4.019	4.238	0.9484	-4.73	-6.103	-588.1	-567.1	21.03	21.71	21.628	4.76E-03	1.00E-04
25	6.23	1.009	0	0	3.981	4.226	0.9421	-4.81	-6.006	-590.05	-567.1	22.98	23.75	23.863	4.74E-03	9.98E-05
26	6.29	1.069	0	0	3.929	4.214	0.9325	-4.89	-5.912	-592.33	-567.1	25.26	26.16	26.141	4.73E-03	9.95E-05
27	6.34	1.129	0	0	3.888	4.202	0.9254	-4.95	-5.834	-594.05	-567.1	26.98	27.98	28.056	4.72E-03	9.92E-05
28	6.4	1.189	0	0	3.878	4.19	0.9256	-5.03	-5.743	-596	-567.1	28.93	29.92	30.373	4.70E-03	9.89E-05
29	6.45	1.249	0	0	3.836	4.178	0.9181	-5.1	-5.668	-597.21	-567.1	30.14	31.24	32.302	4.69E-03	9.87E-05
30	6.51	1.309	0	0	3.807	4.166	0.9138	-5.18	-5.581	-600.03	-567.1	32.96	34.12	34.617	4.68E-03	9.84E-05
31	6.56	1.369	0	0	3.798	4.155	0.9142	-5.24	-5.51	-602.02	-567.1	34.95	36.1	36.53	4.66E-03	9.81E-05
32	6.62	1.429	0	0	3.783	4.143	0.9131	-5.32	-5.426	-604.55	-567.1	37.48	38.65	38.813	4.65E-03	9.78E-05
33	6.68	1.489	0	0	3.711	4.131	0.8982	-5.4	-5.344	-606.05	-567.1	38.98	40.36	41.071	4.64E-03	9.76E-05
34	6.75	1.549	0	0	3.685	4.12	0.8944	-5.49	-5.251	-607.99	-567.1	40.92	42.35	43.675	4.63E-03	9.73E-05
35	6.81	1.609	0	0	3.651	4.109	0.8886	-5.56	-5.173	-610.79	-567.1	43.72	45.24	45.869	4.61E-03	9.70E-05
36	6.88	1.669	0	0	3.615	4.097	0.8823	-5.65	-5.084	-613.25	-567.1	46.18	47.79	48.393	4.60E-03	9.68E-05
37	6.94	1.719	0	0	3.59	4.088	0.8782	-5.72	-5.01	-615.59	-567.1	48.52	50.19	50.523	4.59E-03	9.65E-05
38	7.02	1.769	0	0	3.574	4.079	0.8763	-5.82	-4.913	-618.68	-567.1	51.61	53.31	53.326	4.58E-03	9.63E-05
39	7.09	1.819	0	0	3.568	4.069	0.8768	-5.9	-4.83	-620.73	-567.1	53.66	55.35	55.732	4.57E-03	9.61E-05
40	7.18	1.869	0	0	3.538	4.06	0.8714	-6.01	-4.726	-624.89	-567.1	57.82	59.59	58.782	4.56E-03	9.59E-05
41	7.28	1.919	0	0	3.493	4.051	0.8623	-6.12	-4.614	-627.88	-567.1	60.81	62.71	62.115	4.55E-03	9.57E-05

42	7.37	1.959	0	0	3.487	4.043	0.8624	-6.22	-4.515	-630.31	-567.1	63.24	65.14	65.071	4.54E-03	9.55E-05
43	7.48	1.999	0	0	3.485	4.036	0.8635	-6.34	-4.396	-633.72	-567.1	66.65	68.54	68.645	4.53E-03	9.53E-05
44	7.59	2.039	0	0	3.48	4.029	0.8638	-6.46	-4.28	-637.67	-567.1	70.6	72.48	72.184	4.52E-03	9.51E-05
45	7.73	2.079	0	0	3.471	4.021	0.8631	-6.61	-4.135	-641.85	-567.1	74.78	76.67	76.665	4.52E-03	9.50E-05
46	7.84	2.109	0	0	3.465	4.016	0.8628	-6.73	-4.023	-645.8	-567.1	78.73	80.63	80.182	4.51E-03	9.48E-05
47	7.99	2.149	0	0	3.46	4.009	0.8631	-6.9	-3.873	-650.52	-567.1	83.45	85.34	84.993	4.50E-03	9.47E-05
48	8.1	2.179	0	0	3.435	4.003	0.858	-7.02	-3.765	-653.86	-567.1	86.79	88.76	88.548	4.49E-03	9.45E-05
49	8.19	2.209	0	0	3.433	3.998	0.8587	-7.12	-3.678	-657.22	-567.1	90.15	92.11	91.476	4.49E-03	9.44E-05
50	8.32	2.249	0	0	3.428	3.991	0.859	-7.26	-3.554	-661.25	-567.1	94.18	96.13	95.754	4.48E-03	9.42E-05
51	8.39	2.279	0	0	3.381	3.985	0.8483	-7.34	-3.489	-664.08	-567.1	97.01	99.12	98.074	4.47E-03	9.41E-05
52	8.46	2.309	0	0	3.374	3.98	0.8477	-7.42	-3.425	-666.12	-567.1	99.05	101.2	100.41	4.47E-03	9.40E-05
53	8.53	2.339	0	0	3.371	3.975	0.8481	-7.5	-3.362	-668.3	-567.1	101.2	103.3	102.76	4.46E-03	9.39E-05
54	8.58	2.369	0	0	3.36	3.969	0.8465	-7.56	-3.317	-669.86	-567.1	102.8	104.9	104.44	4.46E-03	9.37E-05
55	8.64	2.399	0	0	3.355	3.964	0.8463	-7.63	-3.265	-671.95	-567.1	104.9	107	106.47	4.45E-03	9.36E-05
56	8.69	2.429	0	0	3.348	3.959	0.8457	-7.69	-3.222	-673.25	-567.1	106.2	108.3	108.15	4.45E-03	9.35E-05
57	8.75	2.469	0	0	3.344	3.952	0.8462	-7.75	-3.172	-675.33	-567.1	108.3	110.4	110.17	4.44E-03	9.33E-05
58	8.8	2.509	0	0	3.336	3.945	0.8457	-7.81	-3.131	-676.55	-567.1	109.5	111.6	111.84	4.43E-03	9.32E-05
59	8.86	2.549	0	0	3.334	3.938	0.8467	-7.88	-3.082	-679.03	-567.1	112	114.1	113.84	4.42E-03	9.30E-05
60	8.91	2.589	0	0	3.307	3.931	0.8413	-7.94	-3.043	-680.12	-567.1	113.1	115.3	115.49	4.41E-03	9.28E-05
61	8.97	2.639	0	0	3.289	3.922	0.8385	-8	-2.998	-682.84	-567.1	115.8	118	117.45	4.40E-03	9.26E-05
62	9.03	2.699	0	0	3.26	3.912	0.8333	-8.07	-2.954	-684.2	-567.1	117.1	119.5	119.36	4.39E-03	9.24E-05
63	9.08	2.749	0	0	3.253	3.903	0.8334	-8.12	-2.919	-685.35	-567.1	118.3	120.6	120.93	4.38E-03	9.22E-05
64	9.14	2.799	0	0	3.249	3.895	0.8342	-8.19	-2.878	-687.32	-567.1	120.3	122.6	122.78	4.37E-03	9.20E-05
65	9.2	2.859	0	0	3.244	3.885	0.8351	-8.25	-2.839	-689.2	-567.1	122.1	124.4	124.57	4.36E-03	9.17E-05
66	9.26	2.929	0	0	3.24	3.873	0.8366	-8.31	-2.802	-691.55	-567.1	124.5	126.8	126.29	4.35E-03	9.15E-05
67	9.36	3.029	0	0	3.233	3.856	0.8384	-8.4	-2.744	-693.99	-567.1	126.9	129.2	129.01	4.33E-03	9.11E-05
68	9.46	3.149	0	0	3.225	3.836	0.8407	-8.49	-2.692	-696.31	-567.1	129.2	131.5	131.5	4.31E-03	9.06E-05
69	9.56	3.259	0	0	3.184	3.818	0.8339	-8.57	-2.646	-698.33	-567.1	131.3	133.6	133.77	4.29E-03	9.02E-05
70	9.66	3.369	0	0	3.159	3.8	0.8313	-8.64	-2.606	-699.87	-567.1	132.8	135.2	135.79	4.27E-03	8.97E-05
71	9.77	3.489	0	0	3.135	3.781	0.8292	-8.71	-2.568	-701.71	-567.1	134.6	137	137.74	4.25E-03	8.93E-05
72	9.85	3.569	0	0	3.131	3.768	0.831	-8.75	-2.544	-702.56	-567.1	135.5	137.9	138.98	4.23E-03	8.90E-05
73	9.92	3.659	0	0	3.128	3.754	0.8333	-8.78	-2.526	-704.09	-567.1	137	139.4	139.93	4.21E-03	8.86E-05
74	9.97	3.709	0	0	3.125	3.746	0.8343	-8.81	-2.514	-704.72	-567.1	137.7	140	140.56	4.21E-03	8.85E-05
75	10	3.759	0	0	3.111	3.738	0.8323	-8.83	-2.501	-705.97	-567.1	138.9	141.3	141.27	4.20E-03	8.83E-05
76	10.1	3.809	0	0	3.099	3.73	0.8308	-8.85	-2.492	-706.46	-567.1	139.4	141.8	141.8	4.19E-03	8.81E-05
77	10.1	3.859	0	0	3.099	3.722	0.8326	-8.87	-2.483	-707.35	-567.1	140.3	142.6	142.28	4.18E-03	8.79E-05
78	10.2	3.929	0	0	3.068	3.711	0.8266	-8.88	-2.475	-707.59	-567.1	140.5	143	142.71	4.17E-03	8.76E-05
79	10.2	3.983	0	0	3.042	3.703	0.8215	-8.9	-2.469	-708.03	-567.1	141	143.5	143.13	4.16E-03	8.74E-05
80	10.3	4.049	0	0	3.029	3.693	0.8202	-8.91	-2.463	-708.51	-567.1	141.4	144	143.5	4.15E-03	8.72E-05

0.2 Overall fit of CCFC in ECFC/mV

ini-V	ini-LT	ini-MT/M	ini-E	ini-Ip
20	0	0.0001	-567	4.4

2 No. of protonation constants

LogKa:

9.5

6.5

3 No. of ML and M(HL) complexes

Log(I	M	L	H	Refir	RefInd
6.7	1	1	0	1	1

Stand. deviation in Log(beta)

###	COVAR for this log				
9.6	1	2	0	1	1
###	Stand. deviation in Log(beta)				
###	COVAR for this log				
12	1	1	1	1	1
###	Stand. deviation in Log(beta)				
###	COVAR for this log				

7	No. of MOH and ML(OH) complexes				
Log(I	M	L	OH	Refir	RefInd
3.9	1	0	1	0	0
7.7	1	0	2	0	0
10	1	0	3	0	0
12	1	0	4	0	1
5.1	2	0	1	0	1
24	4	0	4	0	0
12	1	2	1	1	0
0.6	Stand. deviation in Log(beta)				
0.4	COVAR for this log				
Temp	I-strer	pKw	SLOI	n-ELECTRONS	
25	0.1	13.78	30	2	
AMA	APOS	ANEG			
4	1	4			
Software indicators					
1	1	1	1	1	1
0					

12. GEP data for Cd-Cy_2EN system

TASK	ZBAR	1	HCH0	COMPL	WITH	Cd(II)								
MODL	Cd+2	HCH0	H	1										
CPLX	0	0	-13.78	H	+1(	-1)								
CPLX	0	0	9.483	HCH0(	1)	H	+1(	1)						
CPLX	0	0	15.94	HCH0(	1)	H	+1(	2)						
CPLX	0	0	-9.88	Cd+2(	1)	H	+1(	-1)						
CPLX	0	0	-19.86	Cd+2(	1)	H	+1(	-2)						
CPLX	0	0	-31.04	Cd+2(	1)	H	+1(	-3)						
CPLX	0	0	-43.12	Cd+2(	1)	H	+1(	-4)						
CPLX	0	0	-8.72	Cd+2(	2)	H	+1(	-1)						
CPLX	0	0	-31.42	Cd+2(	4)	H	+1(	-4)						
CPLX	1	0	12.1	Cd+2(	1)	HCH0(	1)	H	+1(	1)				
CPLX	1	0	6.185	Cd+2(	1)	HCH0(	1)							
CPLX	1	0	9.388	Cd+2(	1)	HCH0(	2)							
CPLX	1	0	-3.776	Cd+2(	1)	HCH0(	1)	H	+1(	-1)				
CPLX	1	0	-15.17	Cd+2(	1)	HCH0(	1)	H	+1(	-2)				
CONC														
VESL	IVOL	15	0	0										
VESL	H + 1	0.01064	0	0										
VESL	Cd+2	0.00195	0	0										
VESL	HCH0	0.00199	0	0										
BUR1	H + 1	-0.01	0	0										
ELEC														
ZERO	H + 1	402.37	0	0										
GRAD	H + 1	58.782	0	0										
DATA														
EMF		PH			ZBAR(H)		POINT		PA			ZBAR(M)		POINT
OBS	OBS	CALC	RESID	OBS	CALC	RESID	RESID	OBS	CALC	RESID	OBS	CALC	RESID	RESID
203.4	3.385	3.388	-0.003	2	2	-0.002	0.004	12.076	12.069	0.007	0	0	0.001	0.007
200.5	3.434	3.436	-0.002	2	2	-0.001	0.002	11.979	11.975	0.004	0	0	0.001	0.004
197.2	3.49	3.49	0	2	2	0	0	11.868	11.869	-0.001	0	0	0	0.001
193.6	3.552	3.551	0.001	2	2	0	0.001	11.748	11.749	-0.002	0	0	0	0.002
189.3	3.625	3.62	0.004	2	2	0.002	0.005	11.603	11.612	-0.009	0	0	-0.001	0.009
184.2	3.712	3.703	0.009	2	2	0.003	0.01	11.431	11.45	-0.019	0	0	-0.002	0.019
178.1	3.815	3.802	0.013	2	2	0.004	0.014	11.225	11.252	-0.027	0	0	-0.002	0.027
170.3	3.948	3.928	0.02	2	2	0.004	0.02	10.962	11.002	-0.04	0	0	-0.002	0.04
159.7	4.128	4.099	0.03	2	1.99	0.004	0.03	10.604	10.664	-0.06	0	0	-0.002	0.06
144.5	4.387	4.345	0.042	1.99	1.99	0.003	0.042	10.091	10.175	-0.084	0	0	-0.002	0.084
125.4	4.712	4.678	0.034	1.98	1.98	0.001	0.034	9.448	9.515	-0.067	0	0	-0.001	0.067
110	4.974	4.976	-0.002	1.95	1.95	0	0.002	8.935	8.931	0.004	0.01	0.01	0	0.004
99.2	5.158	5.179	-0.022	1.92	1.92	0	0.022	8.579	8.536	0.043	0.02	0.02	0.001	0.043
91.3	5.292	5.324	-0.032	1.89	1.89	0	0.032	8.323	8.26	0.063	0.03	0.02	0.003	0.063
85.2	5.396	5.435	-0.039	1.86	1.86	0	0.039	8.129	8.053	0.076	0.03	0.03	0.004	0.076
80.2	5.481	5.524	-0.044	1.82	1.82	0	0.044	7.972	7.887	0.085	0.04	0.04	0.005	0.085
76	5.552	5.6	-0.048	1.79	1.79	0	0.048	7.843	7.75	0.093	0.05	0.05	0.006	0.093
72.4	5.613	5.666	-0.052	1.76	1.76	0	0.052	7.734	7.633	0.101	0.06	0.06	0.007	0.101
69.1	5.67	5.724	-0.054	1.72	1.72	0	0.054	7.636	7.531	0.104	0.08	0.07	0.008	0.105
66.1	5.721	5.777	-0.056	1.69	1.69	0	0.056	7.548	7.441	0.107	0.09	0.08	0.009	0.107
63.3	5.768	5.825	-0.057	1.66	1.66	0	0.057	7.467	7.359	0.108	0.1	0.09	0.01	0.108
60.7	5.812	5.87	-0.057	1.62	1.62	0	0.057	7.394	7.285	0.108	0.11	0.1	0.011	0.109
58.3	5.853	5.912	-0.058	1.59	1.59	0	0.058	7.327	7.217	0.11	0.12	0.11	0.011	0.11

56.1	5.891	5.951	-0.06	1.56	1.56	0	0.06	7.267	7.154	0.113	0.13	0.12	0.012	0.114
53.9	5.928	5.989	-0.061	1.52	1.52	0	0.061	7.208	7.095	0.113	0.14	0.13	0.013	0.114
51.8	5.964	6.025	-0.061	1.49	1.49	0	0.061	7.153	7.04	0.113	0.16	0.14	0.014	0.114
49.7	6	6.059	-0.06	1.46	1.46	0	0.06	7.098	6.987	0.11	0.17	0.15	0.014	0.111
47.8	6.032	6.093	-0.061	1.42	1.42	0	0.061	7.05	6.938	0.112	0.18	0.17	0.014	0.113
45.9	6.064	6.126	-0.061	1.39	1.39	0	0.061	7.002	6.891	0.112	0.19	0.18	0.015	0.113
44	6.097	6.157	-0.061	1.36	1.36	0	0.061	6.956	6.846	0.11	0.21	0.19	0.015	0.111
42.2	6.127	6.188	-0.061	1.32	1.32	0	0.061	6.912	6.802	0.11	0.22	0.2	0.015	0.111
40.4	6.158	6.219	-0.061	1.29	1.29	0	0.061	6.87	6.76	0.109	0.23	0.22	0.016	0.11
38.6	6.188	6.249	-0.061	1.26	1.26	0	0.061	6.828	6.72	0.108	0.24	0.23	0.016	0.109
37.4	6.209	6.279	-0.07	1.22	1.22	0	0.07	6.805	6.681	0.124	0.26	0.24	0.018	0.125
36	6.233	6.309	-0.076	1.19	1.19	0	0.076	6.776	6.643	0.133	0.28	0.26	0.02	0.135
34.4	6.26	6.338	-0.078	1.16	1.16	0	0.078	6.742	6.606	0.136	0.29	0.27	0.02	0.138
32.5	6.292	6.368	-0.075	1.12	1.12	0	0.075	6.7	6.57	0.13	0.3	0.28	0.02	0.132
30.6	6.325	6.397	-0.072	1.09	1.09	0	0.072	6.658	6.534	0.124	0.32	0.3	0.019	0.126
28.6	6.359	6.427	-0.068	1.06	1.06	0	0.068	6.615	6.499	0.116	0.33	0.31	0.018	0.117
26.5	6.394	6.456	-0.062	1.02	1.02	0	0.062	6.569	6.465	0.104	0.34	0.33	0.016	0.106
24.4	6.43	6.486	-0.056	0.99	0.99	0	0.056	6.525	6.431	0.094	0.36	0.34	0.015	0.095
22.3	6.466	6.517	-0.051	0.95	0.95	0	0.051	6.482	6.398	0.084	0.37	0.36	0.013	0.085
20.1	6.503	6.548	-0.044	0.92	0.92	0	0.044	6.437	6.365	0.072	0.38	0.37	0.011	0.073
18	6.539	6.579	-0.04	0.89	0.89	0	0.04	6.396	6.332	0.065	0.4	0.39	0.01	0.065
16.1	6.571	6.611	-0.04	0.85	0.85	0	0.04	6.362	6.299	0.063	0.41	0.4	0.01	0.064
14	6.607	6.644	-0.037	0.82	0.82	0	0.037	6.324	6.266	0.058	0.43	0.42	0.009	0.059
12	6.641	6.677	-0.036	0.79	0.79	0	0.036	6.29	6.234	0.057	0.45	0.44	0.008	0.057
9.9	6.677	6.712	-0.035	0.75	0.75	0	0.035	6.255	6.201	0.054	0.46	0.45	0.008	0.055
7.7	6.714	6.748	-0.034	0.72	0.72	0	0.034	6.219	6.168	0.051	0.48	0.47	0.007	0.051
5.4	6.753	6.785	-0.032	0.69	0.69	0	0.032	6.182	6.134	0.047	0.5	0.49	0.006	0.048
2.8	6.797	6.823	-0.026	0.65	0.65	0	0.026	6.139	6.101	0.038	0.51	0.51	0.005	0.039
0.3	6.84	6.864	-0.024	0.62	0.62	0	0.024	6.101	6.066	0.034	0.53	0.53	0.004	0.035
-2.4	6.886	6.906	-0.02	0.59	0.59	0	0.02	6.06	6.031	0.029	0.55	0.55	0.003	0.029
-5.2	6.934	6.951	-0.017	0.55	0.55	0	0.017	6.02	5.996	0.024	0.57	0.57	0.003	0.024
-8.2	6.985	6.998	-0.014	0.52	0.52	0	0.014	5.978	5.959	0.019	0.59	0.59	0.002	0.019
-11.3	7.037	7.049	-0.011	0.49	0.49	0	0.011	5.936	5.921	0.015	0.61	0.61	0.002	0.015
-14.7	7.095	7.103	-0.008	0.45	0.45	0	0.008	5.892	5.882	0.01	0.63	0.63	0.001	0.01
-18.4	7.158	7.161	-0.003	0.42	0.42	0	0.003	5.845	5.841	0.004	0.65	0.65	0	0.004
-22.4	7.226	7.225	0.002	0.39	0.39	0	0.002	5.796	5.798	-0.002	0.68	0.68	0	0.002
-26.7	7.299	7.294	0.005	0.35	0.35	0	0.005	5.746	5.752	-0.006	0.7	0.7	0	0.006
-31.5	7.381	7.371	0.01	0.32	0.32	0	0.01	5.692	5.704	-0.012	0.73	0.73	-0.001	0.012
-36.7	7.469	7.457	0.013	0.29	0.29	0	0.013	5.637	5.652	-0.015	0.75	0.75	-0.001	0.015
-42.5	7.568	7.553	0.015	0.25	0.25	0	0.015	5.579	5.596	-0.017	0.78	0.78	-0.001	0.017
-49	7.679	7.663	0.016	0.22	0.22	0	0.016	5.518	5.536	-0.017	0.81	0.81	-0.001	0.017
-56.3	7.803	7.789	0.014	0.19	0.19	0	0.014	5.455	5.471	-0.016	0.84	0.84	0	0.016
-64.4	7.941	7.933	0.008	0.15	0.15	0	0.008	5.394	5.402	-0.009	0.87	0.87	0	0.009
-73.8	8.101	8.096	0.005	0.12	0.12	0	0.005	5.332	5.337	-0.005	0.9	0.9	0	0.005
-83.7	8.269	8.275	-0.006	0.09	0.09	0	0.006	5.295	5.289	0.006	0.93	0.93	0	0.006
-94.2	8.448	8.458	-0.01	0.06	0.06	0	0.01	5.309	5.298	0.011	0.96	0.96	0	0.011
-104.9	8.63	8.631	-0.001	0.03	0.03	0	0.001	5.474	5.473	0.002	0.99	0.99	0	0.002
-115	8.802	8.785	0.017	0	-0.01	0	0.017	0	0	0	0	0	0	0
-123.9	8.953	8.918	0.035	-0.03	-0.03	0.001	0.035	0	0	0	0	0	0	0
-131.7	9.086	9.032	0.054	-0.06	-0.06	0.002	0.054	0	0	0	0	0	0	0
-138.2	9.196	9.13	0.066	-0.09	-0.09	0.004	0.066	0	0	0	0	0	0	0
-143.6	9.288	9.216	0.072	-0.12	-0.12	0.005	0.072	0	0	0	0	0	0	0
-147.9	9.361	9.293	0.068	-0.14	-0.15	0.006	0.069	0	0	0	0	0	0	0
-151.2	9.417	9.362	0.055	-0.17	-0.18	0.005	0.056	0	0	0	0	0	0	0

-154	9.465	9.425	0.04	-0.2	-0.2	0.005	0.041	0	0	0	0	0	0	0
-156.7	9.511	9.482	0.029	-0.23	-0.23	0.004	0.029	0	0	0	0	0	0	0
-159.1	9.552	9.536	0.016	-0.25	-0.26	0.002	0.016	0	0	0	0	0	0	0
-161.6	9.594	9.585	0.009	-0.28	-0.28	0.001	0.009	0	0	0	0	0	0	0
-164.1	9.637	9.632	0.005	-0.31	-0.31	0.001	0.005	0	0	0	0	0	0	0
-166.5	9.678	9.676	0.002	-0.33	-0.33	0	0.002	0	0	0	0	0	0	0
-168.8	9.717	9.718	-0.001	-0.36	-0.36	0	0.001	0	0	0	0	0	0	0
-171.1	9.756	9.757	-0.002	-0.38	-0.38	0	0.002	0	0	0	0	0	0	0
-173.3	9.793	9.795	-0.002	-0.41	-0.41	-0.001	0.002	0	0	0	0	0	0	0
-175.4	9.829	9.832	-0.003	-0.43	-0.43	-0.001	0.003	0	0	0	0	0	0	0
-177.4	9.863	9.867	-0.004	-0.45	-0.45	-0.001	0.004	0	0	0	0	0	0	0
-179.4	9.897	9.9	-0.003	-0.47	-0.47	-0.001	0.003	0	0	0	0	0	0	0
-181.3	9.929	9.932	-0.003	-0.5	-0.5	-0.001	0.003	0	0	0	0	0	0	0
-183.1	9.96	9.964	-0.004	-0.52	-0.52	-0.001	0.004	0	0	0	0	0	0	0
-184.9	9.991	9.994	-0.003	-0.54	-0.54	-0.001	0.003	0	0	0	0	0	0	0

13. GEP data for Pb-Cy_2EN system

```
TASK    ZBAR        1 HCH0  COMP WITH  Pb(II)
MODL    PB+2   HCH0  H            1
CPLX         0       0 -13.78 H       +1(    -1)
CPLX         0       0  9.483 HCH0( 1)      H         +1(      1)
CPLX         0       0  15.94 HCH0( 1)      H         +1(      2)
CPLX         0       0  -7.88 PB+2( 1)      H         +1(     -1)
CPLX         0       0 -16.66 PB+2( 1)      H         +1(     -2)
CPLX         0       0 -27.44 PB+2( 1)      H         +1(     -3)
CPLX         0       0  -6.18 PB+2( 2)      H         +1(     -1)
CPLX         0       0 -20.52 PB+2( 4)      H         +1(     -4)
CPLX         0       0 -23.02 PB+2( 3)      H         +1(     -4)
CPLX         0       0 -43.34 PB+2( 6)      H         +1(     -8)
CPLX         1       0  12.08 PB+2( 1)      HCH0(    1)      H         +1(      1)
CPLX         1       0   6.78 PB+2( 1)      HCH0(    1)
CPLX         1       0 -0.895 PB+2( 1)      HCH0(    1)      H         +1(     -1)
CPLX         1       0  -10.6 PB+2( 1)      HCH0(    1)      H         +1(     -2)
CONC
VESL    IVOL        15       0       0
VESL    H + 1    0.011       0       0
VESL    PB+2     0.002       0       0
VESL    HCH0     0.002       0       0
BUR1    H + 1    -0.01       0       0
ELEC
ZERO    H + 1    403.4       0       0
GRAD    H + 1    58.51       0       0
DATA
EMF            PH                    ZBAR(H)        POINT           PA                    ZBAR(M)        POINT
OBS     OBS    CALC   RESID OBS    CALC   RESID    RESID  OBS      CALC    RESID   OBS     CALC    RESID    RESID

  187.4  3.692  3.686  0.006     2      2   0.002    0.007   11.466  11.479  -0.013     0       0   -0.001    0.013
  181.6  3.791  3.782  0.009     2      2   0.003     0.01   11.269  11.289  -0.019     0       0   -0.001    0.019
  174.4  3.915  3.903  0.012     2      2   0.003    0.012   11.026   11.05  -0.024     0       0   -0.001    0.024
    165  4.075  4.063  0.012     2   1.99   0.002    0.012   10.707  10.732  -0.025     0       0   -0.001    0.025
  151.8  4.301   4.29  0.011  1.99   1.99   0.001    0.011   10.259  10.282  -0.022     0       0   -0.001    0.022
  134.5  4.597  4.595  0.002  1.98   1.98       0    0.002    9.674   9.677  -0.004     0       0        0    0.004
  118.7  4.867  4.872 -0.005  1.95   1.95       0    0.005    9.143   9.133    0.01    0.01    0.01        0     0.01
  107.7  5.055  5.058 -0.003  1.92   1.92       0    0.003    8.778   8.772   0.007    0.02    0.02        0    0.007
   99.9  5.188  5.186  0.002  1.89   1.89       0    0.002    8.524   8.527  -0.003    0.03    0.03        0    0.003
   94.2  5.285  5.283  0.003  1.86   1.86       0    0.003    8.341   8.346  -0.005    0.04    0.04        0    0.005
   89.6  5.364   5.36  0.004  1.83   1.83       0    0.004    8.196   8.204  -0.008    0.05    0.05        0    0.008
   85.7  5.431  5.424  0.006   1.8    1.8       0    0.006    8.075   8.087  -0.012    0.06    0.06   -0.001    0.012
   82.4  5.487   5.48  0.007  1.76   1.76       0    0.007    7.974   7.988  -0.013    0.07    0.07   -0.001    0.013
   79.5  5.537  5.529  0.007  1.73   1.73       0    0.007    7.888   7.902  -0.014    0.09    0.09   -0.001    0.014
   76.8  5.583  5.574  0.009   1.7    1.7       0    0.009    7.808   7.825  -0.017     0.1     0.1   -0.001    0.017
   74.4  5.624  5.615  0.009  1.66   1.66       0    0.009    7.739   7.757  -0.018    0.11    0.11   -0.001    0.018
   72.2  5.661  5.652  0.009  1.63   1.63       0    0.009    7.677   7.694  -0.017    0.12    0.13   -0.001    0.017
   70.1  5.697  5.688   0.01   1.6    1.6       0     0.01    7.619   7.637  -0.018    0.14    0.14   -0.001    0.018
   68.1  5.731  5.721   0.01  1.56   1.56       0     0.01    7.564   7.584   -0.02    0.15    0.15   -0.001     0.02
   66.2  5.764  5.753  0.011  1.53   1.53       0    0.011    7.513   7.534  -0.021    0.16    0.17   -0.002    0.021
   64.4  5.795  5.783  0.012   1.5    1.5       0    0.012    7.465   7.488  -0.022    0.18    0.18   -0.002    0.022
   62.7  5.824  5.812  0.011  1.46   1.46       0    0.011    7.422   7.444  -0.022    0.19    0.19   -0.002    0.022
     61  5.853   5.84  0.012  1.43   1.43       0    0.012    7.378   7.402  -0.023    0.21    0.21   -0.002    0.023
```

59.4	5.88	5.868	0.012	1.4	1.4	0	0.012	7.339	7.362	-0.023	0.22	0.22	-0.002	0.023
57.8	5.908	5.895	0.013	1.36	1.36	0	0.013	7.299	7.324	-0.024	0.23	0.24	-0.002	0.025
56.3	5.933	5.921	0.013	1.33	1.33	0	0.013	7.264	7.287	-0.023	0.25	0.25	-0.002	0.024
54.7	5.961	5.946	0.014	1.3	1.3	0	0.014	7.225	7.252	-0.027	0.26	0.26	-0.003	0.027
53.2	5.986	5.971	0.015	1.26	1.26	0	0.015	7.19	7.218	-0.027	0.28	0.28	-0.003	0.028
51.8	6.01	5.996	0.014	1.23	1.23	0	0.014	7.159	7.185	-0.026	0.29	0.29	-0.003	0.026
50.3	6.036	6.021	0.015	1.2	1.2	0	0.015	7.125	7.153	-0.027	0.31	0.31	-0.003	0.027
48.9	6.06	6.045	0.014	1.16	1.16	0	0.014	7.095	7.122	-0.026	0.32	0.32	-0.003	0.026
47.4	6.085	6.07	0.016	1.13	1.13	0	0.016	7.063	7.091	-0.029	0.34	0.34	-0.003	0.029
46	6.109	6.094	0.015	1.1	1.1	0	0.015	7.034	7.062	-0.028	0.35	0.35	-0.003	0.028
44.5	6.135	6.118	0.017	1.06	1.06	0	0.017	7.002	7.033	-0.031	0.37	0.37	-0.003	0.031
43.1	6.159	6.142	0.017	1.03	1.03	0	0.017	6.974	7.004	-0.03	0.38	0.38	-0.003	0.03
41.7	6.183	6.166	0.016	1	1	0	0.016	6.947	6.976	-0.029	0.4	0.4	-0.003	0.029
40.2	6.208	6.191	0.017	0.96	0.96	0	0.017	6.918	6.949	-0.031	0.41	0.41	-0.003	0.031
38.8	6.232	6.215	0.017	0.93	0.93	0	0.017	6.892	6.922	-0.03	0.43	0.43	-0.003	0.03
37.3	6.258	6.24	0.018	0.9	0.9	0	0.018	6.864	6.895	-0.031	0.44	0.45	-0.003	0.031
35.9	6.282	6.265	0.017	0.86	0.86	0	0.017	6.84	6.869	-0.029	0.46	0.46	-0.003	0.029
34.4	6.307	6.291	0.017	0.83	0.83	0	0.017	6.814	6.843	-0.03	0.48	0.48	-0.003	0.03
32.8	6.335	6.316	0.019	0.8	0.8	0	0.019	6.786	6.818	-0.032	0.49	0.49	-0.003	0.032
31.3	6.36	6.342	0.018	0.77	0.77	0	0.018	6.762	6.793	-0.031	0.51	0.51	-0.003	0.031
29.7	6.388	6.369	0.019	0.73	0.73	0	0.019	6.736	6.768	-0.032	0.52	0.53	-0.003	0.033
28.1	6.415	6.396	0.019	0.7	0.7	0	0.019	6.711	6.744	-0.033	0.54	0.55	-0.003	0.033
26.5	6.443	6.423	0.019	0.67	0.67	0	0.019	6.688	6.72	-0.032	0.56	0.56	-0.003	0.032
24.9	6.47	6.452	0.018	0.63	0.63	0	0.018	6.666	6.697	-0.03	0.58	0.58	-0.003	0.031
23.2	6.499	6.481	0.018	0.6	0.6	0	0.018	6.643	6.674	-0.03	0.59	0.6	-0.003	0.031
21.4	6.53	6.51	0.02	0.57	0.57	0	0.02	6.619	6.651	-0.032	0.61	0.62	-0.003	0.032
19.7	6.559	6.541	0.018	0.53	0.53	0	0.018	6.6	6.629	-0.029	0.63	0.63	-0.003	0.03
17.9	6.59	6.572	0.018	0.5	0.5	0	0.018	6.58	6.608	-0.028	0.65	0.65	-0.002	0.029
16	6.622	6.604	0.018	0.47	0.47	0	0.018	6.56	6.589	-0.029	0.67	0.67	-0.002	0.029
14.1	6.654	6.637	0.017	0.43	0.43	0	0.017	6.543	6.57	-0.027	0.69	0.69	-0.002	0.027
12.1	6.689	6.671	0.018	0.4	0.4	0	0.018	6.526	6.553	-0.027	0.71	0.71	-0.002	0.027
10.2	6.721	6.706	0.015	0.37	0.37	0	0.015	6.516	6.538	-0.023	0.73	0.73	-0.002	0.023
8.6	6.748	6.742	0.006	0.33	0.33	0	0.006	6.517	6.526	-0.009	0.75	0.75	-0.001	0.009
7.2	6.772	6.78	-0.007	0.3	0.3	0	0.007	6.529	6.518	0.011	0.77	0.77	0.001	0.011
5.5	6.801	6.818	-0.016	0.27	0.27	0	0.016	6.538	6.514	0.024	0.8	0.8	0.001	0.024
3.6	6.834	6.857	-0.023	0.23	0.23	0	0.023	6.55	6.517	0.034	0.82	0.82	0.002	0.034
1.5	6.87	6.898	-0.028	0.2	0.2	0	0.028	6.567	6.527	0.04	0.84	0.84	0.002	0.04
-0.6	6.906	6.939	-0.033	0.17	0.17	0	0.033	6.597	6.55	0.046	0.87	0.87	0.002	0.046
-2.8	6.943	6.98	-0.037	0.13	0.13	0	0.037	6.643	6.591	0.052	0.89	0.89	0.001	0.052
-5.1	6.983	7.023	-0.04	0.1	0.1	0	0.04	6.715	6.66	0.055	0.92	0.92	0.001	0.055
-7.5	7.024	7.066	-0.042	0.07	0.07	0	0.042	6.839	6.782	0.057	0.95	0.95	0.001	0.057
-9.9	7.065	7.109	-0.045	0.03	0.03	0	0.045	7.091	7.032	0.059	0.97	0.97	0	0.059
-12.4	7.107	7.153	-0.045	0	0	0	0.045	0	0	0	0	0	0	0
-14.9	7.15	7.196	-0.046	-0.03	-0.03	0	0.046	0	0	0	0	0	0	0
-17.5	7.195	7.24	-0.045	-0.07	-0.07	0	0.045	0	0	0	0	0	0	0
-20.1	7.239	7.283	-0.044	-0.1	-0.1	0	0.044	0	0	0	0	0	0	0
-22.8	7.285	7.327	-0.041	-0.13	-0.13	0	0.041	0	0	0	0	0	0	0
-25.6	7.333	7.37	-0.037	-0.17	-0.17	0	0.037	0	0	0	0	0	0	0
-28.4	7.381	7.413	-0.032	-0.2	-0.2	0	0.032	0	0	0	0	0	0	0
-31.2	7.429	7.456	-0.027	-0.23	-0.23	0	0.027	0	0	0	0	0	0	0
-34.1	7.478	7.499	-0.02	-0.27	-0.27	0	0.02	0	0	0	0	0	0	0
-37.1	7.53	7.541	-0.012	-0.3	-0.3	0	0.012	0	0	0	0	0	0	0
-40.1	7.581	7.585	-0.004	-0.33	-0.33	0	0.004	0	0	0	0	0	0	0
-43.2	7.634	7.628	0.006	-0.37	-0.37	0	0.006	0	0	0	0	0	0	0

14. GEP data for Cu-Cy_2EN system

TASK	ZBAR	1	HCH0	COMPL	WITH	Cu(II)								
MODL	CU+2	HCH0	H	1										
CPLX	0	0	-13.78	H	+1(	-1)								
CPLX	0	0	9.483	HCH0(	1)	H	+1(	1)						
CPLX	0	0	15.94	HCH0(	1)	H	+1(	2)						
CPLX	0	0	-7.68	CU+2(	1)	H	+1(	-1)						
CPLX	0	0	-6.08	CU+2(	2)	H	+1(	-1)						
CPLX	0	0	-10.76	CU+2(	2)	H	+1(	-2)						
CPLX	0	0	-21.42	CU+2(	3)	H	+1(	-4)						
CPLX	1	0	14.19	CU+2(	1)	HCH0(	1)	H	+1(	1)				
CPLX	1	0	11.29	CU+2(	1)	HCH0(	1)							
CPLX	1	0	4.395	CU+2(	1)	HCH0(	1)	H	+1(	-1)				
CPLX	1	0	-4.326	CU+2(	1)	HCH0(	1)	H	+1(	-2)				
CONC														
VESL	IVOL	15	0	0										
VESL	H	0.0105	0	0										
VESL	CU+2	0.002	0	0										
VESL	HCH0	0.002	0	0										
BUR1	H + 1	-0.01	0	0										
ELEC														
ZERO	H + 1	403.82	0	0										
GRAD	H + 1	58.885	0	0										
DATA														
EMF		PH			ZBAR(H)		POINT		PA			ZBAR(M)		POINT
OBS	OBS	CALC	RESID	OBS	CALC	RESID	RESID	OBS	CALC	RESID	OBS	CALC	RESID	RESID
251.4	2.588	2.611	-0.022	1.89	1.98	-0.085	0.088	13.611	13.547	0.063	0.05	0.01	0.043	0.076
250.7	2.6	2.621	-0.021	1.9	1.98	-0.08	0.082	13.588	13.528	0.06	0.05	0.01	0.04	0.072
250.1	2.611	2.632	-0.022	1.9	1.98	-0.081	0.084	13.57	13.508	0.062	0.05	0.01	0.041	0.074
249.4	2.622	2.644	-0.021	1.9	1.98	-0.077	0.08	13.548	13.488	0.06	0.05	0.01	0.038	0.071
248.7	2.634	2.655	-0.021	1.9	1.98	-0.073	0.076	13.526	13.468	0.058	0.05	0.01	0.037	0.068
248.1	2.644	2.666	-0.022	1.9	1.97	-0.077	0.08	13.508	13.447	0.061	0.05	0.01	0.038	0.072
247.4	2.656	2.678	-0.022	1.9	1.97	-0.074	0.077	13.486	13.426	0.06	0.05	0.01	0.037	0.071
246.7	2.668	2.69	-0.022	1.9	1.97	-0.073	0.076	13.464	13.404	0.06	0.05	0.01	0.036	0.07
245.9	2.682	2.702	-0.02	1.91	1.97	-0.066	0.069	13.438	13.383	0.056	0.05	0.01	0.033	0.065
245.2	2.694	2.714	-0.021	1.9	1.97	-0.066	0.069	13.417	13.36	0.056	0.05	0.01	0.033	0.065
244.7	2.702	2.727	-0.025	1.89	1.97	-0.077	0.081	13.405	13.338	0.067	0.05	0.02	0.039	0.077
243.9	2.716	2.74	-0.024	1.9	1.97	-0.073	0.076	13.379	13.314	0.064	0.05	0.02	0.036	0.074
243.2	2.728	2.753	-0.025	1.89	1.97	-0.074	0.078	13.358	13.291	0.067	0.05	0.02	0.037	0.076
242.4	2.741	2.766	-0.025	1.89	1.97	-0.071	0.075	13.332	13.267	0.065	0.05	0.02	0.036	0.074
241.6	2.755	2.779	-0.025	1.9	1.96	-0.069	0.073	13.307	13.242	0.064	0.05	0.02	0.034	0.073
240.8	2.768	2.793	-0.025	1.89	1.96	-0.067	0.072	13.282	13.217	0.064	0.05	0.02	0.034	0.073
239.9	2.784	2.807	-0.023	1.9	1.96	-0.062	0.066	13.252	13.192	0.061	0.05	0.02	0.031	0.068
239.1	2.797	2.821	-0.024	1.9	1.96	-0.062	0.066	13.228	13.166	0.062	0.05	0.02	0.031	0.069
238.2	2.813	2.836	-0.023	1.9	1.96	-0.058	0.063	13.199	13.139	0.06	0.05	0.02	0.029	0.066
237.3	2.828	2.851	-0.023	1.9	1.95	-0.056	0.06	13.17	13.112	0.058	0.05	0.02	0.028	0.064
236.4	2.843	2.866	-0.023	1.9	1.95	-0.054	0.058	13.141	13.084	0.057	0.05	0.02	0.027	0.063
235.5	2.858	2.881	-0.023	1.9	1.95	-0.052	0.057	13.113	13.055	0.058	0.05	0.03	0.026	0.063
234.5	2.875	2.897	-0.022	1.9	1.95	-0.048	0.053	13.081	13.026	0.054	0.05	0.03	0.024	0.059
233.6	2.891	2.913	-0.023	1.9	1.94	-0.048	0.053	13.053	12.997	0.056	0.05	0.03	0.024	0.061
232.6	2.908	2.93	-0.022	1.9	1.94	-0.046	0.051	13.021	12.966	0.055	0.05	0.03	0.023	0.059
231.6	2.925	2.947	-0.022	1.89	1.94	-0.044	0.049	12.989	12.935	0.054	0.05	0.03	0.022	0.058

230.6	2.942	2.964	-0.022	1.89	1.93	-0.043	0.048	12.958	12.904	0.054	0.05	0.03	0.021	0.058
229.5	2.96	2.981	-0.021	1.89	1.93	-0.039	0.045	12.923	12.871	0.051	0.05	0.04	0.02	0.055
228.4	2.979	2.999	-0.02	1.89	1.93	-0.037	0.042	12.888	12.838	0.049	0.06	0.04	0.018	0.053
227.3	2.998	3.018	-0.02	1.89	1.92	-0.035	0.04	12.853	12.805	0.048	0.06	0.04	0.017	0.051
226.2	3.016	3.037	-0.02	1.88	1.92	-0.033	0.039	12.818	12.77	0.048	0.06	0.04	0.017	0.051
225.1	3.035	3.056	-0.021	1.88	1.91	-0.033	0.039	12.784	12.735	0.049	0.06	0.05	0.016	0.051
223.9	3.055	3.075	-0.02	1.87	1.9	-0.03	0.036	12.746	12.7	0.046	0.06	0.05	0.015	0.049
222.7	3.076	3.095	-0.019	1.87	1.9	-0.028	0.034	12.708	12.663	0.045	0.07	0.05	0.014	0.047
221.5	3.096	3.115	-0.019	1.86	1.89	-0.027	0.033	12.671	12.627	0.044	0.07	0.06	0.013	0.046
220.3	3.117	3.136	-0.019	1.86	1.88	-0.026	0.032	12.633	12.589	0.044	0.07	0.06	0.013	0.046
219	3.139	3.156	-0.018	1.85	1.87	-0.023	0.029	12.592	12.552	0.041	0.07	0.06	0.011	0.042
217.8	3.159	3.177	-0.018	1.84	1.86	-0.023	0.029	12.556	12.514	0.042	0.08	0.07	0.011	0.043
216.5	3.181	3.199	-0.017	1.83	1.85	-0.021	0.027	12.515	12.476	0.04	0.08	0.07	0.01	0.041
215.2	3.203	3.22	-0.017	1.82	1.84	-0.019	0.025	12.475	12.437	0.038	0.09	0.08	0.009	0.039
213.9	3.225	3.242	-0.016	1.81	1.83	-0.017	0.024	12.435	12.399	0.037	0.09	0.08	0.009	0.038
212.6	3.247	3.263	-0.016	1.8	1.82	-0.016	0.023	12.396	12.36	0.036	0.1	0.09	0.008	0.037
211.3	3.269	3.285	-0.016	1.79	1.8	-0.015	0.022	12.356	12.321	0.035	0.11	0.1	0.008	0.036
210	3.292	3.307	-0.015	1.78	1.79	-0.014	0.021	12.317	12.283	0.034	0.11	0.1	0.007	0.035
208.7	3.314	3.328	-0.015	1.76	1.77	-0.013	0.02	12.278	12.245	0.033	0.12	0.11	0.007	0.034
207.4	3.336	3.35	-0.015	1.75	1.76	-0.012	0.019	12.24	12.207	0.032	0.13	0.12	0.006	0.033
206.1	3.358	3.372	-0.014	1.73	1.74	-0.011	0.018	12.201	12.17	0.031	0.13	0.13	0.006	0.031
204.9	3.378	3.393	-0.015	1.71	1.72	-0.012	0.019	12.167	12.133	0.033	0.14	0.14	0.006	0.034
203.6	3.4	3.415	-0.014	1.7	1.71	-0.011	0.018	12.129	12.097	0.032	0.15	0.15	0.005	0.032
202.4	3.421	3.436	-0.015	1.68	1.69	-0.011	0.019	12.095	12.061	0.033	0.16	0.16	0.005	0.034
201.1	3.443	3.457	-0.014	1.66	1.67	-0.01	0.017	12.057	12.026	0.031	0.17	0.17	0.005	0.031
199.9	3.463	3.478	-0.015	1.64	1.65	-0.01	0.018	12.024	11.992	0.032	0.18	0.18	0.005	0.032
198.6	3.485	3.498	-0.013	1.62	1.63	-0.008	0.016	11.986	11.958	0.029	0.19	0.19	0.004	0.029
197.4	3.505	3.519	-0.013	1.6	1.6	-0.008	0.016	11.953	11.924	0.029	0.2	0.2	0.004	0.029
196.2	3.526	3.539	-0.013	1.57	1.58	-0.008	0.015	11.92	11.892	0.029	0.21	0.21	0.004	0.029
195.1	3.545	3.559	-0.015	1.55	1.56	-0.008	0.017	11.891	11.859	0.032	0.22	0.22	0.004	0.032
193.9	3.565	3.579	-0.014	1.53	1.53	-0.008	0.016	11.859	11.828	0.031	0.24	0.23	0.004	0.031
192.7	3.585	3.599	-0.014	1.5	1.51	-0.007	0.015	11.826	11.797	0.029	0.25	0.24	0.003	0.029
191.6	3.604	3.619	-0.015	1.48	1.49	-0.007	0.016	11.798	11.766	0.031	0.26	0.26	0.004	0.031
190.4	3.624	3.638	-0.014	1.46	1.46	-0.006	0.015	11.766	11.736	0.029	0.27	0.27	0.003	0.03
189.3	3.643	3.657	-0.014	1.43	1.44	-0.006	0.016	11.738	11.707	0.031	0.28	0.28	0.003	0.031
188.2	3.662	3.677	-0.015	1.4	1.41	-0.006	0.016	11.71	11.678	0.032	0.3	0.29	0.003	0.032
187	3.682	3.696	-0.014	1.38	1.39	-0.006	0.015	11.679	11.649	0.03	0.31	0.31	0.003	0.03
185.9	3.701	3.715	-0.014	1.35	1.36	-0.006	0.015	11.651	11.621	0.03	0.32	0.32	0.003	0.031
184.8	3.719	3.734	-0.015	1.33	1.33	-0.006	0.016	11.624	11.593	0.031	0.34	0.33	0.003	0.031
183.7	3.738	3.753	-0.015	1.3	1.31	-0.006	0.016	11.597	11.565	0.032	0.35	0.35	0.003	0.032
182.5	3.759	3.772	-0.014	1.27	1.28	-0.005	0.015	11.567	11.538	0.029	0.36	0.36	0.002	0.029
181.4	3.777	3.791	-0.014	1.25	1.25	-0.005	0.015	11.54	11.511	0.03	0.38	0.37	0.002	0.03
180.3	3.796	3.81	-0.014	1.22	1.22	-0.005	0.015	11.514	11.484	0.031	0.39	0.39	0.002	0.031
179.2	3.815	3.829	-0.015	1.19	1.2	-0.005	0.016	11.489	11.457	0.031	0.4	0.4	0.002	0.032
178	3.835	3.849	-0.014	1.16	1.17	-0.004	0.014	11.46	11.431	0.029	0.42	0.41	0.002	0.029
176.9	3.854	3.868	-0.014	1.14	1.14	-0.004	0.015	11.434	11.404	0.03	0.43	0.43	0.002	0.03
175.7	3.874	3.887	-0.013	1.11	1.11	-0.004	0.014	11.406	11.378	0.028	0.44	0.44	0.002	0.028
174.6	3.893	3.907	-0.014	1.08	1.08	-0.004	0.015	11.382	11.352	0.03	0.46	0.46	0.002	0.03
173.4	3.913	3.926	-0.013	1.05	1.06	-0.003	0.014	11.354	11.326	0.028	0.47	0.47	0.002	0.028
172.2	3.933	3.946	-0.013	1.02	1.03	-0.003	0.013	11.327	11.299	0.027	0.49	0.49	0.002	0.027
171	3.954	3.966	-0.013	1	1	-0.003	0.013	11.3	11.273	0.026	0.5	0.5	0.001	0.027
169.8	3.974	3.987	-0.013	0.97	0.97	-0.003	0.013	11.273	11.247	0.026	0.52	0.51	0.001	0.026
168.6	3.995	4.007	-0.013	0.94	0.94	-0.003	0.013	11.247	11.221	0.027	0.53	0.53	0.001	0.027
167.4	4.015	4.028	-0.013	0.91	0.91	-0.003	0.014	11.222	11.194	0.028	0.54	0.54	0.001	0.028

166.1	4.037	4.049	-0.012	0.88	0.88	-0.002	0.013	11.193	11.167	0.026	0.56	0.56	0.001	0.026
164.8	4.059	4.071	-0.012	0.85	0.85	-0.002	0.012	11.165	11.14	0.025	0.57	0.57	0.001	0.025
163.5	4.081	4.093	-0.012	0.82	0.82	-0.002	0.012	11.138	11.113	0.025	0.59	0.59	0.001	0.025
162.1	4.105	4.116	-0.011	0.79	0.79	-0.002	0.011	11.108	11.086	0.022	0.6	0.6	0.001	0.022
160.8	4.127	4.139	-0.011	0.76	0.76	-0.002	0.012	11.082	11.058	0.024	0.62	0.62	0.001	0.024
159.4	4.151	4.162	-0.011	0.73	0.73	-0.002	0.011	11.053	11.03	0.024	0.63	0.63	0.001	0.024
157.9	4.176	4.186	-0.01	0.7	0.7	-0.001	0.01	11.022	11.001	0.021	0.65	0.65	0.001	0.021
156.5	4.2	4.211	-0.011	0.67	0.67	-0.002	0.011	10.994	10.971	0.023	0.66	0.66	0.001	0.023
154.9	4.227	4.237	-0.009	0.64	0.64	-0.001	0.01	10.961	10.941	0.02	0.68	0.68	0.001	0.02
153.3	4.254	4.263	-0.009	0.61	0.62	-0.001	0.009	10.929	10.911	0.018	0.69	0.69	0.001	0.018
151.7	4.282	4.291	-0.009	0.58	0.58	-0.001	0.009	10.898	10.879	0.019	0.71	0.71	0.001	0.019
150	4.31	4.319	-0.009	0.55	0.55	-0.001	0.009	10.865	10.847	0.018	0.72	0.72	0	0.018
148.2	4.341	4.349	-0.008	0.52	0.52	-0.001	0.008	10.829	10.813	0.016	0.74	0.74	0	0.016
146.3	4.373	4.38	-0.006	0.49	0.49	-0.001	0.007	10.792	10.779	0.013	0.75	0.75	0	0.013
144.4	4.406	4.412	-0.007	0.46	0.46	-0.001	0.007	10.757	10.743	0.014	0.77	0.77	0	0.014
142.3	4.441	4.447	-0.005	0.43	0.43	0	0.005	10.716	10.705	0.011	0.78	0.78	0	0.011
140.2	4.477	4.483	-0.006	0.4	0.4	0	0.006	10.678	10.666	0.012	0.8	0.8	0	0.012
137.8	4.518	4.521	-0.004	0.37	0.37	0	0.004	10.632	10.625	0.007	0.81	0.81	0	0.007
135.4	4.558	4.562	-0.004	0.34	0.34	0	0.004	10.589	10.581	0.008	0.83	0.83	0	0.008
132.7	4.604	4.607	-0.002	0.31	0.31	0	0.002	10.54	10.535	0.005	0.84	0.84	0	0.005
129.8	4.653	4.655	-0.001	0.28	0.28	0	0.001	10.488	10.485	0.003	0.86	0.86	0	0.003
126.6	4.708	4.707	0.001	0.25	0.25	0	0.001	10.431	10.432	-0.001	0.87	0.87	0	0.001
123	4.769	4.765	0.004	0.22	0.22	0	0.004	10.367	10.375	-0.007	0.89	0.89	0	0.007
119	4.837	4.83	0.006	0.19	0.19	0	0.006	10.299	10.312	-0.013	0.9	0.9	0	0.013
114.4	4.915	4.904	0.011	0.16	0.16	0	0.011	10.221	10.244	-0.022	0.92	0.92	0	0.022
109	5.007	4.99	0.017	0.13	0.13	0	0.017	10.134	10.17	-0.035	0.93	0.93	0	0.035
102.3	5.12	5.09	0.031	0.1	0.1	0.001	0.031	10.03	10.093	-0.063	0.95	0.95	0	0.063
94.1	5.26	5.21	0.05	0.07	0.07	0.001	0.05	9.923	10.026	-0.104	0.97	0.97	0	0.104
83.8	5.435	5.353	0.082	0.04	0.03	0.001	0.082	9.857	10.028	-0.171	0.98	0.98	-0.001	0.171
72.9	5.62	5.517	0.103	0	0	0.001	0.103	10.515	10.81	-0.295	1	1	0	0.295
62.7	5.793	5.687	0.106	-0.03	-0.03	0	0.106	0	0	0	0	0	0	0
54.2	5.937	5.845	0.092	-0.06	-0.06	0	0.092	0	0	0	0	0	0	0
47	6.06	5.982	0.077	-0.09	-0.09	0	0.077	0	0	0	0	0	0	0
40.8	6.165	6.1	0.065	-0.13	-0.13	0	0.065	0	0	0	0	0	0	0
35.5	6.255	6.201	0.054	-0.16	-0.16	0	0.054	0	0	0	0	0	0	0
30.7	6.336	6.291	0.046	-0.19	-0.19	0	0.046	0	0	0	0	0	0	0
26.3	6.411	6.371	0.04	-0.23	-0.23	0	0.04	0	0	0	0	0	0	0
22.3	6.479	6.445	0.034	-0.26	-0.26	0	0.034	0	0	0	0	0	0	0
18.5	6.544	6.514	0.03	-0.29	-0.29	0	0.03	0	0	0	0	0	0	0
15	6.603	6.578	0.025	-0.33	-0.33	0	0.025	0	0	0	0	0	0	0
11.6	6.661	6.639	0.022	-0.36	-0.36	0	0.022	0	0	0	0	0	0	0
8.3	6.717	6.698	0.019	-0.39	-0.39	0	0.019	0	0	0	0	0	0	0
5.2	6.769	6.755	0.015	-0.42	-0.42	0	0.015	0	0	0	0	0	0	0
2.1	6.822	6.81	0.012	-0.46	-0.46	0	0.012	0	0	0	0	0	0	0
-1	6.875	6.864	0.01	-0.49	-0.49	0	0.01	0	0	0	0	0	0	0
-4	6.926	6.918	0.007	-0.52	-0.52	0	0.007	0	0	0	0	0	0	0
-6.9	6.975	6.972	0.003	-0.56	-0.56	0	0.003	0	0	0	0	0	0	0
-9.9	7.026	7.026	0	-0.59	-0.59	0	0	0	0	0	0	0	0	0
-12.8	7.075	7.08	-0.005	-0.62	-0.62	0	0.005	0	0	0	0	0	0	0
-15.7	7.124	7.135	-0.01	-0.66	-0.66	0	0.01	0	0	0	0	0	0	0
-18.6	7.174	7.191	-0.017	-0.69	-0.69	0	0.017	0	0	0	0	0	0	0
-21.5	7.223	7.248	-0.025	-0.72	-0.72	0	0.025	0	0	0	0	0	0	0
-24.5	7.274	7.307	-0.033	-0.75	-0.75	0	0.033	0	0	0	0	0	0	0
-27.5	7.325	7.368	-0.043	-0.79	-0.79	0	0.043	0	0	0	0	0	0	0

-30.6	7.377	7.431	-0.053	-0.82	-0.82	0	0.053	0	0	0	0	0	0	0
-33.7	7.43	7.496	-0.066	-0.85	-0.85	0	0.066	0	0	0	0	0	0	0
-36.9	7.484	7.563	-0.079	-0.89	-0.89	0	0.079	0	0	0	0	0	0	0
-40.2	7.54	7.633	-0.092	-0.92	-0.92	0	0.092	0	0	0	0	0	0	0
-43.8	7.602	7.704	-0.102	-0.95	-0.95	0	0.102	0	0	0	0	0	0	0
-47.5	7.664	7.776	-0.112	-0.99	-0.99	0	0.112	0	0	0	0	0	0	0
-51.4	7.731	7.849	-0.118	-1.02	-1.02	0	0.118	0	0	0	0	0	0	0
-55.6	7.802	7.921	-0.119	-1.05	-1.05	0	0.119	0	0	0	0	0	0	0
-60	7.877	7.992	-0.115	-1.08	-1.08	0	0.115	0	0	0	0	0	0	0
-64.5	7.953	8.061	-0.107	-1.12	-1.12	0	0.107	0	0	0	0	0	0	0
-69.1	8.031	8.127	-0.096	-1.15	-1.15	-0.001	0.096	0	0	0	0	0	0	0
-73.7	8.109	8.192	-0.082	-1.18	-1.18	-0.001	0.082	0	0	0	0	0	0	0
-78.4	8.189	8.254	-0.065	-1.22	-1.21	0	0.065	0	0	0	0	0	0	0

15. GEP data for Ni-Cy_2EN system

TASK	ZBAR		1	HCH0	COMPI	WITH	Ni(II)							
MODL	Ni+2	HCH0	H		1									
CPLX	0	0	-13.78	H	+1(	-1)								
CPLX	0	0	9.483	HCH0(	1)	H	+1(	1)						
CPLX	0	0	15.94	HCH0(	1)	H	+1(	2)						
CPLX	0	0	-9.68	Ni+2(	1)	H	+1(	-1)						
CPLX	0	0	-18.58	Ni+2(	1)	H	+1(	-2)						
CPLX	0	0	-29.34	Ni+2(	1)	H	+1(	-3)						
CPLX	0	0	-26.82	Ni+2(	4)	H	+1(	-4)						
CPLX	1	0	12.34	Ni+2(	1)	HCH0	1)	H	+1(	1)				
CPLX	1	0	7.747	Ni+2(	1)	HCH0	1)							
CPLX	1	0	10.51	Ni+2(	1)	HCH0	2)							
CPLX	1	0	-2.144	Ni+2(	1)	HCH0	1)	H	+1(	-1)				
CPLX	1	0	-12.53	Ni+2(	1)	HCH0	1)	H	+1(	-2)				
CONC														
VESL	IVOL	15	0	0										
VESL	H + 1	0.010511	0	0										
VESL	Ni+2	0.002004	0	0										
VESL	HCH0	0.002001	0	0										
BUR1	H + 1	-0.00993	0	0										
ELEC														
ZERO	H + 1	403.78	0	0										
GRAD	H + 1	58.855	0	0										
DATA														
EMF		PH				ZBAR(H)		POINT		PA			ZBAR(M)		POINT
OBS	OBS	CALC	RESID	OBS	CALC	RESI		RESID	OBS	CALC	RESID	OBS	CALC	RESID	RESID
202.4	3.422	3.46	-0.038	1.97	2	-0.03		0.046	12.006	11.924	0.082	0.01	0	0.013	0.083
199.2	3.476	3.516	-0.04	1.97	2	-0.02		0.047	11.899	11.813	0.086	0.01	0	0.012	0.087
195.5	3.539	3.58	-0.042	1.98	2	-0.02		0.047	11.774	11.686	0.088	0.01	0	0.011	0.089
191.4	3.609	3.655	-0.046	1.98	2	-0.02		0.05	11.637	11.54	0.097	0.01	0	0.01	0.097
186.4	3.693	3.743	-0.049	1.98	2	-0.02		0.052	11.468	11.366	0.102	0.01	0	0.009	0.102
180.5	3.794	3.85	-0.056	1.98	1.99	-0.02		0.059	11.27	11.153	0.116	0.01	0	0.008	0.117
173	3.921	3.987	-0.065	1.98	1.99	-0.01		0.067	11.017	10.883	0.134	0.01	0	0.007	0.134
163.1	4.089	4.164	-0.075	1.98	1.99	-0.01		0.076	10.683	10.531	0.152	0.01	0	0.006	0.152
150.1	4.31	4.379	-0.069	1.97	1.98	-0.01		0.069	10.245	10.106	0.139	0.01	0.01	0.004	0.139
137.2	4.529	4.577	-0.048	1.95	1.96	-0		0.048	9.813	9.717	0.096	0.02	0.02	0.002	0.096
128	4.686	4.722	-0.037	1.93	1.93	-0		0.037	9.509	9.436	0.073	0.03	0.03	0.001	0.073
121.6	4.794	4.828	-0.033	1.9	1.9	-0		0.033	9.301	9.235	0.066	0.04	0.04	0.001	0.066
116.7	4.878	4.909	-0.031	1.87	1.87	-0		0.031	9.144	9.083	0.061	0.05	0.05	0.001	0.061
112.8	4.944	4.974	-0.03	1.84	1.84	-0		0.03	9.022	8.961	0.061	0.07	0.07	0.001	0.061
109.5	5	5.03	-0.03	1.8	1.8	-0		0.03	8.92	8.86	0.06	0.08	0.08	0.001	0.06
106.6	5.049	5.079	-0.029	1.77	1.77	0		0.029	8.832	8.773	0.058	0.1	0.1	0.001	0.058
104	5.094	5.122	-0.029	1.74	1.74	0		0.029	8.754	8.697	0.057	0.11	0.11	0.001	0.057
101.7	5.133	5.161	-0.029	1.71	1.71	0		0.029	8.686	8.629	0.057	0.13	0.13	0.002	0.057
99.6	5.168	5.198	-0.029	1.67	1.67	0		0.029	8.626	8.568	0.058	0.14	0.14	0.002	0.058
97.4	5.206	5.232	-0.026	1.64	1.64	0		0.026	8.562	8.511	0.051	0.16	0.16	0.001	0.051
95.6	5.236	5.263	-0.027	1.61	1.61	0		0.027	8.513	8.459	0.053	0.17	0.17	0.002	0.053
93.9	5.265	5.293	-0.028	1.58	1.58	0		0.028	8.466	8.41	0.056	0.19	0.19	0.002	0.056
92.2	5.294	5.322	-0.028	1.54	1.54	0		0.028	8.42	8.365	0.056	0.2	0.2	0.002	0.056
90.5	5.323	5.35	-0.027	1.51	1.51	0		0.027	8.374	8.321	0.053	0.22	0.22	0.002	0.053
89	5.348	5.377	-0.028	1.48	1.48	0		0.028	8.336	8.28	0.055	0.23	0.23	0.002	0.055
87.4	5.376	5.402	-0.027	1.44	1.44	0		0.027	8.294	8.241	0.053	0.25	0.25	0.002	0.053

86	5.399	5.428	-0.028	1.41	1.41	0	0.028	8.259	8.203	0.056	0.26	0.26	0.002	0.056
84.6	5.423	5.452	-0.029	1.38	1.38	0	0.029	8.224	8.167	0.057	0.28	0.28	0.002	0.057
83.1	5.449	5.477	-0.028	1.35	1.35	0	0.028	8.186	8.132	0.055	0.3	0.29	0.002	0.055
81.7	5.472	5.5	-0.028	1.31	1.31	0	0.028	8.152	8.098	0.055	0.31	0.31	0.002	0.055
80.2	5.498	5.524	-0.026	1.28	1.28	0	0.026	8.115	8.065	0.051	0.33	0.32	0.002	0.051
78.9	5.52	5.547	-0.027	1.25	1.25	0	0.027	8.085	8.032	0.053	0.34	0.34	0.002	0.053
78.3	5.53	5.57	-0.04	1.21	1.21	0	0.04	8.079	8.001	0.078	0.36	0.36	0.003	0.078
77	5.552	5.593	-0.041	1.18	1.18	0	0.041	8.049	7.97	0.08	0.37	0.37	0.003	0.08
75.5	5.578	5.616	-0.039	1.15	1.15	0	0.039	8.014	7.939	0.075	0.39	0.39	0.003	0.075
74.2	5.6	5.639	-0.039	1.12	1.12	0	0.039	7.985	7.909	0.076	0.41	0.4	0.003	0.076
72.8	5.624	5.662	-0.039	1.08	1.08	0	0.039	7.954	7.879	0.074	0.42	0.42	0.003	0.075
71.4	5.647	5.685	-0.038	1.05	1.05	0	0.038	7.923	7.85	0.073	0.44	0.43	0.003	0.073
70	5.671	5.708	-0.037	1.02	1.02	0	0.037	7.893	7.821	0.072	0.45	0.45	0.003	0.072
68.5	5.697	5.732	-0.035	0.98	0.98	0	0.035	7.859	7.792	0.067	0.47	0.47	0.003	0.068
67.1	5.72	5.756	-0.035	0.95	0.95	0	0.035	7.83	7.763	0.067	0.48	0.48	0.003	0.067
65.7	5.744	5.779	-0.035	0.92	0.92	0	0.035	7.802	7.734	0.067	0.5	0.5	0.003	0.067
64.1	5.771	5.804	-0.032	0.88	0.88	0	0.032	7.767	7.706	0.061	0.52	0.51	0.003	0.062
62.6	5.797	5.828	-0.031	0.85	0.85	0	0.031	7.737	7.677	0.06	0.53	0.53	0.003	0.06
61.1	5.822	5.854	-0.031	0.82	0.82	0	0.031	7.707	7.648	0.059	0.55	0.54	0.003	0.059
59.6	5.848	5.879	-0.031	0.79	0.79	0	0.031	7.678	7.619	0.059	0.56	0.56	0.003	0.059
57.9	5.877	5.906	-0.029	0.75	0.75	0	0.029	7.644	7.59	0.054	0.58	0.58	0.003	0.054
56.3	5.904	5.933	-0.029	0.72	0.72	0	0.029	7.614	7.56	0.054	0.6	0.59	0.003	0.054
54.6	5.933	5.961	-0.028	0.69	0.69	0	0.028	7.581	7.53	0.052	0.61	0.61	0.003	0.052
52.8	5.963	5.989	-0.026	0.65	0.65	0	0.026	7.547	7.499	0.048	0.63	0.63	0.002	0.048
50.9	5.996	6.019	-0.023	0.62	0.62	0	0.023	7.511	7.468	0.043	0.64	0.64	0.002	0.043
49	6.028	6.05	-0.022	0.59	0.59	0	0.022	7.477	7.436	0.041	0.66	0.66	0.002	0.041
47	6.062	6.082	-0.02	0.55	0.55	0	0.02	7.441	7.404	0.037	0.68	0.67	0.002	0.038
45.2	6.093	6.116	-0.024	0.52	0.52	0	0.024	7.413	7.37	0.043	0.69	0.69	0.002	0.043
43	6.13	6.152	-0.022	0.49	0.49	0	0.022	7.376	7.336	0.04	0.71	0.71	0.002	0.04
40.7	6.169	6.19	-0.021	0.45	0.45	0	0.021	7.337	7.3	0.037	0.72	0.72	0.002	0.037
38.2	6.212	6.23	-0.019	0.42	0.42	0	0.019	7.295	7.262	0.033	0.74	0.74	0.002	0.033
35.5	6.257	6.273	-0.016	0.39	0.39	0	0.016	7.251	7.223	0.028	0.76	0.76	0.001	0.028
32.5	6.308	6.32	-0.012	0.36	0.36	0	0.012	7.202	7.182	0.02	0.77	0.77	0.001	0.02
29.2	6.364	6.371	-0.006	0.32	0.32	0	0.006	7.149	7.138	0.011	0.79	0.79	0	0.011
25.5	6.427	6.427	0	0.29	0.29	0	0	7.09	7.091	0	0.81	0.81	0	0
21.4	6.497	6.49	0.007	0.26	0.26	0	0.007	7.029	7.04	-0.011	0.82	0.83	0	0.011
16.6	6.579	6.562	0.017	0.22	0.22	0	0.017	6.957	6.984	-0.027	0.84	0.84	-0.001	0.027
10.9	6.675	6.646	0.029	0.19	0.19	0	0.029	6.876	6.921	-0.046	0.86	0.86	-0.002	0.046
3.8	6.796	6.748	0.048	0.16	0.16	0	0.048	6.777	6.849	-0.072	0.88	0.88	-0.002	0.072
-5.4	6.952	6.876	0.076	0.12	0.12	0	0.076	6.656	6.764	-0.107	0.9	0.9	-0.003	0.107
-18.2	7.17	7.051	0.119	0.09	0.09	0	0.119	6.501	6.657	-0.156	0.92	0.92	-0.003	0.156
-36.8	7.486	7.312	0.174	0.06	0.06	0	0.174	6.31	6.518	-0.208	0.94	0.95	-0.002	0.208
-59.5	7.872	7.738	0.133	0.03	0.03	0	0.133	6.228	6.377	-0.15	0.97	0.97	-0.001	0.15
-78.8	8.199	8.233	-0.033	0	0	0	0.033	0	0	0	0	0	0	0
-93.6	8.451	8.553	-0.102	-0.04	-0.03	-0	0.102	0	0	0	0	0	0	0
-105.2	8.648	8.754	-0.106	-0.07	-0.06	-0	0.106	0	0	0	0	0	0	0
-115.5	8.823	8.897	-0.074	-0.1	-0.09	-0	0.074	0	0	0	0	0	0	0
-123.9	8.966	9.008	-0.042	-0.12	-0.12	-0	0.042	0	0	0	0	0	0	0
-130.9	9.085	9.098	-0.013	-0.15	-0.15	-0	0.013	0	0	0	0	0	0	0
-136.9	9.187	9.174	0.013	-0.18	-0.18	0	0.013	0	0	0	0	0	0	0
-142.1	9.275	9.24	0.035	-0.21	-0.21	0	0.035	0	0	0	0	0	0	0
-146.7	9.353	9.299	0.054	-0.23	-0.24	0.01	0.054	0	0	0	0	0	0	0
-150.8	9.423	9.352	0.071	-0.26	-0.27	0.01	0.071	0	0	0	0	0	0	0
-154.4	9.484	9.401	0.083	-0.28	-0.29	0.01	0.084	0	0	0	0	0	0	0

16. GEP data for Zn-Cy_2EN system

TASK	ZBAR	1	HCH0	COMPL	WITH	Zn(II)								
MODL	ZN+2	HCH0	H	1										
CPLX	0	0	-13.78	H	+1(	-1)								
CPLX	0	0	9.483	HCH0(	1)	H	+1(	1)						
CPLX	0	0	15.94	HCH0(	1)	H	+1(	2)						
CPLX	0	0	-9.18	ZN+2(	1)	H	+1(	-1)						
CPLX	0	0	-16.46	ZN+2(	1)	H	+1(	-2)						
CPLX	0	0	-27.74	ZN+2(	1)	H	+1(	-3)						
CPLX	0	0	-40.32	ZN+2(	1)	H	+1(	-4)						
CPLX	0	0	-8.78	ZN+2(	2)	H	+1(	-1)						
CPLX	0	0	-27.22	ZN+2(	4)	H	+1(	-4)						
CPLX	1	0	11.94	ZN+2(	1)	HCH0(	1)	H	+1(	1)				
CPLX	1	0	6.271	ZN+2(	1)	HCH0(	1)							
CPLX	1	0	10.23	ZN+2(	1)	HCH0(	2)							
CPLX	1	0	-1.998	ZN+2(	1)	HCH0(	1)	H	+1(	-1)				
CPLX	1	0	-10.95	ZN+2(	1)	HCH0(	1)	H	+1(	-2)				
CONC														
VESL	IVOL	15	0	0										
VESL	H + 1	0.011	0	0										
VESL	ZN+2	0.002	0	0										
VESL	HCH0	0.002	0	0										
BUR1	H + 1	-0.01	0	0										
ELEC														
ZERO	H + 1	405.7	0	0										
GRAD	H + 1	58.84	0	0										
DATA														
EMF		PH			ZBAR(H)		POINT		PA			ZBAR(M)		POINT
OBS	OBS	CALC	RESID	OBS	CALC	RESID	RESID	OBS	CALC	RESID	OBS	CALC	RESID	RESID
205.6	3.4	3.405	-0.004	2	2	-0.003	0.005	12.043	12.034	0.01	0	0	0.002	0.01
202.7	3.45	3.455	-0.005	2	2	-0.003	0.006	11.946	11.936	0.011	0	0	0.002	0.011
199.4	3.506	3.51	-0.005	2	2	-0.003	0.005	11.836	11.826	0.01	0	0	0.001	0.01
195.6	3.57	3.574	-0.003	2	2	-0.002	0.004	11.708	11.702	0.007	0	0	0.001	0.007
191.3	3.644	3.647	-0.003	2	2	-0.001	0.004	11.564	11.557	0.007	0	0	0.001	0.007
186.1	3.732	3.734	-0.002	2	2	-0.001	0.002	11.389	11.385	0.004	0	0	0	0.004
179.7	3.841	3.841	0	2	2	0	0	11.174	11.174	0	0	0	0	0
171.6	3.978	3.978	0	2	2	0	0	10.9	10.9	0	0	0	0	0
160.4	4.169	4.17	-0.001	1.99	1.99	0	0.001	10.522	10.52	0.002	0	0	0	0.002
143.9	4.449	4.452	-0.003	1.99	1.99	0	0.003	9.966	9.961	0.005	0	0	0	0.005
123.7	4.792	4.798	-0.006	1.97	1.97	0	0.006	9.287	9.276	0.012	0	0	0	0.012
108.7	5.047	5.064	-0.016	1.94	1.94	0	0.016	8.789	8.756	0.032	0.01	0.01	0.001	0.032
98.3	5.224	5.24	-0.016	1.91	1.91	0	0.016	8.448	8.416	0.032	0.02	0.02	0.001	0.032
90.8	5.352	5.367	-0.015	1.88	1.88	0	0.015	8.206	8.176	0.03	0.02	0.02	0.001	0.03
84.9	5.452	5.465	-0.013	1.85	1.85	0	0.013	8.019	7.993	0.026	0.03	0.03	0.001	0.026
80.2	5.532	5.545	-0.013	1.81	1.81	0	0.013	7.873	7.847	0.026	0.04	0.04	0.002	0.026
76.2	5.6	5.613	-0.013	1.78	1.78	0	0.013	7.751	7.725	0.026	0.05	0.05	0.002	0.026
72.7	5.659	5.672	-0.013	1.75	1.75	0	0.013	7.646	7.62	0.025	0.06	0.06	0.002	0.025
69.6	5.712	5.725	-0.013	1.72	1.72	0	0.013	7.554	7.529	0.025	0.07	0.07	0.002	0.025
66.7	5.761	5.773	-0.012	1.68	1.68	0	0.012	7.47	7.448	0.023	0.08	0.08	0.002	0.023
64.2	5.804	5.817	-0.013	1.65	1.65	0	0.013	7.4	7.374	0.025	0.09	0.09	0.002	0.025
61.8	5.844	5.858	-0.013	1.62	1.62	0	0.013	7.333	7.307	0.025	0.1	0.1	0.002	0.025
59.6	5.882	5.896	-0.014	1.58	1.58	0	0.014	7.273	7.246	0.027	0.11	0.11	0.003	0.027

57.4	5.919	5.932	-0.013	1.55	1.55	0	0.013	7.213	7.189	0.024	0.13	0.12	0.003	0.025
55.4	5.953	5.967	-0.013	1.52	1.52	0	0.013	7.161	7.136	0.025	0.14	0.13	0.003	0.025
53.4	5.987	6	-0.013	1.49	1.49	0	0.013	7.109	7.085	0.023	0.15	0.15	0.003	0.023
51.6	6.018	6.031	-0.014	1.45	1.45	0	0.014	7.063	7.038	0.025	0.16	0.16	0.003	0.025
49.7	6.05	6.062	-0.012	1.42	1.42	0	0.012	7.016	6.993	0.022	0.17	0.17	0.003	0.023
48	6.079	6.092	-0.013	1.39	1.39	0	0.013	6.975	6.95	0.024	0.19	0.18	0.003	0.024
46.2	6.11	6.121	-0.012	1.35	1.35	0	0.012	6.931	6.91	0.021	0.2	0.2	0.003	0.022
44.5	6.138	6.15	-0.011	1.32	1.32	0	0.011	6.891	6.87	0.021	0.21	0.21	0.003	0.021
43	6.164	6.178	-0.014	1.29	1.29	0	0.014	6.858	6.832	0.025	0.23	0.22	0.003	0.026
41.3	6.193	6.206	-0.013	1.25	1.25	0	0.013	6.819	6.796	0.023	0.24	0.24	0.003	0.023
39.7	6.22	6.233	-0.013	1.22	1.22	0	0.013	6.784	6.76	0.023	0.25	0.25	0.003	0.023
38.1	6.247	6.26	-0.013	1.19	1.19	0	0.013	6.749	6.726	0.023	0.27	0.26	0.003	0.023
36.5	6.274	6.287	-0.013	1.16	1.16	0	0.013	6.715	6.692	0.023	0.28	0.28	0.003	0.023
34.9	6.302	6.314	-0.013	1.12	1.12	0	0.013	6.682	6.66	0.022	0.29	0.29	0.003	0.022
33.3	6.329	6.341	-0.012	1.09	1.09	0	0.012	6.649	6.628	0.021	0.31	0.3	0.003	0.022
31.7	6.356	6.368	-0.012	1.06	1.06	0	0.012	6.617	6.596	0.021	0.32	0.32	0.003	0.021
30.1	6.383	6.395	-0.012	1.02	1.02	0	0.012	6.586	6.566	0.02	0.34	0.33	0.003	0.021
28.5	6.41	6.422	-0.012	0.99	0.99	0	0.012	6.556	6.535	0.02	0.35	0.35	0.003	0.02
26.9	6.438	6.45	-0.012	0.96	0.96	0	0.012	6.526	6.506	0.021	0.37	0.36	0.003	0.021
25.3	6.465	6.478	-0.013	0.92	0.92	0	0.013	6.498	6.476	0.021	0.38	0.38	0.003	0.022
23.6	6.494	6.506	-0.012	0.89	0.89	0	0.012	6.467	6.447	0.02	0.4	0.39	0.003	0.02
21.9	6.523	6.534	-0.012	0.86	0.86	0	0.012	6.438	6.418	0.019	0.41	0.41	0.003	0.019
20.1	6.553	6.563	-0.01	0.82	0.82	0	0.01	6.407	6.39	0.017	0.43	0.43	0.002	0.017
18.4	6.582	6.593	-0.011	0.79	0.79	0	0.011	6.379	6.362	0.018	0.45	0.44	0.002	0.018
16.6	6.613	6.623	-0.011	0.76	0.76	0	0.011	6.351	6.334	0.017	0.46	0.46	0.002	0.017
14.7	6.645	6.654	-0.01	0.73	0.73	0	0.01	6.321	6.306	0.015	0.48	0.48	0.002	0.015
12.8	6.677	6.686	-0.009	0.69	0.69	0	0.009	6.292	6.278	0.014	0.5	0.49	0.002	0.014
10.9	6.709	6.719	-0.01	0.66	0.66	0	0.01	6.266	6.251	0.015	0.51	0.51	0.002	0.015
8.8	6.745	6.753	-0.008	0.63	0.63	0	0.008	6.235	6.223	0.012	0.53	0.53	0.001	0.012
6.8	6.779	6.788	-0.009	0.59	0.59	0	0.009	6.209	6.196	0.013	0.55	0.55	0.002	0.013
4.7	6.815	6.824	-0.009	0.56	0.56	0	0.009	6.183	6.17	0.013	0.57	0.57	0.001	0.014
2.5	6.852	6.862	-0.009	0.53	0.53	0	0.009	6.156	6.143	0.013	0.59	0.59	0.001	0.013
0.2	6.891	6.9	-0.009	0.49	0.49	0	0.009	6.13	6.117	0.013	0.61	0.61	0.001	0.013
-2.2	6.932	6.941	-0.009	0.46	0.46	0	0.009	6.104	6.092	0.012	0.63	0.63	0.001	0.012
-4.7	6.975	6.983	-0.008	0.43	0.43	0	0.008	6.079	6.067	0.011	0.65	0.65	0.001	0.011
-7.3	7.019	7.027	-0.008	0.39	0.39	0	0.008	6.055	6.044	0.01	0.67	0.67	0.001	0.01
-9.9	7.063	7.072	-0.009	0.36	0.36	0	0.009	6.035	6.023	0.012	0.7	0.7	0.001	0.012
-12.6	7.109	7.119	-0.01	0.33	0.33	0	0.01	6.017	6.004	0.013	0.72	0.72	0.001	0.013
-15.5	7.158	7.167	-0.009	0.3	0.3	0	0.009	6.001	5.989	0.012	0.75	0.74	0.001	0.012
-18.4	7.207	7.217	-0.01	0.26	0.26	0	0.01	5.991	5.979	0.012	0.77	0.77	0.001	0.012
-21.3	7.257	7.268	-0.012	0.23	0.23	0	0.012	5.989	5.975	0.014	0.8	0.8	0.001	0.014
-24.3	7.308	7.32	-0.012	0.2	0.2	0	0.012	5.996	5.981	0.015	0.82	0.82	0.001	0.015
-27.3	7.359	7.372	-0.014	0.16	0.16	0	0.014	6.015	5.999	0.016	0.85	0.85	0	0.016
-30.4	7.411	7.424	-0.013	0.13	0.13	0	0.013	6.052	6.037	0.015	0.88	0.88	0	0.015
-33.5	7.464	7.476	-0.012	0.1	0.1	0	0.012	6.119	6.105	0.014	0.91	0.91	0	0.014
-36.6	7.517	7.527	-0.01	0.06	0.06	0	0.01	6.239	6.227	0.012	0.94	0.94	0	0.012
-39.6	7.568	7.577	-0.009	0.03	0.03	0	0.009	6.495	6.485	0.01	0.97	0.97	0	0.01
-42.6	7.619	7.625	-0.006	0	0	0	0.006	0	0	0	0	0	0	0
-45.6	7.67	7.672	-0.002	-0.03	-0.03	0	0.002	0	0	0	0	0	0	0
-48.5	7.719	7.717	0.002	-0.07	-0.07	0	0.002	0	0	0	0	0	0	0
-51.4	7.768	7.76	0.008	-0.1	-0.1	0	0.008	0	0	0	0	0	0	0
-54.1	7.814	7.802	0.012	-0.13	-0.13	0	0.012	0	0	0	0	0	0	0
-56.7	7.858	7.842	0.016	-0.17	-0.17	0	0.016	0	0	0	0	0	0	0
-59.1	7.899	7.881	0.018	-0.2	-0.2	0	0.018	0	0	0	0	0	0	0

-61.2	7.935	7.918	0.016	-0.23	-0.23	0	0.016	0	0	0	0	0	0	0
-63	7.965	7.955	0.011	-0.27	-0.27	0	0.011	0	0	0	0	0	0	0
-64.6	7.993	7.99	0.003	-0.3	-0.3	0	0.003	0	0	0	0	0	0	0
-66.1	8.018	8.024	-0.006	-0.33	-0.33	0	0.006	0	0	0	0	0	0	0
-67.6	8.044	8.057	-0.014	-0.36	-0.36	0	0.014	0	0	0	0	0	0	0
-69.1	8.069	8.09	-0.021	-0.4	-0.4	0	0.021	0	0	0	0	0	0	0
-70.7	8.096	8.122	-0.025	-0.43	-0.43	0	0.025	0	0	0	0	0	0	0
-72.3	8.124	8.153	-0.029	-0.46	-0.46	0	0.029	0	0	0	0	0	0	0
-74	8.152	8.183	-0.031	-0.5	-0.5	0	0.031	0	0	0	0	0	0	0
-75.8	8.183	8.213	-0.03	-0.53	-0.53	0	0.03	0	0	0	0	0	0	0
-77.6	8.214	8.243	-0.03	-0.56	-0.56	0	0.03	0	0	0	0	0	0	0
-79.5	8.246	8.273	-0.027	-0.59	-0.59	0	0.027	0	0	0	0	0	0	0
-81.5	8.28	8.302	-0.022	-0.63	-0.63	0	0.022	0	0	0	0	0	0	0
-83.5	8.314	8.331	-0.017	-0.66	-0.66	0	0.017	0	0	0	0	0	0	0
-85.5	8.348	8.36	-0.012	-0.69	-0.69	0	0.012	0	0	0	0	0	0	0
-87.6	8.384	8.388	-0.005	-0.73	-0.73	0	0.005	0	0	0	0	0	0	0
-89.8	8.421	8.417	0.004	-0.76	-0.76	0	0.004	0	0	0	0	0	0	0
-92	8.458	8.446	0.013	-0.79	-0.79	0	0.013	0	0	0	0	0	0	0
-94.2	8.496	8.474	0.022	-0.82	-0.82	0	0.022	0	0	0	0	0	0	0
-96.5	8.535	8.503	0.032	-0.86	-0.86	0	0.032	0	0	0	0	0	0	0
-98.8	8.574	8.532	0.042	-0.89	-0.89	0.001	0.042	0	0	0	0	0	0	0